DE GRUYTER

Narendra Reddy, Wenlong Zhou, Mingbo Ma

KERATIN-BASED MATERIALS

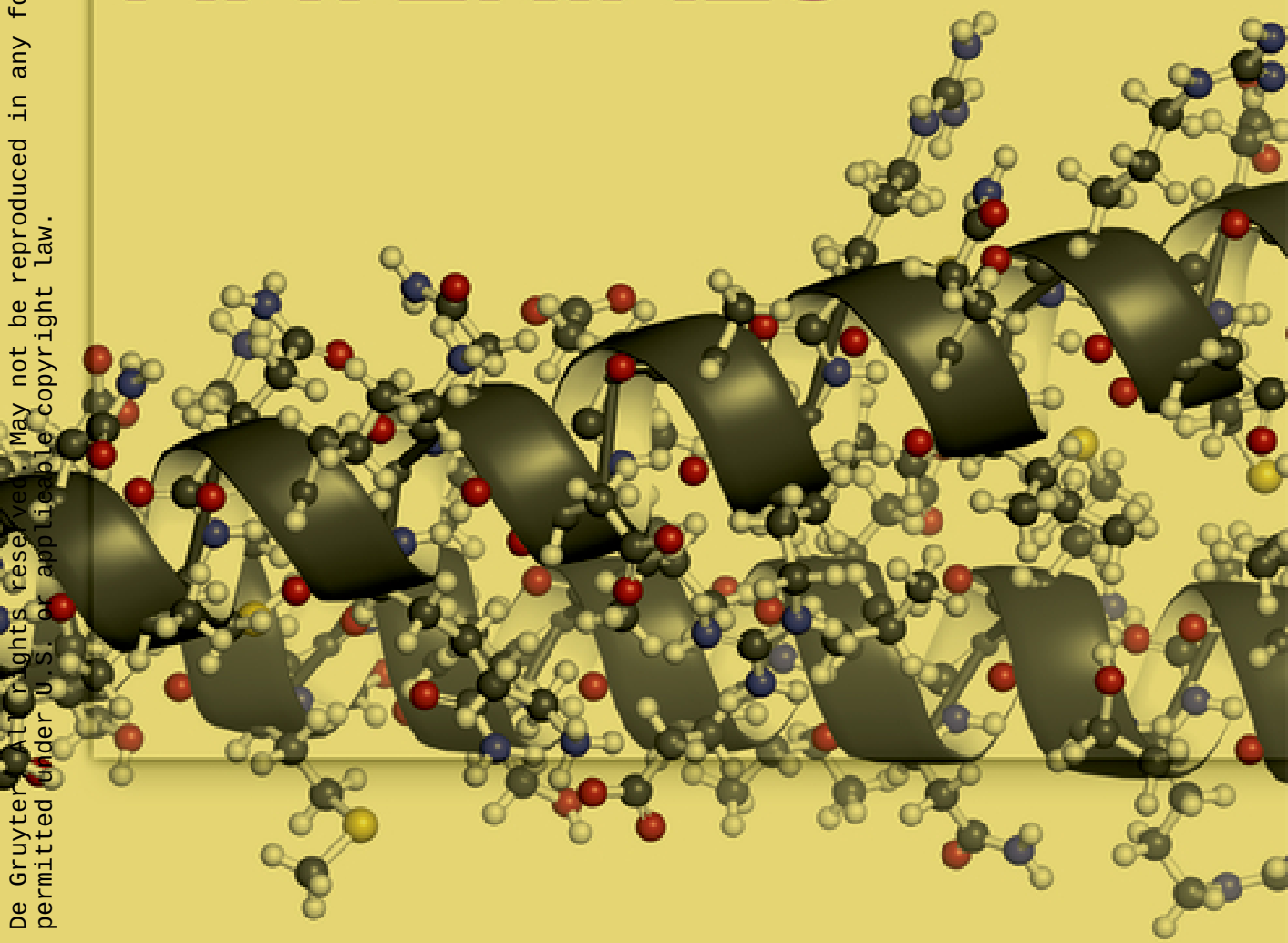

Narendra Reddy, Wenlong Zhou, Mingbo Ma

Keratin-Based Materials

Also of interest

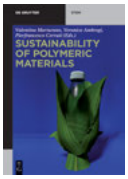

Sustainability of Polymeric Materials
Valentina Marturano, Veronica Ambrogi, Pierfrancesco Cerruti, 2020
ISBN 978-3-11-059093-7, e-ISBN 978-3-11-059058-6

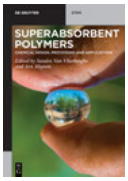

Superabsorbent Polymers.
Chemical Design, Processing and Applications
Sandra Van Vlierberghe, Arn Mignon, 2020
ISBN 978-1-5015-1910-9, e-ISBN 978-1-5015-1911-6

Industrial Biotechnology
Mark Anthony Benvenuto, 2019
ISBN 978-3-11-053639-3, e-ISBN 978-3-11-053662-1

Biosensors.
Fundamentals and Applications
Chandra Mouli Pandey, Bansi Dhar Malotra, 2019
ISBN 978-3-11-063780-9, e-ISBN 978-3-11-064108-0

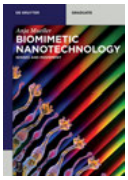

Biomimetic Nanotechnology.
Senses and Movement
Anja Mueller, 2018
ISBN 978-3-11-037914-3, e-ISBN 978-3-11-037916-7

Narendra Reddy, Wenlong Zhou, Mingbo Ma

Keratin-Based Materials

DE GRUYTER

Authors
Dr. Narendra Reddy
Centre for Incubation
Innovation, Research and Consultancy
Jyothy Institute of Technology
Thataguni Post
Bengaluru 560082
India
narendra.r@ciirc.jyothyit.ac.in

Dr. Wenlong Zhou
Department of Textiles and Materials
Engineering
Zhejiang Sci-Tech University
310018 Hangzhou
China
wzhou@zstu.edu.cn

Dr. Mingbo Ma
Department of Textiles and Materials
Engineering
Zhejiang Sci-Tech University
310018 Hangzhou
China
mamingbo@zstu.edu.cn

ISBN 978-1-5015-1913-0
e-ISBN (PDF) 978-1-5015-1176-9
e-ISBN (EPUB) 978-1-5015-1187-5

Library of Congress Control Number: 2020940495

Bibliographic information published by the Deutsche Nationalbibliothek
The Deutsche Nationalbibliothek lists this publication in the Deutsche Nationalbibliografie; detailed bibliographic data are available on the Internet at http://dnb.dnb.de.

Cover image: Molekuul/iStock/Getty Images Plus
Typesetting: Integra Software Services Pvt. Ltd.
Printing and binding: CPI books GmbH, Leck

www.degruyter.com

Preface

Keratin is undoubtedly one of nature's highly sophisticated, unique and versatile materials. From the hollow honeycombs and hierarchical structure in feathers that provide low density, the excellent thermal and acoustic resistances of wool, extraordinary toughness of some mammalian scales and flexibility and diversity of human hairs, keratins have unique structure and properties. Keratins have specific peptide sequences that can promote cell attachment and growth and are preferred for medical applications. Keratins can be made into fibers, films, freeze-dried scaffolds, micro- and nanoparticles. Conventionally, keratin from wool is the only source exploited for commercial applications. In addition to wool, other sources of keratin such as poultry feathers are available in large quantities and at considerably low cost but are not effectively utilized and are mostly disposed as waste. Realizing the importance of keratin, technologies have been developed to extract keratin from feathers, wool and other sources. Studies have also provided better insights into the structure and properties of keratin and have enabled developing newer technologies for extraction of keratin and converting the keratin into biomaterials for various applications. Keratin has been found to be suitable for environmental remediation, biotechnology, medicine, electronics, cosmetics and many other applications. In this book, we present the structure, properties, processability and applications of keratin. Initial chapters discuss on the properties and processing of various sources of keratins. Later, we have divided the chapters based on the forms of keratin. The last chapter reports the recent and most unique applications of keratin. Every effort has been made to provide comprehensive information in each section. However, the contents in this book are mostly designed to give an overview of the keratin and its properties and applications, and readers are urged to refer to the original reports for comprehensive information on specific topics.

https://doi.org/10.1515/9781501511769-202

Contents

Chapter 1
Introduction to keratin

Keratin is one of the most common protein biopolymers found in nature. There are several sources and types of keratin but it has been suggested that keratin from human and bovine sources are similar with respect to charge, size and immunoreactivity. Based on their distinct structure and properties, keratins have been classified as soft and hard keratins. Soft keratins are those found as intermediate filaments (IFs) in the epithelia and arranged in loosely packed bundles and responsible for the mechanical resilience of the epithelial cells. Hard keratins are those found in ordered arrays in matrix of cysteine rich proteins in hairs, nails, claws and beaks and contribute to the tough structure of epidermal appendages (Rouse, 2010; Thibaut, 2003). Keratin exists in mammals, reptiles and birds and fishes as many parts of the body including hoof, horn, fur, wool, skin, quill, feathers, beaks and slime (McKittrick, 2012). Keratin broadly refers to the insoluble proteins found in the IFs which form a major portion of the cytoplasmic epithelia and epidermal appendage structures such as hair, wool, horns and nails. Few keratins are found only in the epithelial cells and are characterized by unique physiochemical properties and their primary function is to protect the epithelial cells from mechanical and nonmechanical stresses that could cause cell death (Coulombe, 2002). Additional functions of keratins include cell signaling, stress response and apoptosis. Although keratin is commonly considered to be a single substance, it is a mixture of proteins and enzymes. Other characteristics of keratin include indigestibility to pepsin or trypsin and also to dilute acids, alkalis, water and organic solvents. Keratins are also generally insoluble in salt solutions but can be made soluble in the presence of urea and other denaturing agents.

Based on their structure, keratins can also be classified as α-keratin or β-keratin. The α-keratin is fibrillar in nature and is composed of helical structure with the micofibrils embedded in an amorphous keratin matrix and aligned along the fiber axis. These amorphous regions have higher sulfur content with considerable amounts of disulfide bonds from the cysteine residues whereas the microfibrillar proteins having relatively low sulfur content are mostly made from hydrogen bonding which are responsible for determining the secondary structure of the proteins (Duer, 2003). α-Keratins can be further classified as the low sulfur containing α-keratins (40–60 kDa) (about 50%–60%) and high sulfur matrix proteins (10–25 kDa). α-Keratins in filament form provide toughness to the hair fibers whereas the α-keratins in matrix proteins provide adhesiveness to cortical cells. Unlike the α-keratins, the β-keratins are synthesized in the form of hard structures (claws and beaks) and are produced in the epidermis of skin appendages (Toni, 2007). β-Keratins have low solubility, have molecular weights between 10 and 25 kDa and are characterized by a distinct X-ray diffraction pattern. Since they form the outer layers, β-keratins have excellent chemical resistance and mechanical strength (Valle, 2010). Filaments in β-keratins have β sheet content

https://doi.org/10.1515/9781501511769-001

that repeats every 3–4 nm and structurally highly resistant compared to α-keratins (Toni, 2007; Valle, 2010). However, the molecular and functional relationship between α- and β-keratins is not clearly understood.

Structurally, molecules in keratin are connected through internal interactions composed of filaments of α-keratins and β-keratins with considerable structural differences between the two keratins. Filaments in α-keratins have diameter of 7 nm compared to 3 nm in β-keratins. All keratin structures are made of units called cortical cells which differ in their subcellular components depending on the source. Major fibrous components of the cells are divided as the intermacrofibrillar materials, macrofibrils and IFs (Bryson, 2009). Length and diameter of the IFs are 10 μm and 7–10 nm, respectively. In terms of morphology, α-keratins are in the form of coiled coils, whereas β-keratins are found in pleated sheets. α-Keratins are made up of low sulfur proteins and high glycine–tyrosine (HGT) proteins (wool, quills, fingernails and horns), whereas β-keratins consist of single proteins commonly seen in feathers, beaks and claws and have scaly surfaces. The α-helix is reported to form the backbone of keratin and is surrounded by the β-sheets and random coils. The extent of helices, β-sheets and random coils varies based on the condition of the keratin and also the method used for analysis (Table 1.1) (Ghosh, 2019). Combining two X-ray techniques (ptychography and nanodiffraction), whole cells in keratin were observed at a resolution of 65 nm (Hemonnot, 2016). From the analysis, it was found that the intracellular bundles in keratin filaments had a radius of 5 nm and were arranged hexagonally. Distance between each filament was 14 nm and diameter of fiber bundles was 70 nm. However, almost all known hard keratins were reported to have a superlattice structure consisting of two infinite lattices and three finite lattices. Equatorial X-ray diffraction patterns (Figure 1.1) demonstrate that the center to center distance of the IFs varies between different keratin sources. A model suggesting a common 62.5 nm lattice with distance between IFs being three times the radius was suggested.

Table 1.1: Variations in the proportions of α-helices, β-sheets and random coils in feather keratin before and after treatment (Ghosh, 2019).

Type of analysis		Isotropic chemical shift (ppm)		Relative proportion (%)		FWHM (ppm)	
		Raw	Pretreated	Raw	Pretreated	Raw	Pretreated
^{13}C-CP-MAS-NMR	β-Sheets + random coils	172	173	65.8	85.9	4.73	4.30
	α-helix	176	175	34.2	14.0	4.84	3.17
^{15}N-CP-MAS-NMR	β-Sheets + random coils	105.5		16.4		12	
	β-Sheets + random coils	117		48.9		11.5	
	α-Helix	126.8		34.7		10	

Note: Reproduced with permission from Elsevier.

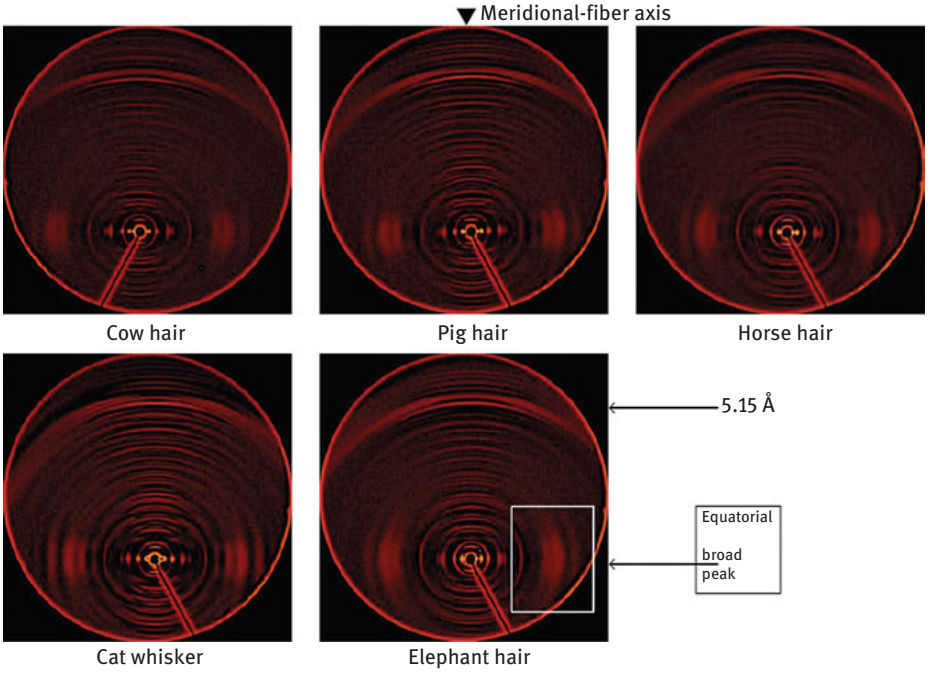

Figure 1.1: Differences in the X-ray diffraction patterns of keratin in hairs of different animals (James, 2011). Reproduced with permission through Open Access publishing.

1.1 General classification and properties of keratin

Depending on their isoelectric point (PI), keratins are classified as acidic (type I) or basic (type II). Type I keratins in humans have a PI between 4.9 and 5.4, whereas type II keratins have a PI between 6.5–8.5. Compared to humans, type I bovine keratins have a PI <5.6 and type II keratins have PI >6.0. Specifically, keratins from hair, nail or wool have a PI between 4.7–5.4. Although keratins have different PIs, the type and sequence of amino acids in the basic and acidic keratin are considered to be similar (Bragulla, 2019). For example, keratin from the skin of humans and various animals have similar amino acid composition. Keratins in horn-cornified tissues and dental enamels have been found to have a constant molecular ratio of histidine, lysine and arginine, irrespective of source (Bragulla, 2019). Although the amino acid content may be similar, the mechanical properties of the keratin materials vary widely depending on the source (Wang, 2016). The types of amino acids and their chemical shifts that were used to judge their molecular conformation are given in Table 1.2.

In addition to the variation in properties of keratin due to structure and composition, the humidity during testing and the location of the keratin from the same source also cause considerable variations in properties. Duer et al. have used solid-state

Table 1.2: Structural features and chemical shifts (^{13}C) in α-keratin (Duer, 2003).

Amino acid	% in α-keratin	Carbonyl α-helix	Carbonyl β-sheet	Carbonyl α-helix	Carbonyl β-sheet	β-Carbon	Y-Carbon	δ-Carbon
Glu	12.1	178.5	175.0	59.2	54.6	28.9	34.6	182.8
Gln	12.1	178.1	174.6	54.0	54.0	28.1	32.2	179.0
Cys	11.2	175.1	172.2	56.1	56.1	26.0	–	–
Ser	10.2	176.0	173.6	56.8	56.8	62.3	–	–
Gly	8.1	175.5	171.9	44.6	44.6	–	–	–
Pro	7.5	179.5	174.8	62.5	62.5	30.6	25.5	48.2
Arg	7.2	179.1	175.0	54.8	54.8	28.8	–	–
Leu	6.9	178.5	175.5	53.9	53.9	40.5	25.2	23.1
Thr	6.5	176.7	174.2	60.6	60.6	68.3	20.1	–
Ala	5.0	176.6	172.2	49.0	49.0	17.7	–	–

Note: Reproduced with permission from Royal Society of Chemistry.

NMR and studied the structure and molecular mobility of α-keratins at various humidity levels. It was observed that the secondary and primary structure of keratin was highly dependent on the level of moisture. A higher degree of ordering and extended conformation of molecules and lower mobility occurs under the dehydrated state. Under the dehydrated condition, disulfide bonds are broken and the changes in the hydrogen bonds lead to loss of motion in the sidechains, which makes the material to become considerably rigid. However, the results have not been substantiated with experimental data (Duer, 2003). Interestingly, human finger nails were reported to have strength of 86 MPa but reduced to 22.5 MPa when completely hydrated with corresponding decrease in modulus from 2.05 to 0.19 GPa. It was also reported that due to the differences in the arrangement of keratin in nails, the energy required to cut a nail longitudinally was about 6 kJ/m^2 compared to about 12kJ/m^2 for cutting the nails transversally (Wang, 2016a).

1.2 Structure and properties of human hair keratin

Human hair is considered to be one of the most complicated natural composite materials. Although mostly composed of keratin, hair fibers have a hierarchical structure and are also made up of micro- to nanoscale materials (Yu, 2017a). In addition, the composition of hair as fiber and its constituents the cortex and cuticle varies considerably. Keratins in humans have been classified based on the source, type of extraction and other factors. Broadly, keratins in humans have been classified into two major classes (type I and type II). Type I keratins are composed of keratins K9–K10, K12 and K28 and K31–K40 compared to type II keratins which consists of K1–K8 and K71–K86 (Schweizer, 2006). In terms of genes, 28 type I keratin genes (17 epithelial and 11 hair keratins) and 26 type II keratin genes (20 epithelial keratins and 6 hair

keratins) have been recognized (Schweizer, 2006) (Table 1.3). Among these (54) types of genes, about 26% are expressed in the hair follicle. Molecular weight of the human keratins has been reported to be between 44 and 66 kDa. Structurally, human hair keratins have a hierarchical arrangement as shown in Figure 1.2 and mainly made up of three main regions: the medulla, cortex and cuticle. IFs form the major constituents of hair keratin and have a central rod with 310 amino acids having α-helical configuration. These IFs are oriented along the fiber axis but disoriented in-plane.

Table 1.3: Various types of keratins found in the different parts of humans (Moll, 2008).

Type of keratin	Type I		Type II	
	New name	Former name	New name	Former name
Epithelial keratins	K9	K9	K1	K1
	K10	K10	K2	K2
	K12	K12	K3	K3
	K13	K13	K4	K4
	K14	K14	K5	K5
	K15	K15	K6a	K6a
	K16	K16	K6b	K6b
	K17	K17	K6c	K6e/h
	K18	K18	K7	K7
	K19	K19	K8	K8
	K20	K20	K76	K2p
	K23*	K23	K77	K1b
	K24*	K24	K78*	K5b
			K79*	K6l
			K80*	Kb20
Hair follicle-specific epithelial keratins (root sheath)	K25	K25irs1	K71	K6irs1
	K26	K25irs2	K72	K6irs2
	K27	K25irs3	K73	K6irs3
	K28	K25irs4	K74	K6irs4
			K75	K6hf
Hair keratins	K31	Ha1	K81	Hb1
	K32	Ha2	K82	Hb2
	K33a	Ha3-I	K83	Hb3
	K33b	Ha3-II	K84	Hb4
	K34	Ha4	K85	Hb5
	K35	Ha5	K86	Hb6
	K36	Ha6		
	K37	Ha7		
	K38	Ha8		
	K39	Ka35		
	K40	Ka36		

Note: Reproduced with permission from Springer.

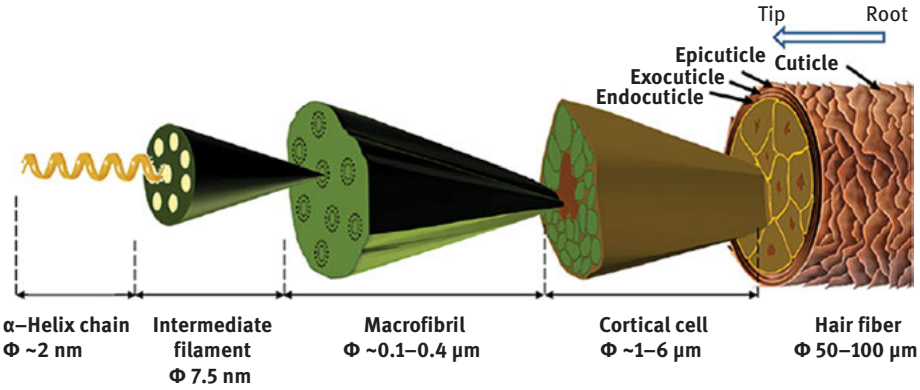

Figure 1.2: Schematic representation of the hierarchical structure of human hair (Yu, 2017a). Reproduced with permission from Elsevier.

Coiled-coil structures (heterodimers) connect together to form IFs which are further networked to form the macrofibrils. Recent studies have revealed that a new region exists between the cortex and cuticle boundary, where IFs are aligned both along the axis and also in-plane (Figure 1.3). Until recently, IFs were considered to be the basic structural units of human hair. However, in a recent study, it has been shown that the human hair (cortex) can be further broken down in hierarchical microparticles (HMPs) and hierarchical nanoparticles (HNPs) with diameter of about 100 nm. HMPs and HNPs extracted from keratin did not show any immunogenicity or cytotoxicity. These nanoparticles were able to carry drugs and also help prevent UV-induced skin damage, inhibit tumor growth and also used as remedy for preventing vein thrombosis in mice (Zheng, 2018). Similarly, the matrix region of cortex which was previously considered to be amorphous has also been found to be made of grains having size of about 2–4 nm. The size of the grains was dependent on the chemical treatment of the fibers, temperature, humidity and physiological factors in the follicle (Kadir, 2017).

Using small angle diffraction studies, it has also been confirmed that the cuticle is made up of mostly β-keratins contrary to the earlier assumptions that the cuticle region was mostly made to α-keratins (Stanic, 2015). In the aligned region of the cortex, the isotropic ring at 94 Å becomes anisotropic and two new strong peaks appear at 210 and 111 Å and weaker peaks at 53.5, 46.2 and 31 Å (Figure 1.4), which are due to the closely packed and aligned IFs that are absent in α-keratins. Scanning electron microscopic (SEM) images also confirmed the existence of an intermediate layer with thickness of about 0.5 μm (Stanic, 2015).

A typical X-ray diffraction pattern and the position of the different equatorial and meridian reflections from human hair is shown in Figure 1.5 (Rafik, 2004). The position and structural characteristics of IFs are reported to vary between different hard keratins and also for α and β-keratins.

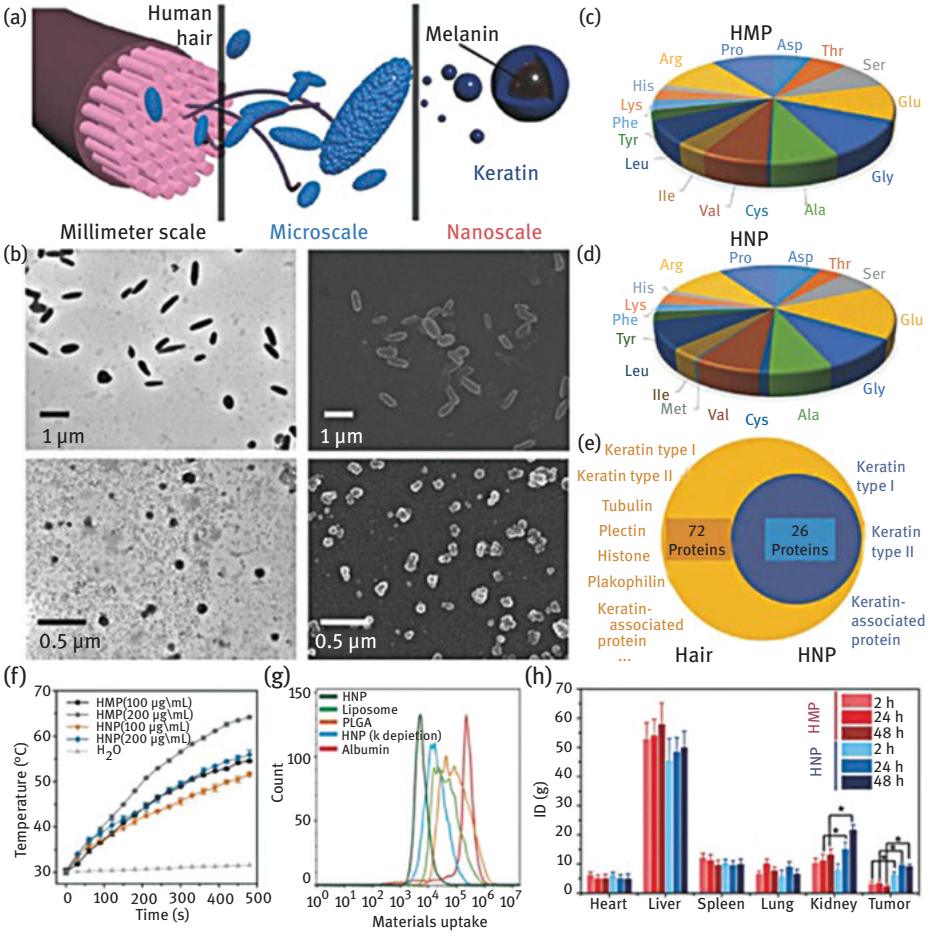

Figure 1.3: Detailed investigations on the structure and applications of nanoparticles and microparticles from the cortex cells in human hair. Hierarchical structural arrangement in human hair (a), TEM and SEM images of micro- and nanoparticles (b), amino acids in microparticles (c) and nanoparticles (d), human hair and HNP (e), photochemical conversion of HMP (e) and HNP (f), cellular uptake of the nanoparticles by the macrophage cells (g) and in vivo distribution of micro- and nanoparticles in tumors in mice (h) (Zheng, 2018). Reproduced with permission from John Wiley and Sons.

Classification of keratins gets updated when new keratins are discovered or new information is obtained on the structure and properties of already existing keratins. Based on latest analysis, the new nomenclature of the human keratins is shown in Table 1.3. The type of keratin and amount of each type of keratin vary between different tissues and cells in the body. For instance, basal cell layers in

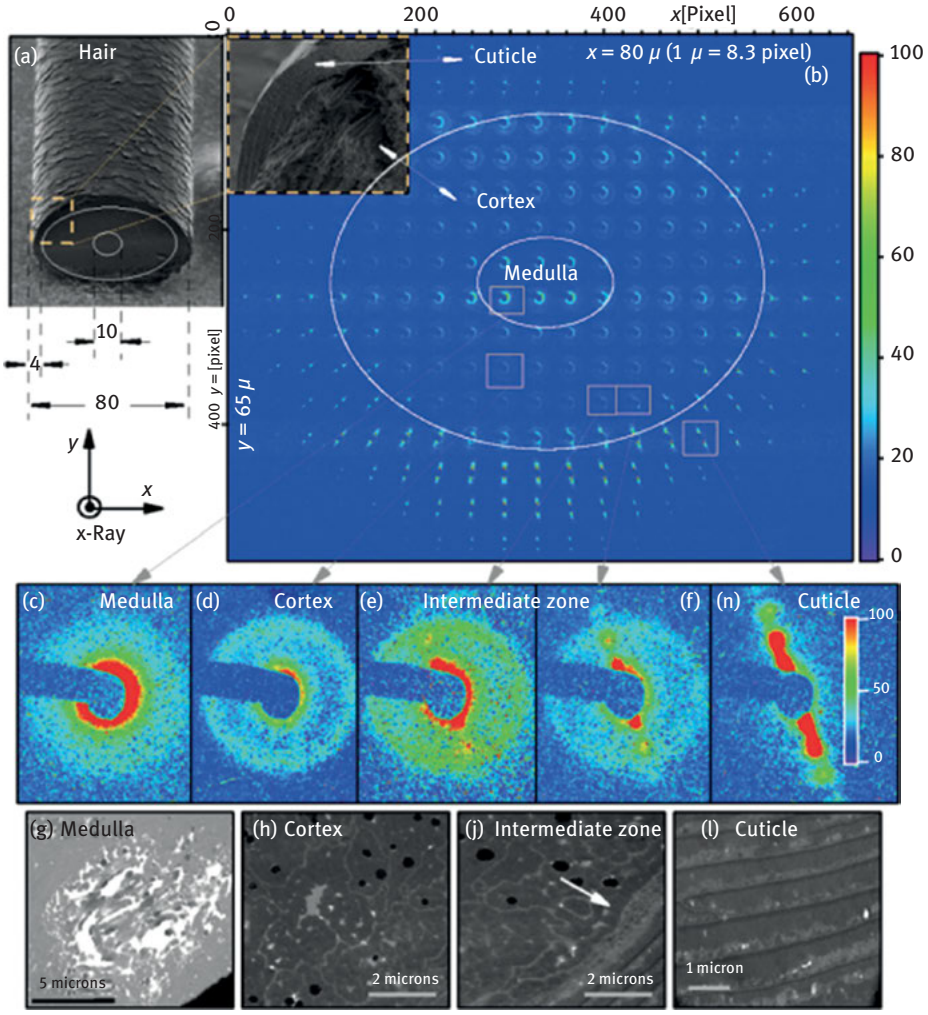

Figure 1.4: SEM image of a human hair (a), SAXS map of human hair (b), SAXS images of the different regions of the hair (c, d, e, f and n) and corresponding SEM images of the regions (g, h, j and l) (Stanic, 2015). Reproduced with permission through Open Access publishing.

normal stratified squamous epithelia contain K5 keratins whereas the suprabasal component contains K10 keratins (Figure 1.6). Even in a single hair or hair follicle, the distribution of the various types of keratin varies significantly and distinctly (Figure 1.7) (Moll, 2008). Similarly, the amino acid composition of hair fibers varies from the cortex to the cuticle (Table 1.4).

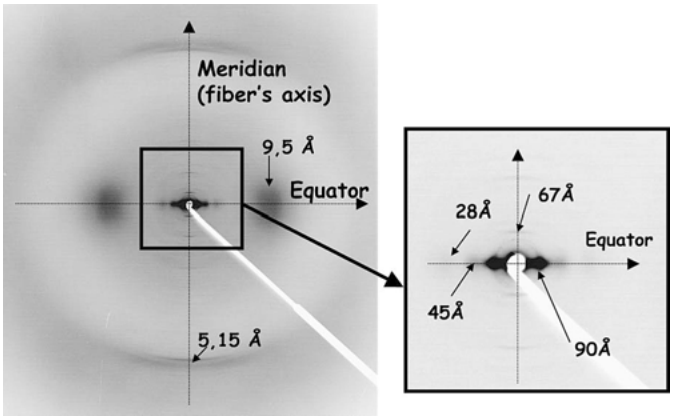

Figure 1.5: Typical X-ray diffraction pattern of human hair keratin with equatorial and meridian lattice positions (Rafik, 2004). Reproduced with open archive publishing from Elsevier.

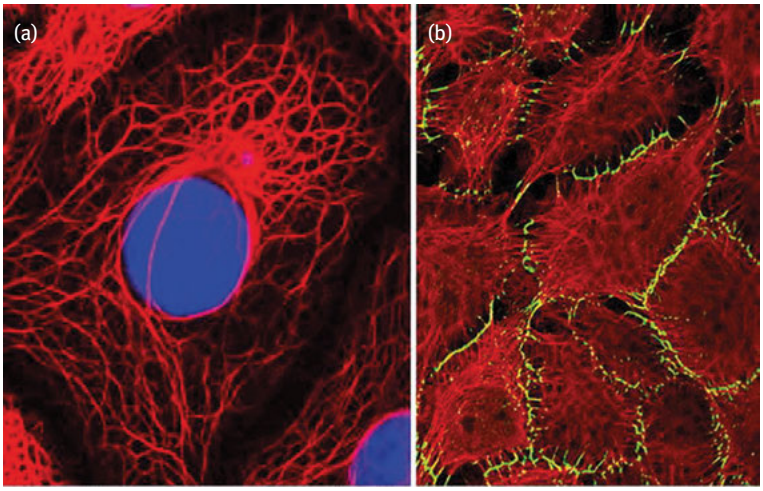

Figure 1.6: Immunofluorescence images of epithelial cells show keratin fibers in red, nuclei in blue and the desmosomal components in green. Reproduced with permission from Springer (Moll, 2008).

1.3 Wool keratin

Compared to feathers, properties of keratin from wool and animal hoofs have been studied to a relatively lesser extent. Detailed characterization of the structure and composition of wool and hoof keratin was done by Zoccola et. al. (Zoccola, 2008). Up to 50% keratin could be extracted from wool but the yield from horn hoof was only 10%. Glutamine, arginine and cysteine were the major amino acids in both

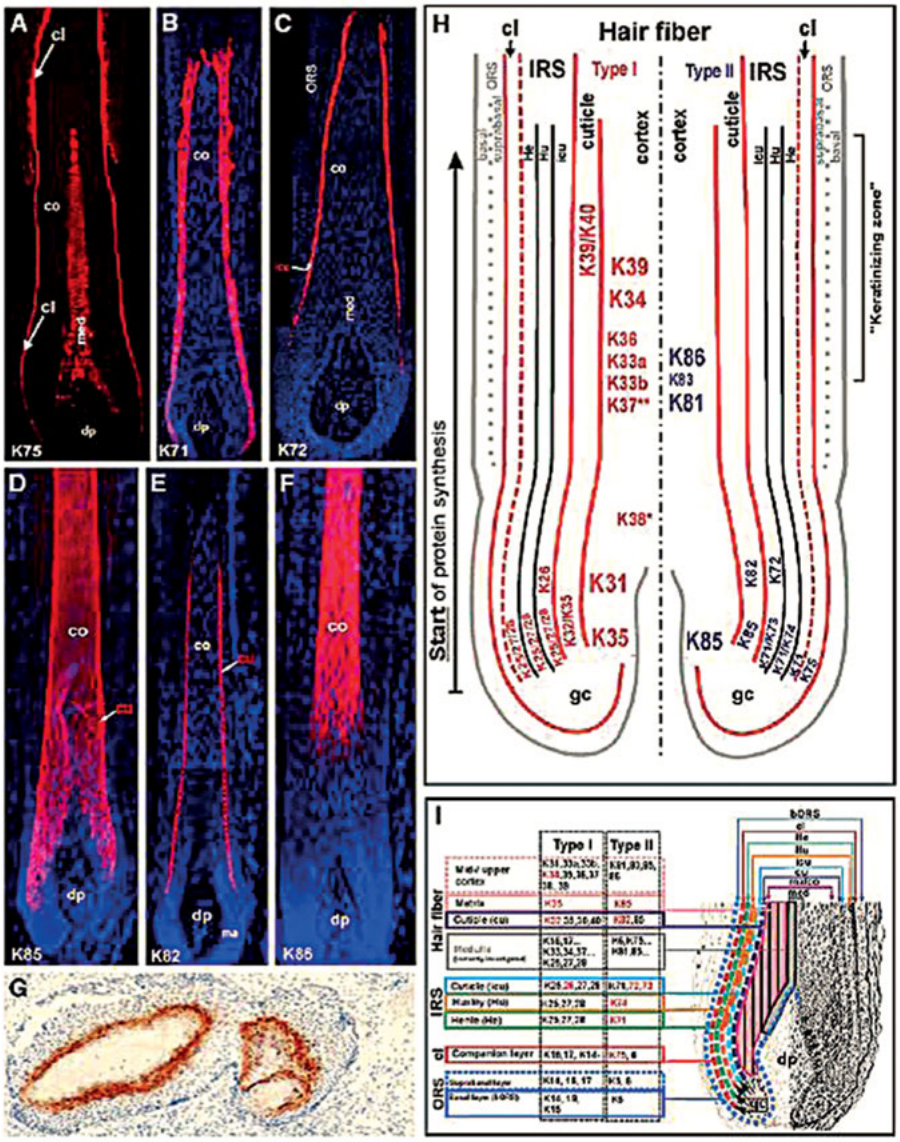

Figure 1.7: Distribution of various keratins in hair and hair follicle. Reproduced with permission from Springer (Moll, 2008).

sources of keratin. However, wool contained a higher level of high-sulfur proteins whereas hooves had glycine and tyrosine that are generally found in cell structures. In terms of structure, higher levels of α-helices and higher levels of crystallinity were found in hoof than in wool. Molecular weights of keratin extracted from wool

Table 1.4: Amino acid composition (μmol/g) of whole human hair and the cortex and cuticle (Popescu, 2007).

Amino acid	Whole hair	Cortex	Cuticle
Cysteic acid	32	27	59
Aspartic acid	399	416	300
Threonine	554	580	412
Serine	967	850	1,628
Glutamic acid/glutamine	916	930	848
Proline	588	532	900
Glycine	437	368	836
Alanine	347	370	500
Valine	405	374	644
Half-cystine	1,435	1,350	1,880
Methionine	13	9	39
Isoleucine	174	172	186
Leucine	457	466	404
Tyrosine	158	162	134
Phenylalanine	124	126	115
Lysine	196	172	331
Histidine	62	65	53
Arginine	466	496	289

Note: Reproduced with permission from Royal Society of Chemistry.

and hoof were mostly between 45 and 60 kDa but some fractions with molecular weight between 11 and 25 kDa were also observed.

In fibrous keratins such as that found in wool, the morphological structure can be classified as macrofibrils, microfibrils and protofibrils in particular hierarchical order (Figures 1.8 and 1.9). Keratin in the protofibrils are entangled in coiled-coil form and linked to the microfibrils which join the macrofibrils inter and intra molecular points through hydrogen, ionic and disulfide linkages (Figure 1.10). These bonds not only provide stability but also determine the processability and potential applications of

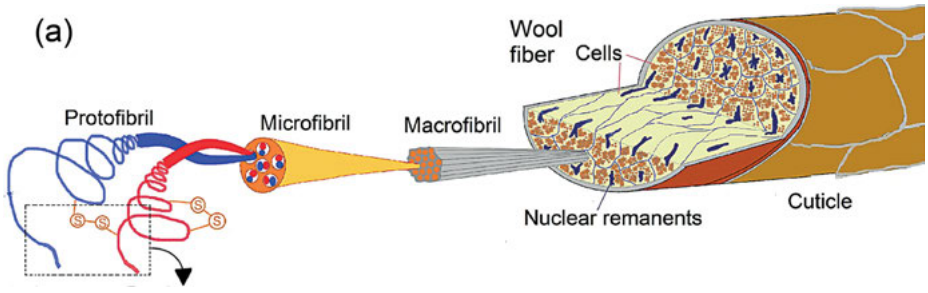

Figure 1.8: Hierarchical arrangement of the fibrils in wool fibers (Fernández-d'Arlas, 2019). Reproduced with permission through Open Access publishing.

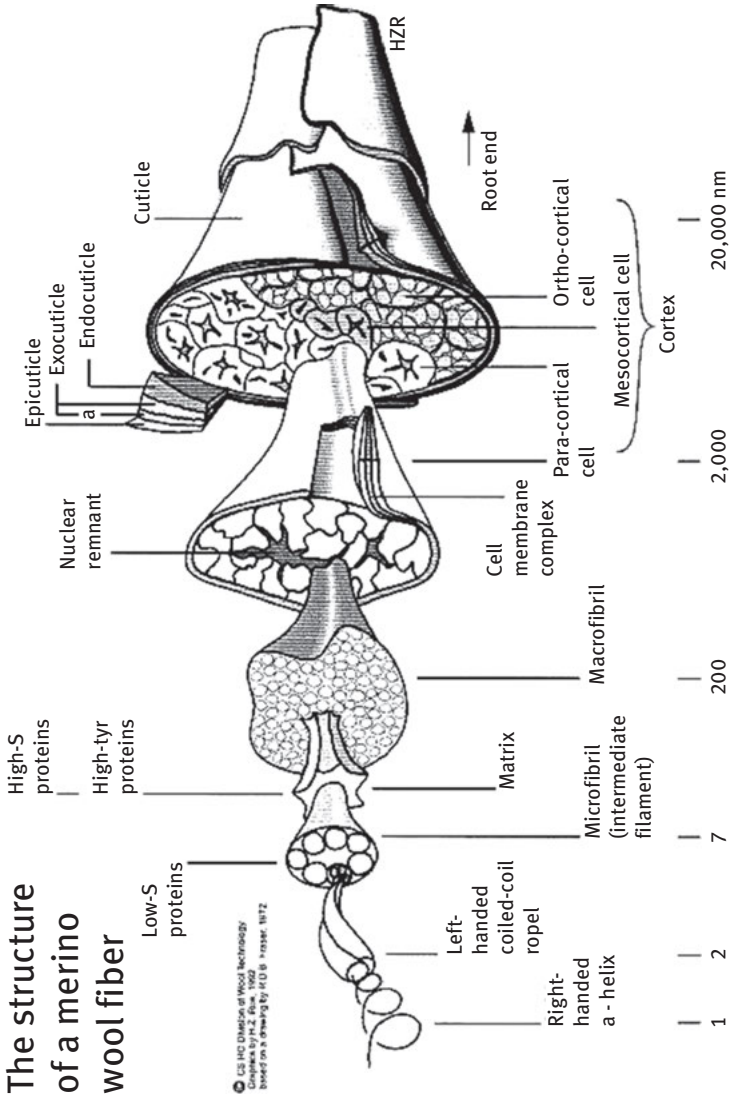

Figure 1.9: Hierarchical arrangement of the structure of wool fibers (Feughelman, 2002). Reproduced with permission from John Wiley and Sons.

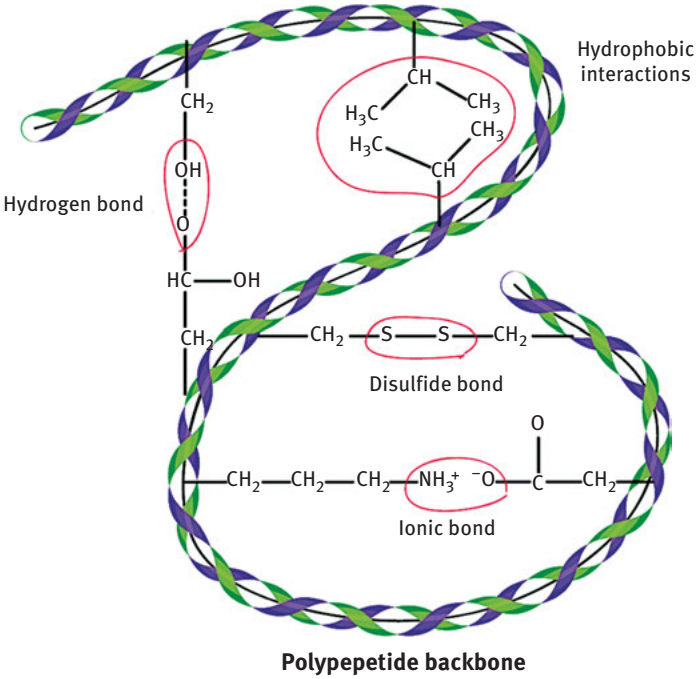

Figure 1.10: Schematic representation of the possible bonds between keratin molecules (Shavandi, 2017). Reproduced with permission from Royal Society of Chemistry.

keratin (Shavandi, 2017; Fernández-d'Arlas, 2019). Further, wool is predominantly composed of α-keratins, which are in turn made up of keratin intermediate filaments. These filaments are embedded in a matrix made of proteins which are called keratin-associated proteins (KAPs). Three types of KAPs are differentiated based on their cysteine content. High sulfur KAPs having less than 30 mol% of cysteine, ultrahigh sulfur proteins KAPs with more than 30% cysteine and HGT containing KAPs with 35–60 mol% of glycine and tyrosine (Gong, 2019). KAPs and IFs are suggested to be linked through disulfide bonds. The KAPs are supposed to play a crucial role in determining the characteristics of wool fibers. HGT-KAPs were found to vary between different traits of sheep and contributed to the variations in the characteristic of the fibers obtained from these sheep (Gong, 2019).

Keratin fibers not only differ in structure and properties but also in morphology. Wool fibers have distinct scales but the size and shape vary between and within species. For instance, considerable variations were observed (Figure 1.11) in the structure of the scales on Alpaca, rabbit, Mohair and merino wool (Thomas, 2012). Diameters of the wool fibers from the different animals varied from 10 to 45 μm with larger fiber diameters also being the straighter ones. Differences were also observed in the amino acid content and profile which would also lead to variations in the properties of the

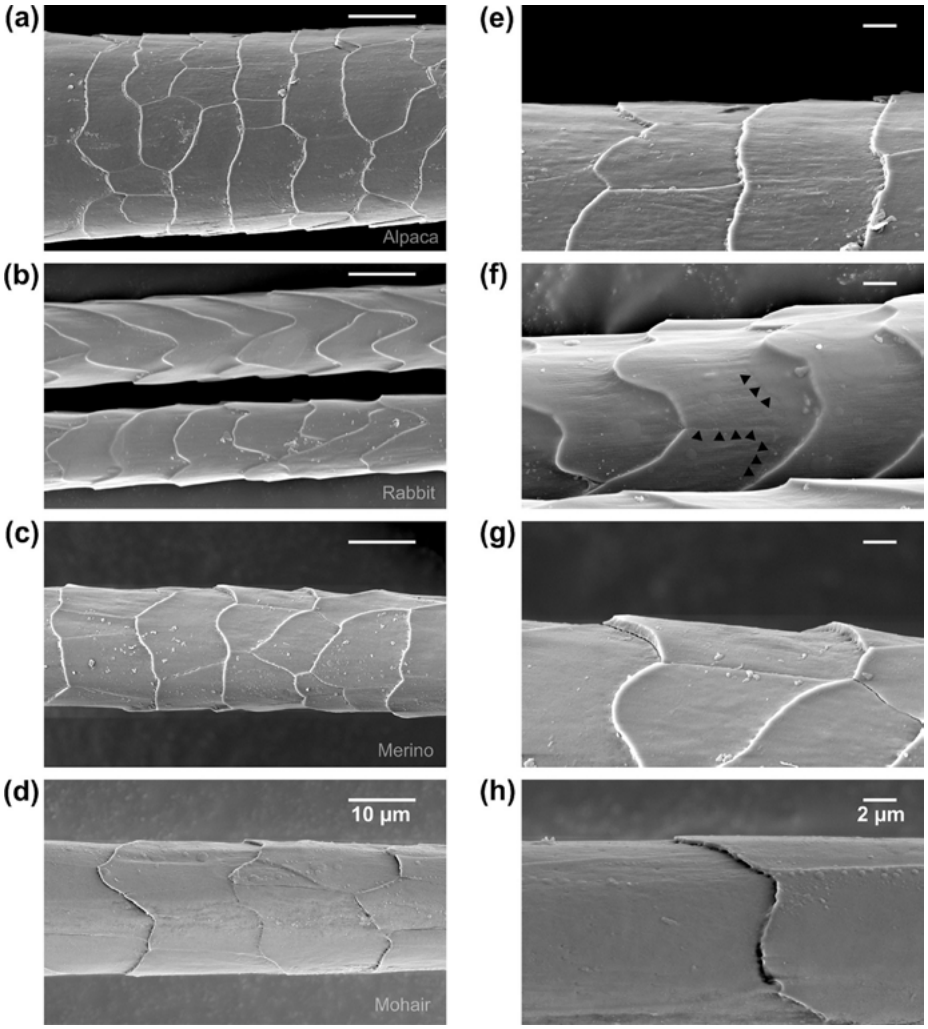

Figure 1.11: Images show the surface morphology and different patterns on the cuticle of alpaca (a and e), rabbit (b and f), merino (c and g) and mohair (d and h) (Thomas, 2012). Reproduced with permission from American Chemical Society.

fibers (Thomas, 2012). A summary of the comparison of the properties of the keratin fibers from different sources is given in Figure 1.12. The shape of hair being either straight or curved is also related to the type and extent of keratin cells in the hair. In straight hair, the cells were arranged annularly along the fiber axis compared to bilateral distribution perpendicular to the fiber axis in curved fibers (Bryson, 2009). Further investigations have shown that the IFs are arranged helically and have a three-dimensional orientation with the helix angle increasing (up to 30°) from the

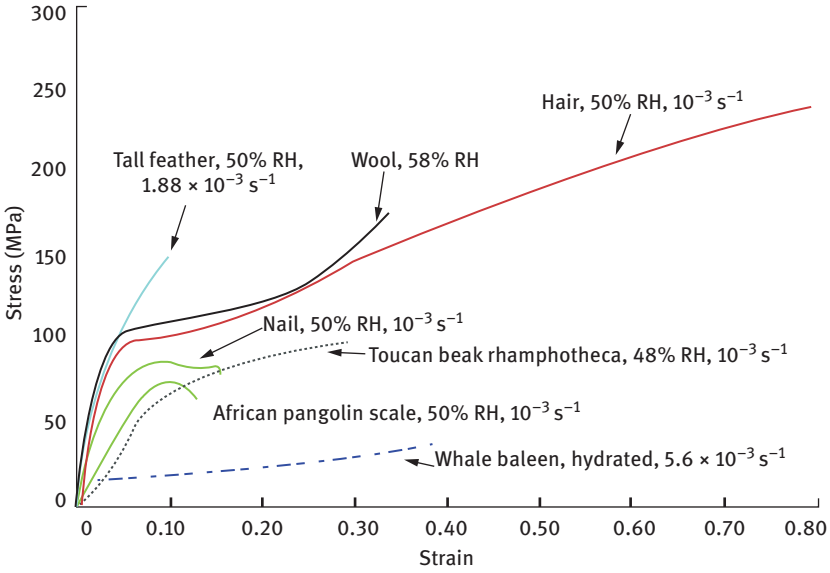

Figure 1.12: Comparison of the properties of the keratin fibers from different sources (Thomas, 2012). Reproduced with permission from American Chemical Society.

center to the outside (Harland, 2019; Caldwell, 2005) with such curvatures suggested to be responsible for the twists in the fibers. Further, the macrofibrils in mammalian cortical cells have been reported to have left handed turns. Similarly, the IFs in the three cortices were found to be predominantly arranged in left-handed concentric helices with the helix angle increasing from center to the periphery of the cortex. Length of each helical path was about 1 μm and the tilt angle of each IF being about 30°. Among the three layers, IFs have a highly ordered arrangement in the mesocortex but considerable variations occur depending on the type of cortex cell and/or extent of crimp in the fibers (Figure 1.13) (Harland, 2011). A report by Deb-Chaudhary indicates that most characteristics of wool fibers are dependent on IFs and the chemical bonds between them and the surrounding matrices made of KAPs (Deb-Chaudhary, 2015). Further, IFs are made up of eight tetramers which further consist of a pair of heterodimers arranged antiparallely and with a slight incline. Unlike IFs, the KAPs are highly disorganized and lack proper secondary structure. Disulfide bridging between and among IFs and KAPs are supposed to occur. It was found that the cysteine residues were involved in forming interdisulfide linkages with keratins and other KAPs. Several peptides were arranged in rod shapes and some of the cysteine residues were exposed on the surface and emerged from the head and tail domains of keratin proteins leading to protein–protein interactions (Deb-Chaudhary, 2015). A schematic representation of the possible interactions between IFs and KAFs through disulfide bonds is shown in Figure 1.14. Extent and

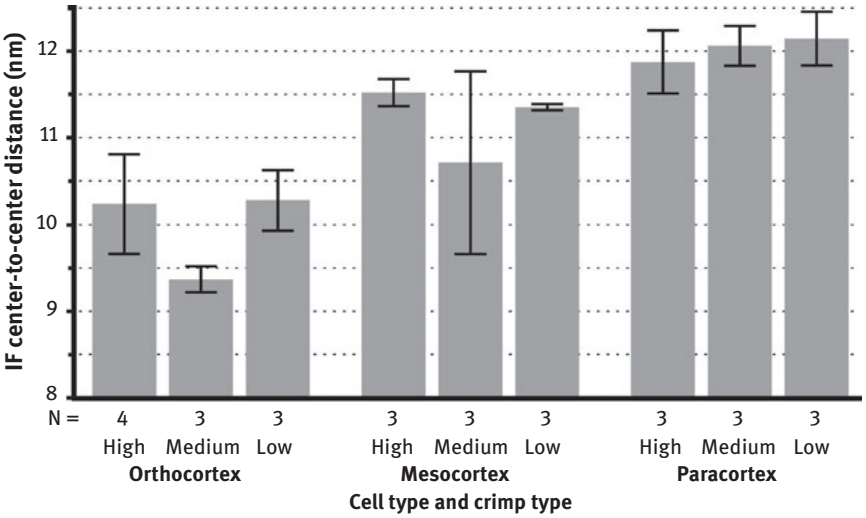

Figure 1.13: Variations in the distance between IFs based on the type of cell and extent of crimp (high, medium and low) (Harland, 2011). Reproduced with permission from Elsevier.

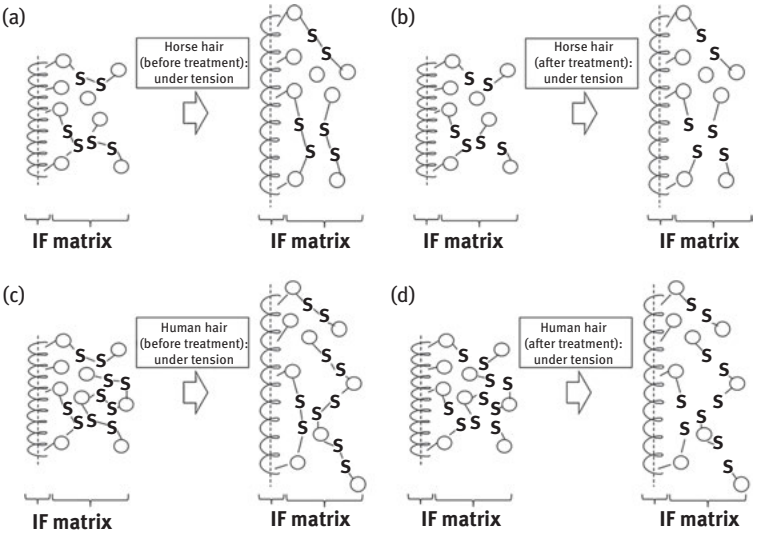

Figure 1.14: Schematic representation of the changes in IFs, matrix and disulfide bonds before and after treatment and with and without any tension (a–d) (Yu, 2017b). Reproduced with permission from Elsevier.

type of bonding is influenced by chemical and physical treatments and responsible for the variations in behavior and properties of hair fibers under different external stimulations (Yu, 2017b). For instance, the elastic modulus of keratin fibers from different animals was dependent on the fiber diameter with increasing diameter decreasing the modulus (Figure 1.15).

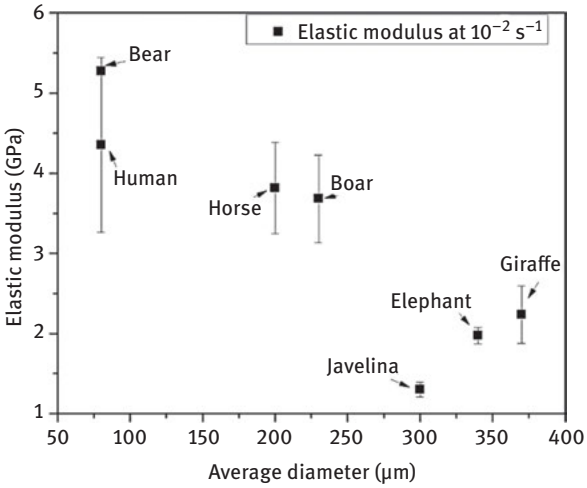

Figure 1.15: Variations in the elastic modulus of hair fibers as a function of fiber diameter (Yu, 2017b). Reproduced with permission from Elsevier.

1.4 Keratins in horns

Keratins in horns and hoofs have different composition (Table 1.5) structure and functionality since horns are subject to extensive impact during interspecific fights when they have to absorb considerable amount of energy. Since horns are made of dead keratin cells which cannot self-heal, the horns are susceptible to mechanical damage. However, studies have shown that keratin in horns have a unique recovery and remodeling mechanism that enables the horns to sustain injuries and retain considerably high strength (Huang, 2019). The hierarchical arrangement contributing to the structure of horn is shown in Figure 1.16. In horns, keratin cells are between 20 and30 μm in diameter and 1–2 μm in thickness and arranged layer by layer. Further, it was found that the cytoskeleton of the cells had macrofibrils of approximately 200 nm in diameter and composed of crystalline IFs of 7–10 nm placed in an amorphous matrix forming a polymer/polymer composite. Structurally, the proteins are made of keratin polypeptide chains having a helical secondary protein structure with α-helices which combine to form the coiled-coil structures seen in the IFs. These IFs were arranged in different orientations (longitudinal, transverse and radial) that provide

Table 1.5: Amino acid content in wool and horn–hoof (Zoccola, 2009).

Amino acid	Wool (%)	Horn–Hoof (%)
Cysteic acid	0.2	0
Aspartic acid	7.0	8.7
Serine	8.5	7.2
Glutamic acid	13.8	16.3
Glycine	4.6	4.0
Histidine	1.3	1.3
Arginine	10.2	10.8
Threonine	6.0	5.1
Alanine	3.3	3.7
Proline	5.7	4.4
Cysteine	10.8	7.1
Tyrosine	5.9	4.5
Valine	5.1	5.3
Methionine	0.6	1.0
Lysine	3.0	4.6
Isoleucine	3.2	4.1
Leucine	7.2	8.7
Phenylalanine	3.6	3.2

Note: Reproduced with permission from Elsevier.

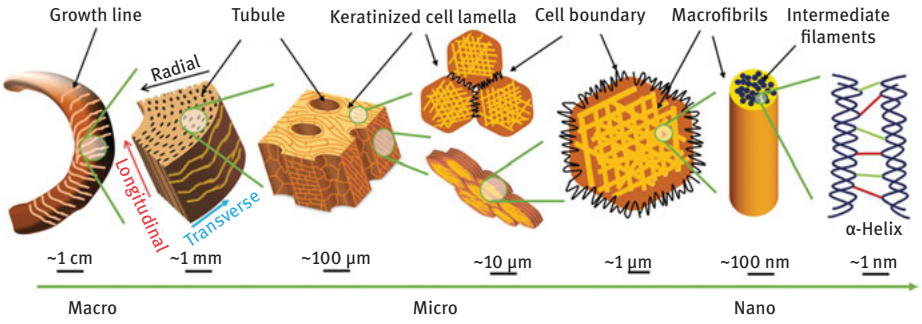

Figure 1.16: Schematic representation of the hierarchical structure of keratin in horns (Huang, 2019). Reproduced with permission from John Wiley and Sons.

resistance to buckling, shear and compressive loadings. In addition to the structural arrangement, mechanical properties of the horn were heavily dependent on the water content. Tensile strength was highest in the dry condition but elongation was higher when the horns were hydrated (Figure 1.17). Fully hydrated samples also had lower modulus and energy absorption capability due to increased mobility of polymer chains (Huang, 2019). However, water was found to only affect the amorphous keratin whereas hydrogen bonds between carbonyl group and amino groups were

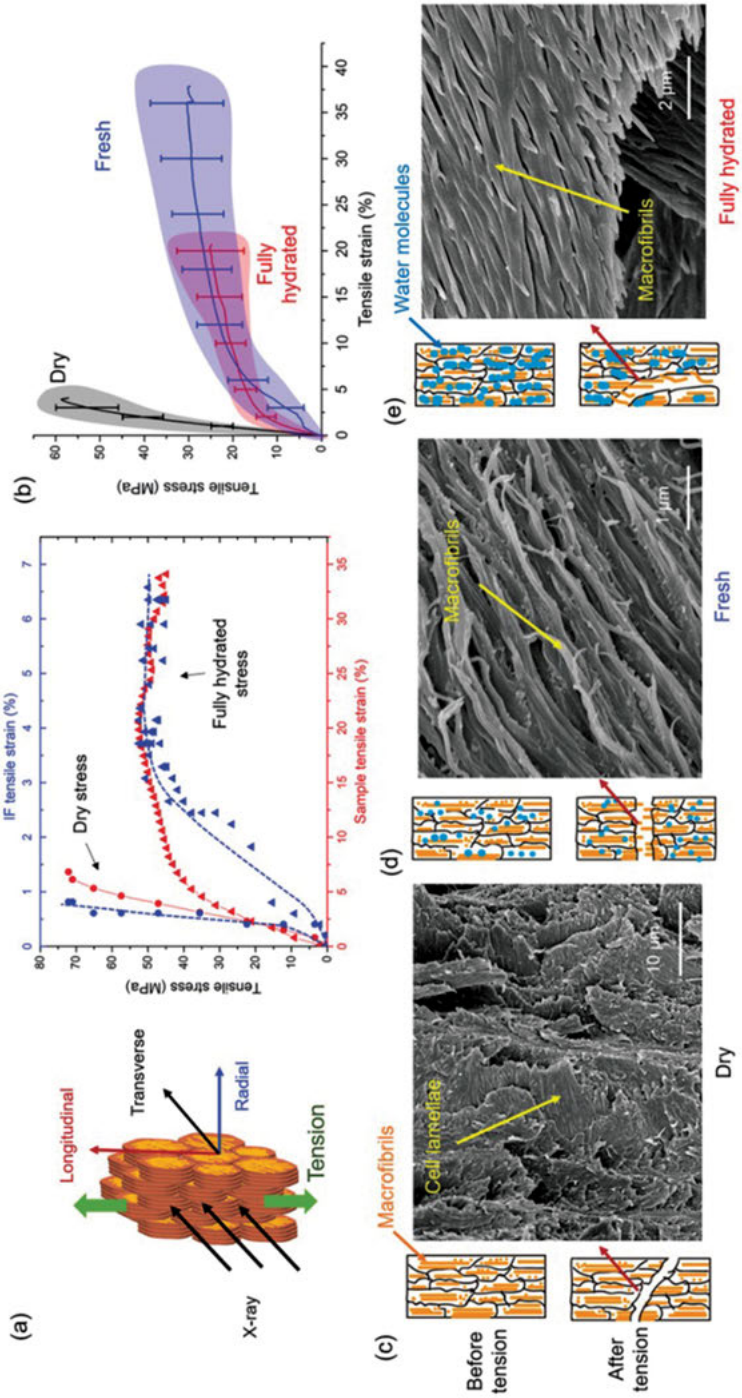

Figure 1.17: Mechanical properties of horn keratin when subjected to ex situ (a) and in situ (b) tensile tests under dry and wet conditions (Huang, 2019). Reproduced with permission from John Wiley and Sons.

broken but the crystalline regions remain unaffected. The keratin structure could be recovered even after 50% compression but only in the radial direction but damage to the structure of keratin in the longitudinal and transverse direction was not recoverable. It was found that the presence of tubules in the keratin cells were responsible for the recoverability of radially stressed horn keratin.

1.5 Keratin in marine animals

Unlike keratin found in animals mostly living on land, substantial changes have been noticed in the structure, properties and functions of keratins found in marine animals. To elucidate such differences, a comparison of the properties of keratin obtained from human hairs and water fowl feathers was made by (Tsuda and Nomura, 2014). Keratin was obtained by hydrolyzing the feather or hairs by treating with NaOH at 120 °C for 10 min. Amino acid analysis (Table 1.6) showed that the feather keratin had considerably higher amounts of glycine and proline whereas the keratin from the water fowl feathers had distinctly high amounts of glutamic acid, lysine and cysteine. High levels of glycine and proline in the feathers suggested elevated levels of β-sheet content.

Table 1.6: Comparison of the amino acid composition (residues/100 residues) of hydrolyzed keratins obtained from human hair and water fowl feathers (Tsuda, 2014).

Amino acid	Hair keratin	Water fowl keratin
Aspartic acid	8.0 ± 0.8	6.9 ± 0.1
Glutamic acid	9.4 ± 0.2	13.7 ± 0.2
Serine	10.8 ± 0.3	13.5 ± 0.1
Threonine	1.7 ± 0.1	8.8 ± 0.1
Tyrosine	2.3 ± 0.3	2.1 ± 0.2
Lysine	0.4 ± 0.2	2.8 ± 0.1
Arginine	2.9 ± 0.1	5.6 ± 0.1
Histidine	0.2 ± 0.0	0.8 ± 0.0
Glycine	18.1 ± 1.5	10.7 ± 0.1
Half-cystine	1.3 ± 0.1	4.4 ± 0.4
Cysteic acid	0.6 ± 0.0	0.9 ± 0.1
Methionine	1.3 ± 0.1	1.2 ± 0.1
Alanine	7.1 ± 0.2	6.3 ± 0.1
Valine	8.4 ± 0.2	5.3 ± 0.1
Proline	12.7 ± 0.3	7.2 ± 0.2
Isoleucine	3.7 ± 0.1	2.6 ± 0.1
Leucine	8.3 ± 0.5	7.7 ± 0.0
Phenylalanine	2.7 ± 0.2	1.7 ± 0.0

Note: Reproduced with permission from John Wiley and Sons.

Keratin found in mammals such as whales are never dried (are always in contact with water) and hence need to have specific structure and functions (Szewciw, 2010). Keratin plates in whales are called baleens which are mostly made up of the hard α-keratins and are embedded in intertubular horns (Figure 1.18). Bristles of baleens are highly calcified but the extent of calcification varies between different species (4% to 1%). Such calcification is not found in nonmammalian keratins and is suggested to be responsible for the properties, particularly strength and modulus. As given in Table 1.7, amount of calcium, phosphorus and sulfur varies considerably between the three species of whales and is generally higher than that found in wool. Presence of higher calcium influences tensile properties (Table 1.7) and compensates the lack of hardening and curing seen in α-keratins found in nonaquatic species (Szewciw, 2010).

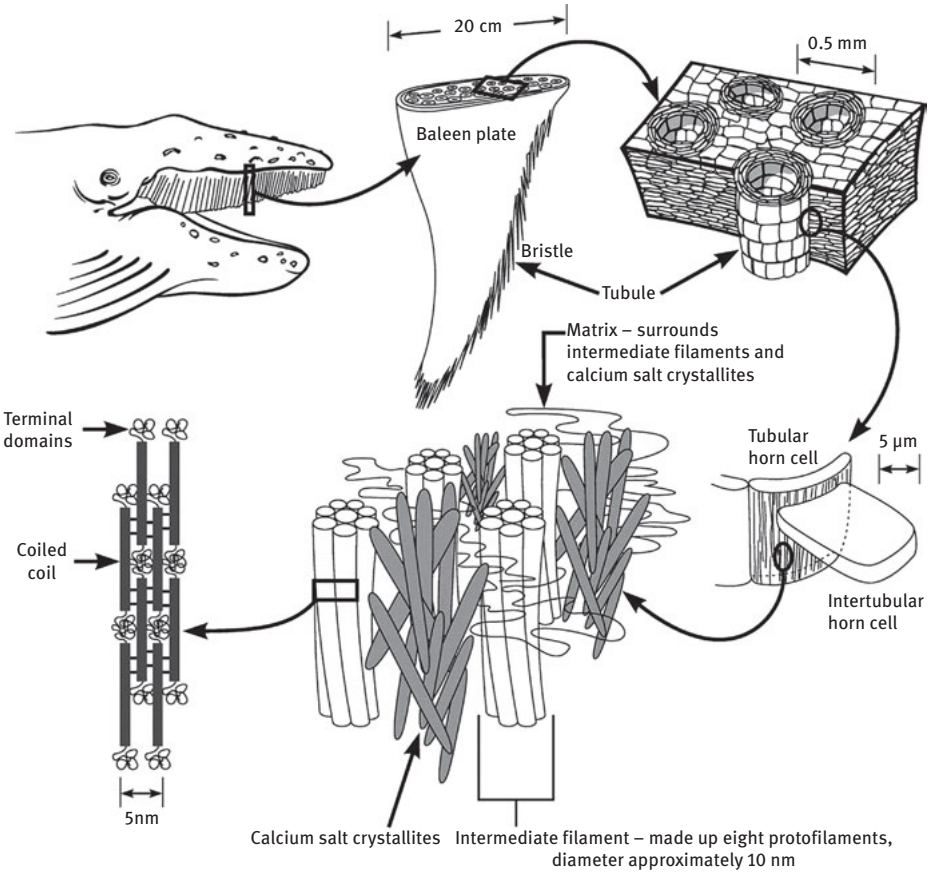

Figure 1.18: Schematic representations of the baleen plates and bristles seen in humpback whales and the hierarchical nature of the keratin in bristles and suggested arrangement of calcified material (Szewciw, 2010). Reproduced with permission from Royal Society of Chemistry.

Table 1.7: Composition and tensile properties of baleen bristles in three different species of whales in comparison to wool fibers before and after decalcification (Szewciw, 2010).

Source	Calcium (μg/g)	Phosphorus (μg/g)	Sulfur (μg/g)	Modulus (MPa)	Yield stress (MPa)	Yield strain (%)	Breaking stress (MPa)	Breaking strain (%)
Wool	2,800	150	31,000	1,216	24	0.028	110	0.50
D-wool	32	120	32,000	1,269	24	0.024	118	0.50
Sei	41,000	18,000	23,000	1,188	11	0.012	30	0.35
D-Sei	180	390	28,000	637	6.7	0.014	18	0.52
Humpback	7,900	2,900	39,000	1,225	15	0.015	36	0.53
D-Humpback	670	780	34,000	971	11	0.013	33	0.47
Minke	2,500	1,400	27,000	652	7.1	0.014	27	0.47
D-Minke	21	260	27,000	636	7.2	0.014	26	0.49

Note: Reproduced with permission from Royal Society of Chemistry.

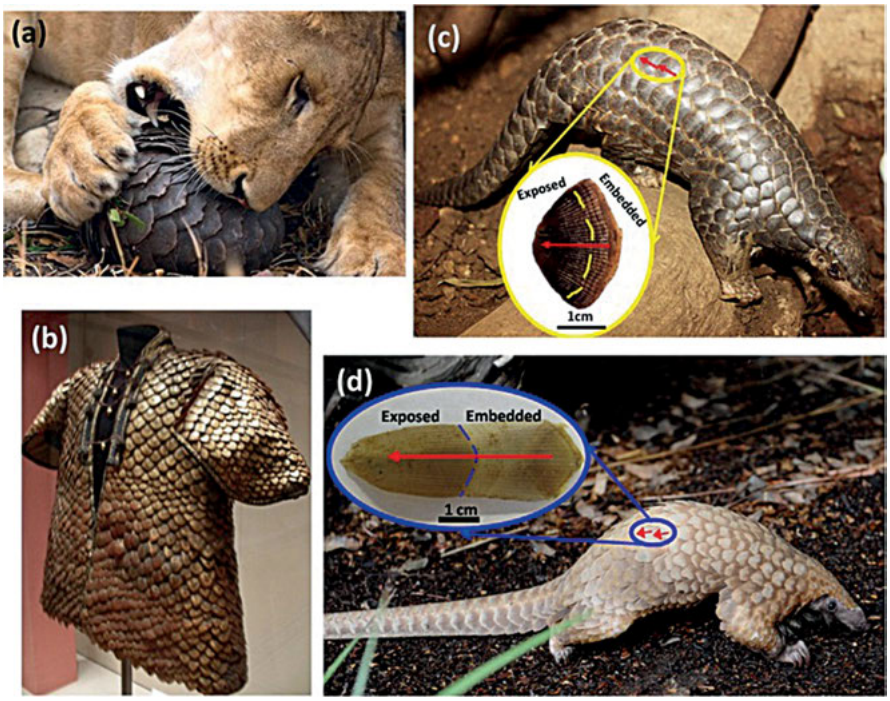

Figure 1.19: Digital images of a pangolin scale resisting attack (a), armor made of pangolin scales (b), African (c) and Chinese pangolin (d). Reproduced with permission from Elsevier.

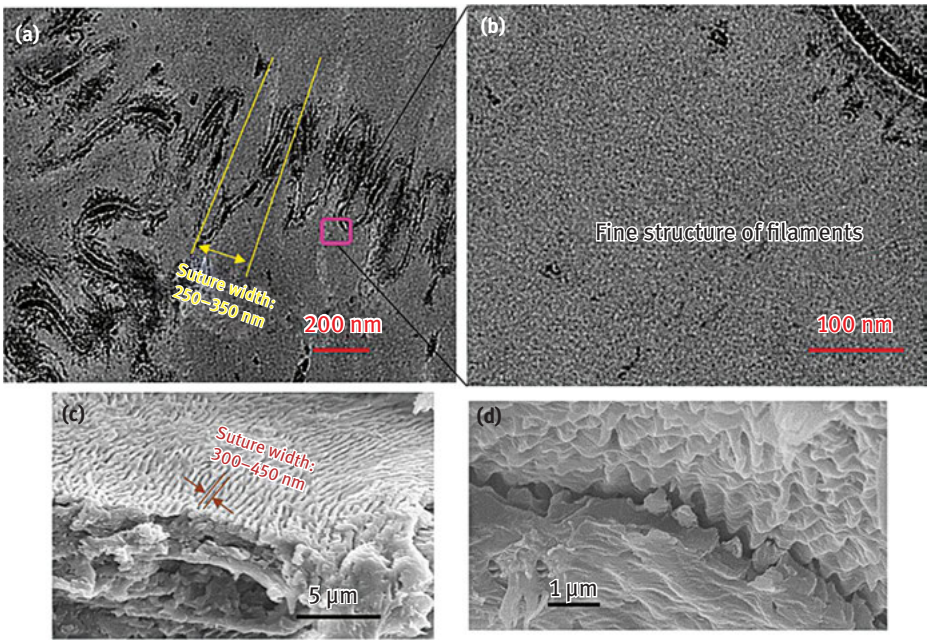

Figure 1.20: TEM (a and b) and SEM (c and d) images of pangolin scales demonstrates the fine structure (Wang, 2016). Reproduced with permission from Elsevier.

Table 1.8: Tensile properties of pangolin scales made of keratin tested in longitudinal and transverse directions (Wang, 2016).

		Strain rate per sec	Young's modulus (GPa)	Tensile strength (MPa)	Breaking strain (%)	Work of rupture (MJ/m^2)
African	Longitudinal	10^{-5}	1.1 ± 0.3	65.5 ± 6.7	16.8 ± 5.5	8.3 ± 3.3
		10^{-4}	1.1 ± 0.2	71.5 ± 6.6	10.6 ± 2.7	4.9 ± 1.5
		10^{-3}	1.0 ± 0.1	72.4 ± 6.9	12.9 ± 0.3	6.5 ± 0.6
		10^{-2}	1.1 ± 0.1	84.7 ± 9.8	12.6 ± 0.8	7.2 ± 0.7
		10^{-1}	1.5 ± 0.2	109 ± 6.0	12.0 ± 3.6	8.4 ± 3.3
	Transverse	10^{-3}	1.2 ± 0.2	74.2 ± 5.1	8.4 ± 1.4	3.6 ± 0.9
Chinese	Longitudinal	10^{-5}	0.9 ± 0.1	60.4 ± 9.0	11.4 ± 3.8	4.8 ± 2.9
		10^{-4}	1.0 ± 0.1	60.5 ± 6.5	12.0 ± 3.1	4.7 ± 1.8
		10^{-3}	1.0 ± 0.2	66.4 ± 2.7	8.0 ± 1.4	2.7 ± 0.5
		10^{-2}	1.0 ± 0.1	70.8 ± 10.9	8.7 ± 0.7	3.4 ± 0.4
		10^{-1}	1.2 ± 0.1	74.2 ± 2.3	6.8 ± 0.1	2.5 ± 0.1
	Transverse	10^{-3}	1.1 ± 0.1	61.6 ± 2.8	6.1 ± 0.9	2.0 ± 0.5

Note: Reproduced with permission from Elsevier.

1.6 Keratin in pangolin scales

One of the toughest keratin structures able to resist even bites by lions (Figure 1.19) is reported to be found in the scales of the armor of the mammal pangolin (Wang, 2016). Scales in Chinese and African pangolins were found to be arranged in overlapping structure in a hexagonal pattern. Three distinct layers (crossed-lamellar structure, crossed fibers and a nanoscale suture structure) were discovered. The suture structure connects the cell membranes and lamellae providing high bonding and shear resistance. Mechanical properties of the scales varied between different areas of the scales and also depending on the region (Chinese/Africa). Transmission electron microscopic (TEM) and SEM images (Figure 1.20) showed the suture like cell membranes (25–50 nm) that interlock the lamellae and filaments of 3–5 nm in diameter. Some of the tensile properties of the scales from two pangolins in two different testing orientations are given in Table 1.8. It was reported that the modulus, strength and ability to absorb energy at low strain rates were different compared to other keratinous materials but similar to that of hair keratin. However, the properties were considerably affected by water with Young's modulus decreasing from 0.27 GPa to 34 MPa upon hydration (Wang, 2016).

Chapter 2
Extraction of keratin

Keratin has been obtained from various sources using a variety of techniques, chemicals, processing conditions and equipments. A schematic of the possible ways to extract keratin is shown in Figure 2.1 (Shavandi, 2017). A comparative study was done to understand the influence of various extraction conditions on the properties of keratin obtained from wool. Merino wool was subject to either alkali hydrolysis, sulfitolysis, reduction, oxidation or extraction using ionic liquids (Shavandi, 2016). Highest protein yield of 95% was obtained through ionic liquid treatment followed by sulfitolysis (89%). However, proteins with highest molecular weights (>40 kDa) were obtained using oxidation whereas alkali hydrolysis caused significant damage resulting in proteins with molecular weight of less than 10 kDa. Extraction conditions also affected the viscosity but did not change the biocompatibility toward fibroblast cells (Shavandi, 2016). A similar study was also done to understand the effect of extraction conditions on properties of keratin obtained from human hair (Agarwal, 2019). Four different chemical approaches (sodium sulfide, peracetic acid, thioglycolic acid and urea treatments) were used to obtain keratin from human hair. Considerable differences were observed in the appearance (Figure 2.2) structure and properties of the keratin obtained from each method. Sodium sulfide (K1) treatment provided a highest yield of protein (5,372 μg/mL) followed by urea (K2: 4,213 μg/mL), thioglycolic acid (K3: 3,844 μg/mL) and peracetic acid (K4: 52 μg/mL). Amount of α-helices and β-sheet plus random coils also varied between 33–57% and 42–57%, respectively. However, no major differences were observed in the lattice spacings but crystallinity index was highest for K1 (0.275), whereas lowest for K2 (0.119). Ability to obtain high yield without affecting the crystallinity makes K1 a preferred treatment for keratin extraction. All four types of keratin were able to support the attachment and growth of mouse osteoblasts indicating suitability for medical applications (Agarwal, 2019).

2.1 Extraction of keratin using alkali with or without reducing agents

Except for wool and hair, it is generally difficult to use keratin in its native form. Typically, keratin is extracted and used for various applications. One of the simplest and conventional means to extract keratin is through alkaline hydrolysis at high temperature. Wool keratin containing about 90% protein was hydrolyzed using 0.15 M potassium hydroxide (KOH) and 0.05 M sodium hydroxide (NaOH) at 120 °C for 20 min for potential use as fertilizer. Up to 100% solubilization (Table 2.1) could be achieved depending on the conditions used (Gousterova, 2003). Although alkali was used, differences in the yield should be due to the conditions used for extraction.

https://doi.org/10.1515/9781501511769-002

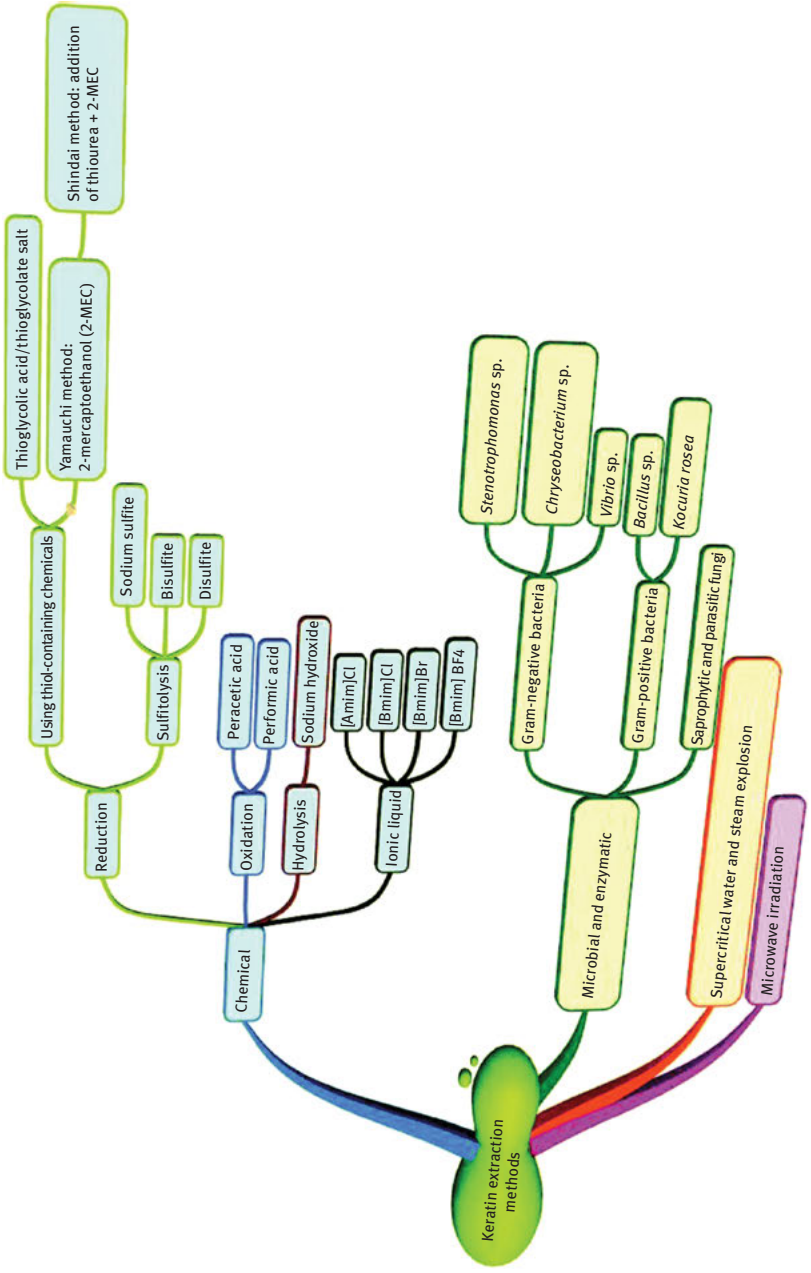

Figure 2.1: Various approaches used to extract keratin (Shavandi, 2017). Reproduced with permission from Royal Society of Chemistry.

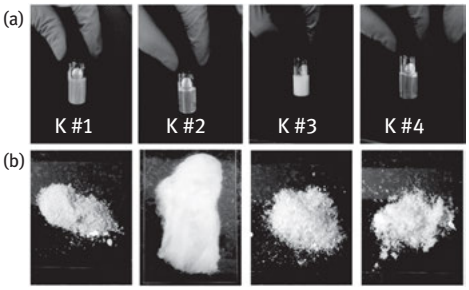

Figure 2.2: Differences in the appearance of keratin in solution (a) and after drying (b) when obtained using four different chemical methods (Agarwal, 2019). Reproduced with permission from Elsevier.

Table 2.1: Yield of keratin and conditions during extraction (Gousterova, 2003).

Wool used (g)	% Solubilized	Nonsoluble residue (g)	% dry matter in solution	pH after hydrolysis	H_3PO_4 required for pH 7 ± 0.1
2.5	100	0.38	4.3	12.9	0.7
5.0	94	0.89	6.5	11.65	0.52
7.5	89	1.54	8.5	10.78	0.5
10.0	82	3.01	10.0	10.56	0.43
12.5	75	4.5	11.2	10.38	0.45
15.0	65	7.15	11.5	10.26	0.41
17.5	57	10.71	11.7	10.23	0.37
20.0	44	15.21	10.6	10.07	0.32

Note: Reproduced with permission from Taylor and Francis.

Keratin has also been obtained from feathers using alkali in the presence of reducing agents. In one such attempt, keratin was extracted from feathers using sodium metabisulfite as the reducing agent in the presence of urea and SDS at 65 °C. Molecular weight of the extracted keratin varied from 10 to 75 kDa depending on the extraction conditions used (Gousterova, 2003).

The effect of reduction and alkali hydrolysis on the structure and composition of wool fibers was investigated in detail. For reduction hydrolysis, wool fibers were treated with 6 M urea, 3 mM ethylenediaminetetraacetic acid (EDTA), 1.4 M 2-mercaptoethanol, 0.1 N NaOH at pH 9.1 for 4 h between 62 and 65 °C. For the alkali hydrolysis, wool fibers were treated with 0.5 N NaOH at pH 13.9 for 3 h at 62–65 °C. A sample of fine wool powder treated in deionized water was used as control (Cardamone, 2010). Sodium dodecyl sulfate-polyacrylamide gel electrophoresis analysis showed that the mercaptoethanol reduced samples had moderate decrease in molecular weight whereas alkali treated samples had complete reduction in the molecular weight. The peptides obtained after the reduction hydrolysis were further separated and homologs

were extracted for Matrix Assisted Laser Desorption/Ionization-Time of Flight (MALDI-TOF) analysis (Cardamone, 2010). Considerable changes were seen between the native keratin in wool and the homologs and alkali extracted wool keratin. In terms of structural changes, the amide I region showed molecular conformation with the reduction hydrolyzed samples having variations in the –OH, –NH and –CO stretching region whereas the alkali hydrolyzed keratin exhibited ionic character due to the formation of sulfoxides. Fourier transform infrared (FTIR) absorption spectra in the amide regions showed that the samples obtained by reduction hydrolysis had higher amide I and amide II content, whereas the α-helix content was lower (Cardamone, 2010). The extraction methods were considered to provide keratin similar to that in native wool and therefore suitable to develop various products with good properties.

Different parts of chicken feathers were used to extract keratin using sodium sulfide and L-cysteine (Pourjavaheri, 2019). Barbs, barbules, rachis or whole feather were immersed in 1:20 ratio of solution containing 0.5 mol/L of sodium sulfide and 8 mol/L urea and 0.165 mol/L of L-cysteine at pH 10.5. Solutions were heated at 40 °C for 6 h and the precipitate obtained as keratin was collected. Treating with reducing agents caused the disulfide bonds in the feathers to be broken down into free thiol and amine groups which get protonated making the keratin soluble. Addition of urea was also done to increase swelling and hence solubility. A yield of 88% keratin was obtained when sodium sulfide was used compared to 66% for L-cysteine. However, no differences in molecular weights (11 kg/mol) were observed between the keratin obtained from the two approaches and the proteins were considered to be relatively pure with a molecular weight of about 11 kg/mol (Pourjavaheri, 2019). In another study, keratin was extracted from wool using L-cysteine as the reducing agent and the properties of the extracted keratin were studied (Wang, 2016c). In this approach, 5 g of wool fibers were treated with 100 mL of 8 M urea solution and 0.165 M L-cysteine (reducing agent) at pH 10.5 for 5 h at 75 °C. Later, dialysis was done against a molecular weight cut off of 8,000–14,000 Da and keratin obtained was freeze dried to form powder for further analysis. Extraction with cysteine resulted in the formation of keratin with molecular weight of 40 to 55 kDa, similar to that of native wool suggesting that no significant degradation occurred during the process of extraction (Figure 2.3) (Wang, 2016c). Compared to dissolution using other reducing agents (Figure 2.4), using L-cysteine resulted in a much higher solubility of 70%. Cleavage of the disufide bonds by L-cysteine (62% lower S–S linkages) resulted in lower thermal resistance and higher amounts of β-sheet structure as observed in other reports (Wang, 2016c). FTIR studies showed that the use of L-cysteine did not affect the peptide bonds but there was minor destabilization of the α-helix structure (Figure 2.5).

Bovine hoofs were pulverized and treated with hexane and dichloromethane to remove oil and other substances. Later, the powdered hoofs were subject to a reduction process (Figure 2.6) and the extracted keratin was used in solution form or lyophilized to form powder (Kakkar, 2014). Keratin extraction was optimum when the

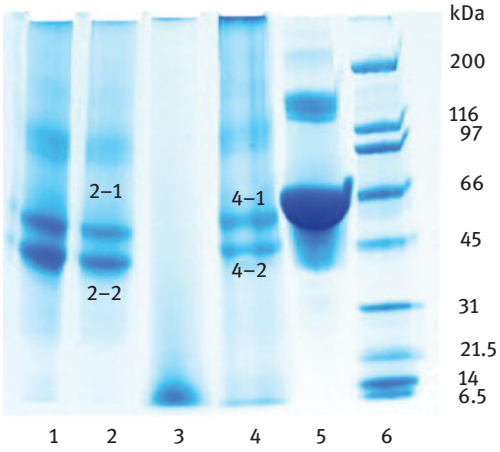

Figure 2.3: SDS PAGE electrophoresis of keratin samples obtained by mercaptoethanol reduction (lanes 1 and 2), alkaline hydrolysis (lane 3), finely pulverized wool powder (lane 4), BSA in lane 5 and molecular markers in lane 6 (Wang, 2016c). Reproduced with permission from Royal Society of Chemistry.

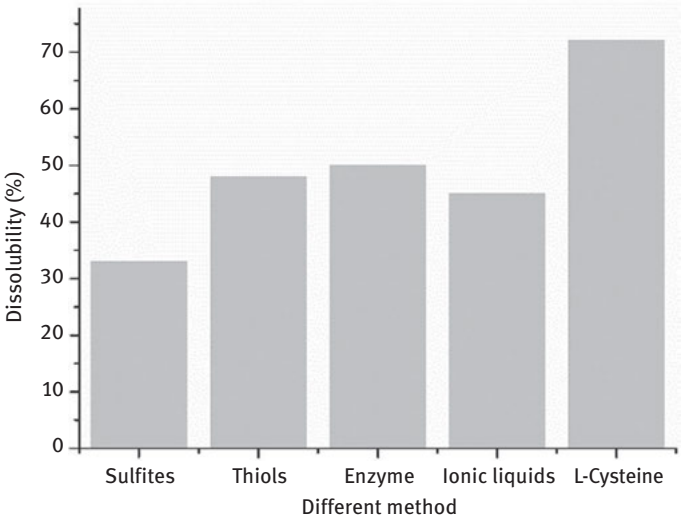

Figure 2.4: Solubility of wool in solutions containing various reducing agents. Reproduced with permission from Royal Society of Chemistry (Wang, 2016c).

pH was between 6 and 8, whereas higher alkaline conditions resulted in hydrolysis. About 44% of the initial weight of the hooves was extracted as keratin with a purity of about 80%. Molecular weight of the keratin was between 45–50 and 55–60 kDa

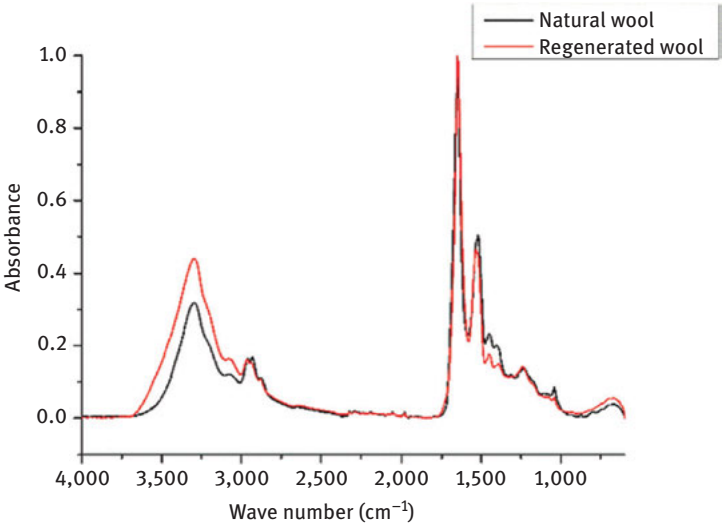

Figure 2.5: Comparison of the FTIR spectrums of raw and regenerated wool keratin. Reproduced with permission from Royal Society of Chemistry (Wang, 2016c).

(Kakkar, 2014). Addition of keratin into 3T3 fibroblast cell solutions (up to 50 μg/mL) did not cause adverse reactions and no decrease in cell viability was noticed (Figure 2.7). Therefore, the hoof keratin was considered to be biocompatible and suitable for medical applications (Kakkar, 2014).

2.2 Ionic liquids for keratin extraction

A series of ionic liquids have been used as green solvents to extract keratin from wool and other protein sources. Two ionic liquids [AMIM] + .Cl^- and [BMIM] + .Cl^- were used to dissolve wool and generate regenerated keratin films (Li, 2013). [AMIM] + .Cl^- was found to have better solubility for wool keratin due to its cationic structure. However, the time required for solubilization was also dependent on the concentration of wool keratin in the solution (Table 2.2). Both FTIR and X-ray diffraction studies indicated that the α-helix structure was destroyed during dissolution which led to increase in the β-sheet content. Substantial changes in the morphology of the keratin fibers occurred before complete dissolution. An initial swelling of the fibers followed by disruption of the cuticle and final disintegration into solution could be clearly observed (Figure 2.8) (Plowman, 2014). After dissolution, the films precipitated using methanol provided higher crystallinity compared to those made using ethanol or water. Complete removal of scales on the surface of the fibers and decrease in thermal stability were negative aspects of the ionic method of

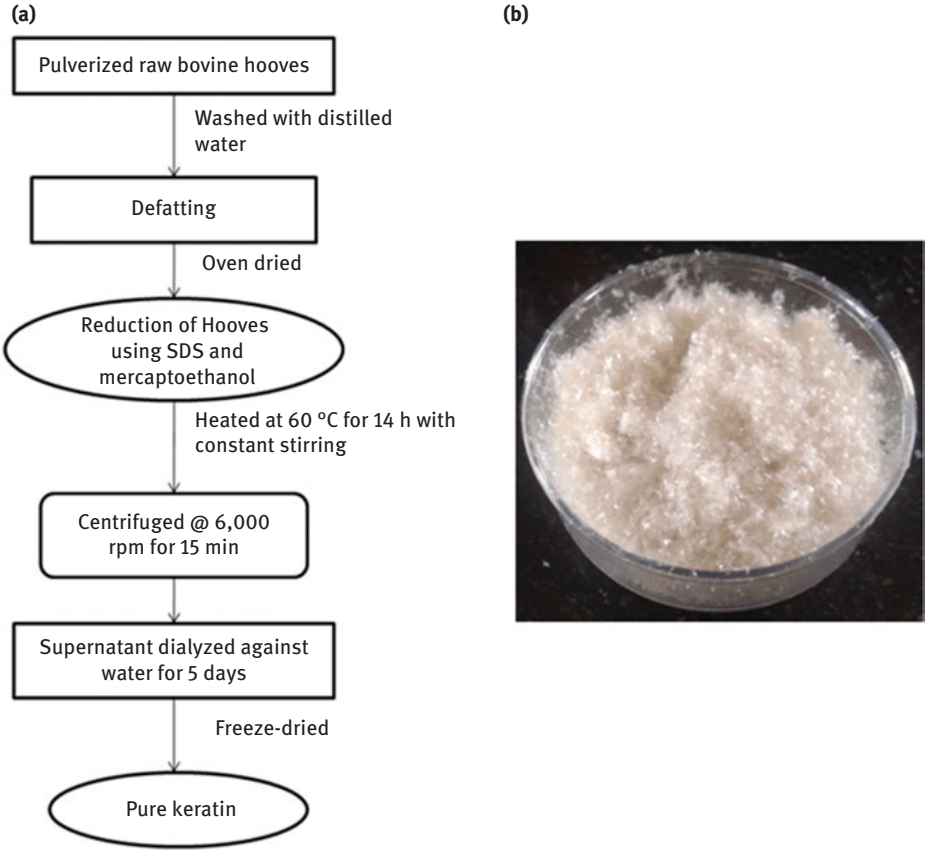

Figure 2.6: Process of extracting keratin from bovine hoofs (a) and a powdered sample of the extracted hoof (b) (Kakkar, 2014). Reproduced with permission from Springer.

dissolution. In addition, the properties of the films obtained using the ionic dissolution were not reported (Plowman, 2014). Ability of [BMIM] + .Cl^- to dissolve wool and cellulose was exploited to develop wool–cellulose blend fibers and films (membranes) (Xie, 2005). Extent of dissolution of wool in the ionic liquid was greatly influenced by the time and temperature and the type of ions in the liquid (Table 2.2).

Although dissolution with ionic liquids requires high temperatures and longer time and the amount of wool that can be dissolved is low, it was shown that ionic liquids in combination with the conventional urea/thiourea extraction (Figure 2.9) of keratin could isolate previously unknown types of keratin peptides (Plowman, 2014). Using a combination of the solvent systems resulted in detection of additional number of keratins. Ionic liquids extracted higher number of lower molecular weight keratins, whereas urea/thiourea system extracted larger number of higher molecular weight peptides (Plowman, 2014). The number of unique keratins extracted

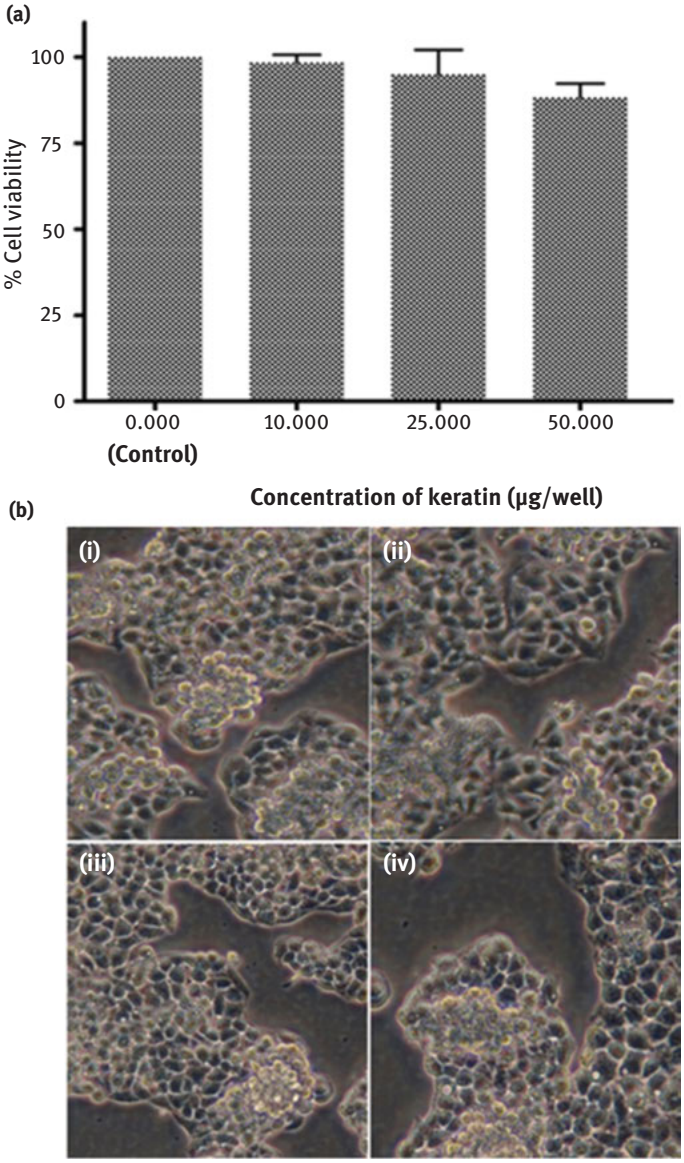

Figure 2.7: Cell culture studies (MTT assay) did not show any decrease in cell viability due to the addition of keratin up to 50 µg/well. Cell morphologies were similar for the control (i) and cell solutions containing 10 µg/well (ii), 25 µg/well and 50 µg/well. Reproduced with permission from Springer (Kakkar, 2014).

Table 2.2: Ionic liquids and conditions required to dissolve wool keratin (Xie, 2005).

Ionic liquids	Temperature (°C)	Time (h)	Solubility (%)
$BMIM^+Cl^-$	100	10	4
	130	10	11
$BMIM^+Br^-$	130	10	2
$AMIM^+Cl^-$	130	10	8
$BMIM^+BF4^-$	130	24	Insoluble
$BMIM^+PF6^-$	130	24	Insoluble

Note: Reproduced with permission from Royal Society of Chemistry.

from the combination system was 9 compared to 15 for the urea/thiourea system and up to 54 keratins were extracted by using both the solvents. It was proposed that the combined extraction system could be used to obtain unique peptides for further understanding of the structure and properties of keratin (Plowman, 2014).

Dissolution of keratin in the ionic liquids was dependent not only on the type of ionic liquid (anionic or cationic) but also on the dissolution time (10–900 min (Zheng, 2015). Generally, anionic liquids provided better dissolution than cationic liquids. Regenerated keratin had a rough and amorphous appearance (Figure 2.10**)** and considerable damage to the crystal structure had occurred as evident from the relatively low degree of crystallinity. Thermal stability of the keratin had also decreased due to the ionic treatment (Zheng, 2015). Although the main amide I, II and III structures were similar between the raw and regenerated keratin, minor changes were discovered in the α-helix and β-sheet content (Figure 2.11). Decrease in α-helix content from 83.8 to as low as 45.1 and corresponding increase in β-sheet content from 16.2 to 54.5 were observed when [Bmim]OAc was used as the solvent. Type of ionic liquid played a significant role in determining the extent of α-helix to β-sheet conversion (Table 2.3) (Zheng, 2015). Nevertheless, the simple procedure, recyclability and low cost were considered beneficial for industrial-scale extraction of keratin using ionic liquids (Zheng, 2015).

Apart from the time or the type of ionic liquid, the temperature used for dissolution also had major influence on the properties of keratin and the products developed from the regenerated keratin (Ghosh, 2014). Wool fabrics were dissolved using (1-butyl-3-methylimidazolium chloride) at temperatures between 120 and 180 °C. Considerable differences in amino acids, particularly cysteine content, was observed with increasing temperature during dissolution. Changes in secondary structure were also observed but dissolution at higher temperatures provided keratin with improved thermal processing. Films made from keratin obtained at high temperatures also had better tensile properties compared to keratin obtained at lower temperatures.

Keratin was extracted from chicken feathers using a hydrophobic ionic liquid (1-hydroxyethyl-3-methylimidazolium bis(trifluoromethanesulfonyl)amide ([HOEMIm]

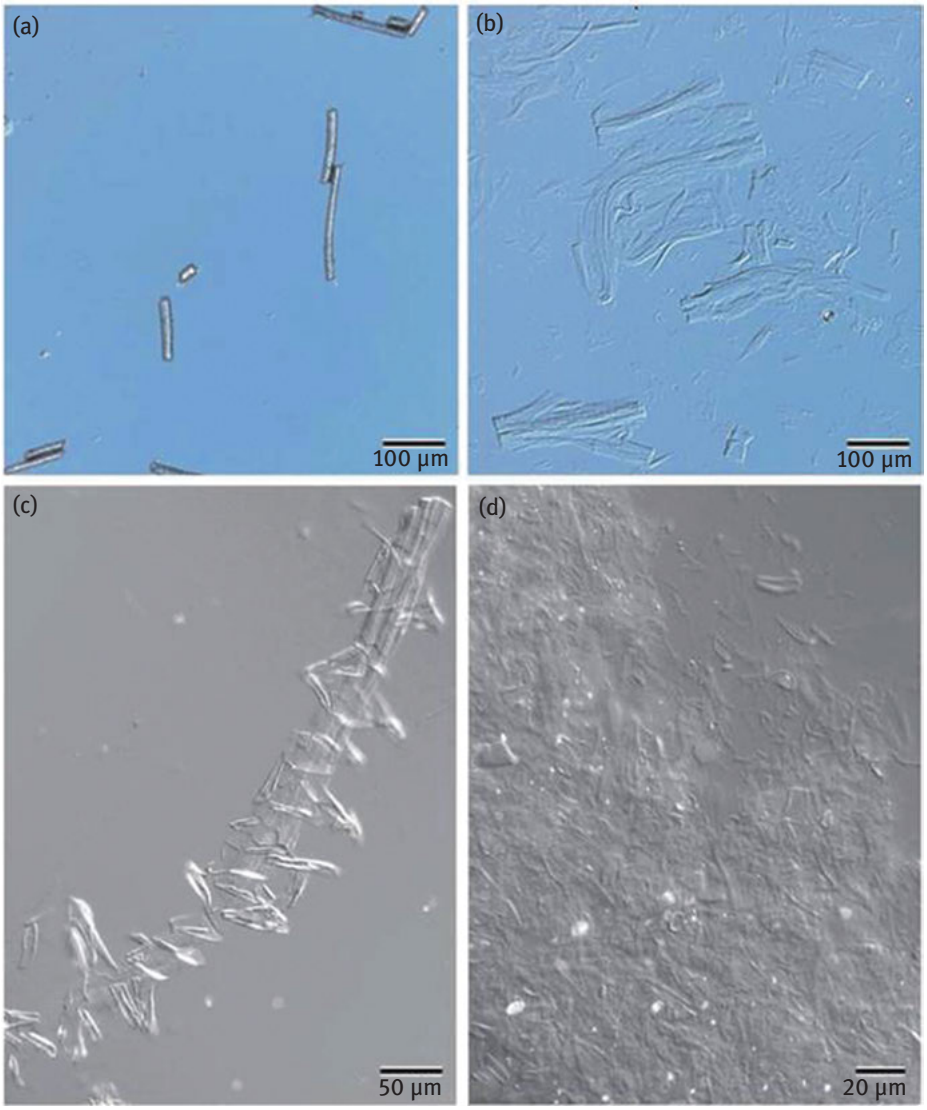

Figure 2.8: Stages in the dissolution of wool using ionic liquid [BMIM] + .Cl^-. Untreated wool fibers (a), swollen wool fragments (b), dissociation of the cuticle cells from fiber fragments (c) and isolated cells and fragments obtained after treating the ionically dissolved keratin with urea/thiourea (d) (Plowman, 2014). Reproduced with permission from Royal Society of Chemistry.

[NTf_2]) and the structure and properties of the extracted keratin were studied (Wang, 2012). To extract the keratin, feathers were immersed in the ionic liquid containing sodium bisulfite at 80 °C for 4 h. About 15–25% of keratin was extracted depending on the time, temperature and ratio of the solvent and reducing agent used. Molecular

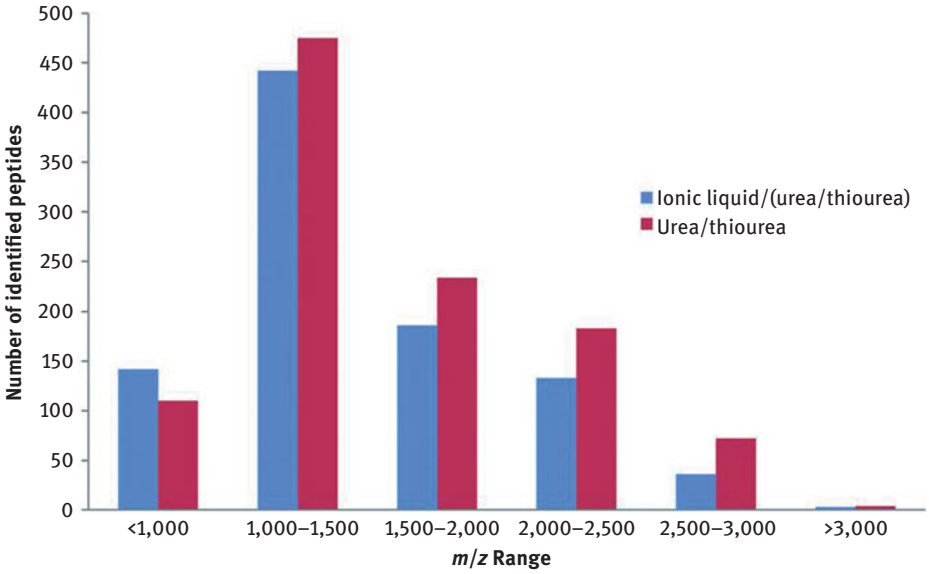

Figure 2.9: Ionic liquids alone were able to extract higher number of lower molecular weight peptides whereas the contrary was true for urea/thiourea system (Plowman, 2014). Reproduced with permission from Royal Society of Chemistry.

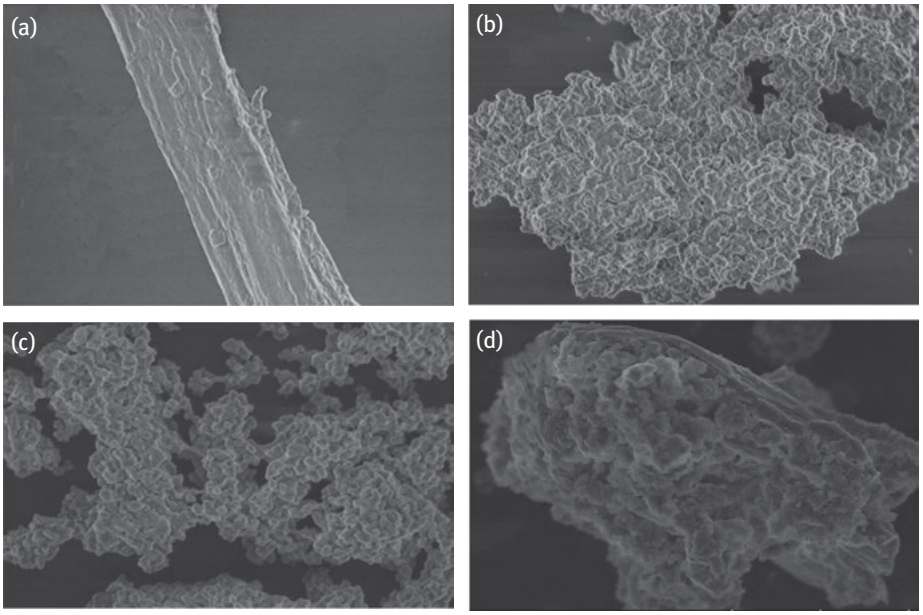

Figure 2.10: SEM images ((a) raw material; regenerated keratin from 8% wool keratin solution of (b) [N2221]DMP; (c) [Bmim]OAc; (d) [Emim]DMP) show the morphological differences after treating with various ionic liquids (Zheng, 2015). Reproduced with permission from American Chemical Society.

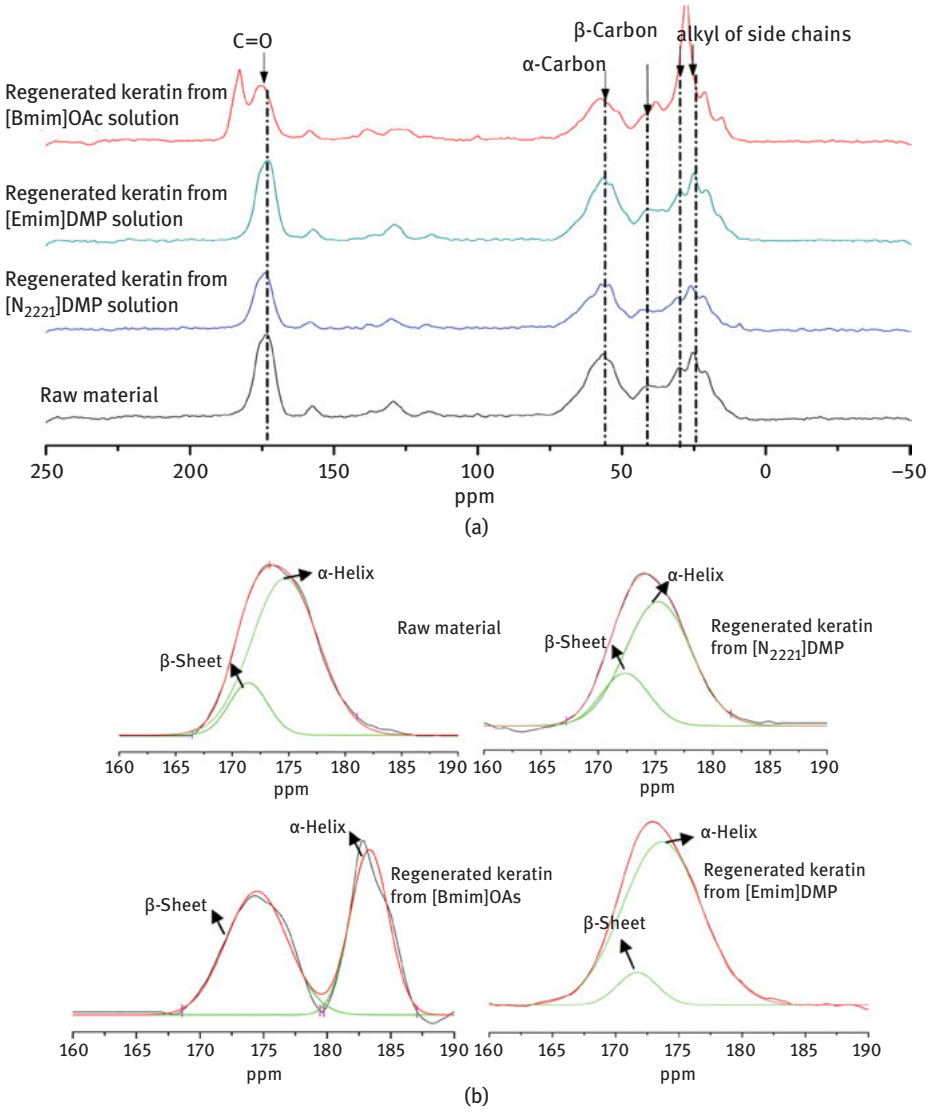

Figure 2.11: Changes in the C=O peaks at 174.7 ppm and 171.4 ppm were used to study the changes in the α-helix and β-sheet content. (a) raw material and regenerated keratin from $[N_{2221}]$DMP, [Bmim]OAc and [Emim]DMP solutions respectively; (b) raw material and regenerated keratin from $[N_{2221}]$DMP, [Bmim]OAc and [Emim]DMP solutions. Reproduced with permission from American Chemical Society (Zheng, 2015).

weight of the keratin extracted was about 10 kDa. Although the ionic liquid used could be collected and reused, the yield and molecular weight of the keratin obtained was considerably low (Wang, 2012). An ionic liquid N-methyl Morpholine N-Oxide (NMMO)

Table 2.3: Ability of various ionic liquids to convert keratin into α-helix or β-sheets (Zheng, 2015).

Peaks	Chemical shift (ppm)	HW (ppm)	Fraction (%)
Raw material			
α-Helix	174.7	5.92	83.8
β-Sheet	171.4	3.38	16.2
Keratin regenerated from $[N_{2221}]$ DMP			
α-Helix	175.4	5.88	78.7
β-Sheet	172.4	3.89	21.3
Keratin regenerated [Bmim]OAc solution			
α-Helix	183.3	3.03	45.5
β-Sheet	175.5	4.84	54.5
Keratin regenerated from [Emim]DMP solution			
α-Helix	173.7	6.26	90.9
β-Sheet	171.7	3.13	9.1

Note: Reproduced with permission from American Chemical Society.

was found to be a strong solvent for chicken feathers to extract keratin. However, about 64% of keratin was degraded into polypeptides with molecular weights of about 2,189 Da compared to 25% keratin that had higher molecular weight of 14,485 Da. A decrease in cysteine content but substantial increase in disulfide bonds was observed. It was proposed that considerable oxidation (Figure 2.12) occurs during the regeneration of feathers into keratin and during drying (Ma, 2017).

Various ionic liquids have also been used to dissolve duck feathers and obtain keratin. The ionic liquids studied were [Amim]Cl, [Bmim]Cl, [Bmim]Br, $[Bmim]NO_3$, $[Hmim]CF_3SO_3$ and $[Bsmim]H_2SO_4$. Dissolution rates of the feathers varied from 5% to 96% with [Amim]Cl providing the highest level of dissolution. (In ionic liquids at 90 °C with 20% feather, complete dissolution of feather was observed.) Scanning electron microscopy images showed severe degradation of the surface after 40 min of treatment. Dissolution rates and yield of keratin was also influenced by the amount of sodium sulfite used as the reducing agent. Complete dissolution of the feathers was achieved in 60 min. Similarly, the temperature and time also changed the amount of keratin extracted. It was suggested that addition of 20% water and 10% of sodium sulfite into the ionic liquids resulted in keratin yield as high as 75% (Ji, 2014). Although high yield of keratin can be obtained using the ionic liquids, the influences of the ionic liquids on the properties of the extracted keratin have to be understood.

Ionic liquids have also been extensively used to extract keratin from unconventional animal sources (Table 2.4) (Shavandi, 2017). Camel hair and cashmere fibers were treated with ionic liquid [BMIM(Cl)] to separate the water soluble and insoluble keratins. Extent of solubility of keratin and primary and secondary structures were affected by the treatment conditions (Yang, 2019). Similarly, amino acid composition

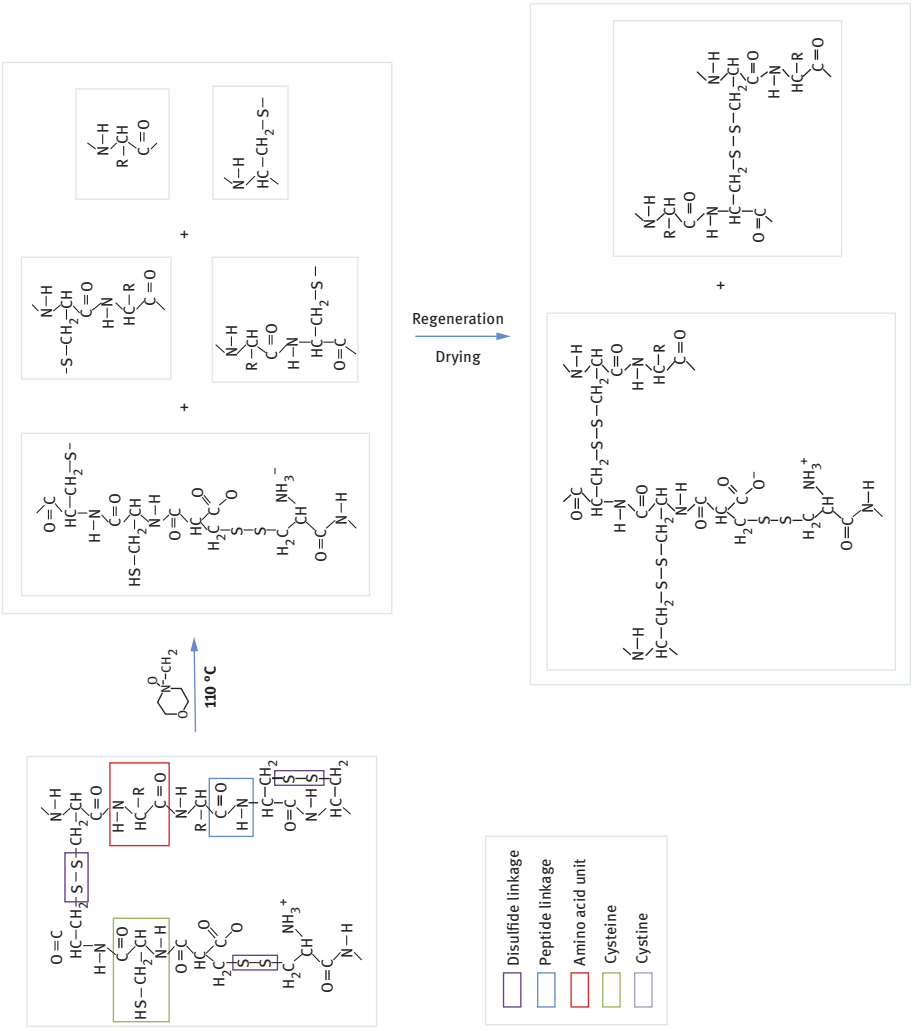

Figure 2.12: Changes in the chemical structure of keratin due to treatment with NMMO (Ma, 2017). Reproduced with permission from Springer Nature.

between the hair and wool fibers and components obtained after treatment were different (Table 2.5). Soluble portion of keratin was used as a replacement for cell culture media without any cytotoxicity to fibroblasts. Ability of various ionic liquids (Figure 2.13) to dissolve goat wool and influence properties of keratin obtained were studied (Liu, 2017). About 8% wool was added into the ionic liquids and heated at 343 K up to 3.5 h for completion dissolution. Keratin yields ranging from 17% to 45% were obtained depending on the specific ionic liquid and treatment time. Crystallinity of the keratin obtained varied from 51% to 62% but the main structure of the keratin was

Table 2.4: Conditions used to extract keratin from various sources using ionic liquids (Shavandi, 2017).

Material	Ionic liquids and additives	Conditions				Yield of keratin
		Temperature (°C)	Solid:liquid ratio	Time	Solubility (wt%)	
Feathers	[Amim]Cl + 10 wt% Na_2SO_3	90	1:20	1 h	4.8%	–
Feathers	[Bmim]Cl + 10 wt% Na_2SO_3	90	1:20	1 h	4.8%	–
Feathers	[Bmim]Br + 10 wt% Na_2SO_3	90	1:20	1 h	4.2%	–
Feathers	[Bmim]NO_3 + 10 wt% Na_2SO_3	90	1:20	1 h	4.2%	–
Feathers	[Hmim]CF_3SO_3 + 10 wt % Na_2SO_3	90	1:20	1 h	0.2%	–
Feathers	[Bmim]HSO_4 + 10 wt% Na_2SO_3	90	1:20	1 h	4.1%	–
Wool	[Bmim]Br	130	–	10 h	2%	–
Wool	[Bmim]Cl	100	–	10 h	4%	–
Wool	[Bmim]Cl	130	–	10 h	11%	–
Wool	[Amim]Cl	130	–	10 h	8%	–
Wool	[Bmim]BF_4	130	–	24 h	Insoluble	–
Wool	[Bmim]PF_6	130	–	24 h	Insoluble	–
Wool	[Amim]Cl	130	–	640 min	21%	–
Wool	[Bmim]Cl	130	–	535 min	15%	–
Wool	[Bmim]Cl	120	1:6	30 min	–	57%
Wool	[Bmim]Cl	150	1:6	30 min	–	35%
Wool	[Bmim]Cl	180	1:6	30 min	–	18%
Feathers	[Bmim]Cl	130	1:2	10 h	50%	60%
Feathers	[Amim]Cl	130	1:2	10 h	50%	60%
Feathers	Choline thioglycolate	130	1:2	10 h	45%	55%
Feathers	[Bmim]Cl	100	–	48 h	23%	–

Table 2.4 (continued)

Material	Ionic liquids and additives	Conditions				Yield of keratin
		Temperature (°C)	Solid:liquid ratio	Time	Solubility (wt%)	
Wool	[Amim][dca]	130	–	–	23%	–
Wool	[Bmim]Cl	130	–—	–	12%	–
Wool	[Amim]Cl	130	–	–	10%	–
Wool	Choline thioglycolate	130	–	–	11%	–
Feathers	[HOEMIm] [NTf2] + 1.0 g $NaHSO_3$					

Note: Reproduced with permission from Royal Society of Chemistry.

Table 2.5: Comparison of the amino acid composition of camel hair and cashmere fibers before and after solubilization in comparison to wool and hair keratin (Yang, 2019).

Cysteine (mol%)	Camel hair			Cashmere			Wool keratin	Human hair keratin
	Raw	Soluble	Insoluble	Raw	Soluble	Insoluble		
Cys	7.9	0.0	0.8	6.3	0.4	1.9	10.4	12.9
Arg	8.1	10.1	9.4	8.1	8.5	8.2	6.6	3.2
Gly	7.8	9.1	8.1	9.4	9.5	8.3	8.2	6.7
Asp	10.4	6.1	6.6	4.9	9.1	7.2	8.5	7.1
Leu	8.1	11.7	11.9	9.4	8.5	10.4	7.0	8.0
Val	6.8	8.5	8.7	7.3	7.1	7.5	5.3	6.9
Glu	11.3	8.6	10.5	7.4	13.8	14.6	13.3	12.8
Ser	8/5	5.9	6.7	8.1	9.5	8.2	10.3	12.2
Ala	6.2	10.4	9.5	8.5	6.8	6.8	5.1	4.7
Ile	3.4	5.2	4.6	4.1	3.8	4.2	2.9	3.6
Thr	5.9	5.1	5.7	6.4	5.8	5.6	6.8	19.6
Met	0.4	0.5	0.5	0.3	0.4	0.5	0.3	0.8
Lys	3.1	3.4	3.8	3.5	3.0	3.6	2.7	2.6
His	0.7	1.0	0.9	0.7	0.7	0.8	0.7	1.1
Phe	2.5	4.6	4.4	4.1	2.7	4.0	2.2	2.2
Tyr	2.1	3.0	2.4	3.5	3.8	2.9	3.4	1.4
Pro	6.9	7.0	5.6	8.2	6.9	5.6	6.1	7.1

Note: Reproduced with permission from Express Polymer Letters.

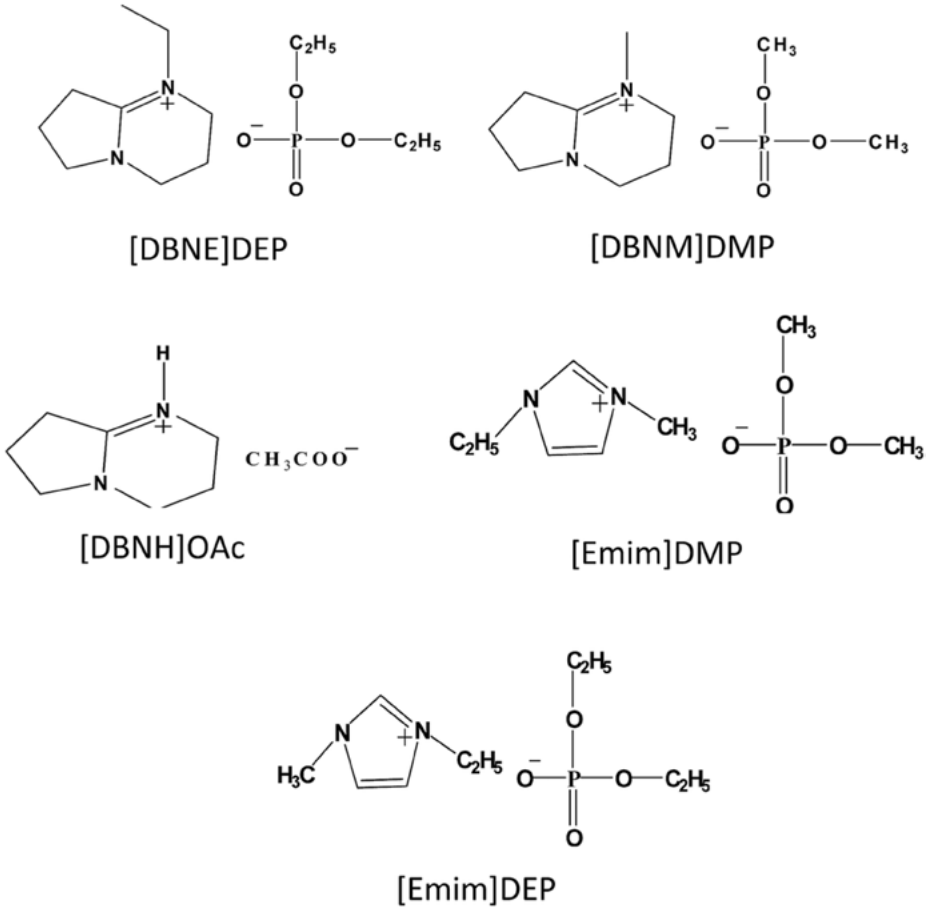

Figure 2.13: Five types of ionic liquids used to dissolve goat wool (Liu, 2017). Reproduced from Royal Society of Chemistry through Creative Commons Licence.

retained as indicated by the NMR results. However, the α-helix and β-sheet content showed substantial changes (Figure 2.14). Untreated wool had 91% α-helices and 9% β-sheets compared to 4% α-helix and 95% β-sheet content (Liu, 2017). Direct relationship was established between the type of ionic liquid, dissolution time, α-helix content and disulfide bond break ratio (Figure 2.15). Ability of the ionic liquids to be recycled and provide keratin with good thermal stability and processability into fibers and other forms makes them suitable for commercial keratin extraction (Liu, 2017). However, it has been reported that the amount of water in recycled ionic liquids affects yield of keratin required to dissolve wool. The extent of conversion of the α-helices and β-sheets was also affected (Zhang, 2017). Treating wool with various ionic liquids results in different extent of disulfide bonds and free sulfhydryl group content which was also influenced by the temperature and duration of treatment. A decrease

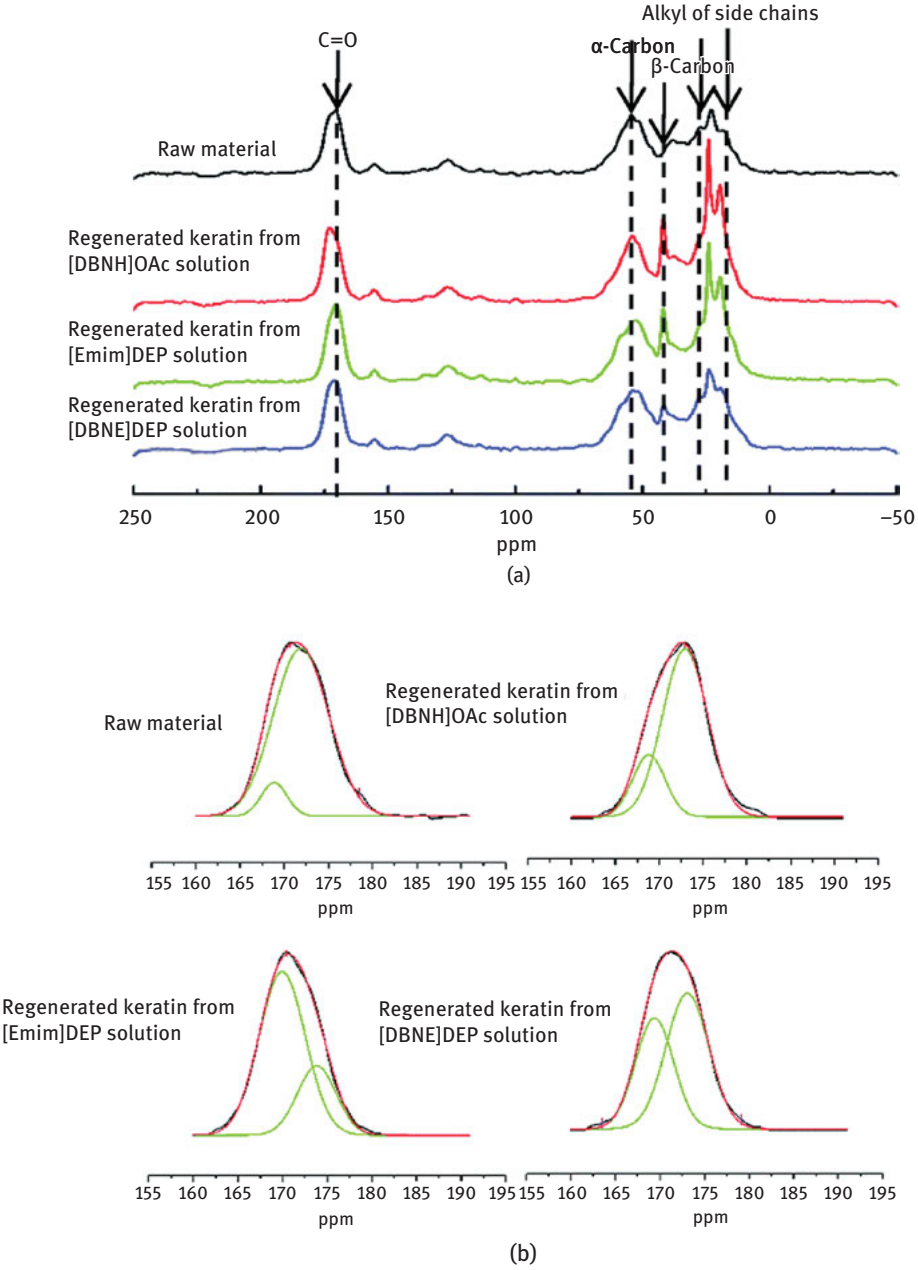

Figure 2.14: Changes in the 13C NMR spectra of goat wool treated with different ionic liquids (a) and deconvolutions of the peaks (b) (Liu, 2017). Reproduced from Royal Society of Chemistry through Creative Commons License.

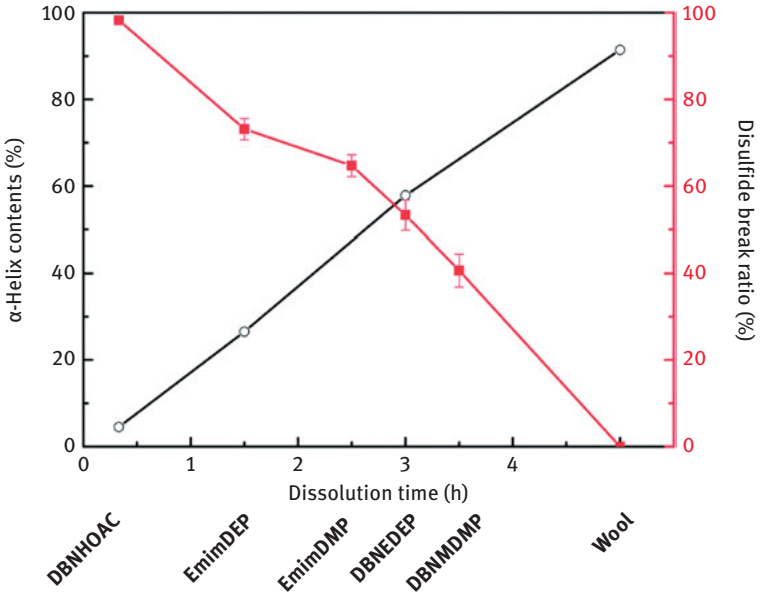

Figure 2.15: Relationship between ionic liquids, extraction time on the α-helix content and disulfide bond break ratio (Liu, 2017). Reproduced from Royal Society of Chemistry through Creative Commons License.

in α-helix content and increase in β-sheet content and disordered regions were observed after treating with the ionic liquids. It was suggested that ionic liquids should cleave 70–80% of the disulfide bonds to avoid excessive degradation.

2.3 Enzymatic extraction of keratin

Extraction conditions not only affect the amino acid composition but also the nutritional value of keratins. Since chemical treatments are harsh and tend to degrade or damage keratin, enzymatic/bacteria/fungi (Table 2.6) keratin extraction has been done to obtain keratin with better properties (Shavandi, 2017). Chicken feathers were subject to in vitro protein digestibility using two enzymes including a nonspecific protease having activity of 12.6 μK/g at pH 7.5. Feathers treated with enzymes were later subject to pressure thermic hydrolysis for 60 or 120 min at 133 °C and 2.4 bar pressure. Alternatively, a nonenzymatic treatment was also done by treating with sodium hydroxide and sodium sulfite at 85 °C for 60 min. Up to 900 g of keratin could be obtained per kilogram of feathers used, making the process suitable for commercial applications. Enzymes were able to degrade the feathers into essential and nonessential amino acids. However, higher amount of sodium and ash in the extracts was considered unsuitable for feed applications (Adler, 2018). It has also

Table 2.6: Some of the possible bacterial/fungal enzymes (keratinases) that have been used to degrade keratin and their processing conditions (Shavandi, 2017).

Bacterial isolate(s)/enzyme	Substrate	Maximum degradation conditions
Chryseobacterium sp. P1-3	Feather meal	Hydrolyzed feather meal within 2 days and possesses a high level of keratinase activity (98 U m/L)
Chryseobacterium sp. strain kr6	Feathers	Complete degradation, optimum growth at pH 8.0 at 30 °C
Vibrio sp. strain kr2	Feathers	Optimum at pH 6.0 and 30 °C
		The hydrolyzate was rich in serine, leucine, alanine and glutamate residues and contains minor amounts of histidine and methionine
Vibrio sp. kr2	Feathers	pH ranging from 6.0 to 8.0, at 30 °C medium containing up to 60 g/L raw feathers, amounts of soluble protein, reaching maximum values around 2.5 g/L
Lysobacter NCIMB 9497	Feathers	Optimum activity occurred at 50 °C, pH 7.5
Stenotrophomonas maltophilia BBE11-1	Feathers	pH 7–11 and temperatures 40–50 °C, 2 days
Stenotrophomonas maltophilia R13	Feathers	pH 7.0 at 30 °C, the maximum yield of the enzyme was 82.3 ± 1.0 U/mL
Stenotrophomonas maltophilia L1	Feathers	pH 7.8 at 40 °C
Bacillus cereus Wu2	Feathers	30 °C and pH 7.0, *B. cereus* possessed disulfite reductase activity along with keratinolytic activity lysine, methionine and threonine
Bacillus subtilis	Feathers	40 °C and pH 11, 7 days

Bacillus sp. MTS	Capable of degrading whole chicken feathers	Bacteria produced extracellular alkaline keratinase and disulfite reductase, for keratinase at pH 8–12, and for disulfite reductase at pH 8–10. The optimum temperature for the extracellular keratinase was 40–70 °C, for disulfite reductase it was 35 °C
Bacillus subtilis DB 100 (p5.2)	37 °C, 700 rpm agitation, released soluble proteins 0.7 mg/mL	Amino acids such as phenylalanine, tyrosine, valine, leucine, isoleucine, serine, alanine, glycine and threonine
Kocuriarosea	Feather degradation up to 51% in 72 h was obtained with a conversion yield in the biomass of 0.32 g/g	At 40 °C, a specific growth rate of 0.17 h^{-1} was attained in basal medium with feathers as a fermentation substrate. Under these conditions, after 36 h of incubation, biomass and caseinolytic activity reached 3.2 g/L and 0.15 U/mL, respectively
***Kocuriarosea* keratinolytic capacity**	Aerobically on submerged feathers	Pepsin digestibility of the fermented product (88%) improved the content of amino acids lysine (3.46%), histidine (0.94%) and methionine (0.69%)
Bacillus pumilus	Bovine hair	pH 8 and 35 °C. Nearly 60% of hair was solubilized after 16 days, and the maximum keratinase production was 54–57 kU/mL, after 9 days
Bacillus safensis LAU 13	Feathers	pH 7.5 and 40 °C, degraded whole chicken feathers after 6 days at 30 ± 2 °C, optimum activity at 50 °C and pH 8.0
Bacillus amyloliquefaciens 6B	Feathers	pH 8.0 and 50 °C completely degrade native feathers in the shortest time period (24 h)

(continued)

Table 2.6 (continued)

Bacterial isolate(s)/enzyme	Substrate	Maximum degradation conditions
Chrysosporium, *Malbranchea*, *Scopulariopsis*, *Microascus* and *Gliocladium*	Human hair	All the test fungi could grow on keratin (human hair) and degrade it
		Maximum cysteine was released in the glucose supplemented medium by *Chrysosporium tropicum* (28 g/mL). Maximum release of protein was by *Scopulariopsis brevicaulis* (65 g/mL)
Chrysosporium species	Hair	28 °C for 14 days
S. brevicaulis, *Trichophyton mentagrophytes*	Feathers	The highest keratinase activity was estimated by *S. brevicaulis* (3.2 kU/mL) and *Trichophyton mentagrophytes* (2.7 kU/mL) in the culture medium with chicken feathers and shows 79% and 72.2% of degrading ability, respectively
Alternaria tenuissima	Feather powder	The highest keratinolytic activities were produced after 4–6 days of cultivation under submerged conditions: 53.8 ± 6.1 U/mL (*Alternaria tenuissima*), 51.2 ± 5.4 U/mL (*Acremonium hyalinum*), 55.4 ± 5.2 U/mL (*Curvularia brachyspira*) and 62.8 ± 4.8 U/mL (*Beauveria bassiana*)
Acremonium hyalinum		
Doratomyces microsporus	Feathers	pH 8–9 and 50 °C
Aspergillus fumigatus	Feathers	pH 9 and 45 °C
A. niger 3T5B8	Feathers	Keratinase activity (172.7 U/mL) after 7 days at pH 5.0
Trichoderma atroviride strain F6	Feathers	5 days with rotary shaking (30 °C, 150 rev./min) pH 8–9 at 50 °C

Note: Reproduced with permission from Royal Society of Chemistry.

been reported that keratin cannot be hydrolyzed by pure keratinase and requires a disulfide bond reductase. Several disulfide bond reductases have been isolated and used for keratin degradation. Seven major types of disulfide reductases that have distinct reaction mechanisms have been reported (Figure 2.16). It was suggested that common keratin reducing agents such as β-mercaptoethanol, dithiothreitol or additional enzymes are necessary for complete degradation of keratin (Peng, 2019). Keratinases extracted from *Bacillus aerius* NSMk2 were found to be halotolerant and have considerable thermal stability (Bhari, 2019). Enzymes extracted had a molecular weight of 9 kDa and specific activity of 30 U/mg. High pH stability between 6.5 and 9.5 and retention of 85% activity at pH 11 even after 4 h of incubation were considered novel. Similarly, the enzymes showed remarkable stability to temperature with 50% residual activity at 70 °C. Presence of inorganic ions such as Na^+, K^+ and Ca^{2+} promoted enzyme activity, whereas Hg^{2+} and Ba^{2+} caused considerable inhibition. Resistance to high salt concentrations (20% NaCl) suggested that the enzymes had halotolerant properties. The enzymes were also able to act as detergents and showed effective removal of hair from goat skin without damaging the structure and properties (Bhari, 2019).

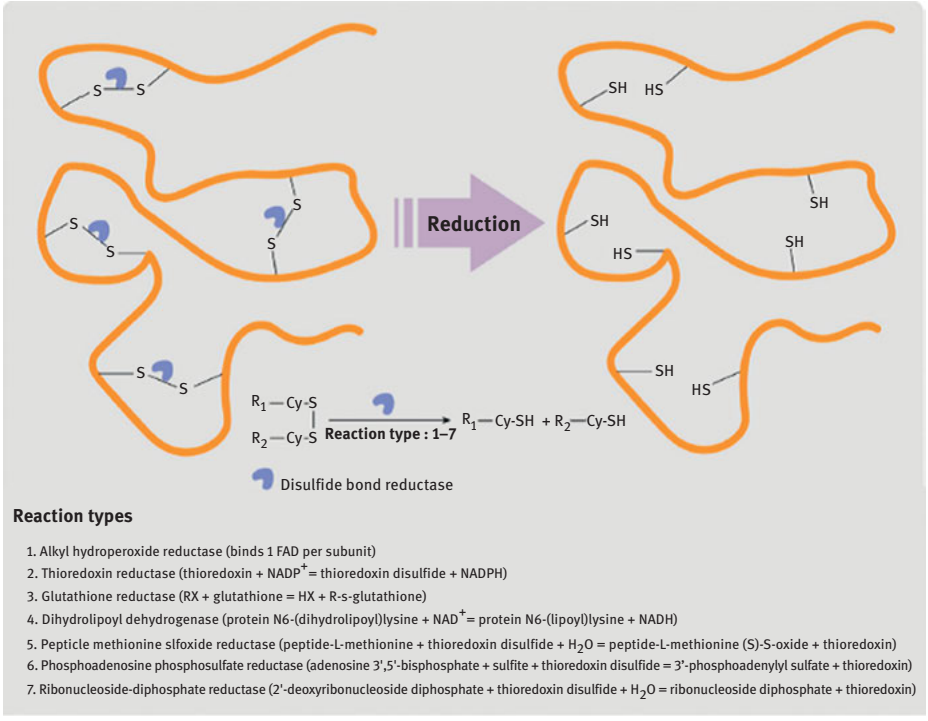

Figure 2.16: Different types of disulfide reductases and their proposed mechanism of action (Peng, 2019). Reproduced with permission from American Chemical Society.

2.4 Microwave-assisted keratin extraction

Instead of using chemical or enzymatic approaches for hydrolysis of keratin, microwave energy has been used for hydrolysis of keratin. Duck feathers were hydrolyzed in an autoclave having a power of 1,200 W at a predetermined pressure and duration. Hydrolyzed keratin obtained was characterized for amino acid content using a Dionex amino acid analyzer (Chen, 2015). Yield and type of amino acids extracted were dependent on the time and temperature of treatment. Increasing treatment time from 10 to 30 min increased the amount of all the amino acids whereas the yield decreased above 30 min. Threonine (up to 8%) was the highest amino acid obtained and asparagine was the lowest. Since no chemicals or catalysts were used, the yield obtained was considered to be high and process was considered to be environmentally friendly (Chen, 2015).

2.5 Steam flash explosion

To avoid the use of chemicals and subsequent hydrolysis of keratin, a steam flash explosion method was used to extract keratin from duck feathers (Zhang, 2015a). Feathers were subject to pressure of 1.4 to 2.0 MPa for 0.5–5 min with saturated steam and then explosion decompressed. Steam exploded feathers were further treated with sodium hydroxide at 25–60 °C for 0.5 to 4 h. Dissolved keratin was precipitated using acid and collected in powder form. Influence of various extraction conditions on the yield of the keratin is shown in Figure 2.17. Increasing volume to weight ratio, concentration of alkali or extraction time increased yield whereas extraction temperature above 40 °C decreased the yield (Zhang, 2015a). A highest extraction rate of 66% was obtained but considerable decrease in molecular weight had occurred since proteins below 10 kDa were seen in the electrophoresis gel (Figure 2.18) (Zhang, 2015a). However, there was no change in the thermal stability of the samples. Steam explosion assisted keratin extraction was suggested to be a simple, economical and environmentally friendly approach to obtain keratin for various applications (Zhang, 2015a).

An attempt was made to understand the possibility of extracting keratin from wool using superheated steam and without the use of any chemicals (Bhavsar, 2017). In this study, wool samples were immersed in water or KOH or CaO solutions in 1:3 ratio. Hydrothermal treatment was done using 140 or 170 °C for 1 h. After treatment, the samples were filtered, freeze dried and collected as powder. pH of superheated water was 7.9 at 140 °C and 5.2 at 170 °C and ranged from 8 to 10.2 for alkali solutions. Treating at 140 °C preserved some of the cuticular structure and morphology but such features were lost and particulate aggregates were formed after treating at 170 °C. Considerable differences were observed in the molecular

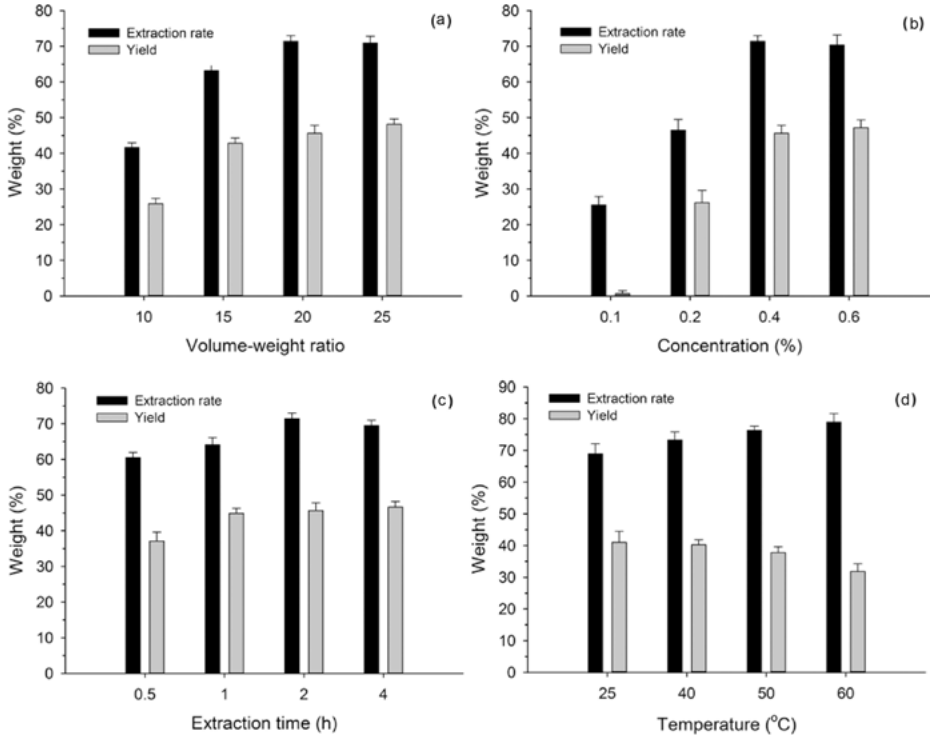

Figure 2.17: Influence of various extraction conditions on the extraction rate and yield of keratin using the steam assisted flash explosion method (Zhang, 2015a). (a) effect of volume/weight ratio of solvent and feather, (b) effect of alkali concentration, (c) effect of extraction time, and (d) effect of extraction temperature. Reproduced with permission from American Chemical Society.

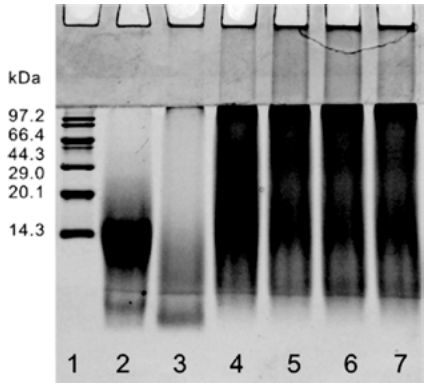

Figure 2.18: SDS-Electrophoresis patterns show the difference in molecular weights of the keratin obtained using various conditions. Standard markers are in lane 1, raw feather in lane 2, keratin extracted using 1 N NaOH in lane 3 and keratin extracted using steam flash explosion at 1.4, 1.6, 1.8 and 2.0 MPa for 1 min are in lanes 4–7, respectively (Zhang, 2015a). Reproduced with permission from American Chemical Society.

weights, and primary and secondary structure of the proteins were obtained at different conditions. Considerable deterioration of the protein structure had occurred under all treatment conditions as the molecular weight of keratin was reduced from 67–43 kDa to 8–3 kDa. Differences were also noticed in the amino acid composition depending on the type of extraction used (Bhavsar, 2017). Proteins obtained using the super-heated steam approach were suggested to be suitable as food, biostimulants and fertilizer.

2.6 Extraction of keratin from horn and hoofs

Buffalo horns have also been used as a source of keratin. To extract keratin from the horns, samples were cut from the horn and oxidized using hydrogen peroxide. The oxidation was done using 20% and 30% peroxide concentration for 12 and 48 h at a temperature of 25 °C. Changes in the structure and composition of the keratin were studied and the potential of using the oxidized keratin as scaffolds for tissue engineering were studied (Zhang, 2015b). FTIR spectra showed peaks at 1,650–1,658 cm^{-1} indicating α-helix structure and bands between 1,640 and 1,610 cm^{-1} belonging to the β-sheets were seen in the horn keratin and the oxidized samples. However, the content of the α- and β-sheets in the samples were different (Table 2.7). Increasing the level of oxidation increased the amount of β-sheets but decreased the amount of α -sheets due to the disruption of disulfide bonds and hydrogen bonds and also due to reduction in crystallinity. Mechanical properties of the horn keratin also varied due to oxidation (Table 2.8).

After oxidation, considerable decrease in tensile strength was observed whereas the elongation increased by more than 300%. Decrease in the strength and modulus is due to the disruption of the chemical bonds during oxidation. However, increase in the β-sheet content makes keratin more flexible and hence the elongation increased after oxidation (Zhang, 2015b). In terms of biocompatibility, the oxidized samples had a hemolysis rate of less than 5% which indicates their suitability for medical applications. Similarly, there was no platelet aggregation or activation suggesting the keratin would not clot the blood. Cells (3T3 and Human Umbilical Vein Endothelial Cells (HUVECs)) growth and viability was found to be the same for serum (control), horn and oxidized horn keratin samples (Zhang, 2015b). Untreated and oxidized keratin samples when subcutaneously injected into mice resulted in an initial inflammatory response which was typical to any foreign body. The inflammation subsidized and healthy tissue growth was observed after 3 weeks, suggesting that the implanted keratin had good biocompatibility and useful for clinical applications (Zhang, 2015b).

Table 2.7: Comparison of the amide bands and α-helix and β-sheet content in the horn and oxidized keratin samples obtained from the horns (Zhang, 2015b).

Sample	α-Helix		β-Sheet	
	Band position (cm^{-1})	Area (%)	Band position (cm^{-1})	Area (%)
Horn	1,650.8	48.74	1,617.0 and 1,631.2	31.69
Oxidized 12–20	1,652.3	45.80	1,617.1 and 1,632.3	35.35
Oxidized 12–30	1,653.9	42.42	1,619.9 and 1,634.0	38.15
Oxidized 48–30	1,656.2	37.66	1,620.3 and 1,634.3	42.10

Note: Reproduced with permission from Elsevier.

Table 2.8: Mechanical properties of raw and oxidized horn keratin samples (Zhang, 2015b).

Sample	Tensile strength (MPa)	Modulus (GPa)	Fracture strain (%)
Horn	118 ± 3.2	1.5 ± 0.03	24.6 ± 3.6
Oxidized 12–20	100 ± 2.3	1.1 ± 0.03	37.6 ± 4.1
Oxidized 12–30	86 ± 5.4	0.9 ± 0.02	56.2 ± 4.3
Oxidized 48–30	73 ± 2.1	0.7 ± 0.02	70.5 ± 6.4

Note: Reproduced with permission from Elsevier.

2.7 Keratin obtained using eutectic solvent system

Ability of a new method called deep eutectic solvent (DES) mixture which consists of two or three components to extract keratin from wool at low temperatures was investigated (Wang, 2018a). In the DES mixture, two solvents choline chloride (ChCl) and urea, glycerol, ethanol, oxalic acid, citric acid and acetic acid were found to dissolve wool and obtain keratin (Figure 2.19). A combination of ChCl and oxalic acid at 1:2 molar ratio and treatment at 110–125 °C for 2 h was found to provide keratin with molecular weights between 3.3 and 7.8 kDa. Up to 100% solubility of wool was obtained depending on the extraction conditions. Differences were also observed in the crystalline structure, thermal behavior, molecular weight and morphology of wool and extracted keratin (Wang, 2018a). Using the eutectic solvent approach, Nuutinen (2019) regenerated keratin from feathers and studied the structure and properties of the extracted keratin. The eutectic solvents were prepared by combining extra pure sodium acetate and urea in specific ratios with or without water and heating the mixture at 150 °C until a clear solution was formed. Three forms of keratin were obtained after treating the feathers as shown in Figure 2.20. Up to 45% regenerated keratin could be obtained depending on the composition of the solvent and temperature and time during dissolution. Similarly, the α-helix and β-sheet content also varied with dissolution time (Figure 2.20). It was suggested that the eutectic solvent system is more gentle,

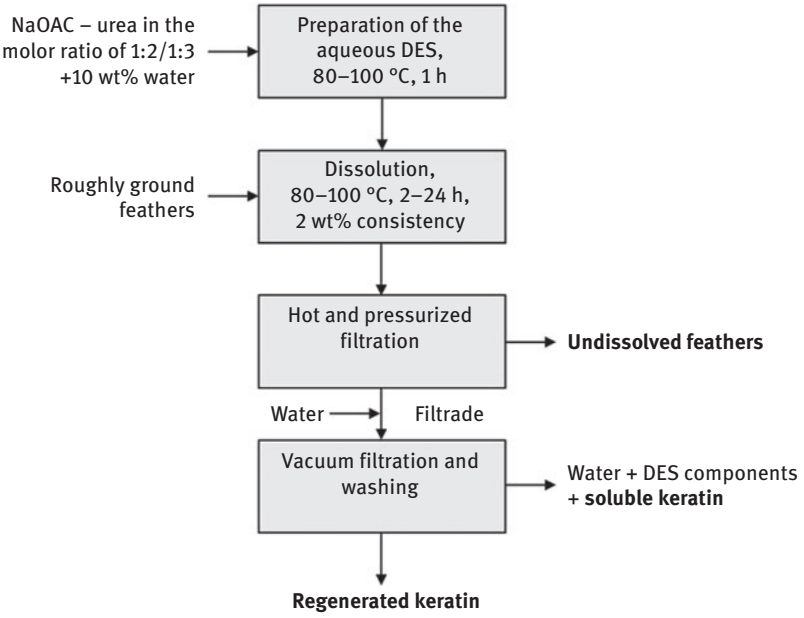

Figure 2.19: Steps involved in the dissolution of feather keratin using deep eutectic solvent system and the three fractions of keratins obtained (Nuutinen, 2019). Reproduced with permission from Royal Society of Chemistry through Open Access publishing.

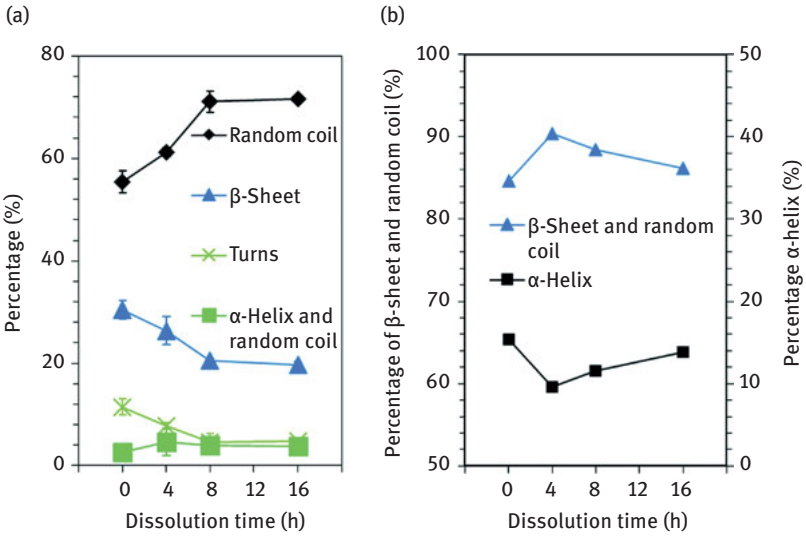

Figure 2.20: Changes in the secondary structure of keratin with dissolution time (Nuutinen, 2019). (a) the FTIR spectra band fitting and (b) the NMR spectra peak fitting. Reproduced with permission from Royal Society of Chemistry through Open Access publishing.

environmentally friendly and inexpensive compared to previous methods of keratin extraction from protein sources (Nuutinen, 2019).

2.8 Pretreatment/oxidation of keratin materials

Not just the method and chemicals used for extraction but even the purification approach is reported to have an effect on the structure and properties of the keratin obtained (Potter, 2018). Instead of the conventional purification, an additional step of solution aggregation was used to purify and allow self-assembly of type I and type II hard keratins. Human hair fibers were treated with peracetic acid at 37 °C for 12 h for oxidation to occur and keratin to be converted into keratose. The keratose formed was purified either using ultrapure water (WKOS) or dialyzed against phosphate buffer and later against water (BKOS) to control the aggregation of the peptides. Keratose powder extracted was dissolved in water with the addition of 1,4-butanediol diglycidyl ether as the cross-linking agent (12%). Solutions were cast onto silicon molds and incubated for 72 h for the hydrogel formation to occur. Dialysis using water resulted in excessive aggregation of proteins due to the ready self-assembly behavior of keratin. Such aggregation results in a lesser purity of peptides and provides lower stability to materials developed from the proteins. Proteins obtained after dialysis using buffer solutions could be made into hydrogels using low concentrations and with better elasticity. However, the proteins were more susceptible to enzymatic degradation compared to those obtained using water purification alone. It was suggested that both mechanical and biochemical properties of keratin-based materials could be altered by adopting different purification methods (Potter, 2018).

To improve the yield of intact cortical cells (keratin) from wool, it was suggested that a descaling and mild oxidation using peracetic acid would be useful (Fan, 2012). In this approach, degreased wool fibers were descaled by treating with formic acid and later treated with peracetic acid for varying time to oxidize the fibers. Later, the fibers were reduced to cortical cells through ultrasonication, washed and dried. Increase in percentage of cortical cells from 16% to 30% (Table 2.9) was seen when the oxidation was done for 2 h. However, further increase in oxidation time to 25 h resulted in severe loss of cells. Such drastic change was attributed to the decrease in crystallinity and reduction in the disulfide bonds (Fan, 2012). The simple approach of oxidation to increase yield of keratin was considered to be suitable for industrial-scale production of keratin.

Soluble keratin with low molecular weight was prepared from merino wool using thioglycolic acid (TGA) for potential hair treatment. To purify the wool, fibers were treated with TGA at pH 13 and 13.5 and the reaction was carried out between 50 and 60 °C with shaking for 3–6 h. After the reaction, the pH was reduced to 4 for the proteins to precipitate and the extracted proteins were freeze-dried. Extracted keratin was used for permanent waving treatment of human hair using 6% solution of

Table 2.9: Effect of oxidation time on the yield of wool keratin (Fan, 2012).

Oxidation time	% Intact cortical cells	% Disrupted cortical cells	% Residual fibers	% Loss
No treatment	16.7	18.0	63.6	1.7
30 min	23.3	18.2	56.7	1.8
1 h	26.7	29.3	42.0	2.0
2 h	30.4	37.4	29.7	2.5
25 h	–	22.6	–	77.4

Note: Reproduced with permission from Springer.

keratin. After treatment, the fibers were washed and oxidized with 8% sodium bromate. This procedure was repeated three times and a permanent bleached waved hair was obtained (Hirata, 2013). When observed using SDS-PAGE, untreated wool had molecular weights in two regions (62–48 kDa and between 12 and 17 kDa), whereas the oxidized wool has a smear throughout the lane and no distinct bands were observed indicating severe hydrolysis (Hirata, 2013). Scanning electron microscopy images did not show any major changes in the surface features of the treated hair, and therefore, the extracted keratin could be used for protecting hair from any potential damage.

Chapter 3
Applications of keratin hydrolysates

3.1 Degradation of keratin using bacteria and fungi

Keratin has been degraded (hydrolyzed) to obtain hydrolysates, amino acids, enzymes and other products. Physical, chemical, biological and a combination of these methods have been used to generate keratin hydrolysates. In a simple method, hydrothermal treatment was done at high pressure (10–15 PSI) and/or high temperature (80–140 °C) using acids or alkalis to degrade keratin. Such treatment disrupts the disulfide bonds and results in soluble peptides or amino acids (Karthikeyan, 2007). Although hydrothermal treatments are simple and effective, it is difficult to control the extent of degradation. Alternatively, enzymatic approaches have been used to degrade keratin and obtain hydrolysates for various applications. Although common proteolytic enzymes cannot degrade keratin, keratinases have been effective in degrading keratin and used in many industries. For instance, a two-step alkali and enzymatic degradation was used to produce feather hydrolysate using mild reaction conditions (Mokrejs, 2010). Schematic of the process used for production of the keratin hydrolysate is in Figure 3.1. The two-step process in which the second step involved treating with 5% enzyme and 0.1% KOH at 70 °C resulted in a high yield of keratin (about 91%). The process used was low cost, suitable for commercial-scale production and the hydrolysate obtained was suggested to be suitable as animal feed and also to develop packaging films and capsules (Mokrejs, 2010).

Various bacteria and fungi are also capable of degrading keratin and producing enzymes. However, the extent of degradation depends on the conditions such as pH and temperature used during degradation. Table 3.1 lists some of the microorganisms and their ability to produce protein and the enzyme keratinase (Singh, 2015). Fungal strains isolated from alkaline soil were studied for their ability to produce keratinolytic enzymes using feathers as a substrate (Cavello, 2013) in solid state and submerged cultures. Among the different strains studied, *Purpureocillium. lilacinum* produced the highest proteolytic and keratinolytic activities. Highest enzyme production obtained was 15.96 Uc/mL. Enzymes produced from keratin waste were *considered* to be suitable to treat leather (hydrolyze) waste and consequently reduce environmental pollution (Cavello, 2013).

Poor degradation of keratin is one of the major limitations for the application of keratin. Several studies have been conducted on identifying bacteria and fungi that are capable of degrading keratin wastes. A gram-negative bacteria *Stenotrophomonas maltophilia* DHHJ was used to ferment chicken feathers in large quantities and the compositional analysis and degradation products obtained from the feathers were analyzed (Cao, 2011). Protein concentration obtained was up to 0.45 g/L and amino acid

https://doi.org/10.1515/9781501511769-003

concentration was up to 0.6 g/L. Feather fermentation broth when used as fertilizer increased plant growth substantially. Similarly, the mechanical properties of hair were improved after treating with the feather broth (Cao, 2011).

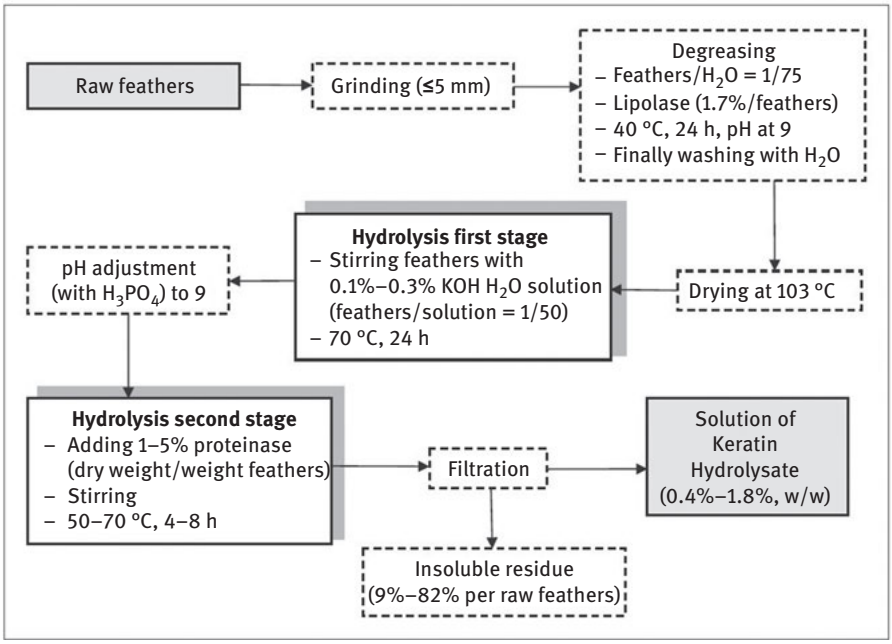

Figure 3.1: Process of obtaining keratin hydrolysate from raw feathers (Mokrejs, 2010). Reproduced with permission through Open Access publishing.

Table 3.1: Microorganisms reported to be capable of degrading keratin and their ability to produce keratinase (Singh, 2015).

S.no.	Fungi tested	Accession number	Total* protein (µg/mL)	Keratinase (Ku/mL)
1.	*Acremonium* sp.1	GPCK 506	366.99	115.8
2.	*Acremonium* sp.2	GPCK 537	494.33	117.6
3.	*Acremonium* sp.3	GPCK 538	441.33	116.5
4.	*Acremonium* sp.4	GPCK 539	417.66	115.2
5.	*Acremonium* sp.5	GPCK 540	312.33	116.6
6.	*Acremonium* sp.6	GPCK 541	351.00	114.5

Table 3.1 (continued)

S.no.	Fungi tested	Accession number	Total* protein (µg/mL)	Keratinase (Ku/mL)
7.	*Acremonium* sp.7	GPCK 542	313.99	112.3
8.	*Acremonium* sp.8	GPCK 543	269.66	110.5
9.	*Acremonium* sp.9	GPCK 544	215.33	110.2
10.	*Acremonium* sp.10	GPCK 545	213.66	110.1
11.	*Acremonium* sp.11	GPCK 546	196.99	76.9
12.	*Acremonium* sp.12	GPCK 547	189.66	69.2
13.	*Acremonium* sp.13	GPCK 548	87.32	16.5
14.	*Acremonium* sp.14	GPCK 549	147.99	88.8
15.	*Acremonium* sp.15	GPCK 550	107.66	18.2
16.	*Acremonium* sp.16	GPCK 551	106.00	17.5
17.	*Acremonium* sp.17	GPCK 640	158.33	114.6
18.	*Acremonium implicatum*	FMR 6212	187.33	115.3
19.	*Acremonium hennebertii*	FMR 6213	195.33	118.6
20.	*Acremonium hennebertii*	FMR 6214	185.66	114.2
26.	*Chrysosporium europae*	FMR 300	457.33	116.6
27.	*Chrysosporium cuniculi*	GPCK 673	231.66	114.2
28.	*Chrysosporium indicum*	GPCK 502	132.00	17.8
29.	*Chrysosporium indicum*	GPCK 639	110.99	16.6
30.	*Chrysosporium indicum*	GPCK 648	154.33	18.5
31.	*Chrysosporium indicum*	GPCK 649	300.33	115.3
32.	*Chrysosporium indicum*	GPCK 650	195.99	110.9
33.	*Chrysosporium indicum*	GPCK 651	228.33	111.6
34.	*Chrysosporium indicum*	GPCK 652	294.99	115.8
35.	*Chrysosporium indicum*	GPCK 653	123.99	110.2
36.	*Chrysosporium indicum*	GPCK 654	156.00	111.5
37.	*Chrysosporium indicum*	GPCK 655	241.32	112.4
38.	*Chrysosporium indicum*	GPCK 656	173.66	110.0

Table 3.1 (continued)

S.no.	Fungi tested	Accession number	Total* protein (µg/mL)	Keratinase (Ku/mL)
39.	*Chrysosporium indicum*	GPCK 657	106.66	17.2
40.	*Chrysosporium indicum*	ITCC 4730	184.66	112.0
41.	*Chrysosporium keratinophilum*	GPCK 501	185.99	75.0
42.	*Chrysosporium keratinophilum*	GPCK 614	384.33	115.9
43.	*Chrysosporium keratinophilum*	GPCK 658	416.99	118.8
44.	*Chrysosporium keratinophilum*	GPCK 659	151.66	115.1
45.	*Chrysosporium keratinophilum*	GPCK 660	137.66	110.0
46.	*Chrysosporium keratinophilum*	GPCK 661	397.33	112.0
47.	*Chrysosporium keratinophilum*	GPCK 662	345.66	115.4
48.	*Chrysosporium keratinophilum*	GPCK 663	172.99	48.8
49.	*Chrysosporium keratinophilum*	GPCK 773	107.99	37.9
50.	*Chrysosporium keratinophilum*	ITCC 4729	179.33	110.3
51.	*Chrysosporium keratinophilum*	P 318	141.33	114.5
52.	*Chrysosporium pannicola*	GPCK 612	140.66	114.1
53.	*Chrysosporium pannicola*	GPCK 670	354.32	116.6
54.	*Chrysosporium pannicola*	GPCK 671	114.33	111.1
55.	*Chrysosporium pannicola*	GPCK 672	179.00	49.6
56.	*Chrysosporium pseudomerdarium*	GPCK 674	214.99	115.9
57.	*Chrysosporium queenslandicum*	ITCC 4731	137.66	57.8
58.	*Chrysosporium queenslandicum*	GPCK 664	196.66	110.5
59.	*Chrysosporium queenslandicum*	GPCK 665	145.99	114.2
60.	*Chrysosporium queenslandicum*	GPCK 666	159.00	112.5
61.	*Chrysosporium queenslandicum*	GPCK 667	210.66	113.6
62.	*Chrysosporium queenslandicum*	GPCK 668	217.00	113.8
63.	*Chrysosporium queenslandicum*	GPCK 669	157.99	79.4
64.	*Chrysosporium tropicum*	GPCK 644	271.33	114.8
65.	*Chrysosporium tropicum*	GPCK 645	355.66	118.5

Table 3.1 (continued)

S.no.	Fungi tested	Accession number	Total* protein (µg/mL)	Keratinase (Ku/mL)
66.	*Chrysosporium tropicum*	GPCK 646	159.99	110.5
67.	*Chrysosporium tropicum*	GPCK 647	206.33	111.2
68.	*Chrysosporium sulfurium*	GPCK 675	336.32	113.7
69.	*Chrysosporium sulfurium*	GPCK 676	224.99	119.9
70.	*Chrysosporium zonatum*	ITCC 4732	236.32	110.4
71.	*Chrysosporium zonatum*	GPCK 698	423.99	118.5

Note: Reproduced with permission from Pelagia Research Library.

Feather waste was used as substrate to produce proteases that were active ingredients for various detergents (Cavello, 2012). *Paecilomyces lilacinus* strain LPS #876 was used to generate the proteases and the protease activity was measured in terms of the azocasein unit (Uc). Feathers were completely degraded after 70 h of incubation at 28 °C. Protease activity increased up to pH 10 and later decreased. Similarly, the highest protease activity was obtained at a temperature of 60 °C (Cavello, 2012). Since detergents contain various chemicals including oxidizing agents, ability of the proteases to be active was studied. Activity from 11% to 110% was observed based on the type of chemicals (inhibitors and metal ions) used (Table 3.2). When used with various detergents, the activity varied from 32% to 100%. Hydrogen peroxide had the most reduction in activity whereas proteases from other sources showed high stabil-

Table 3.2: Changes in protease activity and residual activity with the addition of different chemicals (Cavello, 2012).

Chemicals	Concentration	Residual activity (%)
None	–	100 ± 1.2
PMSF	2 mM	11.8 ± 3.5
Iodoacetate	10 mM	99.0 ± 2.3
EDTA	5 mM	81.1 ± 0.9
1,10-Phenanthroline	1 mM	95.0 ± 0.2
Pepstatin A	100 µg/mL	99.0 ± 4.2
Ca^{2+}	1 mM	110 ± 1.0
Zn^{2+}	1 mM	84.0 ± 2.0
Mg^{2+}	1 mM	95.0 ± 3.0
Hg^{2+}	1 mM	15.3 ± 1.0

Note: Reproduced with permission from Springer.

ity to peroxide (80–85%). The proteases obtained also had excellent stability to both anionic and nonionic surfactants even at high temperatures (40 °C). It was suggested that *P. lilacinus* was capable of generating proteases with excellent stability that could be suitable for use in commercial laundry detergents (Table 3.3) (Cavello, 2012).

Table 3.3: Stability of protease when used with commercially available surfactants and oxidizing agents (Cavello, 2012).

Chemical	Concentration (%)	Residual activity		
		Room temperature	30 °C	40 °C
Control	–	100 ± 1.2	100 ± 2.5	100 ± 1.6
Triton X-100	1	100 ± 3.7	100 ± 3.6	94 ± 1.1
	5	100 ± 2.0	100 ± 2.2	100 ± 2.2
Tween 20	1	100 ± 3.5	100 ± 1.5	100 ± 2.3
	5	100 ± 3.7	95 ± 1.9	100 ± 1.5
Tween 85	1	100 ± 2.0	100 ± 0.9	100 ± 2.5
	5	88 ± 0.9	100 ± 3.2	100 ± 3.6
SDS	0.1	100 ± 2.3	97 ± 1.7	83 ± 2.7
	0.5	89 ± 0.7	68 ± 3.7	62 ± 2.6
	1	100 ± 1.4	99 ± 2.1	100 ± 3.9
Sodium perborate	0.2	100 ± 0.5	100 ± 2.9	100 ± 2.7
	0.5	100 ± 0.9	98.5 ± 3.0	86 ± 1.4
	1	100 ± 1.9	97.6 ± 2.3	80 ± 2.1
H_2O_2	1	100 ± 2.5	100 ± 1.6	80 ± 4.0
	2	118 ± 0.5	118 ± 2.4	54 ± 2.9
	3	96 ± 0.9	106 ± 0.5	33 ± 1.4

Note: Reproduced with permission from Springer.

Keratin hydrolysates were obtained from feathers using *Bacillus subtilis* AMR without the need for any other chemicals (Villa, 2013). In this method, feathers were washed and treated with chloroform and methanol to remove soluble substances. Later, the treated feathers were added into the bacterial solution and allowed to grow for 5 days at 28 °C during which the feathers were completely converted into hydrolysate (Figure 3.2). Crude hydrolysate formed was concentrated, dried and collected. Keratin hydrolysate obtained had molecular weights between 800 and 1,079 Da, lower than that of commercial hydrolysate (900–1,400 Da) (Figure 3.3) Low molecular peptides are able to penetrate into the hair fibers more easily and therefore provide better finishing. When used in a shampoo and conditioner, the keratin hydrolysate improved hydration, brightness and softness suggesting that the hydrolysate was suitable for cosmetic applications (Villa, 2013).

Ability of a few gram-positive and gram-negative bacteria to degrade α- and β-keratin was investigated (Bach, 2015). Three gram-negative bacteria (*Chryseobacterium*

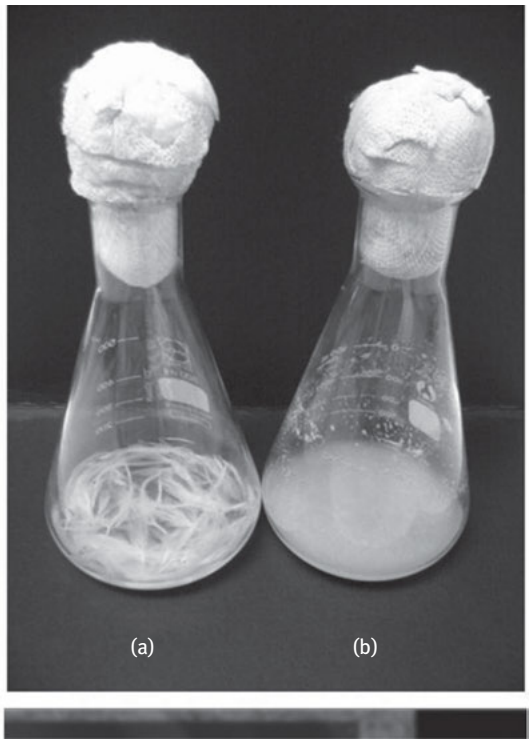

Figure 3.2: Digital images of keratin before (a) and after treating (b) with the bacteria for 5 days (Villa, 2013). Reproduced with permission from. Biomed Central Limited.

indologenes A22 and *Aeromonas hydrophila* K12 and *Serratia marcescens* P3) were used to degrade wool, chicken feathers and human hair. Strains A22 and K12 degraded feather relatively easily compared to hair and wool due to the lower amount of α-keratin in feathers (Table 3.4). Keratinase production was about 15 g/L from feather meal compared to 13% for hair and 24% for wool depending on the strain and culture conditions used (Bach, 2015).

3.2 Treating keratin for conversion into animal feed

One of the major applications of chicken feathers is animal feed. However, feathers have low digestibility and it has been reported that only 16% of the feathers are digestible in rumens. Various chemical, physical and biological treatments are done to improve digestibility. A simple approach of preparing feather meal is by treating the feathers under pressure for various periods of time either in a continuous or batch process (Table 3.5) (Latshaw, 1994). Such treatment results in considerable changes in the amino acid composition and subsequently the digestibility (Table 3.6) (Latshaw, 1994).

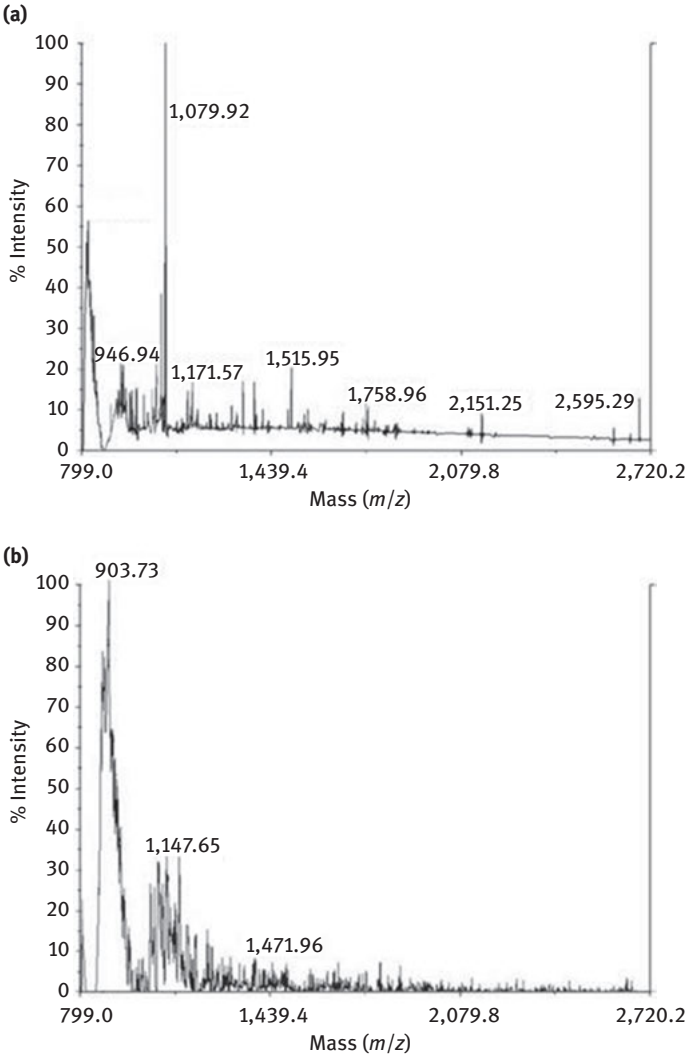

Figure 3.3: Comparison of the MALDI-TOF-MS analysis of peptides obtained by the **e**nzymatic keratin hydrolysates from feather keratin using *Bacillus subtilis* (a) compared to commercially available keratin (b) (Villa, 2013). Reproduced with permission from Biomed Central Limited.

The effect of different processing conditions on the amino acid digestibility of feather meal was determined by chicken assay (Papanapodoulous, 1985). In this approach, three treatment conditions and three processing times were used to determine the amino acid digestibility. Considerable variations were found in the amino acid digestibility depending on the conditions used. Among the different amino acids, lysine had a digestibility of 22.5% compared to 82.4% for isoleucine, 36.3% for aspartic acid and 86.5% for isoleucine. Although some of the amino acids had

Table 3.4: Amount of soluble protein extracted from feather broth (FB), wool broth (WB) and hair broth (HB) by the three different strains and the pH values of the broth (Bach, 2015).

Isolate	Soluble protein (mg/mL)			pH		
	FB	HB	WB	FB	HB	WB
C. indologenes A22	2.57 ± 0.48	2.94 ± 0.03	0.75 ± 0.5	7.0 ± 0.2	7.5 ± 0.2	7.5 ± 0.1
A. hydrophila K12,	0.47 ± 0.12	3.07 ± 0.04	0.13 ± 0.36	8.0 ± 0.2	5.0 ± 0.1	6.0 ± 0.1
S. marcescens P3	0 ± 0.04	–	–	7.0 ± 0.2	–	–

Note: Reproduced with permission from Elsevier.

Table 3.5: Conditions of hydrolyzing feathers in a continuous and batch process and resulting properties of the feather hydrolysate (Latshaw, 1994).

	Type of feather hydrolyzation				
	None	Continuous hydrolyzation (kPa)			Batch
		207	310	414	283
Hydrolyzer pressure (kPa)	–	207	310	414	283
Pressure range (kPa)	–	±5	±8	±6	±6
Hydrolyzing time (min)	–	24	24	24	16 + 43 + 57
Total cycle time (min)	–	24	24	24	116
End point moisture (g/kg)	–	25	20	25	12
End product					
Moisture (g/kg)	59	56	79	44	44
Protein (g/kg)	922	866	853	893	903
Fat (g/kg)	7	27	24	44	18
Fiber (g/kg)	12	7	10	8	11
Ash (g/kg)	2	19	20	23	19
Total	1,002	975	986	1,012	995
Bulk density (kg/m^3)	39.1	135	158.9	182.3	207.7
Pepsin digestible protein	0.16	0.658	0.766	0.806	0.790

Note: Reproduced with permission from Elsevier.

high digestibility, the essential amino acids such as lysine, histidine and methionine were not easily digestible. Since treatment time and presence of enzymes and alkali were critical for digestion, it was suggested that appropriate conditions were to be chosen to obtain the required level of digestibility (Papanapodoulous, 1985).

Since animal feed has to be inexpensive and expensive chemical modifications cannot be adopted; feathers were treated with lime (calcium hydroxide) at various conditions and the changes in digestibility were studied (Coward-Kelly, 2006a,b). When heated at 150 °C for various time periods, untreated feathers had maximum digestibility of about 20%. Increasing concentration of hydroxide increases conversion and a conversion rate of 100% was possible after heating for 100 min. Considerable changes in

Table 3.6: Amino acid content of the feather meals as affected by the processing condition expressed in terms of g/kg (Latshaw, 1994).

	Type of feather hydrolyzation				
	None	Continuous hydrolyzation (kPa)			Batch
		207	310	414	283
Alanine	28.8	37.7	35.3	35.7	34.1
Glycine	51.8	50.7	50.7	56.8	59.5
Isoleucine	39.4	41.3	39.2	42.5	44.5
Leucine	56.9	68.8	63.7	67.1	66.3
Valine	53.0	44.0	42.7	46.3	48.9
Phenylalanine	34.6	40.1	39.4	42.5	45.7
Arginine	67.6	62.5	61.7	65.6	50.8
Histidine	2.3	8.6	7.7	7.1	6.5
Lysine	15.4	22.6	24.6	23.1	17.7
Aspartic acid	41.8	55.9	55.8	57.7	59.2
Glutamic acid	82.2	72.3	72.3	76.5	80.0
Serine	87.3	72.1	68.1	76.2	84.5
Threonine	34.5	36.5	36.3	36.9	39.5
Proline	73.9	74.8	69.3	78.5	85.8
Cysteine	65.8	48.7	43.0	42.1	48.5
Lanthionine	0.8	5.3	5.4	5.4	7.8
Methionine	7.1	6.3	6.3	6.7	6.5
Total	743.2	748.2	721.5	767.0	785.8

Note: Reproduced with permission from Elsevier.

protein conversion could also be achieved with changes in temperature. However, temperatures above 125 °C were necessary to achieve 100% conversion. Although higher temperatures provide better conversion, there could be a risk of degradation of the proteins and loss of valuable amino acids when high temperatures are used.

Amino acid content of the solubilized keratin was similar to that of unhydrolyzed keratin except for proline which showed considerable increase when heated for 150 °C (Coward-Kelly, 2006a,b). Hydrolyzed feathers had amino acid content that was suitable to satisfy the nutrients requirements for different animals and was therefore considered to be an inexpensive and readily available source for animal feed.

Instead of using chemical or physical means, biological treatments particularly those using bacteria have been extensively studied to hydrolyze feather and improve its digestibility when used as animal feed. A feather degrading bacterial strain *Kocuria rosea* LPB 3 was isolated from the soil and cultured aerobically on submerged feathers to obtain fermented feather meal. Extent of degradation and changes in the amino acid composition were compared with respect to commercially available feather meal (Table 3.7) (Berstch, 2005). In vitro digestibility of the fermented feather meal at 88% was similar to that of the commercial feather meal

Table 3.7: Comparison of the amino acid digestibility between fermented feather meal and commercially available feather meal (Berstch, 2005).

Amino acid,%	Fermented meal	Commercial feather meal
Lysine	77.45	68.29
Histidine	84.05	79.63
Methionine	81.91	72.58
Cysteine	96.03	91.61
Threonine	95.48	80.0
Asparagine	91.61	84.21
Proline	99.81	99.86
Glutamine	87.83	87.03
Alanine	98.78	98.46
Leucine	95.15	95.64
Glycine	88.71	90.78
Valine	83.29	58.18
Ile	93.15	94.09
Phenylalanine	92.79	93.42
Tyrosine	81.75	85.0
Serine	91.63	93.59

Note: Reproduced with permission from Elsevier.

(87%) but protein content in the fermented meal was 71% compared to 81% in the commercial meal. However, the fermented meal had higher protein digestibility than raw feather (26%) and hence the bacterial treatment was considered effective to obtain feather hydrolysate as animal feed (Berstch, 2005). Results reported were using in vitro digestion. However, in vivo digestion studies should be considered before the meal can be considered suitable as animal feed.

In a similar study, feathers were hydrolyzed using a bacterial strain *Vibrio* sp. strain kr2 and the obtained hydrolysate was studied for potential use as animal feed (Grazziotin, 2006, 2007). Either the entire bacterial culture (whole culture) or only the supernatant from the culture were used to treat the feathers. Extent of degradation and type and amount of amino acids produced varied depending on whether the whole culture or the supernatant were used. Up to 90% digestibility compared to 72% was obtained for the whole and supernatant cultures, respectively. Nutritional quality of the hydrolysate measured in terms of the protein digestibility-corrected amino acid scoring (PDCAAS) was low suggesting that addition of other amino acids would be required to use the hydrolysate as meal. The low PDCAAS value was reported to be due to the low levels of methionine and lysine (Grazziotin, 2006, 2007). The same bacterial strain was reported to completely degrade feather and produce feather protein hydrolysate even at a high raw feather concentration of 60 g/L in the culture media. Highest amounts of

soluble proteins were obtained when the pH was between 6 and 8 and temperature was 30 °C (Grazziotin, 2006, 2007).

In addition to chicken feathers, cow hairs have also been studied as potential source of keratin for animal feed (Coward-Kelly, 2006a,b). Extraction of keratin was done in an autoclave using various concentrations of calcium chloride (lime) under nitrogen atmosphere. Total nitrogen and type of amino acids in the extracted keratin was estimated using standard techniques (Coward-Kelly, 2006a,b). Percent conversion of the hair into solubilized keratin increased with increasing reaction time whereas no significant decrease was observed with change in the concentration of the feathers in the reaction. Amount of lime used directly influenced conversion with increasing amount of lime increasing the conversion up to about 60% when extraction time was 8 h. Keratin extracted from cow hairs had a highest amino acid content of 14.5% glutamine followed by leucine (9.8%) compared to 8.2% glycine and 7.4% proline for the keratin from chicken feathers. Type and amount of amino acid obtained also varied depending on the time of treatment. It was hypothesized that the poorly soluble calcium hydroxide would provide a weak and stable alkaline condition and therefore cause less damage to the amino acids produced than using strong alkali. A step-wise thermochemical treatment was suggested in order to preserve the amino acids and obtain the keratin hydrolysate with better nutritional value (Coward-Kelly, 2006a,b).

3.3 Biofuel from keratin

Degradation of feathers produces ammonia which is a biogas useful as fuel. To improve degradability and increase production of ammonia, feathers were subject to thermal, enzymatic and combined thermal-enzymatic treatments. Treatment conditions such as enzyme load, pretreatment time and inclusion enzyme on the production of methane was studied (Forgacs, 2013). Thermal treatment was done in an autoclave at 120 °C for 10 min and enzymatic hydrolysis was performed with alkaline serine protease at 55 °C for 2 or 24 h. Both batch and semicontinuous assays were done under anaerobic conditions for digesting the feathers for up to 50 days and the amount and concentration of gas released was measured. Considerable variations were observed in the degree of solubilization depending on the presence or absence of thermal and enzymatic treatments. The variations observed corresponded to the differences in the α-helix and β-sheet content (Table 3.8). A highest solubilization degree of 94% was obtained when an enzyme concentration of 2.66 mL/g was used along with thermal treatment for 24 h. The highest digestion led to the production of a considerably higher level of chemical oxygen demand (COD) at 24,400 mg/L (Forgacs, 2013). However, it was found that harsher treatment conditions may not be necessary when combined pretreatment was used and that the hydrolysis was independent of the enzyme treatment time (Forgacs, 2013).

Table 3.8: Pretreatment conditions and extent of solubilization and corresponding changes in the structure of feathers that produced various levels of ammonia (Forgacs, 2013).

Pretreatment			sCOD (mg/L)	Solubilization degree (%)	α-Helix (%)	β-Sheet (%)	Disordered region (%)
Thermal	Enzyme (mL/g)	Time (h)					
0	0	0	120	0.5	39.3	37.6	23.1
1	0	0	1,100	4.2	45.4	45.7	8.9
1	0.53	2	10,200	39.3	27.5	63.7	8.8
1	0.53	24	12,200	47.0	31.4	60.2	8.3
0	0.53	2	4,150	16.0	35.5	60.4	6.1
0	0.53	24	8,350	32.2	35.0	60.7	4.3
1	2.66	2	13,500	52.0	27.6	65.2	6.2
1	2.66	24	24,400	94.0	30.4	66.2	3.3
0	2.66	2	4,400	17.0	27.5	68.3	5.2
0	2.66	24	10,450	40.2	30.4	64.6	5.0

Note: Reproduced with permission from Springer.

3.4 Bacterial degradation of keratin

Feather degrading bacteria (wild and mutant type) were isolated from a local feather waste site and used for production of keratinase (Cai, 2008). Effect of culture conditions on the production of keratinase and residual hydrolysates were studied. Keratinolyte production was about 55 U/mL for the mutant strain compared to 25 U/mL for the wild type strain. Increasing feather content from 1 to 10 g/L increased the keratinolytic activity from 36 to 70 U/mL and a corresponding increase in residual hydrolysate was also observed (Cai, 2008). Similarly, pH of 7.5 produced enzymes with the highest activity and pH of 6.5 gave the highest residual content (Cai, 2008). Highest enzyme activity of 71 U/mL was observed at a temperature of 28 °C. Analysis of the residual content showed that cysteine content was highest at about 0.15 mg/mL followed by valine, glutamic acid and tyrosine. The new bacterial strain was found to be an effective substrate for enzyme production (Cai, 2008). Another strain *Bacillus* sp. isolated from the soil near a feather disposal site was used for production of keratinase (Cai, 2008). Chicken feathers were treated with the bacteria between pH 6 and 10 using an initial cell count of 5×10^7 cell/mL and incubating for up to 5 days. After incubation, the culture was filtered, remaining feather was collected and the % degradation was estimated. Activity of the enzyme, amount of protein generated and the molecular weight of the keratinase was determined. Enzyme activity increased from 60 to 134 kU/mL when the incubation time was increased from 1 to 5 days. About 1.6% of crude protein was extracted with a molecular weight of about 32 kDa. Enzymes

obtained from the study were considered to be suitable to replace sodium sulfide for tanning and other applications (Deivasigamani, 2008).

Feathers were degraded using a *Bacillus* strain SAA5 isolated from a feather dumping site and used as a source for production of amino acids and keratinase (Srivastava, 2011). Fermentation conditions such as time, temperature, pH and feather concentration influenced the extent of feather degradation and consequently production of enzymes (Srivastava, 2011). Up to 90% degradation of feathers and an enzyme activity of 100 U/mL were obtained. In another study, *Aspergillus flavus* and *Fusarium solani* were isolated from a feather degrading site and used to study their ability to degrade feathers and produce enzymes (Kannahi, 2012). About 0.9 and 0.6 U/mL of protease and 0.7 and 0.8 U/mL of lipase were produced. Addition of carbon, particularly sucrose increased the lipase and protease production to 61 and 71 U/mL, respectively. *A. flavus* and *F. solani* were considered to be suitable for production of enzymes from feathers (Kannahi, 2012).

Feathers were considered as cheap substrate for the production of the enzymes α-amylases and proteases using strains *Bacillus mojavensis* A21, *Bacillus licheniformis* NH1, *B. subtilis* A26, *Bacillus amyloliquefaciens* An6 *and Bacillus pumilus* A1. Medium used for culture consisted of potassium phosphate, magnesium sulfate and sodium chloride at pH 7. Incubation was done at 37 °C for 24 and 48 h (Hmidet, 2010; Gupta, 2006). Activity of the enzymes after culture was determined using standard assays and the percentage degradation of feather was determined based on the weight loss. Influence of the carbon and nitrogen sources on the production of the enzymes was also investigated. Degradation of the feathers varied from 70% to 100% depending on the bacterial strain used. When only feathers were used as the carbon source, amylase activity ranged from 0 to 6.0 U/mL and protease activity was from 170 to 2,800 U/mL. Changes in the production levels of amylase and protease by *B. licheniformis NH1* were observed when various concentrations of feathers were used. Increasing concentration of feathers up to 7.5 g/L increased the activity but higher feather concentration leads to a decrease in the activity. Supplementing the medium with yeast as a source of nitrogen increased the protease activity to 3,950 U/mL and α-amylase activity to 9.2 U/mL. Addition of glucose did not show appreciable increase in the protease activity but amylase activity increased to 9.9 U/mL (Gupta, 2006). It was concluded that feathers could be inexpensive substrates for industrial-scale production of protease and amylases.

A highly thermally resistant bacterial species *Thermoactinomyces* sp. strain CDF was found to completely degrade feather at 55 °C and was used as a single carbon and nitrogen source for the production of keratinolytic protease using chicken feathers as the substrate (Wang, 2015). A considerably high proteolytic activity as high as 267 U/mg was obtained when chopped feathers were used as the substrate and the culture was maintained at 80 °C (Table 3.9). Ability of *Thermoactinomyces* sp. to sustain temperatures as high as 80 °C was considered advantageous for large-scale enzyme production (Wang, 2015).

Table 3.9: Comparison of the proteolytic activity (specific activity U/mg) obtained using different types of substrates (Wang, 2015).

Substrate	Protease C2		Proteinase K	
	60 °C	80 °C	60 °C	80 °C
Azocasein	$(18.0 \pm 0.8) \times 10^3$	$(18.0 \pm 0.8) \times 10^3$	$(17.6 \pm 0.6) \times 10^3$	–
BSA	$(1.5 \pm 0.1) \times 10^3$	–	$(1.1 \pm 0.2) \times 10^3$	–
Azocoll	$(4.2 \pm 0.2) \times 10^3$	–	$(3.9 \pm 0.8) \times 10^3$	–
Elastin-orcein	2.0 ± 0.4	–	1.9 ± 0.4	–
Keratin-azure	17.5 ± 2.2	–	17.8 ± 2.2	–
Chopped bovine	34.5 ± 10.6	79.7 ± 7.0	49.9 ± 8.9	24.3 ± 1.5
hair	48.1 ± 4.6	87.4 ± 6.4	57.9 ± 11.5	28.7 ± 5.6
Chopped chicken	67.8 ± 5.7	125.8 ± 14.5	94.0 ± 9.8	29.6 ± 8.0
feathers	76.9 ± 8.4	268.5 ± 35.2	105.4 ± 10.0	46.8 ± 8.0

Note: Reproduced with permission from Springer.

A bacteria isolated from soil *B. amyloliquefaciens* 6B U was found to completely degrade feather keratin within 24 h and capable of producing proteases at a considerably high concentration of 610 U/mL. The keratinolytic protease 6B had optimum activity at 50 °C, pH 8 and was resistant to several common solvents and surfactants. Hydrolysates obtained after production of the enzymes were ideal for use as fertilizer (Bose, 2014). Considerable increase in plant height and weight and root length and weight were seen when the hydrolysate was used as fertilizer (Bose, 2014).

Whole chicken feathers were used to produce microbial keratinase using *Bacillus thuringiensis* Bt 407 as the bacterial strain. Amount of keratinase produced varied depending on the source of carbon, incubation time, strain of bacteria (Table 3.10) and other components used. Maximum enzyme yield was 94.5 U/mL with molecular weight

Table 3.10: Influence of various parameters on the production and activity of keratinase produced from poultry feathers (Uttani, 2018).

Strain/isolate	24 h			48 h			72 h		
	U/mL	Protein/ 100 mL (mg)	Activity (U/mg)	U/mL	Protein/ 100 mL (mg)	Activity (U/mg)	U/mL	Protein/ 100 mL (mg)	Activity (U/mg)
K1	0.22	12	0.001	4	9.6	0.41	0.02	80	0.0002
K5	0.89	30	0.029	2.5	16.5	0.15	1.34	67	0.002
K6	2.65	15	0.177	23.7	14	1.68	7.24	34	0.212
K10	1.85	10	5.40	62.6	5.2	11.96	34.6	18.4	1.880
K12	0.72	16	0.045	4.5	28.2	0.16	5.6	12	0.466

Note: Reproduced with permission through Open Access publishing.

of 33 kDa and optimum enzyme activity was observed at 55 °C and pH 8. Addition of metal ions such as Ca^{2+}, Mg^{2+} and Ba^{2+} increased enzyme activity whereas Cd^{2+}, Cu^{2+} and Fe^{+3} decreased the activity. Enzymes obtained were suitable for use as detergent (Uttani, 2018).

Instead of the conventional one-step approach, a new method of two-stage submerged fermentation was used to extract 73% of protein in pig hair and produce about 89 g/L of protein rich hydrolysate (Falco, 2019). Porcine bristles were thermally treated at 150 °C, 600 kPa for 20 min and later powdered to obtain particles of size 1.4 mm or lesser. Microorganism for the study was from the strain *Amycolatopsis keratiniphila* D2. The culture broth was inoculated with 1 mL of bacterial cells and incubated for 120 h. After the treatment, the broth was centrifuged for 5 min and the keratinase obtained was stored at −80 °C. Various conditions such as incubation temperature and meal concentration were varied to generate optimum enzyme production (Figure 3.4). In addition to the flask method, a two stage fermentation process was also used to generate the proteins and the enzymes. A maximum keratinase production of 204 kU/L was obtained after the initial step of batch fermentation compared to 148 kU/L when flask approach was used. Crude proteins obtained after the first stage were used to hydrolyze the pig bristles and obtain proteins (Falco, 2019). The two stage approach provided much higher enzymes at about 427 mg/L/h compared to 117 mg/L/h for single stage process and hence considered suitable for commercial-scale production.

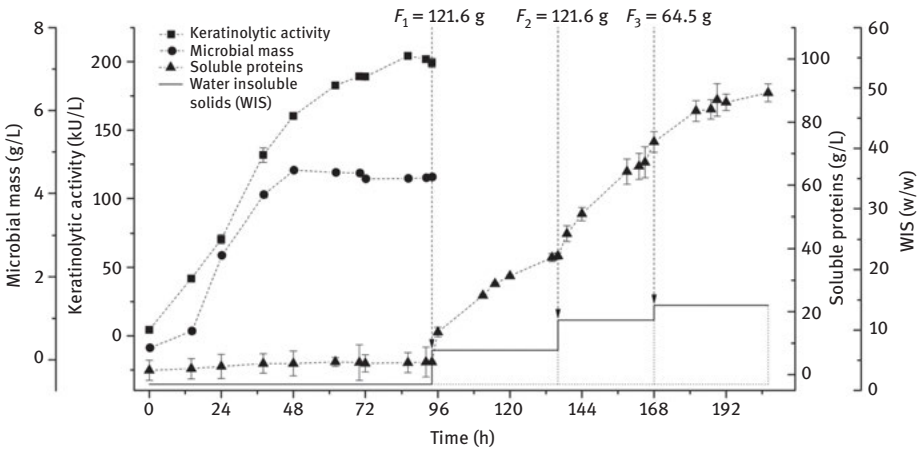

Figure 3.4: Effect of microbial concentration and incubation time on enzyme activity and soluble protein yield (Falco, 2019). Reproduced with permission from Elsevier.

3.5 Fungal strains used for keratin extraction

Similar to bacteria, several fungi have also shown to degrade feather and produce enzymes. Potential of using one of the most common fungi (*Aspergillus niger*) that is considered to be generally safe was studied for its potential to produce enzymes using keratin from various sources as the substrate (Bose, 2014). Human hair, pig hair, feather meal, chicken feathers and bovine horn were used as both the carbon and nitrogen source for the fungi at various pH to obtain different enzymes. Proteolytic and keratinolytic activity varied between the substrates and also as the culture period increased (Figure 3.5). Activity of proteolytic enzyme decreased considerably with increasing pH whereas the activity of keratinolytic enzymes increased up to pH 6.5 and later decreased (Figure 3.6). Feather meal provided both highest proteolytic and keratinolytic activity although longer time was necessary to achieve peak production of keratinase (Lopez, 2011). Feathers were exposed to considerable heat and pressure which caused partial hydrolysis that assisted in increasing the levels of enzyme production. A pH of 4.5 and culture time of 96 h was found to be optimum for production of protease compared to pH 6.5 and 48 h culture time for keratinase production (Lopez, 2011).

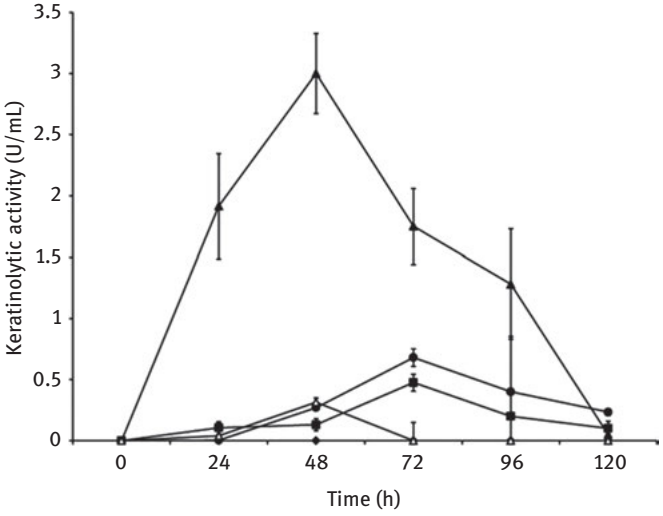

Figure 3.5: Changes in the production of protease and keratinase using various keratin sources and increasing culture time (Lopez, 2011) (■) Bovine horn, (△) chicken feathers, (▲) feather meal, (◆) human hair and (●) pig hair. Reproduced with permission from Hindawi Publishing Corporation.

A white rot wood fungus *Pleurotus pulmonarius* was used to produce keratinolytic enzyme using hair as the substrate (Inacio, 2018). The fungus was inoculated onto agar plates containing mineral media and supplemented with glucose and hair. Cultures

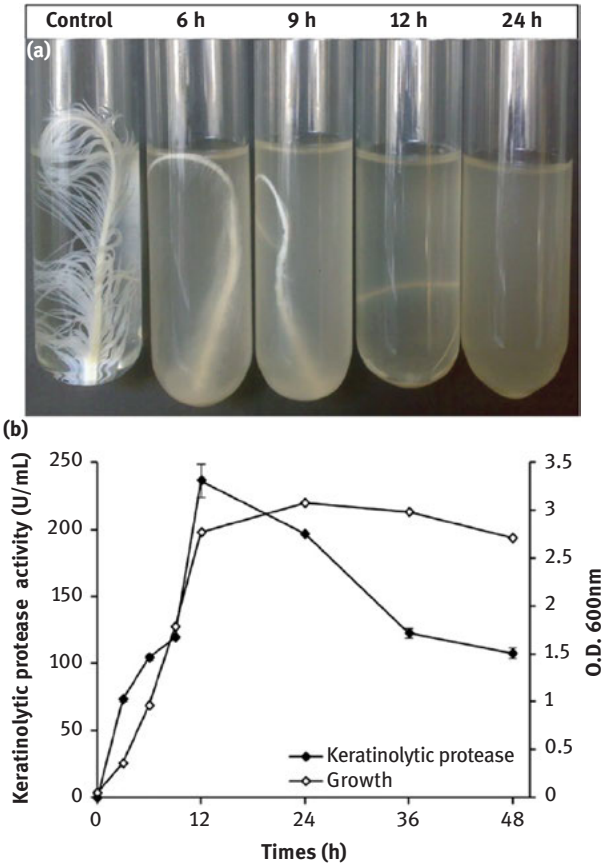

Figure 3.6: Level of proteolytic (a) and keratinolytic (b) activities with change in pH (Lopez, 2011). Reproduced with permission from Hindawi Publishing Corporation.

were maintained in the dark for 25 days at 28 °C. Later, the media was filtered and crude enzymes were extracted and used without further purification. In vitro studies were done to determine the ability of the enzyme to degrade hair, feathers, wool and beef skin. A keratinolytic activity of 26 U/mL was obtained after 15 days and about 30% of hair fibers could be degraded after 48 h. However, the enzymes were able to degrade feathers and beef skin to a considerably lower level of 23.5% and 16%, respectively (Inacio, 2018). The keratinase enzymes generated had a molecular weight of 16 kDa, similar to those produced earlier but using a different approach. A propeptide engineering approach where specific peptides were truncated and replaced with different amino acids was done to improve yield and efficiency of the enzymes produced (Su, 2019). It was found that the enzyme activity was significantly affected by the type of propeptide sequence. A full length propeptide was necessary to achieve proper folding and expression of the keratinase gene

from *B. pumilus (KerBp)*. Molecular weight of the enzyme obtained was between 30 and 40 kDa (Figure 3.7). An enzyme activity of 3,000 unit/mL which was substantially higher than previously reported using any approach was achieved using the engineered peptides (Su, 2019).

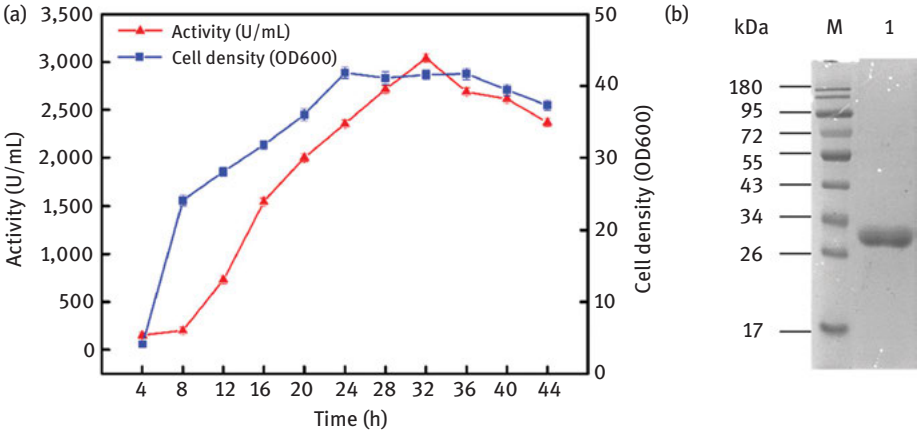

Figure 3.7: Activity, cell density (a) and molecular weight (b) of enzymes produced from the proengineered keratin at various culturing times (Su, 2019). Reproduced with permission from American Chemical Society.

Ability of various fungi isolated from soil to degrade keratin in horse hair was studied by Calin (2017). After 21 days of culture, it was observed that each fungi had a different effect on the morphology, particularly surface degradation. It was also observed that degradation was mainly due to the breakage of disulfide bonds and formation of sulfoxide (S=O) bonds. Highest amount of sulfoxide bonds were found in samples inoculated with *Fusarium* sp. strain 1A. Thermal degradation of the treated keratin was also affected with weight loss ranging from 74% to 82%, highest being for *Fusarium* sp. which was suggested to be suitable for commercial-scale degradation of keratin (Calin, 2017).

Chapter 4
Films/membranes from keratin and their applications

4.1 Pure keratin films

Films are the easiest biomaterials that can be fabricated and have been widely studied for food, medical, cosmetic, electronics and other applications. Hence, keratin from different sources has been made into films using physical, chemical and biological approaches either in 100% forms or as blends with other bio- and synthetic polymers. Keratin-based films have also been extensively studied for food, medical, biotechnology and other applications. Although keratin has been made into films, there are several limitations that lead to poor properties and limited uses. One of the major limitations of films developed from feathers is their poor stability under aqueous conditions or high humidity. Similarly, keratin films have poor flexibility and hence low elongation.

Plasticizers are extensively used to increase the elongation of films. In one such attempt, glycerol was used as the plasticizer and films were developed by solution casting (Moore, 2006). Feathers (35 g) were immersed in 400 mL of water containing 8 M urea, 30 g sodium dodecyl sulfate (SDS), mercaptoethanol and a pH 9 buffer to extract keratin. The extracted keratin was cast into films after adding either 1%, 3%, 5%, 7% or 9% of glycerol. Considerable increase in elongation of the films was obtained depending on the extent of glycerol present, but addition of glycerol considerably increases the solubility and swelling and also leads to lower mechanical properties (Table 4.1). However, changes in the mechanical properties with increasing levels of glycerol were considered as a positive attribute to control the mechanical properties of the films to the desired level. In another study, keratin extracted (79.6%) from feathers was dissolved using NaOH and combined with various amounts of glycerol. The blend solution was then cast and dried to obtain the bioplastic films (Ramakrishnan, 2018). Addition of glycerol substantially increased the plasticity of the films and hence thermal stability decreased with increasing concentration of glycerol. Similarly, tensile strength decreased from 0.3 to 0.02 MPa and modulus from 25 to 2.5 MPa when the extent of glycerol varied from 0% to 10%. Tensile properties of the films were lower compared to other reports on keratin films. Also, the elongation which should improve with addition of glycerol was not reported. Films were easily hydrolyzable when treated with protease enzymes at pH 7.5 for 10 h (Ramakrishnan, 2018).

Wool fibers treated to form cortical cells, and short fibrils were used to prepare porous biocomposite films for absorbent and biomedical applications (Patrucco, 2013). Glycerol as plasticizer was added into the keratin, and films were prepared by casting. Scanning electron microscopic image shows uniform fibers with dimensions similar to that of the cortical cells. Films made from the fibrils were highly

https://doi.org/10.1515/9781501511769-004

Table 4.1: Properties of feather keratin film containing various levels of glycerol (Moore, 2006).

Glycerol (g/g)	Water solubility (%)	Swelling index (%)	Glass transition temperature (°C)	Mechanical properties		
				Tensile strength (MPa)	Elongation at break (%)	Young's modulus (MPa)
0.00	30.7 ± 1.5	155 ± 7	70	16.6 ± 5.5	1.7 ± 0.2	10.2 ± 7.1
0.01	–	–	–	6.3 ± 0.7	11.9 ± 2.6	2.0 ± 0.8
0.03	37.0 ± 1.3	182 ± 2	67.5	7.6 ± 0.6	13.8 ± 2.4	2.1 ± 0.6
0.05	40.6 ± 3.8	191 ± 35	64.5	5.3 ± 0.7	19.8 ± 4.1	1.2 ± 0.2
0.07	48.3 ± 2.7	207 ± 15	56.3	5.4 ± 0.5	30.5 ± 7.7	0.9 ± 0.6
0.09	50.7 ± 1.0	110 ± 13	–	2.0 ± 0.2	31.9 ± 4.5	0.2 ± 0.0

Note: Reproduced with permission from Elsevier.

compact whereas films made from the cortical cells were highly porous. As observed in other studies, addition of glycerol decreases the tensile strength and modulus but increased the elongation. Although the films had good tensile properties (Table 4.2), addition of glycerol will make the fibers susceptible to water. It is also not evident if the mechanical properties are suitable for specific applications. However, both the compact and the porous films had similar moisture regain when the absorption was studied for 1,500 min (Patrucco, 2013). Instead of using glycerol, effect of sorbitol as a plasticizer for feather keratin based films was studied by Martelli (2006). Keratin was extracted from feathers using urea, SDS and mercaptoethanol, and the aqueous dispersion of keratin was combined with various concentrations of sorbitol and cast into films. As observed for glycerol, increasing concentration of sorbitol increased water solubility and water vapor permeability of the films. Tensile strength of the films decreased from 5.1 to 0.5 MPa when concentration of sorbitol was increased from 0% to 30% (Table 4.3). Interestingly, the unplasticized films had a considerably high breaking elongation of 16% which increased up to 53% just by the addition of

Table 4.2: Tensile properties of keratin films containing various levels of glycerol (Patrucco, 2013).

Samples	Tensile strength (MPa)	Elongation (%)	Modulus (MPa)
Compact film	4.0–7.9	1.4–3.1	260–297
Porous film	11.4 ± 2.4	3.2 ± 0.2	451 ± 57
Porous film + 1% glycerol	12.4 ± 1.7	3.4 ± 0.9	467 ± 24
Porous film + 5% glycerol	12.3 ± 2.1	3.5 ± 1.1	430 ± 28
Porous film + 20% glycerol	9.6 ± 2.3	7.8 ± 3.6	310 ± 48
Porous film + 50% glycerol	4.1 ± 1.3	20.8 ± 3.2	82 ± 41

Note: Reproduced with permission from Sage Publications.

Table 4.3: Tensile properties of chicken feather keratin films containing various amounts of sorbitol as the plasticizer (Martelli, 2006).

Sorbitol (g/g)	Tensile strength (MPa)	Elongation (%)	Modulus (MPa)
0.00	5.1 ± 0.2	16.3 ± 2.0	125 ± 23
0.02	3.4 ± 0.5	52.8 ± 5.6	28 ± 8
0.05	1.8 ± 0.1	42.7 ± 3.4	19 ± 4
0.10	1.2 ± 0.1	38.4 ± 3.8	9 ± 1
0.20	0.8 ± 0.1	39.5 ± 2.5	5 ± 2
0.30	0.5 ± 0.0	31.7 ± 3.5	3 ± 0

Note: Reproduced with permission from Springer.

2% of sorbital. Modulus of the films decreasing from 125 to 3 MPa occurred due to the increase in plasticizer content.

Pure keratin films were prepared by treating feather fibers using 8 mol urea, L-cysteine at pH 10.5 and stirring the mixture for 12 h at 70 °C. Dissolved keratin was precipitated by adding dilute acid and sodium sulfate, and later it was dried and powdered to obtain a yield of about 60%. To form the films, extracted keratin (15%) was added into 0.1 M sodium carbonate–sodium bicarbonate buffer having a pH of 9.5. About 10% surfactant (SDS) was also added to facilitate formation of macromolecular chains. The solution was heated at 90 °C for 1 h and aged for 24 h at room temperature. Solution formed was cast onto molds and evaporated to form the films. The films were immersed in a coagulation bath and later in a glycerol solution before conditioning and testing (Ma, 2016). Presence of SDS led to the unfolding of keratin macromolecular chains, and also prevented agglomeration of the reduced keratin and provided a homogenous solution. Amount of α-helix in keratin decreased after regeneration and β-sheet content was higher than in raw feathers. Membranes obtained had tensile strength of 3.5 MPa and high elongation of 127% suitable for various applications (Ma, 2016).

Transparent films were prepared from keratin extracted from wool, which was dissolved in alkaline solutions, and combined with sunflower oil or glycerol as plasticizer and SDS as dispersing agent. Films developed had transparency (Figure 4.1) similar to that of polyethylene and also had high thermal stability with degradation occurring at 320 °C. However, the films were affected by humidity with strength decreasing but water sorption and elongation increasing with increase in humidity. Similar observation was also seen with the addition of glycerol as plasticizer. Addition of formaldehyde decreased mechanical properties but thermal treatment at 80 °C for 24 h lead to unprecedented increase in toughness of the 28% glycerol-containing films to 19 MJ/m (Fernández-d'Arlas, 2019). Strength and elongation of the keratin films was considerably higher when compared to many other protein-based thermoplastic films (Figure 4.2).

Figure 4.1: Transparent films prepared from wool keratin using sunflower oil (left) as plasticizer compared to glycerol (right) (Fernández-d'Arlas, 2019). Reproduced with permission through Open Access publication.

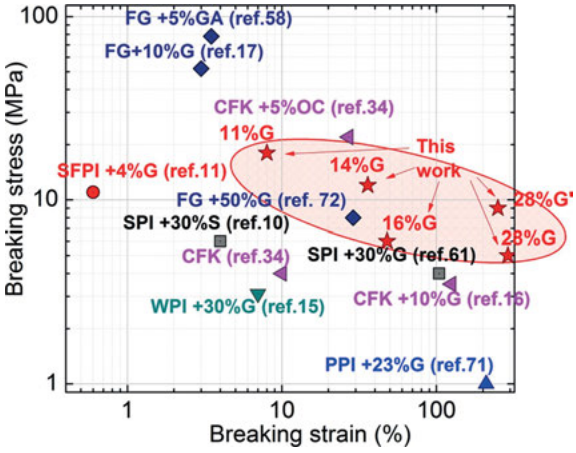

Figure 4.2: Comparison of the properties of films developed from wool keratin, plasticized with glycerol and thermally treated to achieve exceptionally high strength (Fernández-d'Arlas, 2019). Reproduced with permission through Open Access publishing.

Addition of L-cysteine (5%) into keratin solution prepared from duck feathers lead to considerable increase in mechanical properties and biocompatibility. Films containing cysteine were immersed in 10% methanol and 10% acetic acid for 2 h and glycerol was included as plasticizer. Size of cysteine was between 200 nm and 4 μm which influenced mechanical properties. A maximum tensile strength of 52 MPa was obtained but the strength decreased drastically to about 6 MPa when the films were immersed in water. Cysteine reinforcement was found to increase the mechanical properties considerably higher than that possible with previous approaches

(Table 4.4). The films were highly transparent and also supported the growth and proliferation of L929 mouse fibroblast cells (Mi, 2019).

Table 4.4: Comparison of properties of keratin films developed from various sources and using different modifications (Mi, 2019).

Material	Tensile strength (MPa)	Elongation (%)	Humidity (%)
Feather keratin	16.6 ± 5.5	1.7 ± 0.2	–
Feather keratin, Na_2S	60	–	65
Feather keratin, Na_2S	60	–	65
Carboxymethylated keratin, 15–23%	30	50	50
glycerol	17.5	–	–
Hair keratin	6.2	75	50
Wool keratin, transglutaminase, glycerol	4.7 ± 0.9	10 ± 2.3	50
Feather keratin, glycerol/sorbitol 1:3	4.2 ± 0.3	16.5 ± 2.0	50
Feather keratin (nanoclay)	5.1 ± 0.2	16.3 ± 2.0	75
Feather keratin	1.2 ± 0.1	38.4 ± 3.8	75
Feather keratin (10% sorbitol)	7.6	111	–
Feather keratin (30% glycerol)			

Note: Reproduced with permission from Elsevier.

Films in the form of biomatrices developed from wool keratin were functionalized using methylene blue for potential wound dressing and tissue engineering applications. Wool keratin was degreased and later treated with urea, sodium metabisulfite and SDS at 65 °C. Dissolved keratin was dialyzed against a 12–14 kDa membrane for 3 days and later freeze-dried to obtain the dry powder (Aluigi, 2016). To prepare films, keratin powder was dissolved (15%) in formic acid at room temperature. Films without methylene blue and with 50 and 400 μg of dye were prepared by solution casting. Dye-containing films were subject to light activation to generate reactive oxygen species that would provide antibacterial properties. Extent of antibacterial activity was directly related to the amount of reactive oxygen species (ROS) generated which was proportional to the dye content (Aluigi, 2016). Photooxidation affected protein folding and decreased the β-sheet content but marginally increased the α-helix content. Before light irradiation, the α-helix, β-sheet and β-turn content was 14%, 48% and 38%, respectively, which changed to 22%, 30% and 48% after treatment. Although no major changes were observed in the structure, the films inhibited up to 99% of *S. aureus* suggesting that the films would be suitable for medical applications (Aluigi, 2016).

Keratin extracted from human hair by the Shindai extraction method were formed into films and used as substrates for cell culture (Reichl, 2009). Extracted keratin had molecular weights in two ranges with one range being from 40 to 60 kDa and the other range between 10 and 20 kDa. The keratin dialysate was precipitated onto culture plates to form clear films after wetting and drying the solution. Films obtained were

used to culture as many as 12 different types of cells extracted from different origins. Cell proliferation studies showed that when compared to polystyrene, substantially higher cell growth was observed for the keratin-coated scaffolds, particularly for the clear films. However, the improvements obtained were dependent on the type of cells. For example, corneal epithelial cells showed improved growth whereas RPMI 2650 and PHK cells did not show any significant increase (Reichl, 2009). Coating of cell culture plates with keratin extracts was considered to be a promising approach for improved cell culture.

One of the challenges in obtaining films from keratin sources is the difficulties in dissolving using common solvents. Strong and expensive reducing agents such as mercaptoethanol are able to dissolve keratin, but result in considerable decrease in molecular weights, and hence materials made from the degraded keratin will not be suitable for industrial applications. Similarly, use of high concentration of alkali also results in severe hydrolysis and therefore poor properties of the products. To overcome this limitation, the potential of dissolving feathers using sodium sulfide and developing films was studied (Poole, 2011). For dissolution, feathers were first milled to about 3.2 mm and then digested using various concentrations of sodium sulfide at 30 °C for various time periods. Solubilized feather was centrifuged to collect the supernatant solution. Films were obtained by casting the solution and allowing the solution to dry. Water insoluble films were obtained after drying, and the excess sodium sulfide was removed through washing. It was found that the extent of dissolution of the feathers was directly proportional to the solubilization time and the concentration of sodium sulfide used. Extent of dissolution was up to 60% when the concentration of sulfide was 10 g/L and time was around 20 h. However, longer treatment times resulted in lower molecular weight keratin (10 kDa). Films cast from the sodium sulfide-treated feather solution had tensile strength ranging from 37 to 61 MPa (Table 4.5) which was higher than the strength

Table 4.5: Dry and wet (soaked in water for 30 min) tensile properties of keratin films obtained using various extraction conditions (Poole, 2011).

Sample/treatment	Modulus (MPa)		Strength (MPa)		Elongation (%)	
	Dry	Wet	Dry	Wet	Dry	Wet
0.5 h	1,241 ± 182	121 ± 39	46 ± 9	8 ± 2	7 ± 3	8 ± 3
1.0 h	1,568 ± 271	95 ± 46	61 ± 7	6 ± 2	7 ± 2	10 ± 3
6 h	990 ± 499	23 ± 10	37 ± 21	3 ± 1	5 ± 2	17 ± 4
24 h	–	17 ± 8	–	2 ± 1	–	15 ± 3
1 h + SDS	1,225 ± 73	73 ± 43	48 ± 8	5 ± 1	5 ± 1	15 ± 6
2% ME	1,344	–	30	–	3	–
2% ME + SDS	10	–	17	–	2	–
Polyester resin	4,000	–	48–85	–	2	–

Note: Reproduced with permission from Springer.

of the films obtained using mercaptoethanol as the reducing agent. Films made using sodium sulfide also had higher elongation. However, treating feathers with sulfide for 24 h resulted in films that were too brittle and could not be tested. It was suggested that sodium sulfide was an inexpensive chemical that was suitable for large-scale extraction of keratin for industrial applications but the extraction conditions have to be controlled (Poole, 2011).

Keratin extracted from merino wool was regenerated in the form of films and the properties of the regenerated films were studied. To extract keratin, the wool fibers were put into urea solution (8 M) and m-bisulfite at pH 6.5 along with 5 N NaOH and treated for 2 h at 65 °C. After treatment, the solution was dialyzed against 12,000 to 14,000 molecular weight tube for 3 days at room temperature. The keratin solution was poured onto polyester plates to form the films. In addition to the films formed from the dialyzed solutions, the films were dissolved in concentrated formic acid and again recast into films (Aluigi, 2007). Considerable changes in the amino acid content and molecular weight were seen between the wool, films regenerated from water and that regenerated using formic acid. Regenerated keratin had similar molecular weight as the raw keratin during the initial period of extraction but complete degradation occurred after 3 months. Formic acid regenerated keratin had higher thermal stability due to higher amounts of crystalline structure (Aluigi, 2007). Keratin extracted from wool was mixed with potassium hexatitanate ($K_2Ti_6O_{13}$) whiskers and cast as films. Addition of the whiskers (up to about 3%) increased the strength and elongation but higher whisker content decreased the strength and particularly the elongation to a large extent (Liu, 2010) (Figure 4.3). In addition to the amount of whiskers, the orientation of the whiskers and the presence of coupling agent influenced and increased the tensile properties (Liu, 2010).

In another study, merino wool in fabric form was dissolved using an ionic liquid (1-butyl-3-methylimidazolium chloride ($[BMIM]^+ Cl^-$) at various temperatures (120, 150 and 180 °C) and the changes in structure and properties were determined. The dissolved keratin was dried into powder and later mixed with glycerol and made into films by compression molding at 120 °C and their properties were measured (Ghosh, 2014). Amount of keratin decreased with increasing extraction temperature since water-soluble peptides and amino acids were generated. Highest yield obtained was 57% at 120 °C compared to 18% at 180 °C (Ghosh, 2014). Considerable changes were also observed in the amino acid content in the keratins extracted at various temperatures. Raw wool fibers had molecular weights between 75 and 37 kDa and few low-molecular-weight proteins between 20 and 10 kDa. After hydrolysis in the ionic liquids, the bands between 37–75 kDa disappeared and reappeared as weak bands between 20 and 30 kDa. Structurally, shifting of the β-sheet and α-helix bands was observed and the amount of β-sheet was 25% and α-helix content was 75%. Stress–strain curves show that increasing dissolution temperature decreased the strength but increased the elongation. Decrease in strength was suggested to be mainly due to the reduction in molecular weight.

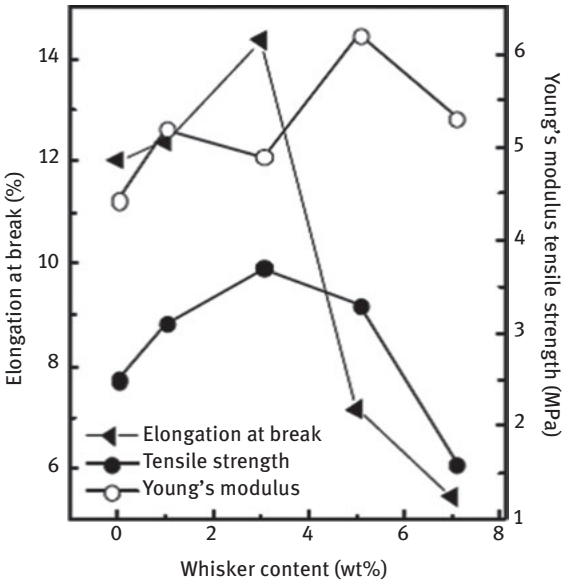

Figure 4.3: Tensile properties of keratin films made using various percentages of potassium hexatitanate whiskers (Liu, 2010). Reproduced with permission from Academic Journals.org.

In a unique approach, keratin extracted from human hair was made into films for periodontal tissue regeneration. The nonimmunogenicity and antibiotic eluting properties of keratin were considered to be ideal for tissue regeneration. Keratins used for this application had molecular weight between 40–60 kDa and formed transparent films with thickness of about 80 μm. Minocyclin loaded on the film had a release rate of 62% to 67% within 48 h depending on the release medium. YD-8 human oral epithelial cells, human gingival fibroblasts (hTERT-hNOF) and human periodontal ligament cells (hPDL) showed excellent proliferation on the keratin films. The cells also expressed high amounts of cytoskeleton and β1 integrins indicating that the cells were adhered on the keratin membranes (Lee, 2015).

In addition to developing films from keratin through solution casting, keratin films have also been made by thermal processing. However, keratins are non-thermoplastic and hence need chemical/physical modifications to convert them into films. Films were developed using wool keratin (S-sulfo keratin) that was extracted using urea and sodium metabisulfite (Katoh, 2004a). Extracted powder was mixed with water and ethanol, and the slurry was compression molded between 70–160 °C at a pressure of 10 MPa for 5 min to form films with thickness between 0.3 and 0.4 mm. Properties of the films were dependent on the molding temperature with temperature between 100 °C and 120 °C providing higher strength and modulus (Table 4.6) since the proteins could melt uniformly at higher temperatures (Katoh, 2004a). Molding temperature also affected the water uptake with 100 °C molded films providing the

Table 4.6: Tensile properties of S-sulfo keratin films made using various compression temperatures (Katoh, 2004a).

Molding temperature (°C)	Strength (MPa)	Elongation (%)	Modulus (MPa)
70	11.5 ± 2.3	2.1 ± 0.5	697 ± 80
80	7.9 ± 2.7	1.1 ± 0.5	879 ± 88
100	25.7 ± 2.6	3.4 ± 0.9	1,168 ± 27
120	27.8 ± 2.9	3.5 ± 0.8	1,218 ± 80
140	21.8 ± 2.7	4.7 ± 0.7	946 ± 27
160	17.7 ± 1.7	3.4 ± 0.6	710 ± 82

Note: Reproduced with permission from Elsevier.

lowest (49%) uptake and the 70 °C compression molded films providing the highest (174% uptake). Water uptake and swelling ratio of the films was also affected by pH with alkaline pH resulting in hydrolysis and, therefore, higher swelling and eventual dissolution of the films (Katoh, 2004a). Fibroblast cells cultured on the films showed similar attachment and proliferation compared to culture plates suggesting that the films could be suitable for medical applications.

4.2 Cross-linking keratin films

Cross-linking is generally done to improve the mechanical and aqueous stability of biopolymeric materials. Keratin extracted using urea, SDS and mercaptoethanol was made into films by solution casting. To improve stability, chitosan was included into the solution and the films were also cross-linked with ethylene glycol diglycidyl ether (EGDE) and glycerol diglycidyl ether (GDE) (Tanabe, 2002; 2004). EGDE provided highest tensile strength of 27 MPa similar to the strength obtained when 30% chitosan was added. Cross-linkers provide higher elongation than addition of chitosan and modulus of cross-linked films was also higher than that of chitosan-containing films (Table 4.7). Cross-linking was also more efficient in reducing the swelling compared to addition of chitosan. Films containing chitosan swelled up to 126% due to the hydrophilicity of chitosan. Cross-linked films were able to maintain their stability and even had higher mechanical properties after immersion in water (Tanabe, 2004). However, presence of chitosan promoted the attachment and proliferation of cells, whereas the cross-linker, particularly GDE, made the films cytotoxic. Observations of the films showed some cell proliferation on the EGDE cross-linked films but the GDE cross-linked films did not show any cell attachment and growth (Tanabe, 2004).

Keratin extracted from chicken feathers was made into films with thickness from 0.07 to 0.12 mm and cross-linked using dialdehyde starch (DAS) for potential use in food packaging (Dou, 2015). Glycerol was added to improve plasticity of the films. Aldehyde groups in starch could react with the functional groups in the

Table 4.7: Tensile properties of keratin films after cross-linking or addition of chitosan. Weight of keratin used for film formation was 100 mg (Tanabe, 2004).

Treatment	Strength (MPa)	Elongation (%)	Modulus (MPa)
EGDE, 7.5 mg	27 ± 6	6 ± 1	350 ± 74
EGDE, 15 mg	23 ± 6	12 ± 6	372 ± 235
EGDE, 30 mg	10 ± 1	14 ± 8	250 ± 70
GDE, 7.5	15 ± 7	13 ± 5	210 ± 73
GDE, 15 mg	11 ± 6	8 ± 2	250 ± 92
GDE, 30 mg	8 ± 2	14 ± 6	178 ± 38
Chitosan, 20 mg	34 ± 8	7 ± 2	176 ± 82
Chitosan, 30 mg	27 ± 9	5 ± 2	310 ± 161

Note: Reproduced with permission from Elsevier.

proteins leading to the formation of inter- and intramolecular cross-links. Further, the aldehyde groups in starch could react with the hydroxyl groups in keratin leading to hemiacetal cross-linking. Such extensive cross-linking was suggested to provide substantial improvements in stability and mechanical properties. Films obtained had good transparency (Figure 4.4) but increasing content of DAS turned the films brownish due to Maillard reaction. Tensile properties of the films showed that addition of glycerol was necessary to obtain flexible films. Tensile strength decreased but elongation increases more than 200% when the glycerol content was increased to 40% from 30%. Addition of cross-linking agent (DAS) decreased strength which was suggested to be due to the counter action of plasticization and cross-linking. However, solubility of the films decreased after cross-linking and water vapor permeability showed marginal changes (Table 4.8**)** (Dou, 2015).

Figure 4.4: Transparent films were obtained by combing feathers with dialdehyde starch (Dou, 2015). Reproduced with permission from Royal Society of Chemistry.

Table 4.8: Tensile properties of keratin films containing 30% and 40% glycerol and cross-linked with 2%, 5% or 10% dialdehyde starch (Dou, 2015).

Sample glycerol-DAS	Moisture content (%)	Solubility (%)	Strength (MPa)	Elongation (%)	Water vapor permeability (10^{-10} g/m^2 s Pa)
30–0	21.8 ± 1.1	44.7 ± 2.1	4.5 ± 1.2	19.0 ± 10.0	3.5 ± 0.2
30–2	17.3 ± 0.9	39.3 ± 0.8	2.9 ± 0.8	22.3 ± 1.8	4.1 ± 0.1
30–5	14.8 ± 1.5	41.0 ± 1.1	4.1 ± 0.4	11.3 ± 3.7	3.1 ± 0.4
30–10	18.0 ± 0.4	36.0 ± 8.3	2.8 ± 0.4	9.1 ± 4.2	3.1 ± 0.2
40–0	20.7 ± 2.5	61.9 ± 3.1	3.8 ± 0.7	38.0 ± 11.4	4.6 ± 0.8
40–2	17.6 ± 1.2	54 ± 1.8	1.3 ± 0.1	36.0 ± 0.9	5.3 ± 0.6
40–5	15.2 ± 0.9	47.6 ± 0.7	1.2 ± 0.1	38.0 ± 3.5	4.4 ± 0.8
40–10	18.9 ± 1.3	48.4 ± 2.3	1.5 ± 0.3	36.7 ± 11.8	3.6 ± 0.3

Note: Reproduced with permission from Royal Society of Chemistry.

Feathers or other sources of keratin have been hydrolyzed and made into films. Typically, hydrolysis is done using alkali or strong reducing agents such as mercaptoethanol (Poole, 2015). However, such strong hydrolysis results in considerable decrease in molecular weight resulting in poor properties of the products. To overcome this limitation, feathers were digested using sodium sulfide as the reducing agent since it can evaporate and does not leave any trace in the products to be developed (Poole, 2015). Reduction was performed by treating 50 g of feathers with 10 g/L Na_2S under nitrogen atmosphere. Keratin extracted had a molecular weight of about 10 kDa and some 20 kDa dimers. Supernatant obtained during reduction of the keratin was poured onto petri dishes and formed into films. Several physical and chemical treatments including cross-linking and addition of nanoparticles were done to improve the mechanical properties of the films. Cross-linking the films with formaldehyde led to substantial increase in dry strength, but the wet strength did not show any improvement. Similarly, dry and wet modulus both increased after cross-linking. However, addition of microcrystalline cellulose decreased the strength and modulus appreciably due to inhomogeneous dispersion and poor compatibility (Table 4.9). Tensile properties of the keratin films obtained in this research were considered to be better than protein films previously reported and comparable to that of synthetic polymer-based films (Poole, 2015). Hydrolyzed feather keratin was combined with porcine gelatin and made into films and electrospun membranes. Later, the materials were cross-linked with g-glycidyloxypropyl trimethoxysilane (Fortunato, 2019). Electrospun samples had fibers with diameters of 1.7 ± 0.35 μm when electrospun at 35 kV and 1 μm when electrospun at 50 kV. Elastic modulus of the films varied from 100 to 750 kPa compared to 30–70 MPa for the electrospun membranes, similar to that of skin. The modulus of the membranes was controllable based on the ratio of keratin and gelatin. Membranes were biocompatible

Table 4.9: Comparison of the dry and wet tensile properties of keratin films cross-linked or containing various levels of microparticles (Poole, 2015).

Sample	Strength (MPa)		Modulus (MPa)	
	Dry	Wet	Dry	Wet
Control	56 ± 9.3	7.1 ± 1.5	1406 ± 366	79 ± 24
Formaldehyde 21 °C	79 ± 1.9	8.7 ± 0.4	1632 ± 52	90 ± 4.7
Formaldehyde 105 °C	62 ± 3.2	8.5 ± 0.6	1727 ± 58	84 ± 7.8
Glutaraldehyde 21 °C	66 ± 2.7	8.2 ± 0.4	1391 ± 86	79 ± 3.8
Metal catalyzed	56 ± 1.5	7.0 ± 0.7	1160 ± 86	57 ± 3.7
MC Avicel PH101	52 ± 2.1	4.3 ± 0.1	1132 ± 51	32 ± 2.0
MC Novagel GP 2180	40 ± 3.0	5.1 ± 0.3	853 ± 64	40 ± 2.2
MC Novagel GP 3282	33 ± 6.1	2.7 ± 0.3	748 ± 125	25 ± 2.3
Montmorillonite	54 ± 2.6	4.6 ± 0.2	1133 ± 49	35 ± 3.1

Note: Reproduced with permission from Springer.

and supported the colonization of epithelial cells, rat neurons and primary fibroblasts, suggesting their suitability for tissue engineering and regenerative medicine (Fortunato, 2019).

Keratin was extracted from duck feathers by treating with urea, SDS and sodium bisulfite and heating the solution at 90 °C for 4 h. Obtained keratin was dispersed in-water and alcohol with the addition of plasticizer along with formaldehyde (37–40%) as the cross-linking agent. Keratin was also made into films by treating the films with DMF for 2 h at 90 °C and without using the reducing agents. Properties of the films obtained are given in Table 4.10. Increase in elongation but decrease in strength was observed with the addition of the plasticizer. Cross-linking with formaldehyde made the films resistant to water but caused cytotoxicity. 1,8-Octanediol

Table 4.10: Properties of films made from duck feather keratin plasticized with 1,8-octanediol (OD) or glycerol (gly) and cross-linked with formaldehyde (Liu, 2018a).

Plasticizer, (g/g)	Moisture content (g/g)	WVP × 10^{-10} [g/(m.s.Pa)]	Thickness (mm)	Tensile strength (MPa)	Elongation at break (%)
0	0.13 ± 0.026	0.106 ± 0.024	0.219 ± 0.026	12.1 ± 0.2	2.3 ± 0.5
0.05– OD	0.18 ± 0.033	0.259 ± 0.007	0.220 ± 0.017	11.6 ± 0.3	4.3 ± 0.2
0.10– OD	0.19 ± 0.064	0.344 ± 0.022	0.256 ± 0.009	10.7 ± 0.1	6.0 ± 0.2
0.20– OD	0.22 ± 0.037	0.651 ± 0.078	0.247 ± 0.012	9.4 ± 0.6	8.2 ± 0.7
0.30– OD	0.29 ± 0.020	0.808 ± 0.040	0.248 ± 0.021	8.0 ± 0.3	11.6 ± 0.4
0.20–gly	–	3.218 ± 0.235	0.235 ± 0.018	5.4 ± 0.4	18.4 ± 1.8
0.30–gly	–	3.748 ± 0.146	0.225 ± 0.011	3.6 ± 0.2	22.5 ± 4.5

Note: Reproduced with permission from John Wiley and Sons.

was suggested to provide lower flexibility but better hydrophobicity compared to glycerol as plasticizer (Liu, 2018a).

Ability of human hair keratin to be made into membranes suitable for guided tissue regeneration were developed using dityrosine bonding (Navarro, 2019). Extracted keratin was dissolved using phosphate-buffered saline (PBS) (pH 7.4) at 4% concentration and combined with a photosensitive initiator–catalyst–inhibitor solution. This mixture was exposed to UV light for the cross-linking/curing to occur and form a resin (Figure 4.5). Extent of cross-linking and properties of the resin could be controlled by varying the UV light intensity, exposure time, resin volume and so on. The proposed mechanism of formation of the resin through free-radical reactions, process of preparing the resin and actual resin samples are shown in Figure 4.5. A parameter called energy density was calculated to relate the composition and processing of the resin with its mechanical and performance properties. As shown in Figure 4.6, the percentage of swelling, compressive stress, transport properties and ultimate stress could be controlled by varying the energy density. Protein-based biodegradable membranes suitable for guided tissue regeneration for surgical reconstruction of periodontal and bone defects could be developed using this approach (Navarro, 2019).

In addition to cross-linking using chemicals, films made from wool keratin have been cross-linked using transglutaminase (Cui, 2013). The enzyme was added into the keratin solution along with 15 g/L glycerol and 10 mmol/L dithiothreitol, and the mixture was poured onto glass plates and made into films. Increasing concentration of the enzyme or the cross-linking time increased the strength of the films but decreased the elongation (Cui, 2013) (Figure 4.7). Molecular weight of keratin had also increased from 66 kDa to about 116 kDa due to cross-linking. More importantly, the solubility of the films in PBS and in artificial gastric juice (AGJ) decreased considerably after cross-linking (Figure 4.8). As scaffold for drug delivery, the films showed about 80% cumulative release of diclofenac after 25 h in PBS solution but the release was only about 12% in AGJ. As can be expected, the cross-linked films have slower release than the noncross-linked samples. Keratin films were also reported to support the growth of cells and hence were suitable for tissue engineering applications (Cui, 2013).

4.3 Blends of keratin with other biopolymers

Keratin was combined with hydroxyapatite (HA) and made into dense and porous films and implanted in the long bones of sheep for up to 18 weeks (Dias, 2010). Nanoindentation tests were done to determine the mechanical properties of the films and tissue formed during the study period. Up to 40% hydroxyapatite was used in the films similar to that found in commercial biomaterials used for bone regeneration. Keratin–HA films did not have any inflammation or cause infection during the entire period of study. These films had similar performance compared to

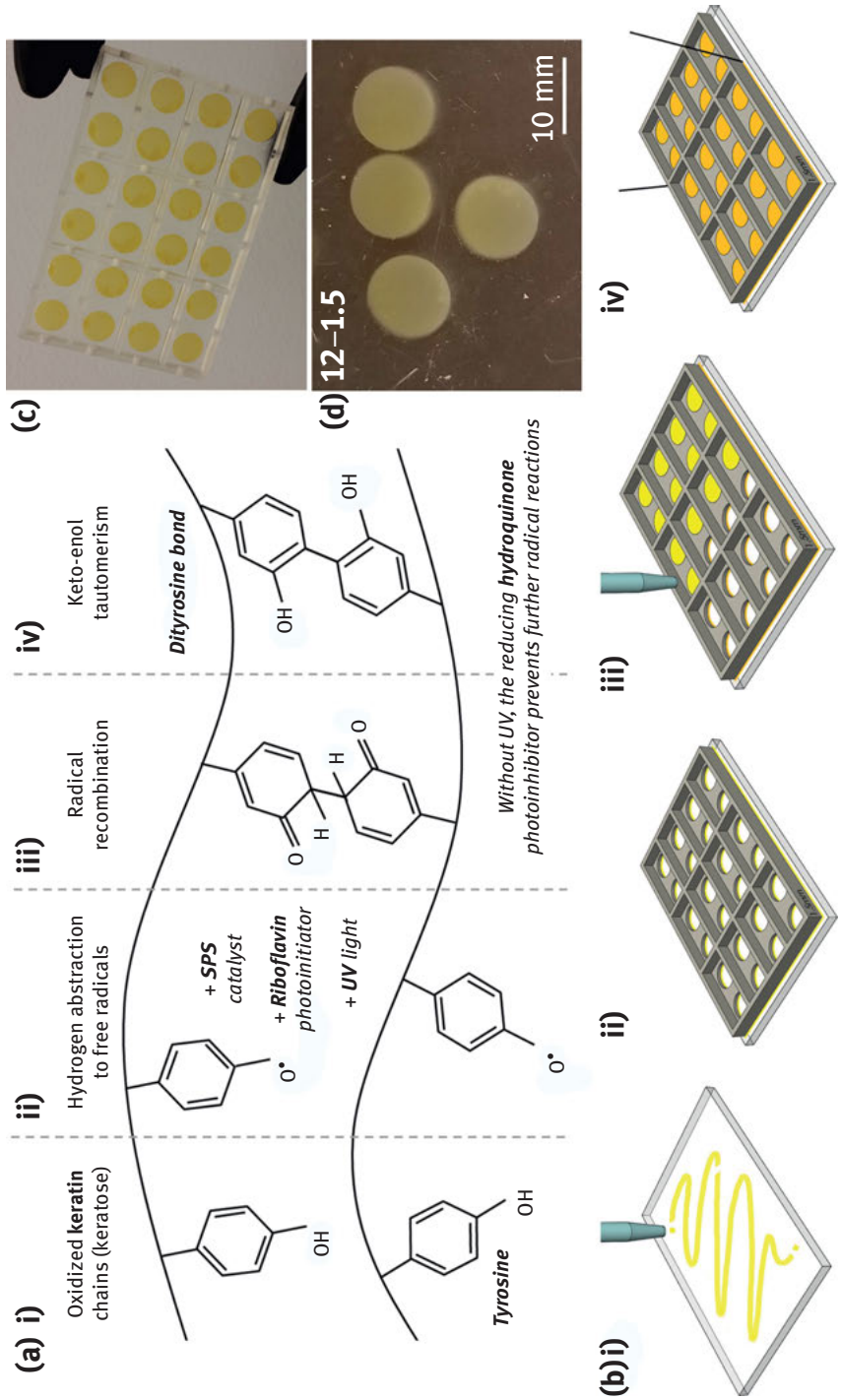

Figure 4.5: Steps involved in the formation of cross-linked membranes through UV-induced free-radical reactions (a), converting the solution into resins (membranes) (b), membranes in molds (c) and in PBS solution (d) (Navarro, 2019). Reproduced with permission from Elsevier.

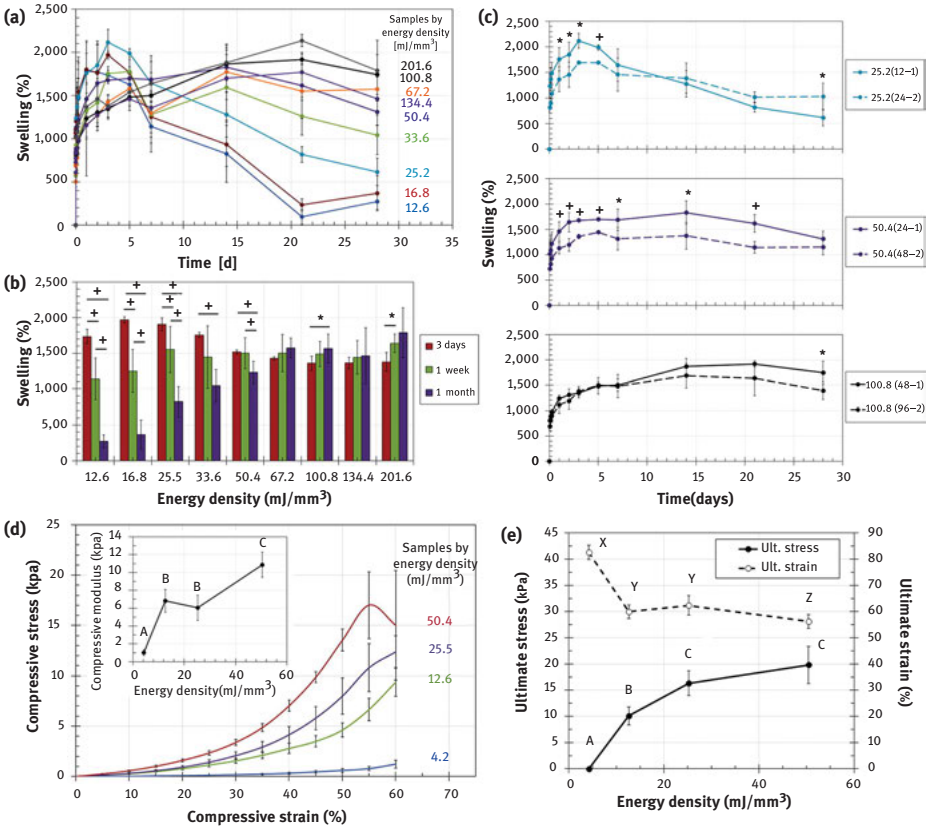

Figure 4.6: Influence of energy density on the properties of membranes prepared from keratin as resin for guided tissue regeneration (Navarro, 2019). (a) Swelling profiles of keratin hydrogels in MEM as a function of ED; (b) The drop in swelling capacity between days 3 and 28; (c) Viability of the ED parameter at different combinations of thickness and exposure time; (d-e) Mechanical characterization of the hydrogels shows the relation between ED and elastic modulus, ultimate stress, and ultimate strain. Reproduced with permission from Elsevier.

the commercially available poly(lactic acid) (PLA)–HA scaffold. However, the porous keratin–HA films had considerably higher healing ability than PLA–HA or the dense keratin–HA films (Dias, 2010). Bone filling defect had completely healed and indentation studies showed that the mature bone formation had occurred when the porous scaffolds were used. Reconstituted keratin–HA scaffolds were considered ideal as bone graft materials (Dias, 2010). To mimic the properties of biominerals, HA crystals were deposited onto keratin extracted from wool and form a bionanocomposite film (Li, 2012). Wool was dissolved in alkali solution and keratin obtained was dried and formed into powder. HA was added into various concentrations of the keratin solution and coprecipitated to form the composite. Up to 86% HA crystals

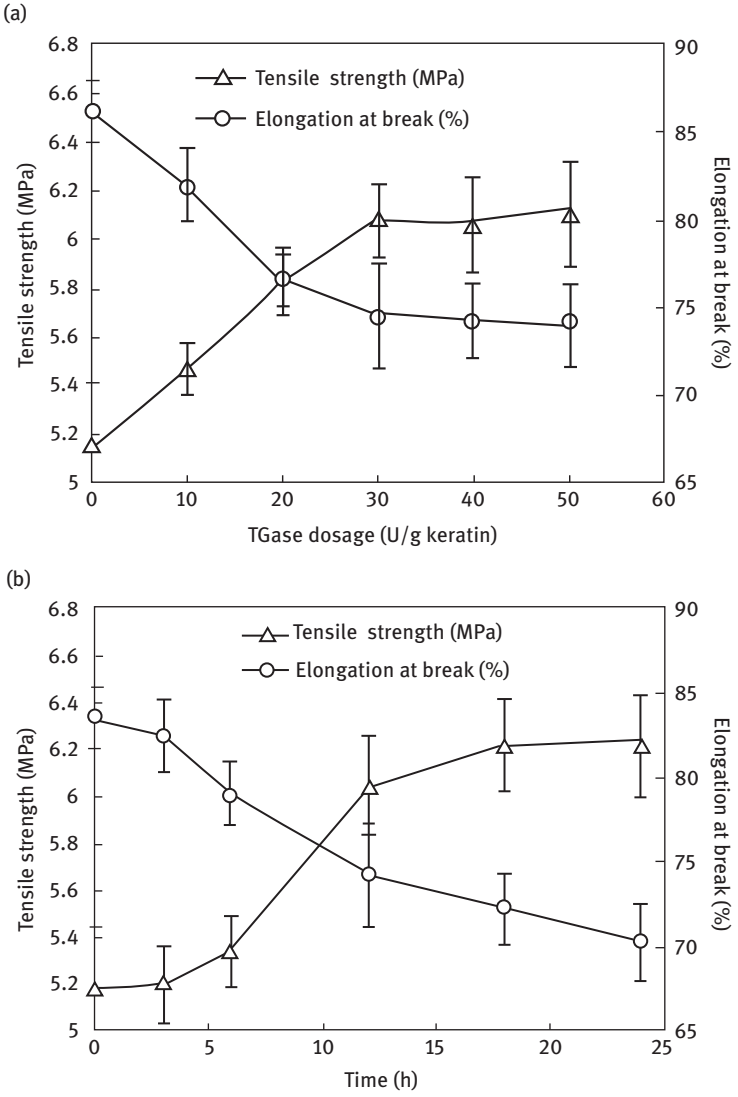

Figure 4.7: (a) and (b) Changes in the tensile strength and elongation of noncross-linked and TGase cross-linked keratin films with increasing concentration of enzyme and cross-linking time (Cui, 2013). Reproduced with permission from John Wiley and Sons (Cui, 2013).

(20–50 nm in length and about 10 nm in width) could be added to the keratin depending on the concentration of the keratin in the solution. It was suggested that the amount of HA on the keratin was similar to that found in natural bones (69–80%) and therefore the scaffold could be suited for bone tissue engineering (Kavitha, 2005). When osteoblasts were seeded onto the HA and the keratin/HA nanocomposite, higher

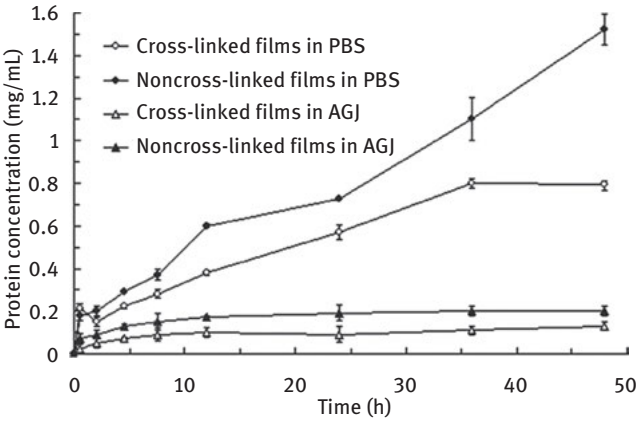

Figure 4.8: Cross-linked films have lower solubility than the uncross-linked films in both phosphate-buffered saline and artificial gastric juice (Cui, 2013). Reproduced with permission from John Wiley and Sons.

number of live cells and higher cell proliferation was observed on the composite films suggesting suitability for tissue engineering applications (Kavitha, 2005). In another study, keratin obtained from wool was combined with various ratios of HA and made into films for tissue engineering and other applications (Tu, 2016). Predetermined (0% to 35%) HA along with 2% glycerol was added into keratin solution and the blend was cast onto plates and dried at 50% humidity, 25 °C for 48 h to form the films. Agglomeration of the HA particles (70–100 nm in length and 20–30 nm in width) was observed in the fibers. Phase separation between the two polymers and decrease in transparency of the films was observed as the amount of HA increased.

Keratin extracted from bovine horns was combined with chitosan and made into films (referred as biosheets) for potential use as tissue engineering scaffold (Singaravelu, 2015). Films developed were tested for their mechanical properties, thermal stability and potential to support the attachment and proliferation of mouse fibroblast cells (Singaravelu, 2015). Increasing ratio of chitosan increased strength and modulus substantially but decreased elongation by more than 50%. Addition of chitosan increased the swelling of the films which was considered to be beneficial for wound healing. Mupirocin loaded on the films showed a burst release of about 32% within 1 h but a sustained release of up to 64% was obtained at the end of 92 h. The sheets were found to be biocompatible with more than 90% cell viability. In fact, the keratin sheets showed higher attachment and proliferation than the chitosan sheets (Singaravelu, 2015). Presence of chitosan also imparted the fibers with antimicrobial properties making the films suitable for wound dressing applications.

Keratin extracted from feathers was made into particles, and later combined with glycerol and microcrystalline cellulose and the solution was cast into films (Sharma, 2018). Before the extraction, feathers were treated with petroleum ether to

remove grease and any microorganisms. Keratin was extracted from the feathers by immersing the feathers in 100 to 500 mM of sodium sulfide and digesting at temperatures between 30 °C and 65 °C for 1–6 h, and the solution formed was freeze-dried to obtain powdered keratin with a yield of about 82%. To obtain films, keratin was dissolved in NaOH for 48 h at 60 °C and combined with 3.5% glycerol and 0.2% microcrystalline cellulose. Blend solution was poured onto Petri plates and allowed to air dry and form films. Keratin after extraction had increased β-sheet content and decreased α-helix content compared to untreated feathers (Figure 4.9). X-ray diffraction studies confirmed increase in β-sheet content but a decrease in crystallinity was also observed. Films prepared were transparent, (Figure 4.10) and mechanical properties were mainly dependent on the amount of glycerol added. Tensile strength varied from 1.7 to 3.6 MPa and elongation up to 31% (Sharma, 2018). Films were considered to be ecofriendly as they were developed using natural polymers.

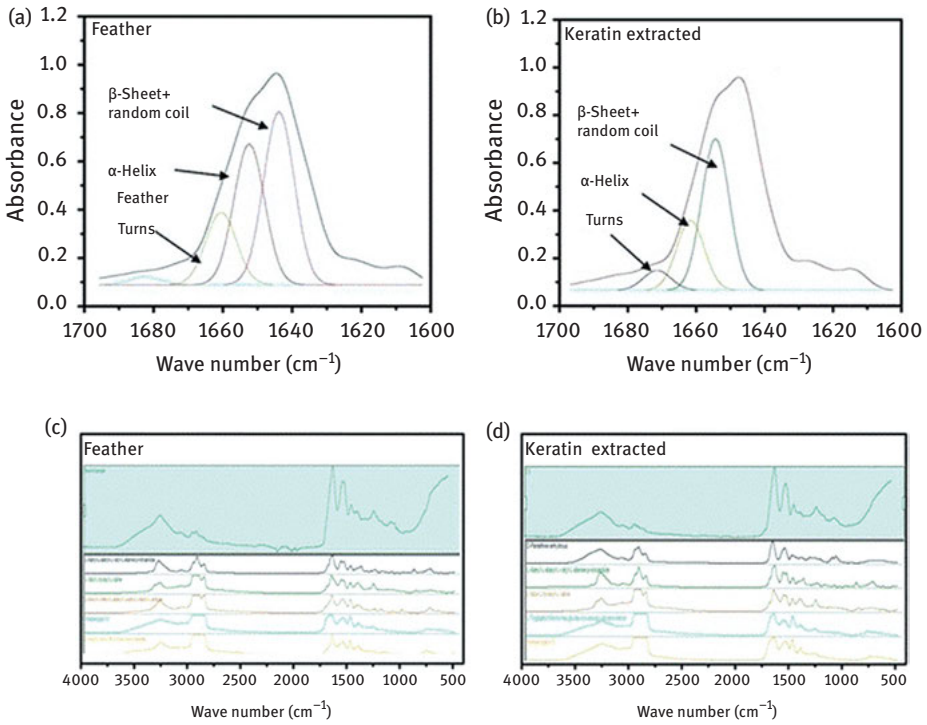

Figure 4.9: Changes in the β-sheet and α-helix content of feathers (a, c) and keratin extracted (b, d) from the feathers based on FTIR studies (Sharma, 2018). Reproduced with permission from Springer.

In another study, keratin was made into films by blending with sodium alginate and substantial changes were observed in the structure and properties of keratin depending on the ratio of the two polymers (He, 2017). Feathers were treated with per acetic

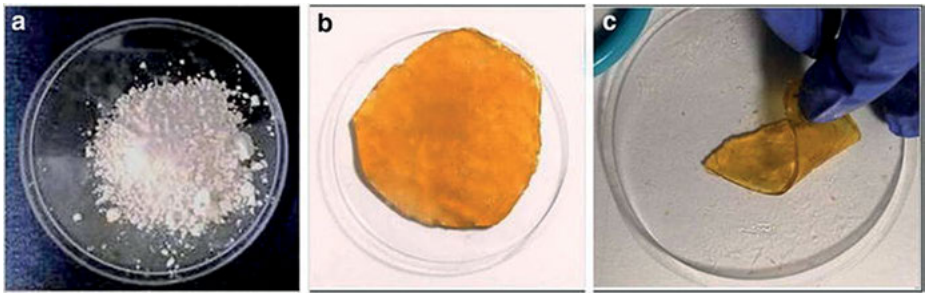

Figure 4.10: Digital images of keratin powder (a), transparent film without glycerol (b) and after addition of glycerol (c) (Sharma, 2018). Reproduced with permission from Springer.

acid at 60 °C for 100 min and the solution was later dialyzed to obtain keratin powder. Blend films were prepared by combining keratin powder with sodium alginate under alkaline conditions (pH 9.5) and sorbital (24%) was added as the plasticizer. Fourier-transform infrared spectroscopy (FTIR) studies showed good interaction between keratin and alginate due to the formation of hydrogen bonds. Such good interaction between the two polymers led to high mechanical properties of films (Table 4.11). A marginal increase in thermal stability of the films was also observed. It was suggested that alginate provided keratin with properties required for use in packaging and biomedical applications (He, 2017).

Table 4.11: Properties of pure keratin and films containing 10% to 50% alginate (He, 2017).

Sample	Thickness (mm)	Tensile strength (MPa)	Elongation (%)	Moisture content (%)	Water vapor permeability ($\times 10^{-10}$ g/(m^2 s Pa^2))
Pure keratin	0.171 ± 0.006	2.83 ± 0.21	25.5 ± 2.4	8.3 ± 0.4	3.6 ± 0.2
10% alginate	0.163 ± 0.006	6.03 ± 0.24	27.6 ± 3.3	8.4 ± 0.3	3.4 ± 0.2
20% alginate	0.147 ± 0.006	8.95 ± 0.42	24.8 ± 6.8	9.9 ± 0.6	3.1 ± 0.3
30% alginate	0.140 ± 0.010	10.60 ± 0.71	28.0 ± 3.5	9.3 ± 0.2	2.8 ± 0.2
40% alginate	0.137 ± 0.006	13.21 ± 1.81	25.2 ± 2.1	9.2 ± 0.3	3.2 ± 0.3
50% alginate	0.120 ± 0.006	16.30 ± 0.15	29.2 ± 0.3	9.4 ± 0.4	3.7 ± 0.2

Note: Reproduced with permission from John Wiley and Sons.

A blend of silk sericin and wool keratin was made into transparent films with properties suitable for medical, electronics and other applications (Tu, 2016, Chen, 2017). It was hypothesized that wool keratin and silk sericin had distinct and considerably different secondary structures and the interaction between these two molecules was not predictable (Tu, 2016). However, interactions between keratin and fibroin chains led to the formation of β-crystallites due to the assembly of several β-strands and gradual assembly of the layers and eventual cross-linking (Figure 4.11). Studies showed that a

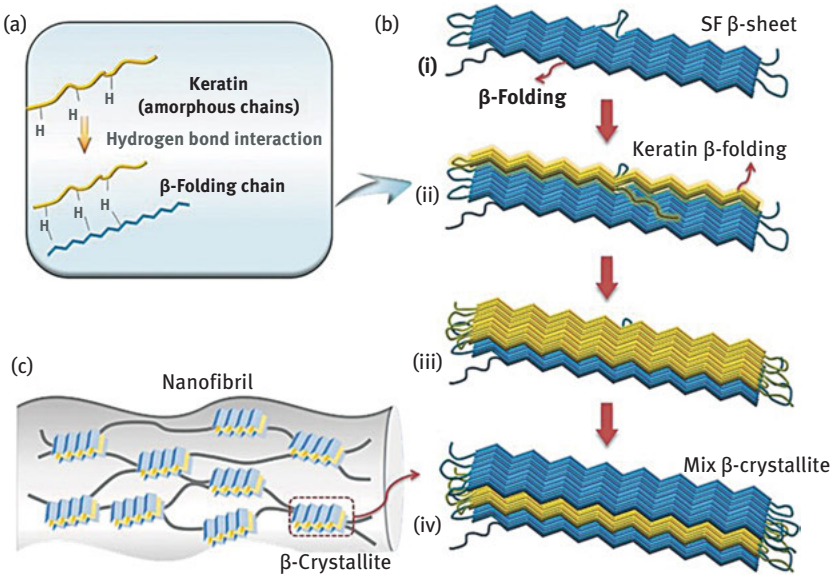

Figure 4.11: Schematic representations of potential hydrogen bonding between keratin and silk proteins (a), formation of β-crystallites in a layer-by-layer form [(b) i–iv], cross-linking of β-crystallites with amorphous chains to form the network structure (c) (Tu, 2016). Reproduced with permission from John Wiley and Sons.

gradual transition of β-sheets in silk into α-helices occurred with increase in keratin content. For instance, β-sheet content decreased to 15% from 39% and α-helix content increased from 8 to 18%. It was suggested that interactions between sericin and keratin through cross-linking of hydrogen bonds and rearrangement of secondary structure would have occurred. Interestingly, it was demonstrated that increase in β-sheet content led to a linear increase in stress and modulus and decrease elongation (Figure 4.12). Blend films showed significant absorption of UV light and hence suggested to be useful for protection against UV degradation (Chen, 2018a).

Composite films composed of keratin, with cellulose and/or chitosan were prepared using the ionic solvent ($[BMIm^+Cl^-]$). The process used to form the composite films is shown in Figure 4.13 (Tran, 2016). Cellulose–keratin blends had higher tensile strength and thermal stability compared to cellulose–chitosan blends. Keratin in the blends had lower α-helix and higher β-sheet content but no changes were observed in the primary structure of either keratin, cellulose or chitosan after dissolution in the ionic liquid. It was suggested that appropriate selection of the ratio of cellulose or chitosan would enable development of keratin films with desired properties for specific applications (Tran, 2016). Keratin from human hair was combined with chitosan azide solution and the blend polymers were cast into films (Lin, 2018). Transparent films were obtained since there was good interaction between the

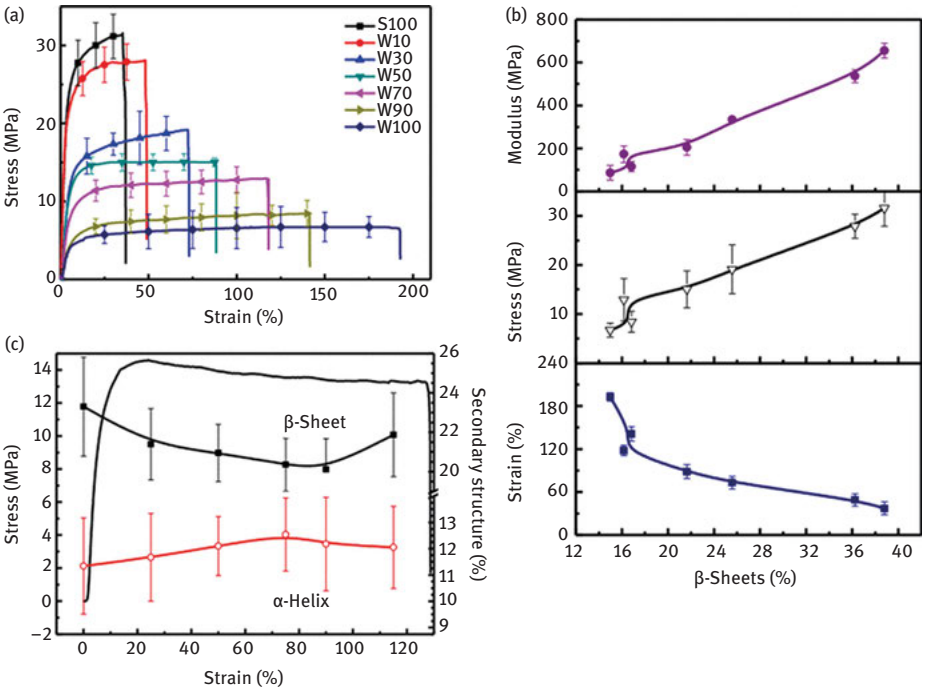

Figure 4.12: Influence of wool keratin and β-sheet content on the mechanical properties of sericin–keratin blend films (Chen, 2018a). (a) Stress–strain curve of SS–WK films; (b) the transition of the secondary structures of SS–WK films with the variety of beta sheet. Reproduced with permission from Springer Nature.

two polymers. The cast films were exposed to UV radiation for 15 min and later dried under ambient conditions. Presence of a peak at 2,118 cm^{-1} in the FTIR spectrum confirmed grafting of the azide group on chitosan and good interaction between chitosan and keratin. Water sorption of the films increased as the keratin content increased but no major change was observed in the strength of the films (22 to 28 MPa). L929 cells seeded on the blend films showed substantially increased attachment and spreading including formation of pseudopodia when the ratio of keratin was high at 50%. Similar results were also obtained when the membranes were used for a scratch wound test. Keratin–chitosan membranes were able to support hASC cell attachment and proliferation indicating their suitability for healing wounds.

Highly transparent keratin films (Figure 4.14) were prepared by compression molding keratin hydrogels (Mori, 2018). Hydrogels were prepared by treating wool in 8 M guanidine hydrochloride and 2-mercaptoethanol at 60–70 °C for 18 h. Extract obtained was dialyzed and the proteins obtained were made into hydrogels. These hydrogels were compressed between two aluminum plates at a pressure of 2.8 MPa

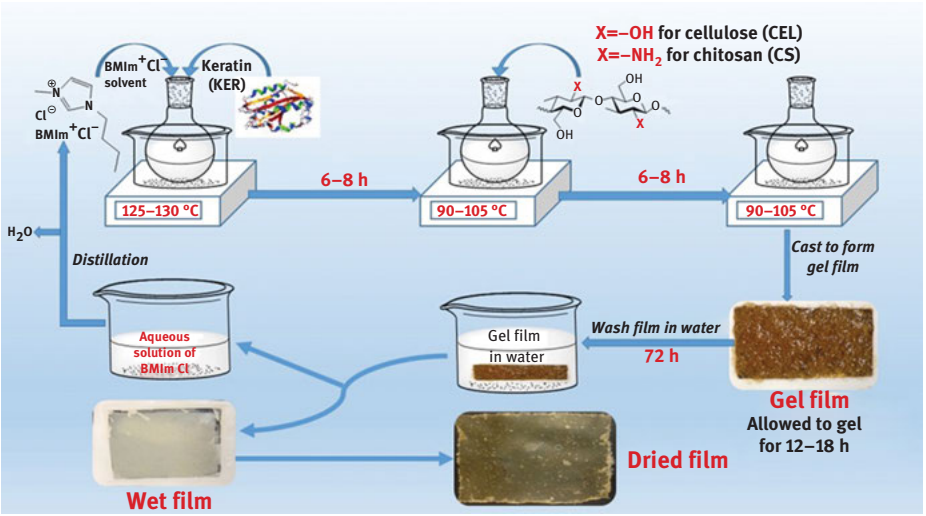

Figure 4.13: Schematic representation of the process used to prepare the composite keratin films and their digital pictures in wet and dry form (Tran, 2016). Reproduced with permission from American Chemical Society.

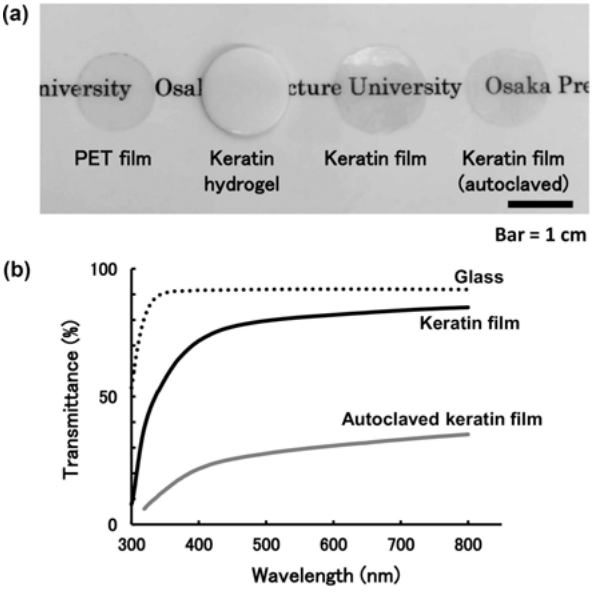

Figure 4.14: Transparent keratin films prepared by compression molding hydrogels in comparison to PET and autoclaved films (a); level of transparency of the films (b) (Mori, 2018). Reproduced with permission from Elsevier.

for 10 s to form films. Converting the hydrogels into films improved the strength from 0.013 to 0.486 MPa and modulus from 0.041 to 0.582 MPa but decreased elongation. Films were also stable in aqueous environments with only 12% degradation after 42 days compared to 50% for the hydrogels. However, films had lower degradation in vivo compared to hydrogels but did not show any inflammation or rejection after subcutaneous implantation (Mori, 2018).

Nonwoven (polyester/viscose 30/70 blend) wound dressings were coated with feather keratin, alginate and chitosan, and studied for their wound healing ability. The nonwoven fabric was immersed in solutions of either keratin, keratin–sodium alginate or keratin–chitosan for different durations and temperatures. Polymers were coated onto the fabric depending on the treatment conditions. Morphological studies showed an even and smooth coating of the polymers on the nonwoven. Although, the coating resulted in a decrease in air permeability (1.7×10^{-4} m^3/s to 0.428×10^{-4} m^3/s), the level was considered suitable for wound dressing. Substantial increase in thickness from 0.22 mm for the untreated nonwoven to 2.89 mm for those treated with keratin and chitosan was also responsible for the lower porosity. Keratin–chitosan-treated samples exhibited excellent antibacterial activity against both gram positive and gram negative strains. Also, no cytotoxicity was observed and cell attachment and

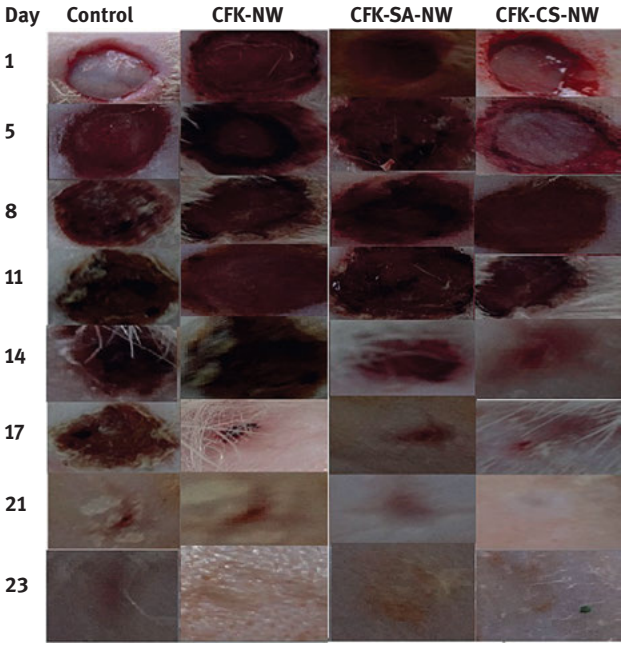

Figure 4.15: Digital images of the wound healing ability of untreated (control), keratin (CFK-NW), keratin–sodium alginate (CFK-SA-NW) and keratin–chitosan (CFK-CS-NW) from 1 to 23 days dressing (Shanmugasundaram, 2018). Reproduced with permission from Elsevier.

proliferation was observed for up to 5 days. Treated nonwovens were used as dressing materials to cure wounds on rats. As shown in Figure 4.15, considerable differences were observed in the wound healing rate depending on the treatments used for the fabrics. A 100% wound healing rate was obtained for the keratin–chitosan-treated sample after 15 days compared to only 58% for the untreated nonwoven (Shanmugasundaram, 2018).

A new technique of pulsed laser deposition (PLD) was used to deposit thin films of keratin onto glass or hemp fabric to impart hydrophilicity and other properties (Cocean, 2019). For the PLD treatment, the horn or wool fibers were ablated using a laser having 10 ns pulse width, wavelength of 532 nm, incident angle of 45° pulse repetition time of 10 Hz, 336 µm, distance between target to support being 3.5 cm and chamber pressure being 3.10^{-2} torr. A schematic of the possible changes in wool/horn due to the laser treatment is shown in Figure 4.16. Transparent films were formed on the top of the substrate and atomic force microscopic (AFM) images revealed that the morphology of deposited keratin was different for the wool and horn keratin. When coated onto hemp fabrics, the surface becomes considerably

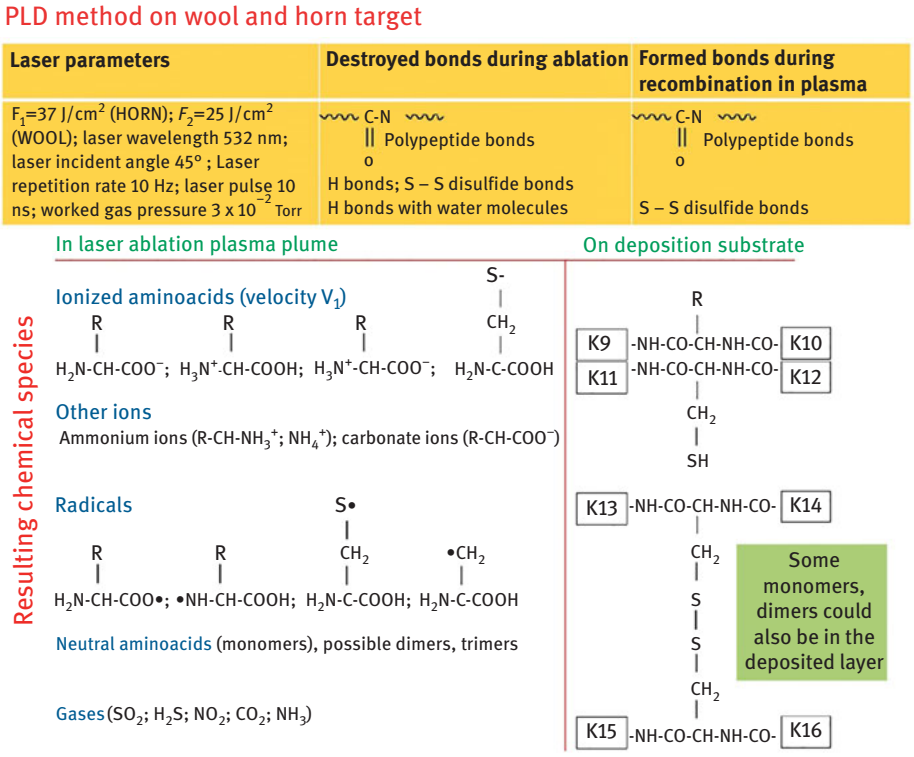

Figure 4.16: Changes in the chemical structure due to the PLD treatment on wool and horn (Cocean, 2019). Reproduced with permission from Elsevier.

hydrophilic compared to the untreated surface. Ability to control the hydrophilicity on the surface and combine a carbohydrate with protein was suggested to be preferable for medical applications (Cocean, 2019).

A layer-by-layer deposition of keratin was done to obtain multilayer films for potential tissue engineering use (Yang, 2009). The multilayer films were deposited onto poly(diallyldimethylammonium chloride) (PDDA) and polyacrylic acid (PAA) which was the substrate since keratin acts as polyanion and polycation depending on the pH. Before the deposition, keratin extracted from wool was treated with iodoacetic acid to protect the thiol groups and obtain carboxyl methyl keratin with an isoelectric point of 3.8. To form the films, slides treated with the substrate were dipped in the modified keratin solution (1.5 mg/mL) for 20 min and later dried. This procedure was followed several times to obtain the multilayer film. Up to eight bilayers were formed with the average thickness of the multilayer film being 220 nm and each bilayer was of 18 nm when deposited on PDDA whereas the thickness was 1,050 nm and each bilayer was 61 nm when PAA–keratin was used (Yang, 2009). Such large variation in thickness was considered to be due to the polyelectrolytic differences between PDDA and PAA. Ability to build thick films quickly using inexpensive and biocompatible keratin was considered to be ideal for tissue engineering applications (Yang, 2009).

4.4 Keratin films with synthetic polymer blends

Since addition of glycerol increases hydrophilicity and decreases mechanical properties, various ratios of polyethylene glycol (PEG) of different molecular weights were combined with keratin extracted from feathers that were later made into films (Martelli, 2012). Addition of PEG decreased the hydrophilicity with increasing molecular weight of PEG providing higher resistance to moisture. Subsequently, films containing PEG had lower solubility after immersion in water. It was suggested that feathers were a good source to develop biothermoplastics with the addition of PEG (Martelli, 2012).

Surface characteristics of blend films made from raw feather and nylon 6 were studied by Akhlaghi (2012). Raw feather cut into lengths of 3–4 cm was mixed with nylon 6 dissolved in formic acid. Various ratios of the feathers were combined with nylon and films were spin cast onto silicon wafers. Some of the properties of the films are listed in Table 4.12. Stiffness of the films decreased with increasing proportion of feathers whereas adhesion parameter increased and surface roughness did not show significant changes. AFM images (Figure 4.17) showed that there was considerable phase separation between feather and nylon. Also, films containing higher amounts of feathers had larger surface roughness than those containing higher amounts of nylon. The nylon component was found to increase elastic modulus and stiffness whereas feather provided higher pull-off force and work of adhesion in the samples (Akhlaghi, 2012). Based on the results, it was suggested that combining feathers with synthetic polymers may be a good approach to obtain films with good tensile properties and

Table 4.12: Properties of films made from blend of feather keratin (FK) and nylon 6 (NY6) (Akhlaghi, 2012).

Sample	Stiffness (N/m)	Wa (mN/m)	Fa (nN)
NY6	3.64 ± 12	67.2 ± 19	20.8 ± 17
NY6/FK 80/20	2.86 ± 19	68.8 ± 26	21.3 ± 23
NY6/FK 60/40	2.66 ± 22	70.7 ± 26	21.7 ± 26
NY6/FK 40/60	1.97 ± 27	73.3 ± 35	22.3 ± 32
NY6/FK 20/80	1.42 ± 7	74.6 ± 28	22.7 ± 26
FK	1.15 ± 26	76.5 ± 28	23.1 ± 27

Note: Reproduced with permission from John Wiley and Sons.

aqueous stability. However, the approach of blending nylon with feathers results in physical blending with limited chemical bonding. Therefore, significant improvement in properties cannot be expected. Also, blending a synthetic polymer with a biopolymer would decrease the biodegradability of the product developed.

Keratin extracted from feathers was dissolved using tris(hydroxymethyl)aminomethane (Tris), which also acts as a plasticizer. Dissolved solution was combined with PVA and made into films. Control films of keratin and PVA without Tris but with glycerol as plasticizer were also made for comparison (Chen, 2018b). Disappearance of the FTIR peak at 1,589.5 cm^{-1} suggested hydrogen bonding between Tris and keratin molecules (Figure 4.18). Similarly, characteristic absorption peaks at 1632.8, 1533.3 and 1235.4 were shifted to 1637.4, 1539 and 1,238 cm^{-1} due to the interaction between PVA, keratin and Tris. Shifting of peaks associated to N–H and O–H suggested hydrogen bonding and good compatibility between the molecules. Such changes also lead to the reduction in β-sheet content and increase in β-turn and random coils. Tensile properties of the films were dependent on the ratio of keratin/PVA and more predominantly on the Tris/glycerol content (Table 4.13). Increasing PVA and Tris led to increased elongation. However, Tris also made the films more hydrophilic and susceptible to water vapor. Hydrolyzed goose feather keratin was obtained using superheated water as solvent. Keratin solution obtained was combined with methylcellulose dissolved in aqueous ethanol. The blend solution was homogenized and cast onto plates to form films with or without the addition of glycerol (Liebeck, 2017). Addition of keratin into methyl cellulose increased flexibility but decreased tensile strength (Table 4.14). However, thermal stability and water resistance of the films decreased as the amount of keratin in the films increased.

Similar to blending with PVA, keratin-based films were prepared by combining keratin with PLA and solution casting into films (Fortunati, 2015). Merino wool and brown alpaca fibers were used to extract keratin using the sulfitolysis reaction, dialyzed and freeze-dried to obtain powder. The powder obtained was combined with PLA dissolved in chloroform and cast into films. For comparison, a commercially

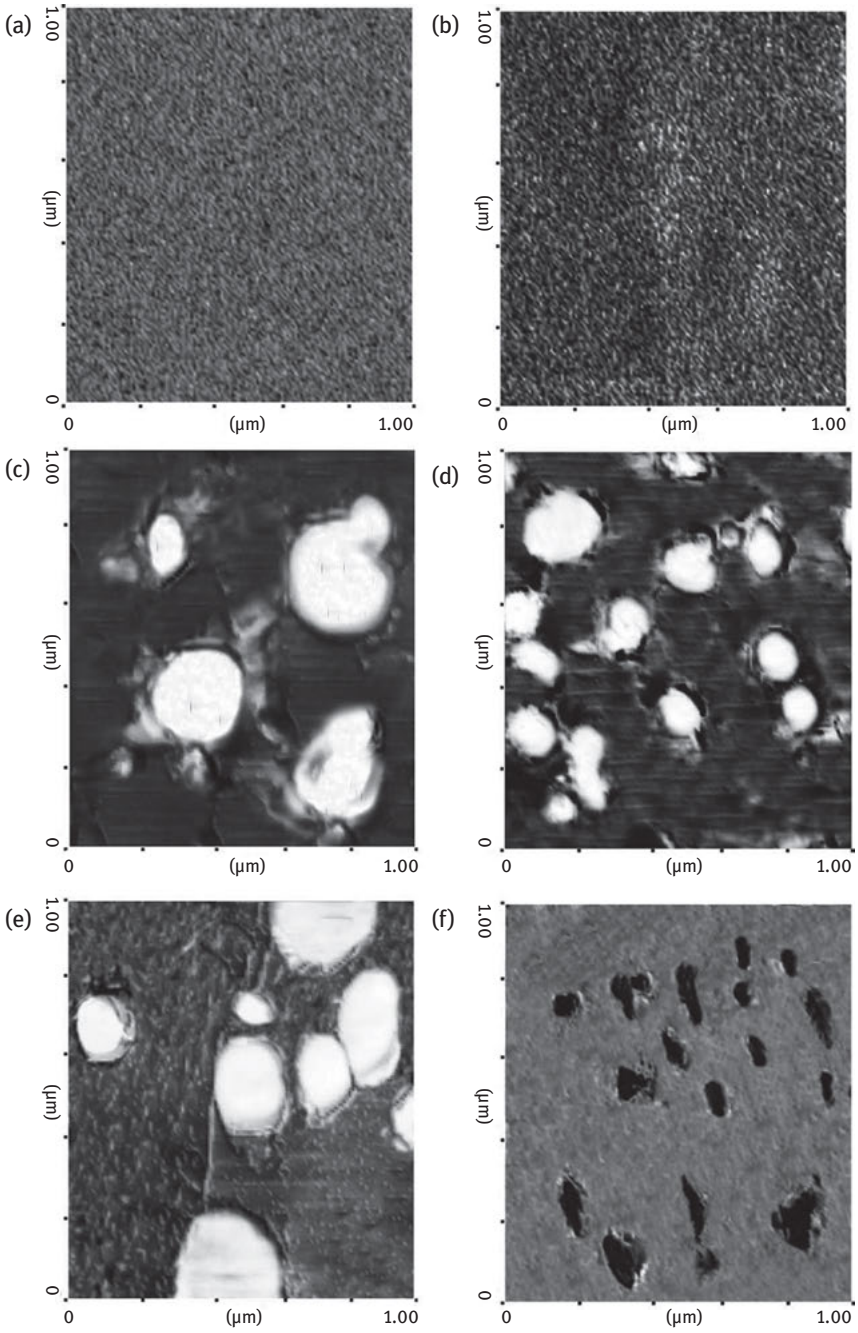

Figure 4.17: AFM images of pure nylon 6 (a), pure feather keratin (b) and 20/80 nylon/feather (c), 40/60 nylon/feather (d), 60/40 nylon/feather (e) and 80/20 nylon/feather composite films (f) (Akhlaghi, 2012). Reproduced with permission from John Wiley and Sons.

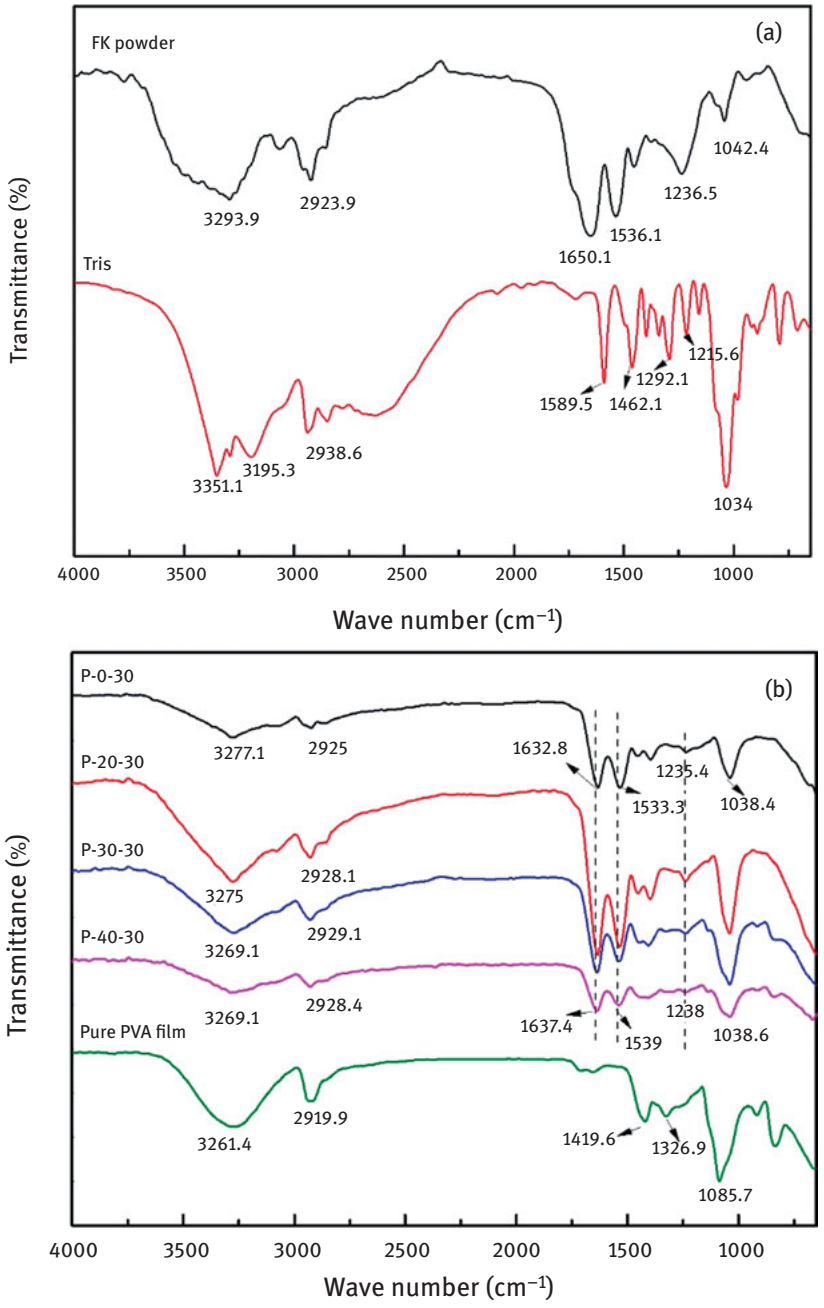

Figure 4.18: Changes in the FTIR spectra of films made using various ratios of keratin, tris (a) and PVA (b) (Chen, 2018b). Reproduced with permission through open access publishing.

Table 4.13: Changes in the tensile properties of keratin films containing varying ratios of PVA and Tris or glycerol (Chen, 2018b).

Keratin/PVA (%) Tris	Modulus (MPa)	Elongation (%)	Strength (MPa)
90–10, 30	494 ± 22	1.75 ± 0.35	7.0 ± 0.7
80–20, 30	324 ± 17	2 ± 0	5.1 ± 0.1
70–30, 30	323 ± 39	7 ± 0.7	8.9 ± 0.07
60–40, 30	311 ± 25	24 ± 3.5	8.1 ± 0.6
50–50, 30	215 ± 16	179 ± 9	9.5 ± 1.1
60–40, 15	2,007 ± 39	1.5 ± 0	22.9 ± 0.2
60–40, 20	742 ± 46	2.7 ± 0.2	12.2 ± 0.9
60–40, 25	417 ± 17	10.8 ± 1.0	9.6 ± 0.4
60–40, 30	311 ± 25	23.7 ± 3.5	8.1 ± 0.6
60–40, 40	422 ± 45	16.7 ± 0.9	5.9 ± 0.2
60–40–0 glycerol	1,258 ± 29	1.5 ± 0	8.9 ± 0.01
60–40, 15 glycerol	16 ± 5	262 ± 0.7	3.9 ± 0.3

Note: Reproduced with permission through Open Access publishing.

Table 4.14: Influence of keratin addition on the properties of methylcellulose and keratin films prepared using glycerol as plasticizer (Liebeck, 2017).

Ratio of cellulose/keratin	Modulus (MPa)	Strength (MPa)	Elongation (%)
78/22	544 ± 17	28 ± 1.9	45 ± 6
44/56	474 ± 66	25 ± 2.4	49 ± 4
45/55	274 ± 27	18 ± 2.4	73 ± 5
50/50	169 ± 20	13 ± 0.5	81 ± 1
42/58	149 ± 13	11 ± 1.1	94 ± 2

Note: Reproduced with permission through the Creative Commons Attribution License.

available hydrolyzed keratin obtained from rabbit skin was also used as reinforcement. Unlike the merino and alpaca keratin, the hydrolyzed keratin obtained from rabbit skin had a circular shape with mean particulate diameter between 40–100 μm (Fortunati, 2015). Hydrolyzed keratin powder had lower melting temperature and thermal stability than the keratin extracted from wool. Films obtained had considerably different morphology depending on the contact with the casting plate and type and amount of keratin used as reinforcement (Table 4.15). Increasing the amount of keratin led to an increase in pore size for all the films. Pore sizes in the films ranged from 1 to 14 μm and the films containing hydrolyzed keratin had larger pores corresponding with the size of the particles used. However, the hydrolyzed keratin particles had better compatibility and binding with PLA due to their spherical shape. Wettability and thermal properties also showed that the hydrolyzed keratin was better suited as reinforcement. In terms of mechanical properties, increasing amount of keratin from 1% to 5% increased strength but decreased the elongation for the alpaca

Table 4.15: Contact angle, thermal stability and percentage of crystallinity changes with addition of keratin into PLA films. KA, KM and KH represent keratin extracted from alpaca wool, merino wool and hydrolyzed keratin from rabbit skin, respectively (Fortunati, 2015).

	Wettability, contact angle (degree)		Thermal stability			Crystallinity (%)
	Upper surface	Lower surface	T_g (°C)	ΔH_{cryst} (J/g)	T_m (°C)	
PLLA	79 ± 1	76 ± 1	64.5 ± 0.3	22.1 ± 0.5	180.0 ± 0.3	9.5 ± 2.6
PLLA/1%KA	76 ± 1	70 ± 4	64.5 ± 0.6	14.1 ± 0.1	180.5 ± 0.3	17.7 ± 2.1
PLLA/5%KA	94 ± 1	71 ± 4	62.0 ± 0.1	8.2 ± 0.2	180.2 ± 0.4	23.8 ± 0.5
PLLA/1%KM	92 ± 2	67 ± 2	62.9 ± 0.4	18.3 ± 1.3	181.2 ± 0.6	10.3 ± 1.5
PLLA/5%KM	74 ± 2	66 ± 3	62.1 ± 0.2	8.0 ± 0.4	179.9 ± 0.4	22.7 ± 0.5
PLLA/1%KH	78 ± 2	77 ± 1	61.9 ± 0.2	23.4 ± 1.1	180.7 ± 0.7	8.0 ± 1.0
PLLA/5%KH	81 ± 1	70 ± 3	61.3 ± 0.2	15.1 ± 0.7	179.8 ± 0.2	16.1 ± 1.6

Note: Reproduced with permission from Elsevier.

keratin (Table 4.16). For the merino wool keratin, about 20% decrease in strength but no major change in elongation was observed with increasing keratin concentration. Highest strength was obtained when 5% hydrolyzed keratin was used. Films had good absorption of proteins (bovine serum albumin) and supported the attachment and growth of mesenchymal stem cells suggesting that the films are useful for medical applications. Alpaca and merino wool fibers were dissolved and treated to obtain keratin particles with average diameter of 33 and 19 μm, respectively (Aluigi, 2014). Keratin yield from the merino wool fibers was 14% whereas 38% from alpaca. The obtained keratin was dissolved using chloroform along with PLA and cast into films onto a Teflon surface. Two major molecular weight bands between 62 and 43 kDa and between 28 and 9 kDa were observed in the gel electrophoresis patterns. α-Helix

Table 4.16: Tensile properties of biocomposite films prepared from PLA and different types and ratios of keratin. KA, KM and KH represent keratin extracted from alpaca wool, merino wool and hydrolyzed keratin from rabbit skin, respectively (Fortunati, 2015).

	Tensile		Yield		Modulus (MPa)
	Strength (MPa)	Elongation (%)	Strength (MPa)	Elongation (%)	
PLLA	18.6 ± 3.7	12.9 ± 1.7	17.5 ± 2.5	131.5 ± 25.7	600 ± 50
PLLA/1%KA	15.3 ± 12	14.7 ± 0.5	15.3 ± 1.5	82.9 ± 9.6	420 ± 10
PLLA/5%KA	22.3 ± 3.0	3.9 ± 0.3	21.1 ± 4.3	11.8 ± 1.8	800 ± 40
PLLA/1%KM	30.1 ± 3.5	3.7 ± 0.5	23.4 ± 1.9	30.0 ± 7.2	1,200 ± 70
PLLA/5%KM	25.4 ± 3.1	3.6 ± 0.5	20.0 ± 2.5	9.1 ± 2.0	980 ± 50
PLLA/1%KH	12.3 ± 3.3	15.8 ± 2.2	12.8 ± 3.3	197 ± 27.9	610 ± 70
PLLA/5%KH	33.3 ± 3.3	4.1 ± 0.4	28.1 ± 3.3	37.6 ± 8.8	1,190 ± 70

Note: Reproduced with permission from Elsevier.

and β-sheet content also varied with the source of keratin and the extraction process. Addition of the keratin fibers into PLA increased the modulus from 600 to 1,200 MPa. The keratin–PLA blend films were suggested to be biocompatible but a detailed investigation was not done (Aluigi, 2014). In another study, keratin was made water soluble, combined with polyethylene oxide (PEO) and electrospun into membranes after making the solution stable using EDGE. Later the membranes were recross-linked in an oxygen atmosphere for 8 days.

Bionanocomposites in the form of keratin– PEO films were prepared through ultrasonically functionalized graphene. In this study, keratin was combined with PEO and also with PEO grafted with graphene, and the blends were made into films by solution casting. FTIR analysis showed changes in the asymmetric and symmetric vibrations of ether C–O–C bonds and CH_2 group deformation which suggested some level of interaction between the graphene–PEO and keratin molecules (Martelli, 2006; Grkovic, 2015) (Figure 4.19). Morphological images showed good binding between the PEO and keratin fiber surfaces and thermal analysis revealed that addition of the keratin-G into PEO increased the thermal stability. However, addition of graphene structures decreased the thermal stability of the nanocomposite films. In terms of mechanical properties, inclusion of even 0.3 wt % of P–G increased the modulus and hardness of PEO by 5% and 33%, respectively. Similarly, functionalization with graphene increased the modulus and hardness by 92% and 190%. It was suggested that graphene functionalization and blending with PEO was a simple and effective method to increase the mechanical properties of the keratin films (Martelli, 2006).

Studies have also been done to improve the properties of keratin films by the addition of graphene oxide (GO). About 1 wt% of GO was added into keratin solution and stirred for 3 h at room temperature and later for 4–5 h in an ultrasonicator at 40 °C for homogenous mixing. The blend solution was cast onto glass and allowed to dry for 24 h at 40 °C to form the films. Addition of GO made the surface of the films smoother and removed many defects. However, no changes were observed in the molecular weight of the samples and no reaction was observed between GO and keratin. Considerable increase in strength (14.7 MPa) and elongation from 0.67% to 3.65% occurred due to the presence of GO (Li, 2018a).

Electrospun films/membranes made using 90/10 ratio of keratin/PEO showed considerable bead formation (Figure 4.20) due to the low viscosity of the solution. Addition of EDGE increases the molecular weight and hence the viscosity of the solution leading to considerably uniform nanofibers. EDGE was used as the primary cross-linking and the cross-linked mats were exposed to oxygen atmosphere for 8 days to further improve properties, particularly water stability. Although secondary cross-linking did not alter the appearance of the fibers, swelling of fibers was observed after immersion in water but the membranes were able to maintain their integrity (Fan, 2016). Primary and secondary cross-linking increased the thermal stability of the samples from 150–280 °C to 260–420 °C and 290–420 °C, respectively.

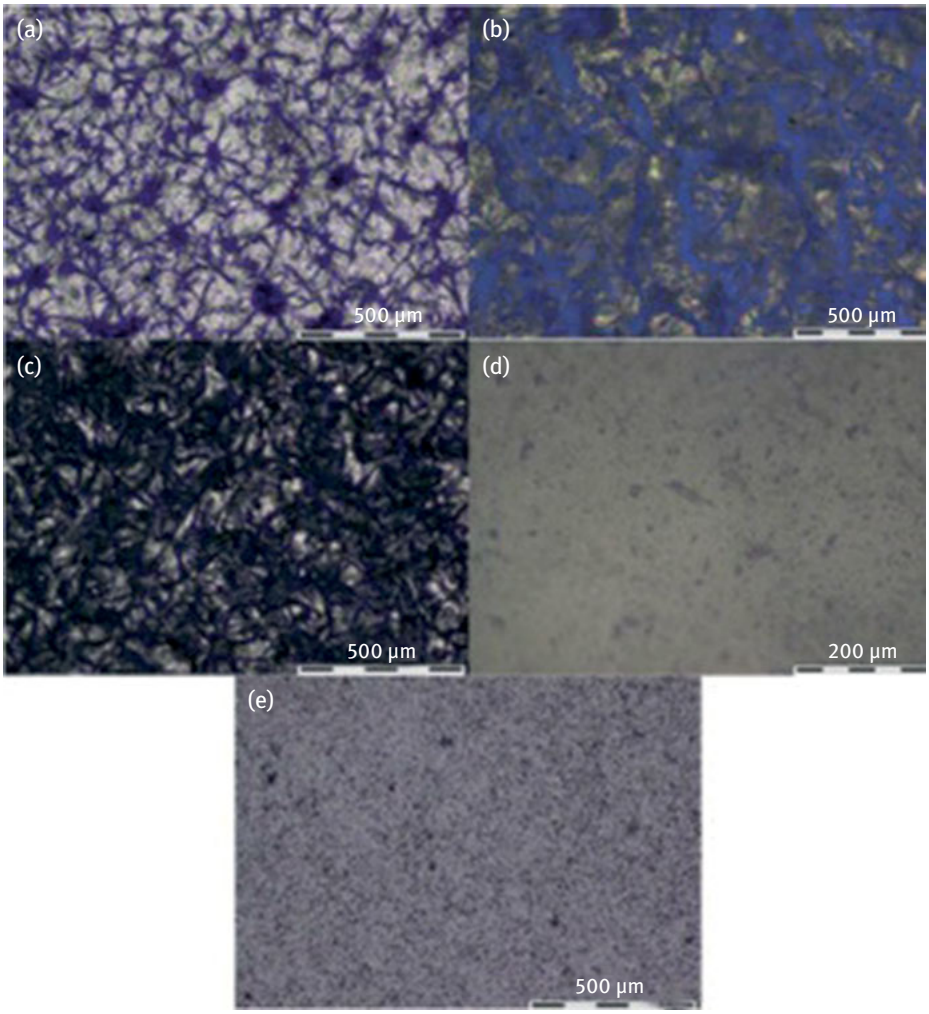

Figure 4.19: Optical images of the neat PEO (a), blends of PEO/p-g (b), PEO/f-G (c), keratin-PEO (d) and keratin-PEO/f-G (e) (Martelli, 2006). Reproduced with permission from Royal Society of Chemistry.

L929 cells seeded on the secondary cross-linked keratin films showed excellent cell attachment (Figure 4.20) and exponential proliferation demonstrating the suitability of the membranes for tissue engineering and other medical applications (Fan, 2016).

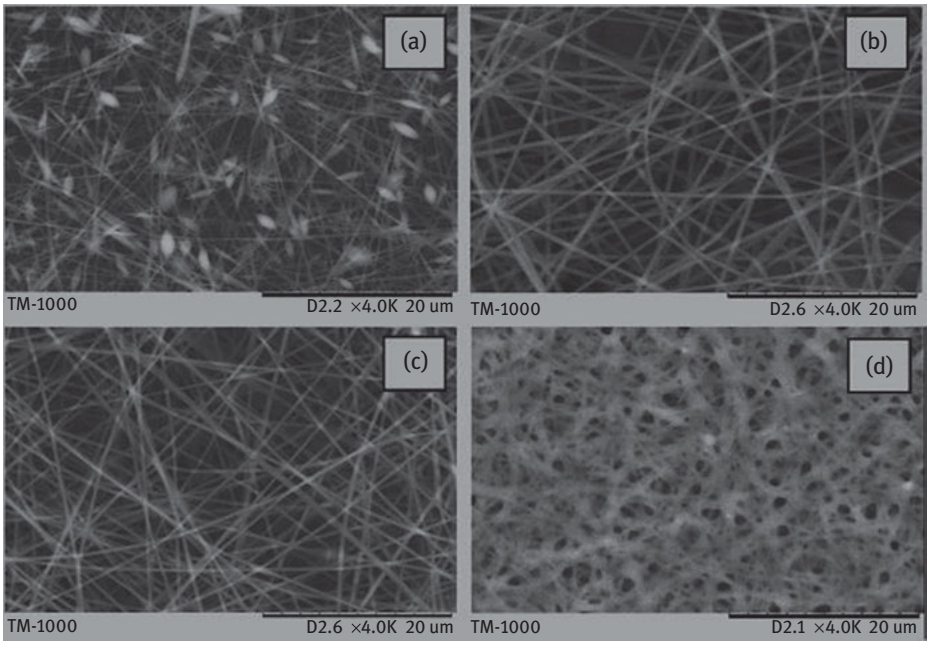

Figure 4.20: Morphology of fibers obtained using various ratios of keratin and PEO. Uncross-linked blend (a); primary cross-linked fibers (b); secondary cross-linked fibers (c); and secondary cross-linked fibers after immersion in water for 24 h (d) (Fan, 2016). Reproduced with permission from Elsevier.

4.5 Thermoplastic feather films

Compression or injection molding is another common method of developing films. It is generally considered that feathers are nonthermoplastic and therefore cannot be injection or compression molded. However, Barone et al. combined feather powder with glycerol and extruded the mixture in a twin-screw extruder. This process converted the feathers into thermoplastics and the samples could be compression molded into films at 160 °C. Glycerol and the compression molding conditions played a critical role in the formation and the properties of the films (Barone, 2005a–c). Addition of glycerol increased the elongation but decreased the strength and modulus substantially. Elongation of the film was as high as 100%. However, addition of glycerol above 30% increased the water absorption and hence made the films very weak. The water stability of the films was poor and therefore applicability of the films would be limited (Barone, 2005a–c).

In a novel approach, feathers were hydrolyzed to various extents using alkali and it was found that the hydrolyzed feathers could be compression molded into composites using glycerol (30%) as plasticizer (Reddy, 2013). In addition to the concentration

of alkali used for hydrolysis, compression time and temperature were also found to influence mechanical properties of the films. Peak stress of the films varied from 2.7 to 9.0 MPa and elongation varied between 3.8% and 30% depending on the extent of hydrolysis and compression conditions used. However, films developed were unstable and disintegrated in water. To improve stability, feathers were cross-linked using citric acid. After cross-linking, the films were stable in water but lost up to 80% of their strength in the wet condition. A digital image of the hydrolyzed feather and film developed by compression molding are shown in Figure 4.21. It was suggested that the films could be suitable as scaffolds for tissue engineering since the cross-linker used was noncytotoxic (Reddy, 2013).

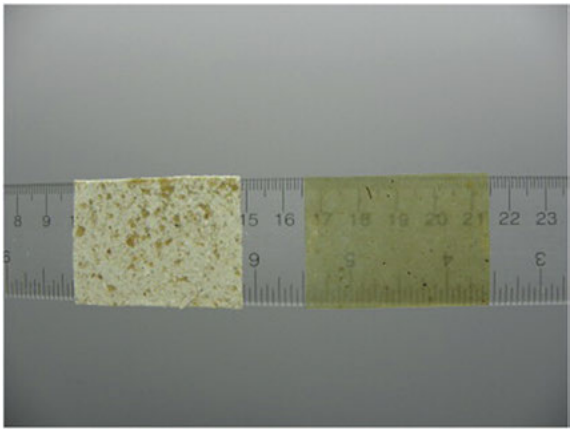

Figure 4.21: Digital image of compression molded unhydrolyzed and alkali hydrolyzed keratin that transforms into a transparent film (Reddy, 2013). Reproduced with permission from Elsevier.

Thermoplastics can also be developed from the feather keratin through chemical modifications. Researchers have adopted acetylation, grafting or etherification to modify feathers and develop thermoplastics. Reddy et al. converted feathers into thermoplastic through etherification based on the mechanism shown in Figure 4.22

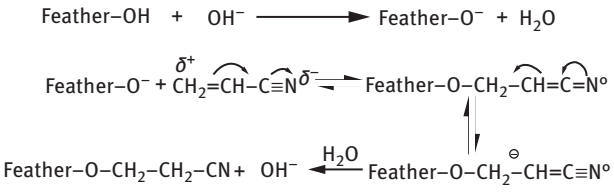

Figure 4.22: Mechanism of etherification of feathers using acrylonitrile (Reddy, 2011). Reproduced with permission from Elsevier.

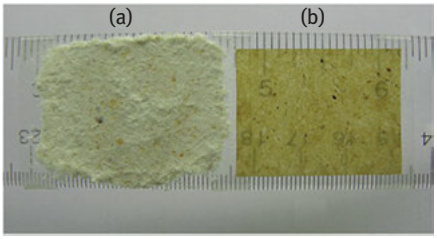

Figure 4.23: Poultry feathers (a) can be made into transparent thermoplastics after etherification (b) (Reddy, 2011). Reproduced with permission from Elsevier.

(Reddy, 2011). Etherification conditions such as time, temperature and catalyst concentration influenced the extent of thermoplasticity achievable. A weight increase of up to 20% was achieved after modification. Unmodified feathers do not melt but cyanoethylated feathers had a melting temperature at about 167 °C. When compression molded after adding 20% glycerol, the modified feathers were converted into transparent thermoplastic films (Reddy, 2011) (Figure 4.23). Tensile strength of the samples varied from 1.6 to 4.2 MPa and modulus varied from 23 to 197 MPa depending on the extent of etherification.

Chapter 5
Keratin made into gels

5.1 Hydrogels, aerogels and nanogels from feather keratin

Hydrogels are structures that have high capacity to hold water and other biological fluids due to their inherent porosity and structure. Due to these reasons, hydrogels are particularly preferred for food and medical applications, primarily for controlled release of neutraceuticals, pharmaceuticals, drugs and so on. Although polysaccharides and synthetic polymers have been made into hydrogels, proteins including keratin are preferred over other biopolymers for medical applications. Keratin contains 7–20 mol% of cysteine residues that can be modulated to achieve different degradation rates of biomaterials and therefore achieve tunable rates of release of therapeutic agents (Tanabe, 2002). The extent of degradation of keratin materials can be controlled depending on properties of keratin and the type of extraction. For instance, oxidatively extracted keratin (keratose) was found to degrade in days to weeks whereas reductively extracted keratin (kerateine) was stable for several months when made into hydrogels (Tanabe, 2002).

A simple approach of oxidation and reduction was used to develop keratin hydrogels with tunable properties (Cao, 2019). The process where intramolecular disulfide bonds use a reducing agent like cysteine to release free thiols is called disulfide shuffling. These free thiols later formed intermolecular disulfide bonds due to oxidation (Figure 5.1). Chicken feather keratin was formed into a powder and dissolved in a buffer containing cysteine. The solution formed a gel after incubation. Similar hydrogels were prepared using different ratios of keratin and with 1.5% or 3.3% cysteine. Ciprofloxacin was added into the hydrogels and their loading and release behavior was studied (Cao, 2019). The disulfide shuffling and amount of keratin and cysteine considerably influenced the properties of the hydrogels and also gel forming properties. Gelation time decreases from 3 days without use of cysteine (conventional approach) to just 10 min when 10% keratin solution containing 3% cysteine was used. A 1.5 to 2 times increase in compressive strength was achieved with the new approach. After 40 days of incubation in phosphate buffered saline (PBS) and reducing media, the degradation of the hydrogels was found to be inversely dependent on cysteine levels. About 94%, 91% and 85% gel was retained when cysteine concentration was 3%, 1.5% and 0%, respectively (Cao, 2019). The release of drug was related to the degradation profile of the gels. Both L929 and rOB cells showed good attachment, growth and proliferation, suggesting that the hydrogels were cytocompatible. When subcutaneously implanted in mice, the cysteine containing gels had 28–40% of original volume whereas the conventional hydrogel was completely degraded. It was clearly evident that the structure, mechanical properties, drug release capability (Figure 5.2) and in vivo degradation could be easily controlled by varying the amount of cysteine used for the disulfide shuffling process (Cao, 2019).

https://doi.org/10.1515/9781501511769-005

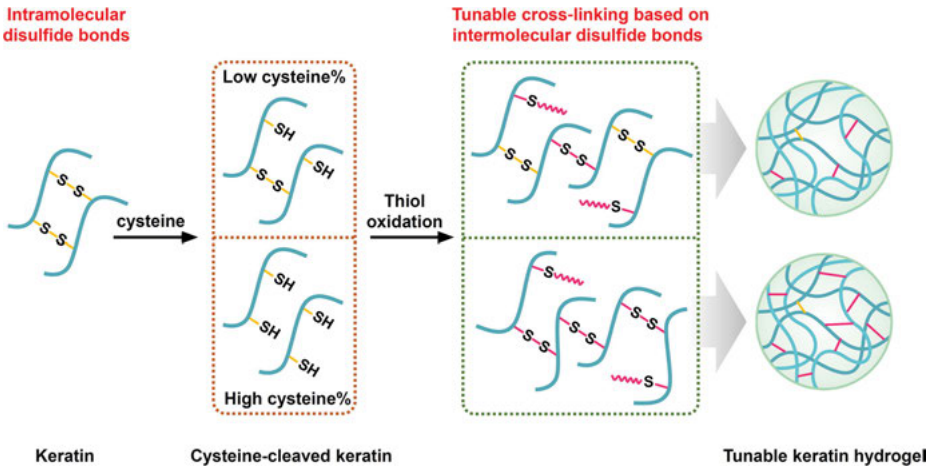

Figure 5.1: Process of disulfide shuffling where intramolecular cross-linkings are converted into intermolecular disulfide bonds (Cao, 2019). Reproduced with permission from Elsevier.

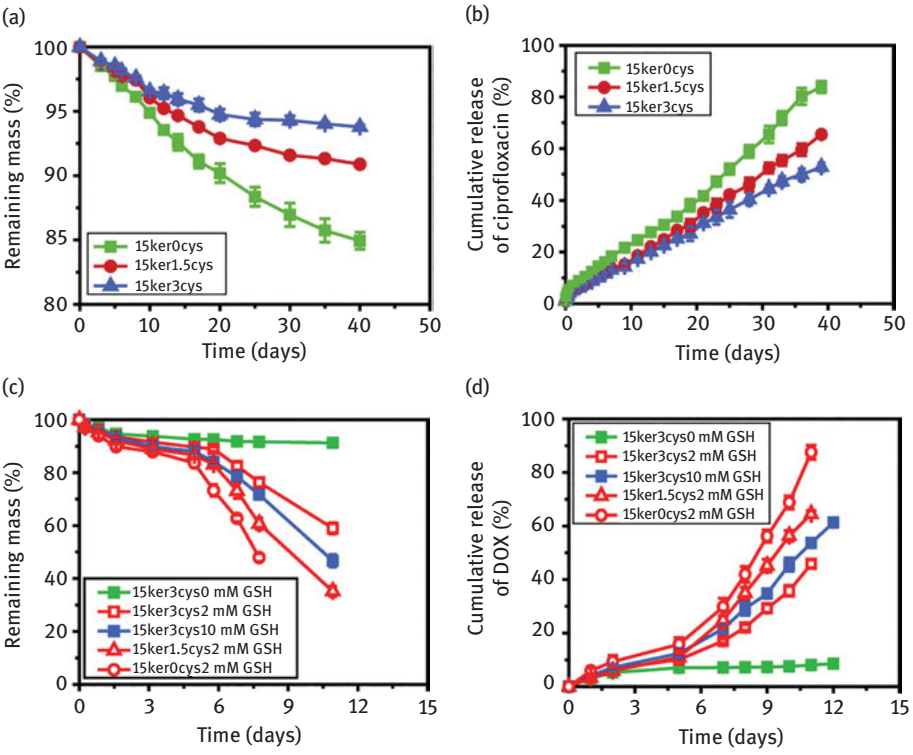

Figure 5.2: Cumulative drug release (b and d) and remaining mass (%) (a and c) of scaffolds made using different ratios of cysteine (Cao, 2019). Reproduced with permission from Elsevier.

Keratin was extracted from feathers and made into hydrogels using freeze-drying. To further improve the properties of keratin hydrogels, acrylic acid monomers were grafted using N, N'-Methylenebisacrylamide, sodium bisulfite and potassium persulfate. The acrylic acid monomers were grafted by replacing the amide bonds onto the primary chains of the hydrolyzed feather keratin (Wattie, 2018). Addition of acrylamide increased the thermal stability and reduced swelling. Swelling also varied with pH and was between 10 and 500 g/g. pH between 5 and 7 provided highest swelling and interestingly, the gels could shrink and expand as the pH was varied between 2 and 8. A highest swelling of 501 g/g could be achieved in water and the gels were suggested to be suitable for agriculture and other applications.

Hydrogels were prepared through chemical modification of kerateine, keratose and alkali-modified kerateine for controlled release of therapeutic agents including ciprofloxacin, recombinant human insulin-like growth factor and recombinant human bone morphogenetic proteins. The chemical modification done was to "cap" the cysteine residues with iodoacetamide and reduce the concentration of the thiol groups from 270 nM of Thiol per mg of protein to about 25 nM per gram. Morphologically, the hydrogels had a highly porous structure but no major difference was observed in the morphology between the different types of keratins used. Swelling ratio was highest for keratose hydrogels but these hydrogels were unstable and could not be tested for mechanical properties. Compressive modulus was highest for the 74% cross- linked hydrogels (Tanabe, 2002). Keratin was extracted from chicken feathers using the enzyme savinase in the presence of sodium dodecyl sulfate (SDS) and a reducing agent (sodium sulfite) at 55 °C for up to 6 h. Dissolved keratin was precipitated and later dialyzed against 3.5 kDa tube and collected. Keratin solution was combined with polyvinyl alcohol (PVA) and mixed at room temperature for 6 h, and the mixture was lyophilized for 48 h at −54 °C to form sponges. Proteins with molecular weights between 10–12 kDa similar to that found in native feathers were extracted. Pore size in the pure keratin sponges was between 50–100 μm compared to 5–10 μm in the keratin–PVA blended sponge. The blend scaffold had an oil absorption capacity of 50 g/g compared to 0.993 g/g for the pure PVA sponges. Similarly, the air permeability of the keratin–PVA sponge was 369 mm/S and water vapor permeability was 6.5×10^{-7}/GPa s m, considerably higher compared to other keratin sponges developed (Sadeghi, 2018).

Keratin extracted from chicken feathers was reduced using dithiotheritol and made into hydrogels by freeze-drying. To prepare the gel, about 1% of keratin was dispersed in 8 mol urea solution at 65 °C and heated for 2 h along with the reducing agents and other chemicals. Gels formed had a clear appearance but became hard and brittle after drying (Figure 5.3). Since hydrogels are prone to swelling, the swelling ratio was determined in various pH (4.5, 6.5, 7.0 and 7.8). Considerably lower swelling was observed in the biological fluids. Variation in the swelling of the gels was considered to be due to the changes in the salt and pH sensitiveness. For instance, swelling of the hydrogel was considerably higher in sodium chloride than calcium chloride probably due to the easy dissociation of sodium chloride

(Guo, 2015). To understand the ability of the hydrogels to load and release drugs, a model compound Rhodamine B and protein macromolecule bovine serum albumin (BSA) were added and the release profile of the drugs from the hydrogel were studied. Hydrogels provided controlled release for both rhodamine B and BSA with cumulative release of 97% and 89%, respectively. Study showed that the release of the drugs could be controlled by varying the pH.

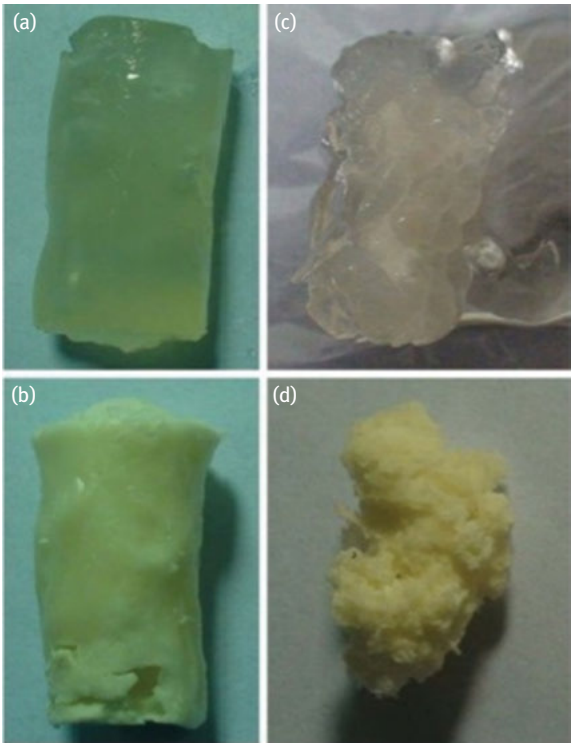

Figure 5.3: Digital images of the hydrogel without any treatment (a), gel swollen in ethanol (b), swollen in water (c) and a dried hydrogel (d) (Guo, 2015). Reproduced with permission from John Wiley and Sons.

Amount of drug released typically depends on the pH and the other release conditions used. Rhodamine had higher amount released (up to 95%) and the highest amount of BSA released was about 90% (Figure 5.4). For BSA, the release was considerably higher in pH 7.4 whereas rhodamine had similar release at pH 7.4 and 8.4 and considerably low release at pH 3.0 (Figure 5.5). Differences in the release of the drugs were due to the size of the molecule and the extent of attraction between the drug and the functional groups in the hydrogels (Guo, 2015).

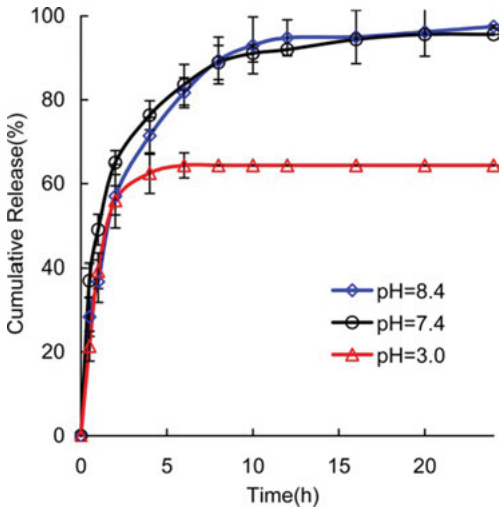

Figure 5.4: Release of rhodamine B from the feather keratin hydrogel at different pHs at 37 °C. Reproduced with permission from John Wiley and Sons (Guo, 2015).

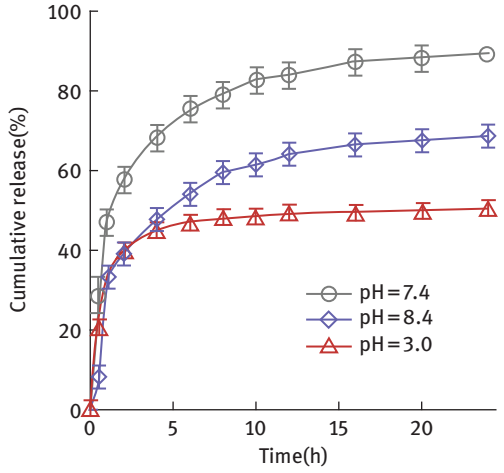

Figure 5.5: Release of bovine serum albumin from the keratin hydrogel at 37 °C at different pHs (Guo, 2015). Reproduced with permission from John Wiley and Sons.

5.2 Hydrogels from wool keratin

Highly porous microfibrillar keratin sponges were manufactured by treating wool fibers with 0.1 N sodium hydroxide at 60 °C for 24 h (Patrucco, 2015). Coarse fiber

fragments remaining after the treatment were removed and the dissolved cortical cells were used to form the sponge. Sodium chloride having particles with diameters between 400–500 μm was also added to assist in the pore formation since the salt could be leached resulting in pores. Sponges obtained were treated at 180 °C to thermally cross-link the keratin molecules. Microporous sponges with even and distributed pores were obtained with pore sizes having diameters ranging from 190 to 560 μm. Cross-section of the sponges clearly showed the formation of fibrils that could help to improve the stability and mechanical properties of the scaffolds. Sponges had a porosity of 93% and a density of 1.32 g/cm^3. Extraction of keratin and formation of the sponges resulted in a decrease of cysteine from 10.83to 2.39 mol%, whereas all other amino acids in the sponges were comparable to that in the wool fibers. Cross-linked sponges had tensile strength of 0.103 MPa and elongation was 1.5% with cross-linking also providing higher thermal stability. Osteoblasts (SAOS-2) cells seeded on the sponge showed good attachment and subsequently up to fourfold increase in cell numbers when cultured for 7 days indicating the biocompatibility of the scaffolds (Patrucco, 2015).

In another study, wool keratoses were used to prepare hydrogels for potential tissue engineering applications (Sando, 2010). Wool fibers were treated with peracetic acid at 37 °C overnight and the keratoses formed was extracted using a Tris-base and precipitated using alkali to obtain α-keratose and with acid to form β-keratose. Substantial variations were observed in the amino acid composition of the two keratins obtained before and after cross-linking (Table 5.1). Primary difference between the two keratoses was the lower level of cysteine in α-keratoses than in β-keratose. Gels were prepared from the keratose solution using molds and later cross-linked through UV irradiation in the presence of a metal oxide. Tensile properties (Table 5.2) and moisture absorption of the gels were determined and the gels were used as substrates for tissue engineering. NIH3T3 cells were seeded on the gels and the adhesion was determined using DNA quantification assays (Sando, 2010). Tensile properties, tissue adhesion and wettability depended on the type of buffer and cross-linker used. Cells seeded on the scaffold were able to attach and proliferate suggesting that the

Table 5.1: Properties of hydrogels prepared from keratin and modified keratin (Sando, 2010).

Specimen	Swelling ratio (Q)	Compressive modulus (kPa)	Cross-link density (μmol/cm^3)	Mol. wt. between cross-links (M_c) in kg/mol
Keratose	1.18 ± 0.26	–	–	–
7% S-S MKTN	1.07 ± 0.01	10.4 ± 1.98	4.12 ± 0.79	87.7 ± 19.9
74% S-S MKTN	1.06 ± 0.02	53.0 ± 19.8	21.1 ± 7.90	19.2 ± 9.4
80% S-S MKTN	1.05 ± 0.01	26.4 ± 2.4	10.6 ± 0.96	33.4 ± 3.2
Kerateine	1.01 ± 0.01	42.8 ± 8.9	17.3 ± 3.58	21.1 ± 5.2

Note: Reproduced with permission from John Wiley and Sons.

Table 5.2: Properties of hydrogels made from α-keratose (Sando, 2010).

Buffer	Tensile properties		Tissue adhesion	Wettability	
	Elastic modulus (kPa)	Mass between cross-links (kg/mol)	Stress at break (kPa)	Swelling ratio (%)	Contact angle (degree)
Tris HCl					
– 20 mM SPS	20.6 ± 1.4	18.0 ± 0.4	90.1 ± 2.4	−6.0 ± 1.4	73.2 ± 2.0
– 40 mM SPS	37.8 ± 1.9	14.4 ± 0.3	94.0 ± 1.0	−11.2 ± 1.8	72.4 ± 1.8
+2.5 glycerol					
– 20 mM SPS	12.5 ± 0.8	20.3 ± 0.3	81.8 ± 2.4	26.4 ± 13.4	72.9 ± 7.3
– 40 mM SPS	18.6 ± 2.5	18.5 ± 0.6	91.0 ± 1.9	25.8 ± 23.3	71.2 ± 2.4
PBS					
– 20 mM SPS	30.4 ± 3.8	15.8 ± 0.8	83.9 ± 2.2	−11.7 ± 0.8	72.3 ± 5.0
– 40 mM SPS	53.5 ± 4.3	12.2 ± 0.5	92.1 ± 2.2	−9.3 ± 0.4	76.5 ± 3.5
+2.5 glycerol					
– 20 mM SPS	9.5 ± 2.6	21.4 ± 0.9	87.3 ± 2.4	−2.4 ± 4.2	66.7 ± 6.3
– 40 mM SPS	17.7 ± 2.3	18.8 ± 0.6	87.9 ± 1.9	−1.8 ± 2.7	73.1 ± 6.9

Note: Reproduced with permission from John Wiley and Sons.

α-keratose cross-linked with UV irradiation was suitable for tissue-engineering applications. Keratin extracted from wool and made into sponges (10 mm diameter and 2 mm thickness) was conjugated with lysozymes and cross-linked. Disulfide-linked keratin showed gradual release of the lysozyme but ether cross-linkages were necessary to maintain a stable structure (Kurimoto, 2003).

Sponges with controlled porosity and pore sizes were developed using sulfated wool keratin through compression molding and particulate leaching approach (Katoh, 2004b). Keratin powder (45,000–60,000 Da and 16,000 Da molecular weight bands) were mixed with sodium chloride particles of various sizes along with urea and the samples were compression molded at 140 °C for 5 min. The composites formed were immersed in ethanol to remove urea and salts and form the porous scaffolds. Pore size was directly dependent on the size of the sodium chloride particle used and the presence of urea resulted in smooth scaffolds (Table 5.3). Scanning electron microscopic (SEM) images revealed the difference in pore size with change in particle size. Changes in the pore size also affected the density and the water absorption of the scaffolds. Particles having size between 300–500 μm provided a porosity of 93.4% and water uptake of 946%. Sponges showed higher swelling at pH 7.4 and even dissolved when the pH was 9.1. Ability to control the porosity and swelling were considered desirable properties for medical applications (Katoh, 2004b).

Table 5.3: Changes in the porosity and water uptake of the keratin sponges made using various amounts of salt (Katoh, 2004b).

NaCl/keratin	Apparent density (g/cm^3)	Porosity (%)	Water uptake (%)
0	1.3 ± 0.00	0.0 ± 0.0	87 ± 3
5	0.151 ± 0.003	88.4 ± 0.2	599 ± 20
9	0.106 ± 0.006	91.8 ± 0.4	746 ± 28
15	0.084 ± 0.003	93.5 ± 0.3	1,077 ± 43
20	0.077 ± 0.002	94.1 ± 0.2	1,206 ± 13

Note: Reproduced with permission from Elsevier.

Keratin extracted from wool was made into sponges for long duration tissue engineering. Sponges had pore size of 100 μm and were stable in aqueous media when prepared after 3 days of freezing at −20 °C. The hydrogels were seeded with mouse fibroblast cells (L929) and the ability of the scaffolds to support cell growth was monitored up to 30 days (Tachibana, 2002). Cells were observed to grow rapidly on the scaffolds for 20 days. Although no significant increase in cell numbers was observed above 20 days, cells sustained on the scaffold for up to 30 days. Low degradation of the feather keratin by proteases and the specific amino acid motifs in keratin that promote cell attachment and growth were considered highly desirable for long-term tissue engineering (Tachibana, 2005, 2006).

Unlike most studies where human hair keratin has been used to develop hydrogels, it was demonstrated that similar hydrogels without any cytotoxicity could be developed from feather keratin (Wang, 2017). Hydrogels were fabricated by dissolving lyophilized keratin powder in water and addition of H_2O_2 solution to assist in the formation of disulfide bonds. Gels were obtained after overnight incubation at 37 °C or by lyophilizing at −40 °C. Extracted keratin and the hydrogels formed had similar structure and showed characteristic amide bonds. The gel had a considerably porous structure at the top compared to the bottom (Figure 5.6). No cytotoxicity was observed due to the hydrogel after subcutaneous implantation in mice and none of the organs were affected in reference to untreated mice. Wound closure and healing was considerably improved in the implanted mice compared to the control (Figure 5.7).

Sponges made from the wool keratin were further chemically modified to have carboxyl or amino functional groups (Tachibana, 2006). For carboxyl modification, the sponges were treated with 10 mL of 0.1 iodoacetic acid in 0.5 M Tris HCl at pH 8.5 and for the amino sponges, the material was treated with 2-bromoethylamine under similar conditions. Sponges became considerably harder and the carboxyl content was reported to double after treatment. Treated sponges showed increased absorption of lysozyme with increasing time or amount of lysozyme. Osteoblastic differentiation was considerably higher on the treated sponges with alkaline phosphatase (ALP) activity being about two times higher. Further, the carboxyl-treated sponges had ALP activity

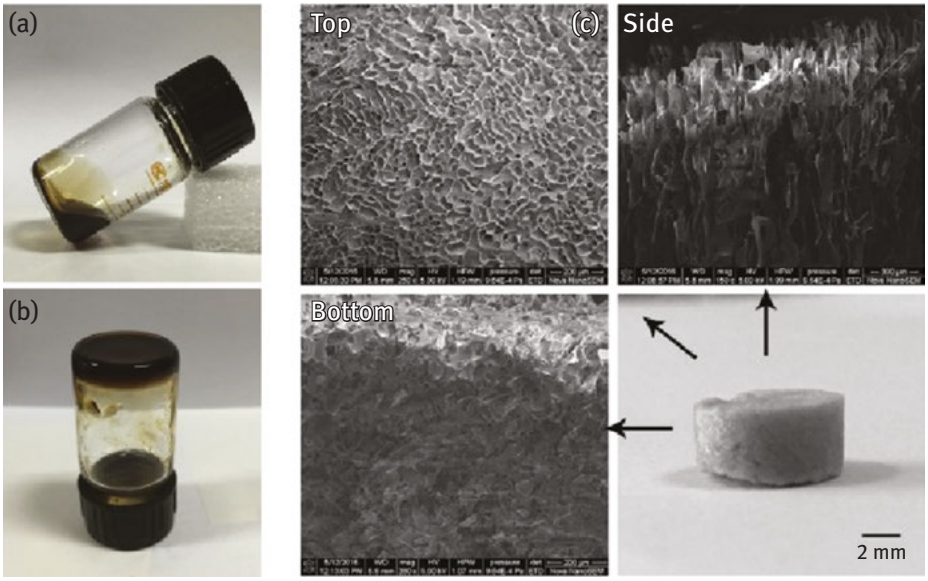

Figure 5.6: Digital image of the keratin hydrogel showing stability in upright (a) and inverted (b) positions. SEM images reveal that the top surface is highly porous (c) compared to the bottom side of the scaffold (Wang, 2017). Reproduced with permission from Elsevier.

of 1.2 compared to 0.4 for the amino-treated sponges due to the basic nature of the ALP proteins that provides better ability to bind to the carboxyl group. The lysozyme showed a release of about 11% under physiological buffer. To enhance the differentiation of cells on the carboxyl and amino-modified keratin scaffolds, the sponges were hybridized with calcium phosphate. Two approaches were used for the calcification of the scaffold. In the first approach, the chemically modified sponges were immersed with buffer containing calcium phosphate ions and in the second approach; hydroxyapatite (HA) particle suspension was added so that the HA particles could be trapped in the scaffold. Calcium phosphate crystals were observed on the surface and inside the scaffold whereas the HA particles were held within the scaffold and did not come out when washed with water. ALP activity was considerably higher on the HA-trapped sponges which was suggested to be due to the crystallinity of the HA. It was concluded that both hybridization methods were suited for better differentiation of osteoblasts (Tachibana, 2005).

Hydrogels were made by blending keratin with another biopolymer, alginate and 2D and 3D scaffolds were developed for tissue engineering applications (Silva, 2014). Keratin was extracted from wool and blended with alginate, and the blends were subject to sonochemical treatment to form the hydrogels. Ultrasound treatment changed the structure of the keratin from α to β with some extent of disordered regions also being present. No significant differences were observed in the thermal behavior of the

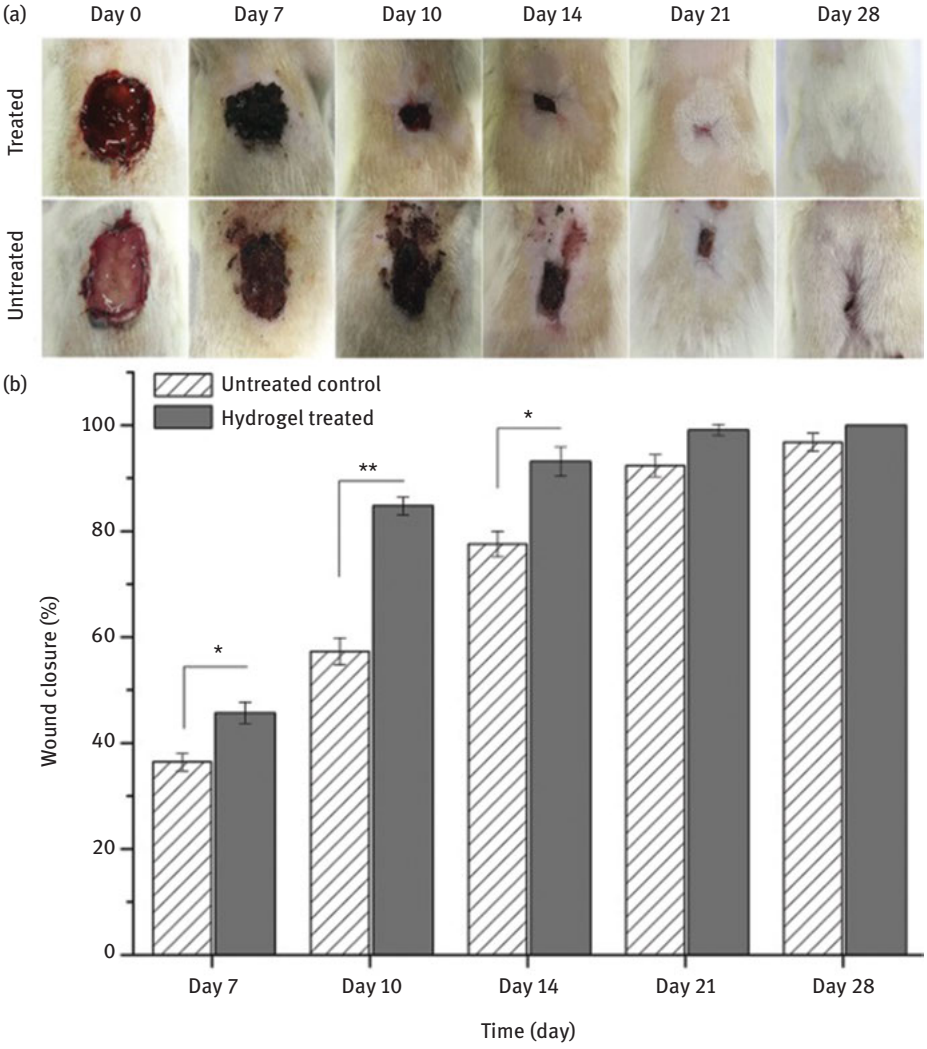

Figure 5.7: (a) and (b) Progressive changes in wound healing and wound closure of rabbits with and without subcutaneously implanted hydrogels (Wang, 2017). Reproduced with permission from Elsevier.

alginate and alginate–keratin blend hydrogels. Addition of keratin increased the water absorption capacity of the hydrogels and the 3D hydrogels had higher absorption than the 2D hydrogels. Similarly, an increase in modulus from 100 to 400 kPa was observed after the addition of keratin. Substantially higher increase in the attachment and proliferation of cells was observed on the blend hydrogel compared to the pure alginate hydrogel (Silva, 2014) (Figure 5.8). Cells encapsulated inside the hydrogels were viable until 4 weeks and were considered suitable for medical applications.

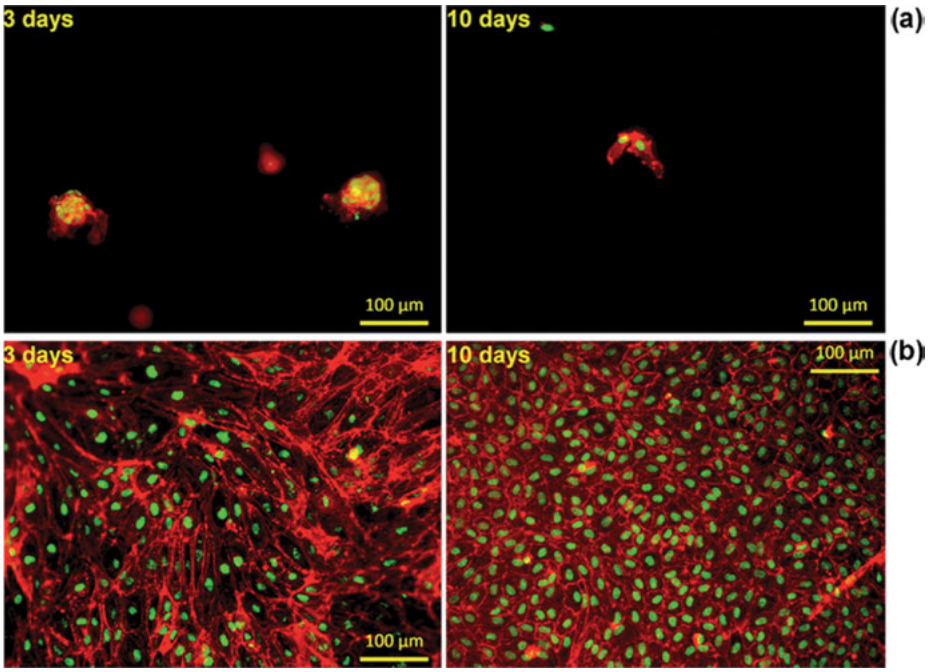

Figure 5.8: (a) and (b) Proliferation of cells on the 2D hydrogels after 3 and 10 days of cultivation (Silva, 2014). Reproduced with permission from Royal Society of Chemistry.

In many instances, a single polymer will not be an able to provide the desired properties and hence, two or more polymers are combined to develop the biomaterial. In one such effort, keratin extracted from wool was combined with alginate and hydrogels were developed. To extract keratin from wool, degraded wool fabrics were immersed in a solution containing 8 M urea, 0.2 M SDS, 0.5 M sodium bisulfite and heated to 60 °C for 12 h. Keratin solution was dialyzed against distilled water using a cellulose tubing with molecular weight cut off of 12,000 to 14,000 Da (Park, 2013). Keratin extracted (sulfitolysis) from wool and human hair was blended with PVA and made into hydrogels. Various ratios of the S-sulfo keratin were added into PVA solution containing 0.01% poly(ethyleneimine) (PEI) and cast into gels (Park, 2013). The gels formed were irradiated with an electron beam at a dose rate between 10 kGy–100 kG at room temperature. Radiation was observed to induce scission reactions and also cross-linking through free-radical reactions. Considerably lower dosage of 10 kGy was possible when 0.01 wt% of PEI was included during irradiation. Swelling ability and strength of the gels decreased above an optimum dosage level. Strength of the wool keratin gel was highest at 20 kGy higher than the strength of hair keratin and PVA gels made under similar conditions (Figure 5.9) (Park, 2013).

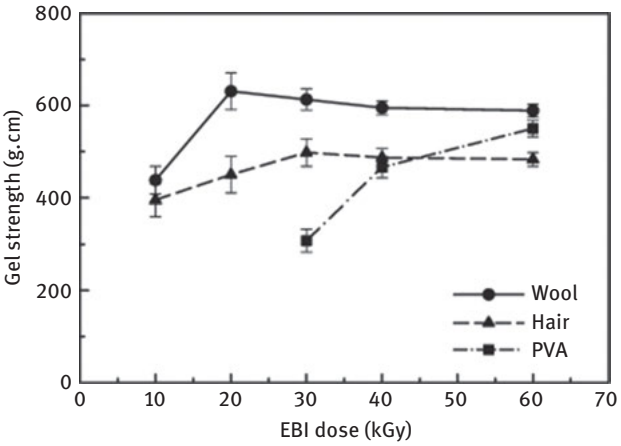

Figure 5.9: Changes in the strength of wool and hair keratin gels after different levels of exposure to irradiation compared to strength of PVA (Park, 2013). Reproduced with permission from Elsevier.

To prepare keratin–alginate hydrogels, wool fabrics were treated with urea, SDS and sodium sulfite and heated to 60 °C for 12 h. After treatment, the hydrolyzed keratin was dialyzed and collected. Alginate and keratin were combined together using sonochemical and pressure-driven extrusion to obtain 3D hydrogels in the form of films and microcapsules (Silva, 2014). Water uptake, weight loss, morphology and mechanical properties of the hydrogels were studied. Water uptake was higher (3,200%) for alginate gels than the alginate–keratin blend (2,000%). Absorption of up to 4,200% was seen in the 3D gels due to the presence of microcapsules (Figure 5.10). When treated in the medium, degradation was up to 60% for the alginate but considerably lower at about 30% for the blend gels. In addition, the blend hydrogels had considerably higher modulus of up to 500 kPa compared to 120 kPa for the pure gels (Silva, 2014). Cells

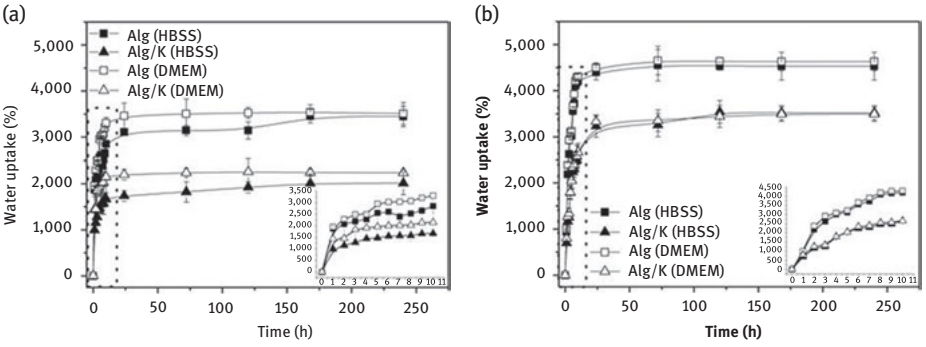

Figure 5.10: (a) and (b) Uptake of water by the 2D and 3D hydrogels in DMEM and HBSS media (Silva, 2014). Reproduced with permission from Royal Society of Chemistry.

seeded on the blend scaffolds showed considerably higher growth and proliferation than the pure scaffold. The blend hydrogels had viability of up to 4 weeks for the cells during which typical morphology and mitochondrial activity was observed suggesting that the hydrogels were suitable for tissue engineering and regenerative medicine applications (Silva, 2014).

Hydrogels and microcapsules for tissue engineering applications were developed by blending keratin with alginate, alginate dialdehyde (ADA) and bioactive glass (Reakasame, 2018). Keratin was extracted from wool fabrics using urea, SDS and sodium sulfite. Dissolved keratin was dialyzed against 12–14 kDa membranes and collected. Hydrogels were prepared by blending keratin with different polymers and formed into hydrogels. These hydrogels were made into microcapsules by extruding through a high-precision fluid dispenser at a pressure of 1–2 bars. Ionic cross-linking of the microcapsules was done by treating with 0.1 M $CaCl_2$. Presence of keratin having molecular weight between 40 and 60 kDa was confirmed in all the blends. Biomineralization had occurred on the surface of the scaffolds after immersion in simulated body fluid for 7 days. Presence of ADA increased the biodegradation compared to alginate or bioactive glass. MG-63 cells grown on the hydrogels for 21 days showed good cell viability for alginate or ADA but slight cytotoxicity was noticed in the presence of bioactive glass (Reakasame, 2018).

5.3 Wool keratin for hydrogels

Highly porous keratin sponges were prepared by treating wool keratin with 8 M guanidine hydrochloride and mercaptoethanol at 60–70 °C for 18 h (Ozaki, 2014). Keratin sponges had a density of 0.188 g/cm^3, strength of 47 MPa and modulus of 102 MPa, considerably higher than that of similar sponges made from collagen. The gels were able to swell up to 874% when immersed in PBS and supported the attachment and growth of PC12, HOS and murine embryonic fibroblasts (MEF) cells. Mechanical properties, biocompatibility and stability under physiological conditions of the hydrogel sponges were considered suitable for tissue engineering applications (Ozaki, 2014).

A particulate leaching and freeze-drying method was used to obtain highly porous and flexible wool keratin sponges (Hamasaki, 2008). In this approach, keratin was combined with dried calcium alginate beads and formed into sponges through lyophilization. The sponges were later treated with EDTA solution to leach out the calcium alginate particles resulting in a porous scaffold. Compared to the keratin sponge that had pore size of 60 μm, the keratin alginate sponge had pore size between 500–600 μm that further increased to about 1,000 μm upon swelling (Hamasaki, 2008). Considerable differences can be observed in not only the morphology but also the physical and mechanical properties of the scaffolds. Sponges formed by particulate leaching had about 1/10th the density of the regular freeze-dried scaffolds and the water uptake was nearly 9 times higher due to the highly porous nature. However, no

significant differences were observed in the cell attachment and growth on the two scaffolds (Hamasaki, 2008).

Pure keratin obtained from either wool or human hair did not gel without the addition of PVA. Further, keratin–PVA blend required a radiation dose above 90 kGy which could potentially damage the proteins. To overcome these limitations, PEI was used as a gel accelerating agent. Solutions containing PEI could gel even when irradiated at 10 kGy indicating that PEI could accelerate gelation (Park, 2013). SEM images showed that the keratin gels had a highly porous structure compared to PVA and that the human hair hydrogel had larger pore size than the wool hydrogel. At low dosage of irradiation, wool-keratin-based hydrogels had higher strength but both PVA and the wool keratin hydrogels had similar strength at high dosage rates. Gels made from keratin extracted from human hair had relatively lower variation in strength with increasing dosage rates. High porosity that provides good swelling, acceptable strength and eliminates the need for chemicals were considered to be advantages of the keratins gels made using this approach (Park, 2013).

5.4 Hydrogels from human hair

Proteins extracted from human hair were coated onto cell culture plates and also made into porous scaffolds for potential use as tissue engineering scaffolds (Verma, 2008). To extract the proteins, human hair was treated with water and later with ethanol to remove lipids. After removal of the lipids, the hairs were immersed in a solution containing urea, thiourea and β-mercaptoethanol for 3 days at 50 °C. Solution containing the extracted proteins was filtered and dialyzed and lyophilized to obtain protein powder. The powder was coated onto tissue culture plates and also formed into porous sponges (Figure 5.11) through lyophilization (Verma, 2008). Proteins extracted from the human hair had molecular weights in two ranges (40–60 kDa and 15–30 kDa) and their isolectric point was between 4.5 and 5.3 (Verma, 2008). Sponges developed had a porous morphology with pore size of about 150 μm. Proteins coated on the culture plates showed similar attachment and proliferation of cells but the sponges had significantly higher proliferation compared to untreated plates. Based on these results, it was suggested that the porous keratin scaffolds could be used as substrates for tissue engineering.

In another investigation, proteins extracted from human hair were made into hydrogels for rapid regeneration of peripheral nerves (Sierpinski, 2008). Hydrogels were irradiated with γ-rays and used for in vitro and in vivo studies. For the in vitro studies, Schwann cells were treated with keratin containing serum and the proliferation of the cells was studied. In case of in vivo analysis, the hydrogels were inserted inside a surgically cut tibial nerve and the regeneration was observed. Six weeks after implantation, the tibial nerve was subject to muscle force measurements and it was determined that the gels had enhanced the strength of the nerves. MTS assay results

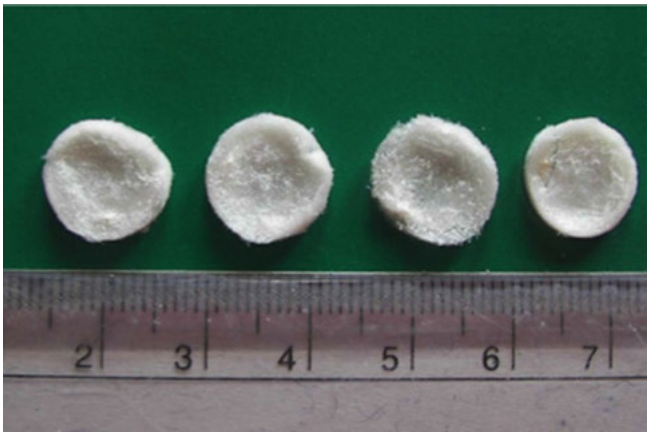

Figure 5.11: Digital images of sponges made from human hair proteins (Verma, 2008). Reproduced from IOP science.

showed that the cells incubated with protein containing media had substantially higher attachment and proliferation compared to the cells cultured with the serum alone. When implanted in vivo, bridging of the nerve gap was observed for the nerve containing the keratin with excellent angiogenic response. However, muscle force had not fully recovered after 6 weeks for any of the samples. Despite this limitation, keratin biomaterials were considered to be neuroconductive and capable of enhancing nerve tissue regeneration (Sierpinski, 2008). Similarly, hydrogels made from human hair were studied as biomaterials that could stimulate regeneration of conduits similar to commercially used autografts (Hill, 2011).

5.5 Formation of hydrogels through oxidation

In a different approach, human hair was oxidized and the changes in structure and properties of the oxidized keratin (keratose) were evaluated. Hydrogels were developed from the oxidized keratin and the potential of using the hydrogels as implants was investigated (Guzman, 2011). To obtain the oxidized keratin, human hair was treated with 20 times its weight of 2% peracetic acid for 10 h at 37 °C. After treatment, the hair was further extracted with ultrapure water and later dialyzed and crude extracted was collected (Guzman, 2011). Keratose formed was freeze-dryed, ground into powder and sterilized using gamma irradiation. The extracted keratose was redissolved in PBS and incubated at 37 °C to form gels. Viscoelastic and mechanical properties of the hydrogels were measured. Scaffolds obtained were highly porous in nature and the porosity was measured to be about 78% and the average diameter of the pore cell was 13 ± 1 μm. Hydrogels were made into scaffolds by placing them into molds and freeze-

drying. Dry scaffold had strength of 1.4 MPa but immersion into PBS turns the scaffold into a highly porous gel having lower strength (Guzman, 2011). Scaffolds were implanted into mice along with scaffolds made from poly(glycolic acid) as the control. Substantial changes in the morphology of the hair were observed with the corticles in hair being completely removed and the keratose sample consisting of only the cuticle portion. As seen from the SEM images (Figure 5.12), the scaffolds retain the structure of

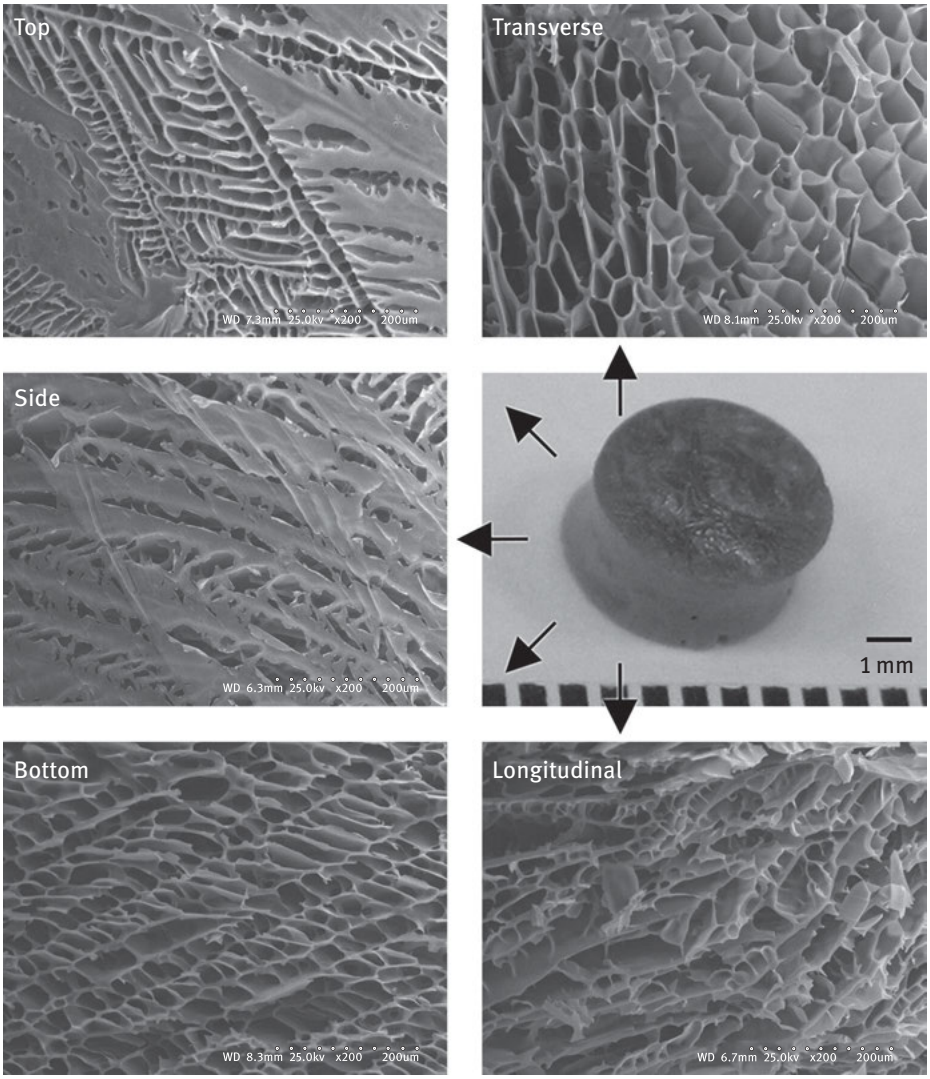

Figure 5.12: SEM images of the keratose scaffolds reveal the porous structure in almost all directions (Guzman, 2011). Reproduced with permission from Elsevier.

the feathers since distorted honeycombs were still intact. The keratose solution when incubated with multiple cell lines did not show any cytotoxicity and was able to pass the in vitro cytotoxicity test as prescribed by ISO 10933 part 5. When subcutaneously implanted in mice, the keratose gel was able to integrate into the tissue and degrade up to 92%. No adverse reactions were observed and it was suggested that the gels could be useful as scaffolds to deliver drugs and other payloads (Guzman, 2011).

In another approach, keratin was made into hydrogels and later oxidized using hydrogen peroxide to convert the keratin into keratose. The conversion was achieved by treating the keratin gels with 5% and 30% hydrogen peroxide at temperatures between 4 and 60 °C for 16 h. Oxidation of keratin to keratose was confirmed using Fourier transform infrared spectroscopy spectrums. Although there was no major structural change in the keratin backbone, kertose hydrogels had higher swelling than keratin. Decrease in β-sheet and increase in sulfonic acid groups allowed easier expansion and hence higher water uptake by the polypeptide chains. The gels also had stimuli response behavior toward pH and specific ions (Figure 5.13) desirable for tissue engineering and controlled drug release applications (Galaburri, 2019).

Instead of blending with another polymer, keratin-based gels were manufactured by chemically modifying the gels through various means. Keratin and modified keratin gels were characterized for their solubility, modulus, swelling and potential to load and release drugs and be used as scaffolds for tissue engineering (Nakata, 2015). Elastic modulus of the gels was dependent on the concentration of keratin used with the modified gels having considerably lower modulus than the native gels when high concentration (180 mg/mL) was used. At low concentrations, the acetamidated keratin hydrogels had substantially higher modulus than the unmodified keratin gels due to better arrangement of the molecules in the hydrogel. Swelling of the hydrogel was dependent on the pH with a swelling ratio of 1,200% when the pH was 10.5 for the unmodified keratin. Carboxymethylated hydrogel dissolved at pH 7.4 and 10.5 due to increased hydrophilicity whereas the acetamidated keratin provided relatively stable hydrogels with swelling ratios of 500 and 600 when the pH was 7.4 and 10.5, respectively (Nakata, 2015). Fibroblast cells were found to attach and proliferate on all the keratin scaffolds similar to that of commercially available culture plates. However, cells were mostly found on the surface and unable to penetrate the gels. When used as a drug carrier, the unmodified and acetamidated hydrogels provided sustained drug release for 3 days but the aminoethylated keratin and carboxymethylated keratin hydrogels released the drugs within 1 day (Nakata, 2015).

Dual-sensitive keratin-based hydrogels were also developed by combining *N*-isopropyl acrylamide and itaconic acid and cross-linking with *N*, *N*-methylene bisacrylamide (MBA) (Figure 5.14). Morphological analysis showed that the three polymers in the blend hydrogels had egg shaped rods of about 60–200 nm which were interconnected and formed an interpenetrating polymer network. However, the blend scaffolds had higher swelling than the individual polymers. Hydrogels showed pH dependent release behavior. A slow release of about 53% after 12 h had occurred at pH

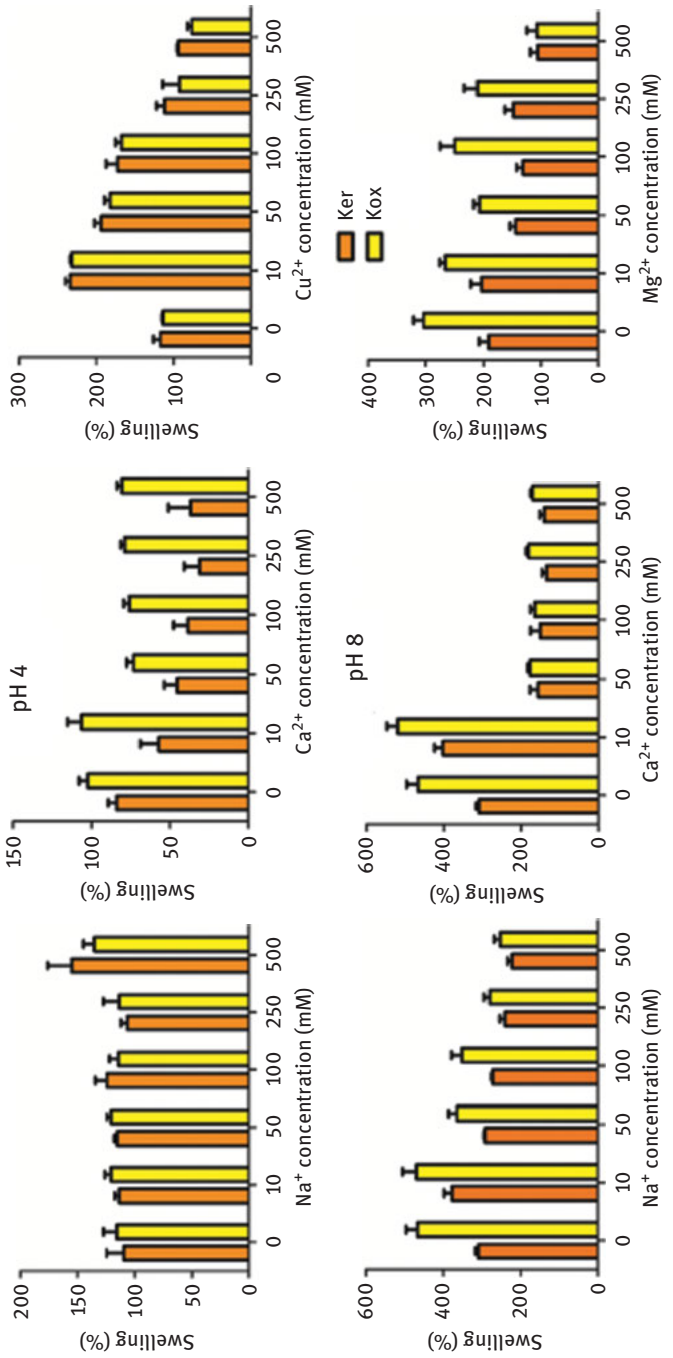

Figure 5.13: Swelling behavior of the keratin and keratinose hydrogels at different cationic conditions (Galaburri, 2019). Reproduced with permission from Elsevier.

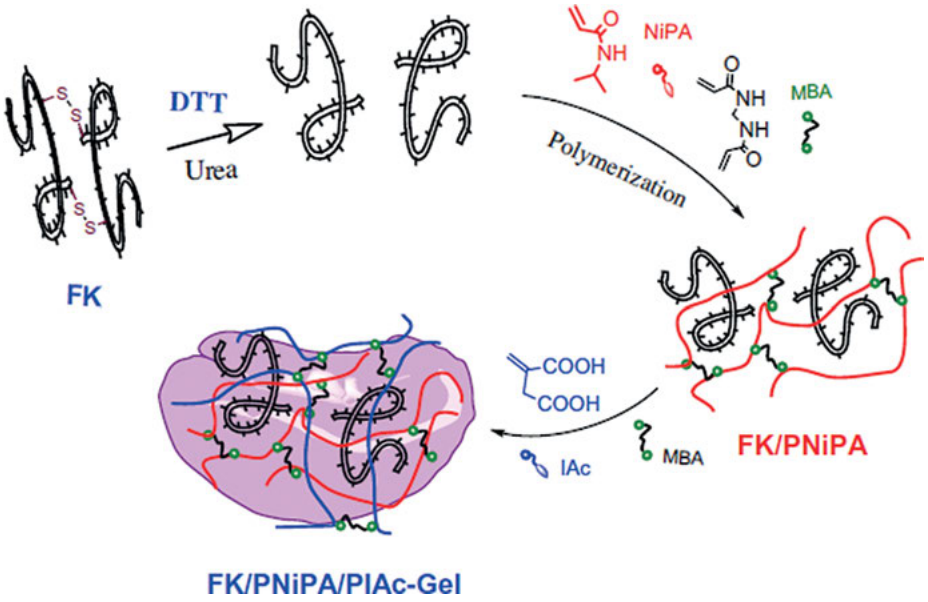

Figure 5.14: Schematic of the process used to prepare the dual sensitive keratin hydrogel (Sun, 2016). Reproduced with permission from Taylor and Francis.

1.2 compared to 84% release at pH 8.4 for rhodamine blue. For the drug Dox-HCl, a release rate of 66% was obtained under acidic environment compared to 93% under neutral and 81% under alkaline environment (Sun, 2016). Release behavior of BSA from the hydrogels was different than the other two drugs with 43% released at pH 1.2 compared to 60% in pH 8.4. In addition to pH response, the hydrogels also showed temperature-dependent release with 60%, 76% and 90% released at 25, 37 and 42 °C, respectively. Ability to control release based on pH and temperature was considered ideal for drug delivery and other medical applications (Sun, 2016).

Keratin extracted from bovine hoofs was combined with tetraethyl orthosilicate (0.4% to 5.6%) to form keratin–silica hydrogels (Kakkar, 2016). Addition of silica increased the hardness of the hydrogels from 46 to 184 g and cohesiveness of the hydrogels from 0.42 to 1.49 g when the silica concentration was increased from 0.4 to 5.6 mg/mL. Similarly, adhesiveness increased from 0.1 to 0.7 mJ and compressive modulus from 1 to 5 kPa. The hydrogels that swelling of about 540% considered to be good for biomedical applications. NIH3T3 cells were able to penetrate the hydrogels and showed good attachment and proliferation. Keratin–silicate hydrogels were suggested to be suitable for wound healing applications (Kakkar, 2016). Keratin extracted from bovine hoofs was combined with two different ratios of graphene oxide (GO) and made into hydrogels for potential use as an absorbent for pollutants, particularly ciproflaxin in wastewater (Ramos, 2018). To prepare the hydrogels, keratin powder was combined with dilute NaOH in ethanol and stored

at 45 °C for 4 h. Later, either 0.5% or 2% of graphene oxide dispersed in ethanol was mixed with the keratin suspension and cast to form hydrogels. Addition of GO increased the storage modulus and hence the stability of the gels but did not change the interaction between keratin chains. The gels were able to swell considerably even after being completely dry, and keratin retained its pH responsive behavior. The gels were able to sorb ciproflaxin and also release the drug easily, making the gels reuseable (Ramos, 2018).

5.6 Hemostatic wound dressings

Expandable sponges with excellent hemostatic ability were made using human hair keratin and acrylamide (Wang, 2019). Desired ratio of keratin and acrylamide were dissolved in 0.3% N,N-methylene bisacrylamide (MBA) and stirred at room temperature. Sponges formed were washed with ethanol and dried at 50–55 °C for 6 h (Wang, 2019). The reaction during the formation of the sponges, morphology of the scaffolds containing different level of keratin and some of the other properties of the sponges are shown in Figure 5.15. The hemostatic ability of the sponges was evaluated in vivo by inserting the sponges in penetrating trauma in mice. Considerable decrease in amount of blood loss and time to hemostatis was possible with 20% keratin-containing sponge compared to gauze or pure acrylamide (Figure 5.15) in both liver and femoral artery transection hemorrhage. Also, the treated sponges were able to biodegrade in the body within 28 days. Human hair keratin made into sponges (200 μm pore size) was also able to promote the regeneration of peripheral nerves in rats (Gao, 2019). Keratin obtained had molecular weight between 40 and 60 kDa, which was coated onto the well plates. Cells (RSC96) seeded on the keratin-coated plates showed about 70% adhesion compared to 45% for the control. When implanted at the peripheral nerve injury site, the keratin sponge was absorbed in the body and completely degraded within 5 weeks. Axon diameter and thickness of myelin sheath in the nerves was higher at the injury site treated with keratin sponge compared to the control. As a direct visualization of the ability of keratin sponge to cure peripheral nerve injury, it was observed that the footprint of the mice approached that of normal mice within 10 days compared to 21 days for the untreated samples. Similarly, sciatic nerve function, weight of muscle and muscle fiber were higher for the keratin-treated injury (Figure 5.16).

Keratin hydrogels prepared from human hair were also able to provide excellent hemostatic resistance. Porous keratin hydrogels were developed and injected in situ into intracerebral hemorrhage surgery to control bleeding. Insertion of the keratin gel was found to substantially reduce hematoma volume, decrease cell apoptosis, neuroinflammatory reaction and neurological deficiencies. Keratin gels were considered to be highly suitable as hemostatic agents without compromising on the biocompatibility (He, 2019). In another study, keratin was extracted from human hair and made into a hydrogel (Aboushwareb, 2009). Keratin extracted had proteins in two molecular

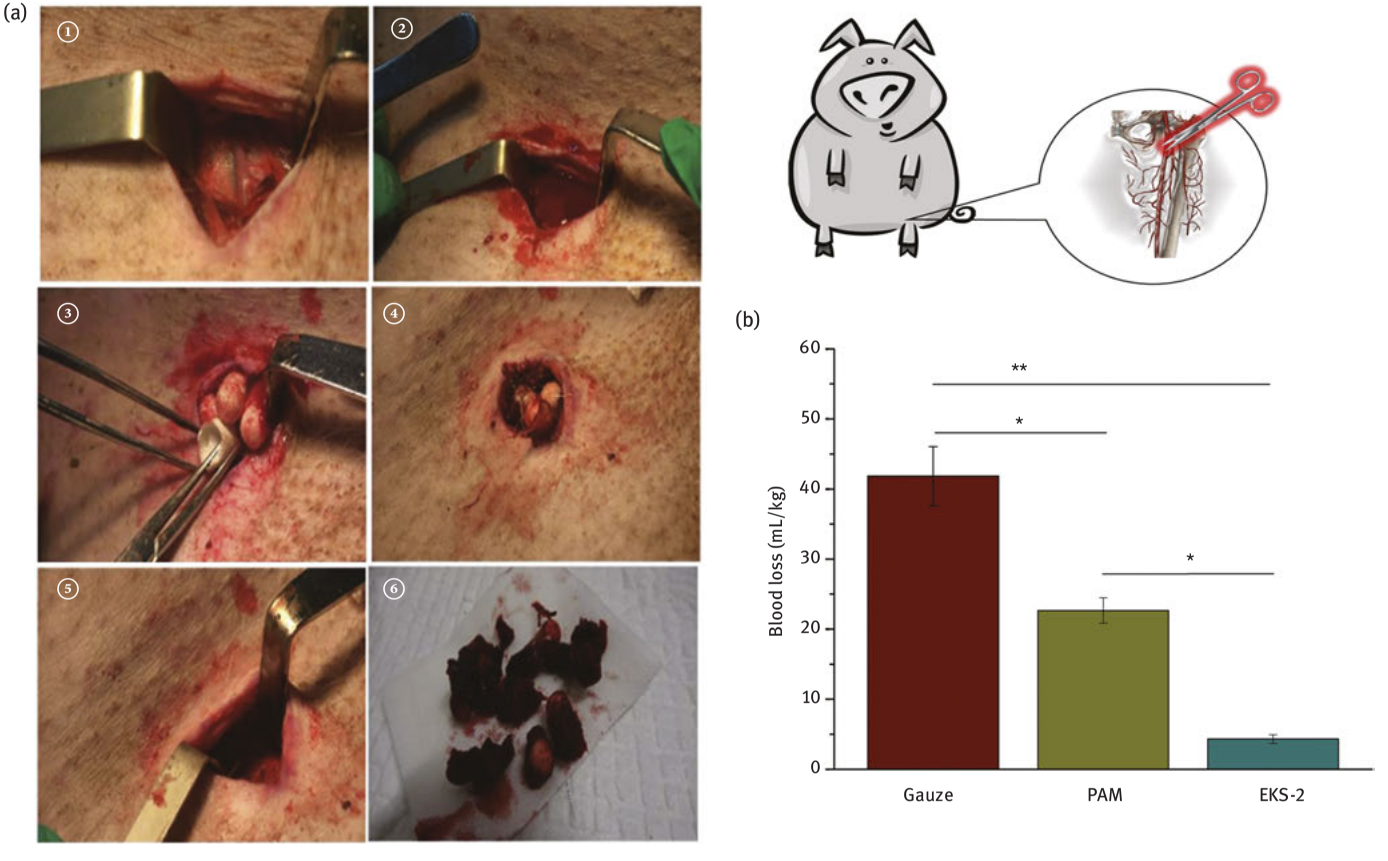

Figure 5.15: Images showing the decrease in hemorrhage after treating with the keratin expandable sponge (a); the sponge has excellent hemostatic ability and resulted in lower blood loss compared to gauze and polyacrylamide (b) (Wang, 2019). Reproduced with permission from Elsevier.

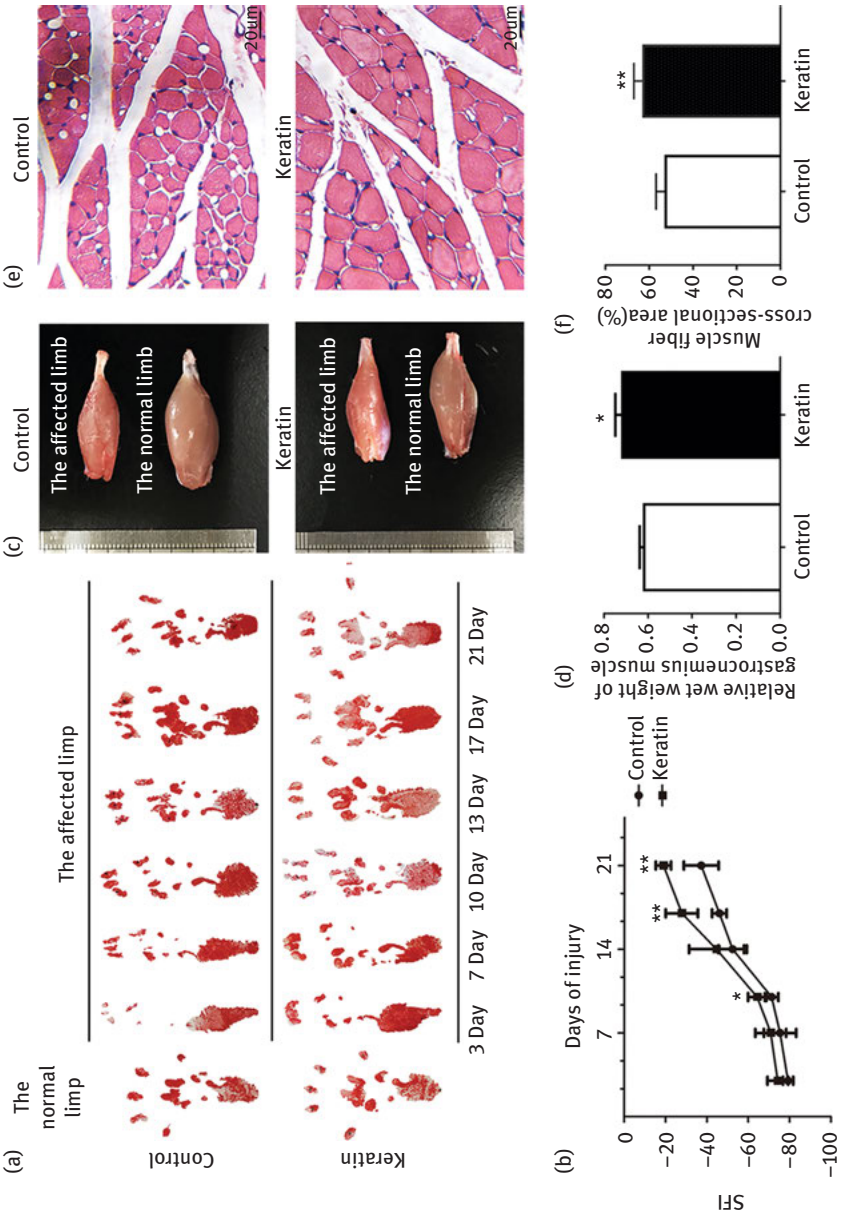

Figure 5.16: Improvement in the footprint of mice with and without the keratin sponge treatment (a); amount of nerve function (b), muscle structure (c), muscle weight (d) and muscle fiber cross-sectional area (e, f) changes with and without the keratin sponge implant (Gao, 2019). Reproduced with permission through open access publishing.

weight groups with most of the proteins between 64 and 43 kDa and some proteins in the 16 to 10 kDa region. Amino acid analysis showed that the keratin had a highest concentration of threonine (19%) and about 12% of serine, cysteine and glutamic acid. Keratin gel was placed in an artificially injured liver in mice (Figure 5.17) and the ability of the keratin gel to reduce hemostatis was studied in comparison to various commercially available hemostatic wound dressings (Aboushwareb, 2009). Blood loss tests (Figure 5.18) showed that the keratin- and QuikClot-treated mice had the lowest amount of loss. Keratin gel was also able to maintain stable mean arterial pressure,

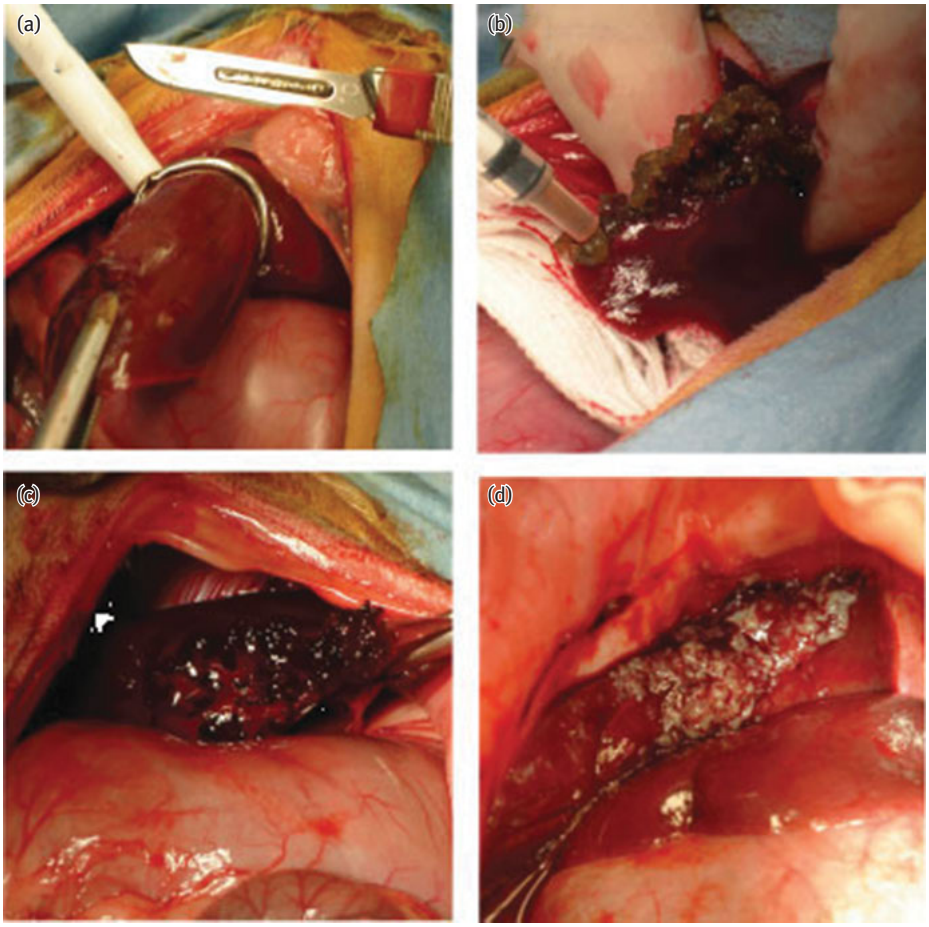

Figure 5.17: Digital pictures show the procedure of implanting and the efficiency of the keratin gel to absorb and stop blood flow. (a) The liver on which the gel would be placed; (b) application of the gel on the traumatized liver; (c) image shown after applying the gel and after 20 min of application; (d) complete stopping of the bleeding 30 min after implanting the gel (Aboushwareb, 2009). Reproduced with permission from John Wiley and Sons.

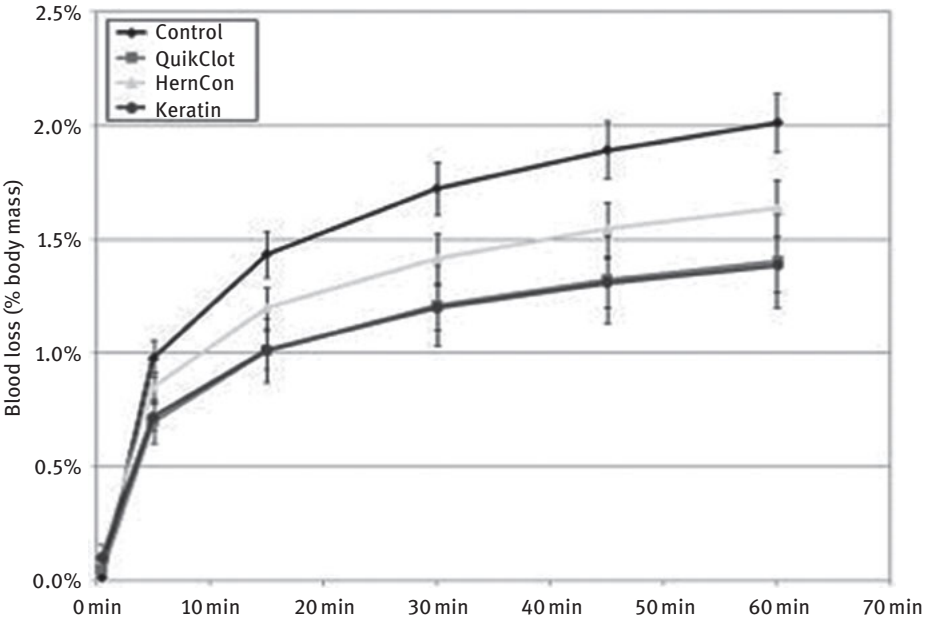

Figure 5.18: Decrease in blood with increasing time after implanting the various hemostatic gels (Aboushwareb, 2009). Reproduced with permission from John Wiley and Sons.

and the shock index was considerably lower when compared to other scaffolds. Further, no negative response from the cells was observed and the keratin gels were considered to be suitable for hemostatic dressings.

5.7 Nanogels and aerogels

Nanogels that are responsive to dual stimuli were prepared by combining human hair keratin and alginate and cross-linking (using hydrogen peroxide) the two polymers (Sun, 2017). Keratin from human hair and alginate solution were combined and made into nanogel particles by freeze-drying after removing unreacted polymers by dialysis. DOX was added into the solution and drug loading and release efficiencies were calculated. A schematic representation of the process used to prepare the nanogels is shown in Figure 5.19. The particles in the gel had an average size distribution between 60 and 90 nm, suitable for passive tumor penetration and accumulation. Also, the nanogels had zeta potential of −46 mV and hence considered to be stable. Extensive formation of disulfide bonds and some hydrogen bonding was observed which led to the stability of the gels. A high drug loading efficiency of 75% was obtained due to the high negative charge on keratin–alginate gel compared to the highly positive charge on the drug.

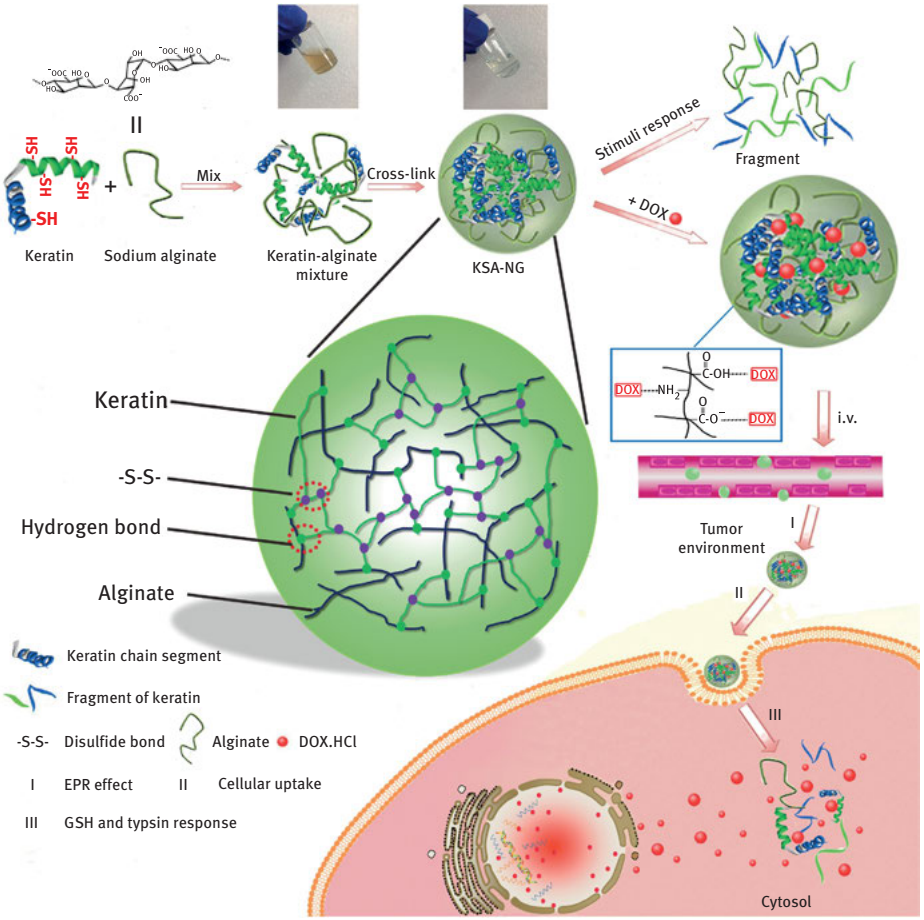

Figure 5.19: Schematic representation of the process used to prepare keratin–alginate nanogels and their anticipated mode of cancer treatment (Sun, 2017). Reproduced with permission from Elsevier.

Similarly, a high release rate of 76% was obtained in the presence of trypsin. The blend nanogels were able to enter and accumulate in tumors and had a longer retention time. The nanogels did not show any cytotoxicity and were hence considered suitable for anticancer drug delivery and therapy (Sun, 2017).

Similar to hydrogels and nanogels, chicken feather fibers were used as reinforcement for PVA–clay aerogels (Sun, 2018). Montmorillonite (clay) was added into water and stirred at 22,000 rpm for 1 min to form a 10% suspension. Later, 5% PVA solution was added into the clay solution and formed into a hydrogel. Similarly, feather fibers were added and made into gels with composition of 1–3% fibers, 5% clay and 2.5% PVA. Compressive strength of the fibers increased with increasing concentration of fibers both for the clay and clay–PVA gels (Figure 5.20). It was suggested that feather

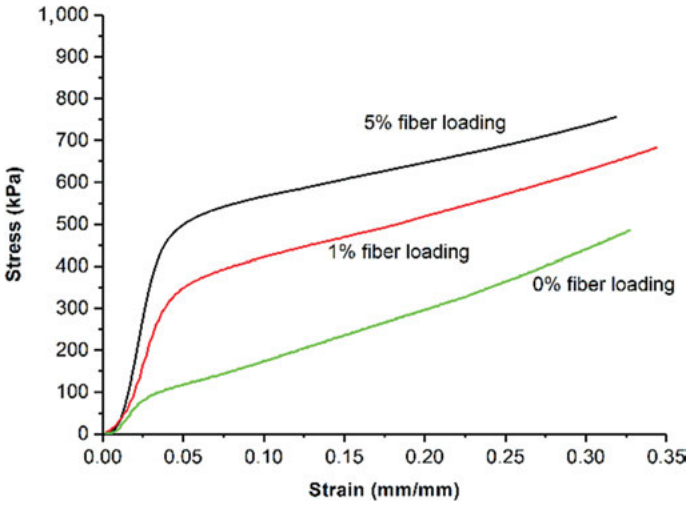

Figure 5.20: Increase in the compressive strength of keratin reinforced PVA–clay aerogels (Sun, 2018). Reproduced with permission from Springer.

fibers consist of hook like structures which will entangle with the matrix and thereby increase the mechanical strength. Also, keratin fibers have good interaction with the polar polymer/clay matrix via hydrogen bonds which will also facilitate improved performance properties. Inclusion of the fibers and its interaction with the matrix substantially altered the morphology including the porosity and pore size. Porous nature of the gels also led to better thermal insulation with thermal conductivity decreasing from 0.075 to 0.058 W/mK, suitable for insulation applications (Sun, 2018).

Chapter 6
Keratin for environmental remediation

Due to the large availability and low cost, keratin from feathers, wool and other sources have been studied as a potential bioabsorbent for various pollutants and also for purification of water. The ability of a keratin colloidal solution to remove Pb(II) from water was studied by Sekimoto (2013). Removal of Pb(II) from water by the keratin colloidal solution was highly dependent on the conditions used for removal. The removal efficiency ranged from 6.7% to as high as 87% (Table 6.1). Absorption of Pb per gram of keratin was between 17% and 43%. Based on adsorption isotherms, it was suggested that the monolayer adsorption of Pb(II) onto keratin occurred due to the presence of the thiol and amino groups on the surface of the particles. Highest absorption by the keratin particles was about 43.3 mg/g, which was higher than that of activated carbon and similar to that of other biomaterials (Sekimoto, 2013). However, the removal of Pb(II) from solutions containing a mixture of binary or tertiary metal ions was lower when compared to the removal of Pb (II) from water (Table 6.2).

Chicken feather barbs were used to absorb zinc ions (Zn^{2+}) in both batch and fixed-bed columns (Aguayo-Villarreal, 2011). Kinetics of sorption were studied and isotherms were developed using a constant ratio of metal solution and feathers. Feathers were considered to have higher specific surface area than other absorbents used for metal sorption. A maximum Zn^{2+} sorption of 7.3 mg/g of feather was obtained at pH 5 and 30 °C. It was suggested that the acidic nature of feathers makes it a natural absorbent for zinc ions.

Chromium (Cr (VI)) is another metal that is prevalent in wastewater discharged by industries. Although several technologies are adopted to remove chromium, feather as bioabsorbent was considered an ideal substrate due to its amino acid composition and large-scale availability (Saucedo-Rivalcoba, 2011). Since keratin is considerably light, it was combined with polyurethane to form a hybrid membrane. Keratin was treated with acid and alkali and also dialyzed before combining with polyurethane. Membranes obtained had pore size ranging from 7 to >50 nm. A maximum removal of 38% of chromium was achieved using alkali-treated feathers in the polyurethane membrane. Keratin extracted from chicken feathers was made into films for potential use as absorbent for chromium. The bioabsorbent was placed in Cr(VI) solution in concentrations between 50 and 500 mg/L for up to 24 h for the sorption to be complete. Mechanical strength of the keratin film was 6.2 MPa, and the porosity was 81%. Absorption increased from 3.7 to 20.3 mg/g when the initial keratin concentration was increased from 50 to 500 mg/L (Aguayo-Villarreal, 2011). However, increasing pH above 6 decreased the uptake capacity,

https://doi.org/10.1515/9781501511769-006

Table 6.1: Efficiency of Pb(II) removal from water by the colloidal keratin solution at various absorption conditions (Sekimoto, 2013).

Initial Pb(II) concentration (mM)	pH of solution	mg of keratin added	Agitation time (min)	% Removal of Pb(II)	Adsorption capacity (mg/g)
1.0	5	1.5	10	31	39
2.0	5	1.5	10	17	43
1.2	5	1.5	10	26	39
0.90	5	1.5	10	33	37
0.70	5	1.5	10	41	36
0.50	5	1.5	10	58	36
0.40	5	1.5	10	71	32
0.30	5	1.5	10	87	35
1.0	5	0.75	10	6.7	17
1.0	5	2.25	10	45	37
1.0	5	3.0	10	62	39
1.0	5	3.75	10	67	33
1.0	5	4.5	10	85	34
1.0	3	4.5	10	71	29
1.0	4	4.5	10	77	32
1.0	6	4.5	10	81	34
1.0	5	4.5	0.17	85	35
1.0	5	4.5	1	87	35
1.0	5	4.5	3	86	35
1.0	5	4.5	5	86	35

Note: Reproduced with permission from Springer.

Table 6.2: Efficiency (%) of removal of Pb(II) from solutions containing binary or tertiary mixture of metal ions (Sekimoto, 2013).

Metal ion	Single metal solution	Binary metal solution			Ternary metal solution		
		Pb ± Zn	Pb ± Cd	Pb ± Hg	Pb ± Zn–Cd	Pb ± Zn ± Hg	Pb ± Cd ± Hg
Pb(II)	85 ± 2.1	72 ± 0.9	66 ± 1.3	54 ± 2.1	65 ± 1.3	55 ± 0.6	57 ± 1.6
Cd (II)	–	–	18 ± 0.8	–	11 ± 1.3	–	8.7 ± 0.8
Zn(II)	–	14 ± 1.5	–	–	15 ± 1.0	3.2 ± 1.1	–
Hg(II)	–	–	–	64 ± 2.1	–	69 ± 1.0	73 ± 2.5

Note: Reproduced with permission from Springer.

which was about 12 mg/g when the pH was 12. The level of bioabsorption achieved in this report was considered to be similar to those obtained using common bioabsorbents. In another study, thermoplastic feather films were studied for their potential to absorb Cr(VI) in solution (Saucedo-Rivalcoba, 2011). In this study, feathers were mixed with glycerol and compression molded at 160 °C for 5 min to form thermoplastic films. The films obtained were immersed in 200 ml/L Cr(VI) solution, and

the absorption studies were conducted (Saucedo-Rivalcoba, 2011). Conditions used during absorption such as temperature and concentration of the ion solution determined the amount of absorption by the films. Under the optimum condition, a high removal of 99.1% and absorption capacity of 75 mg/g was obtained; therefore, the feather films were considered suitable for removing Cr(VI) from wastewater (Saucedo-Rivalcoba, 2011).

In another study, a series of chemical modifications were done to improve sorption of Cr(VI) and Cu(II) ions by chicken feathers (Sun, 2009). Feathers (CF) were initially treated with alkali (NaOH), and fragments of the feather keratin were later cross-linked using epichlorohydrin (EpiCF). Functionalization of the keratin–EpiCF was also done by adding ethylenediamine (EA) to obtain EAEpiCF as the sorbent. A Cr(VI) sorption of 14.4 mg/g was obtained when EAEpiCF was used as the sorbent, considerably higher than other sorbents used for removal of Cr(VI) in previous studies (Table 6.3). Up to 90% removal was achievable when the ion concentration was in the range of 10–80 ppm. In addition, EAEpiCF was also able to desorb up to 90% of the sorbed ions, and up to three resorption cycles (Figure 6.1) could be done without significant decrease in the amount of sorption.

Table 6.3: Sorption conditions and amount of sorption of Cr(VI) by modified keratin and other bioabsorbents (Sun, 2009).

Material	Sorption capacity (mg/g)	Operating parameters			
		pH	*T* (°C)	Initial metal conc. (mg/L)	Biomass conc. (mg/L)
Chlorella vulgaris	2.98	1.0–2.0	25	200	–
Cladophara crispata	6.20	1.0–2.0	25	200	–
Zoogloea ramigera	3.40	1.0–2.0	25	75	–
Rhizopus arrhizus	8.40	1.0–2.0	25	125	–
S. cerevisiae	4.30	1.0–2.0	25	100	–
Pilayella littoralis	6.55	5.5	25	50	2.5
Quercus ilex L. (stem)	0.07	2.7–5.0	22 ± 2	10	10
Quercus ilex L. (leaf)	0.08	2.6–4.8	22 ± 2	10	10
Quercus ilex L. (root)	0.09	2.6–5.4	22 ± 2	10	10
Rhizopus nigricans	12.70	2.0	45	250	10
Rhizopus nigricans	21.22	2.0	–	100	2
Neurospora crassa	15.85	1.0	25	250	1
EAEpiCF	14.47	4.1	20	80	5

Chicken feathers were also found to be suitable to remove Zn^{2+} from wastewater in both continous and batch treatments (Gao, 2014). Temperature, pH and initial metal concentrations were varied to achieve the maximum possible absorption. A maximum absorption of 4.3 mg/g was achieved at a temperature of 30 °C. Compared to other Zn^{2+} sorbents such as activated carbon or sunflower stalks reported in literature, the

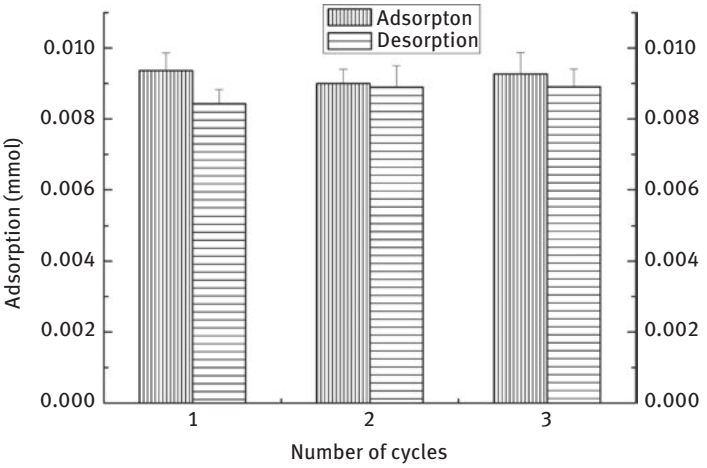

Figure 6.1: Absorption and desorption after three cycles (Sun, 2009). Reproduced with permission from American Chemical Society.

sorption by the feathers was considerably low (Table 6.4). However, feathers are relatively inexpensive and therefore would be suitable as sorbents even though higher amounts may have to be used to achieve the same level of sorption (Gao, 2014). Actual absorption closely followed that of the predicted ones with R^2 values ranging from 0.64 to 0.95. Batch absorption provided lower sorption capacities than continous sorption.

Table 6.4: Comparison of the bioabsorption ability of modified feathers with other common agents (Gao, 2014).

Bioabsorbent	Capacity, (mg/g)	pH	Bioabsorbent concentration (g/L)
Modified chicken feathers	14.47	4.1	5.0
Neurospora crassa	15.85	1.0	1.0
Pilayella littoralis	6.55	5.5	2.5
Palm flower (acid treated)	7.13	4.5	10.0
Activated carbon (coconut tree saw dust)	3.46	8.0	50.0
Ficus carica fiber-based activated carbon	44.84	3.0	10.0
Reprocessed feather	14.80	6.0	12.5

Note: Reproduced with permission from John Wiley and Sons.

Most studies report the ability of keratin to remove a single metal ion in solution. In reality, a complex of metal ions is most commonly found in wastewater. To understand the ability of keratin (chicken feathers) to sorb various metal ions,

individual and three and five metal ion solutions were used (Kar, 2004). The level of removal of ions was dependent on the type of ion and pH during sorption. Removal of cations such as copper and lead was more effective between pH 5 and 6, whereas alkaline pH favored the removal of uranium. Efficiency of removal ranged from 0 to as high as 97% depending on the pH, type of ion and the number of metal ions in the solution (Table 6.5). Initial concentration of the metal ion also influenced the removal efficiency.

Table 6.5: Percentage removal of copper of different initial concentrations and increasing reaction times.

Sample	Temperature		Time (h)		Rate (°C/min)		Residue fraction	S_{BET} (m^2/g)	C_{BET}	V_{mic} (cm^3/g)
	T1	*T2*	*t1*	*t2*	*t1*	*t2*				
1	215	400	24	1	3	3	0.176 ± 0.015	436 ± 4	1,003	0.178
2		450	24	1	3	2				0.196
3	220	450	32	1	3	2	0.101 ± 0.020	460 ± 2	6,330	0.176
4		–	1	–	3	–				0.133
5	220	400	5	1	3	3	0.063 ± 0.010	419 ± 6	845	0.072
6		500	24	1	3	3			832	0.041
7	400	500	26	1	3	2	0.209 ± 0.007	376 ± 0	300	0.002
8		–	24	–	3	–			822	<0.001
	220						0.212 ± 0.018	189 ± 6	68	
									135	
	215						0.011 ± 0.002	114 ± 0		
	220						0.004 ± 0.001	14 ± 0		
	220						0.617 ± 0.022	<1		

Note: Reproduced with permission from *Journal of Chemical Technology and Biotechnology*.

Instead of extracting keratin, feathers were treated with sodium hydroxide or sodium chlorite and ability of the treated feathers to sorb various heavy metals was studied (Sayed, 2005). pH, time, alkali used for treating the feathers and initial metal concentration were all found to influence the metal absorption. Sorption of magnesium ions was considerably low (67%) for feather treated with both the alkali-treated feathers, whereas up to 99.9% sorption was seen for magnesium and iron depending on the pH. In a similar approach, chicken feathers were modified using alkali or anionic surfactant, and their potential to remove copper and zinc was studied (Al-Asheh, 2003). As observed in other studies, amount of metal sorption was highly dependent on the conditions used during sorption. Treating feathers with alkali and surfactant lead to substantial increase in the amount of metal sorption.

Keratin from feather was solubilized by treating under alkaline condition (pH 12) at 150 °C. Four different dopants [poly(ethylene glycol) (PEG); diglycidyl ether; poly

(*N*-isopropylacrylamide); allyl alcohol (AA) and trisilanol cyclohexyl Polyhedral Oligomeric Silsesquioxane (POSS)] were added into the solubilized keratin for in situ modification and increase sorption of arsenic from wastewater (Khosa, 2014). Chemical modifications led to the formation of a hard, crystalline and brittle plastic-like product. Morphologically, feathers were converted into microporous substrates with increased roughness that could lead to higher sorption. Amount of arsenic uptake was considerably different for the untreated and treated feathers. AA and POSS-modified feathers provided higher uptake, whereas PEG-modified feathers had the lowest uptake. Introduction of various functional groups and physical changes to the structure of keratin due to the chemical modifications was suggested to be the reason for higher uptake compared to untreated feathers. Based on isotherms and regression analysis, it was concluded that both monolayer and multilayer absorption of arsenic occurs on the keratin (Khosa, 2014).

In a different approach, chicken feathers were used as a source to prepare carbon–nitrogen fibers by pyrolysis for absorbent applications (Senoz, 2010). Effect of heating the feathers at 215 °C and above 220 °C under nitrogen atmosphere on the amount of residue and pore size and porosity was investigated. Influence of pyrolysis conditions on the amount of nitrogen that the carbonized feathers could absorb is given in Table 6.6. The surface area of the samples obtained was considerably lower compared to the commercial absorbent that had surface areas of about 1,324 and 1,124 m^2/g. X-ray photon spectroscopy (XPS) (Figure 6.2) analysis showed the presence of trace amounts of phosphate and sulfur. Large C1 peaks were observed, and the C/N ratio was five times higher on the surface compared to the bulk. Excess levels of carbon found on the surface were considered to be due to the distribution of randomly oriented carbon chains on the surface of the fibers. Pyrolysis was suggested to be due to side chain

Table 6.6: Amount of nitrogen that can be absorbed by feather keratin pyrolyzed (PCFF) under different conditions (Senoz, 2010).

Sample	S_{BET} (m^2/g)	C_{BET}	V_{mic} (cm^3/g)
PCFF-6	436 ± 4	1,003	0.178
PCFF-7	460 ± 2	6,330	0.196
PCFF-8	419 ± 6	845	0.176
PCFF-10	376 ± 0	832	0.133
PCFF-9	189 ± 6	300	0.072
PCFF-12	114 ± 0	822	0.041
PCFF-11	14 ± 0 < 1	68	0.002
PCFF-13	1,342 ± 6	135	0.001
Darco KB-G	1,124 ± 3	205	0.416
Darco G		774	0.386

Note: Reproduced with permission from John Wiley and Sons.

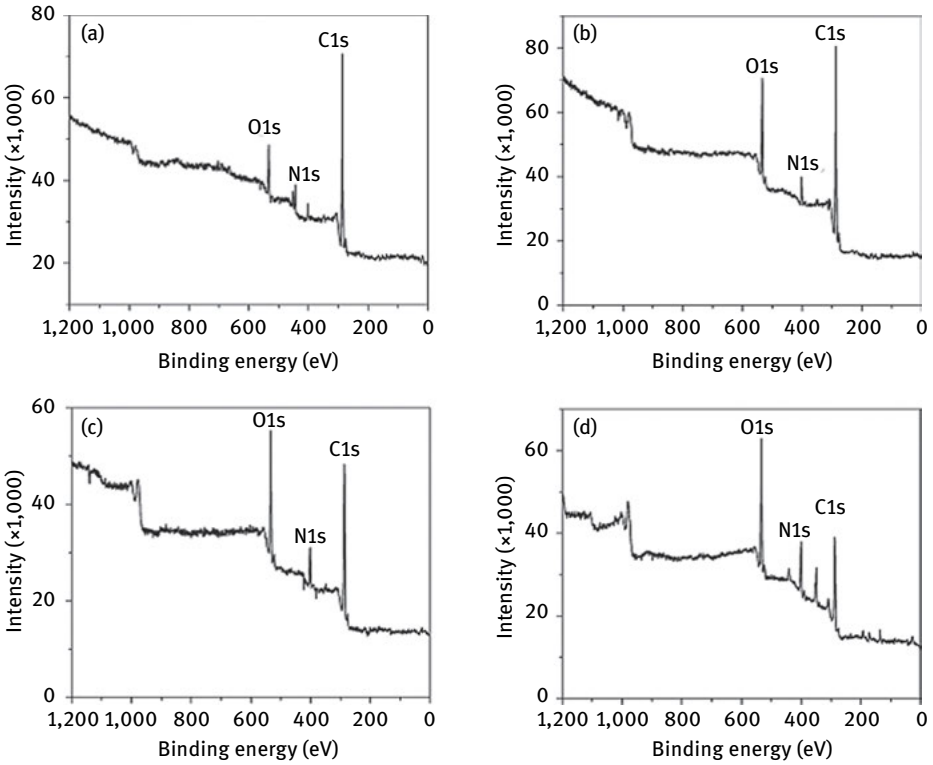

Figure 6.2: XPS spectra of the untreated and feathers treated with 3°C/min and heated to 215°C up to 4 h soaking at 215°C (a), 3°C/min to 215°C and 24 h soak at 215°C (b) and after second pyrolysis done at 3°C/min to 215°C and 4 h soak at 215°C [Senoz, 2010]. Reproduced with permission from John Wiley and Sons.

degradation and modification of the amine bonds. Pore size of the samples was considered to be narrow, which could be the reason for the lower levels of absorption (Senoz, 2010).

6.1 Wool

The ability of wool fibers to absorb metal cations from various solutions at 25 and 50 °C was investigated and the diffusion coefficients were predicted (Sun, 2009). Considerable differences were observed in the absorption depending on the concentration of the solution and the temperatures used. Consequently, the rates of diffusion were different for the different solutions studied. For example, complete removal of mercury was achieved when the temperature was 50 °C, whereas only about 30% of copper ions was absorbed. Differences in size of the ions and their

affinity to wool were considered as reasons for the different absorption behavior. Wool powder prepared after milling and chemical treatments were studied for their ability to absorb and desorb CO^{2+} from two types of buffer solutions (Sayed, 2005). Binding of CO^{2+} was heavily dependent on the pH of the buffer solution with high sorption observed at pH 8 and 10. Making the wool powder finer and exposing the cortical cells by chemical treatment led to an increase in rate and amount of CO^{2+} absorption. The absorbed CO^{2+} could be recovered (up to 70%) by washing in a buffer solution. When wool was dissolved and reused for absorption, up to 80% of the sorption of the fresh CO^{2+} could be achieved, suggesting that fine wool powder was excellent for the absorption of CO^{2+} (Sayed, 2005).

To improve mechanical properties and the amount of sorption, keratin extracted from merino wool was dissolved in formic acid and combined with polyamide 6 and electrospun into nanofibers (Aluigi, 2011). Keratin was dialyzed against a molecular weight cutoff of 11–60 kDa to enable dissolution in formic acid. Diameter of the blend nanofibers varied from 136 to 218 nm with increasing proportion of keratin leading to larger fibers. Similar variations were also observed for porosity and specific surface area. Sorption capacity of Cu^{2+} ions by the membranes was directly dependent on the conditions used. For instance, initial metal ion concentration and sorption time had a significant influence on sorption. The extent of removal of Cu^{2+} ranged from 26% to as high as 97% depending on the ratio of keratin in the membrane and concentration of metal during sorption (Table 6.7). Increasing the ratio of keratin in the membranes increased the removal efficiency irrespective of the concentration of metal ions. The maximum absorption obtained was 103 mg/g when 90% keratin was present. Sorption of Cu^{2+} onto keratin was found to be of pseudo-second order. Formation of complexes between Cu^{2+} ions and the higher carboxyl groups in proteins was suggested to be the reason for high levels of sorption (Aluigi, 2011).

Table 6.7: Influence of initial metal ion concentration on the removal efficiency of Co after 24 h and when sorption was done at pH 5.8 (Aluigi, 2011).

Concentration of Co (mg/L)	Removal efficiency (%)				
	Fabric wool	Nanofiber keratin mat			
		PA6	50%	70%	90%
0/05	68	78	80	84	94
0.3	–	33	49	60	97
1	7	–	31	50	67
10	11	22	28	29	35
35	4	18	26	39	44

Note: Reproduced with permission from Elsevier.

Wool fibers were powdered into four different sizes and were used as sorbents for various metal ions with different sorption conditions (Naik, 2010). Amount of absorption was highly dependent on the pH, time and temperature during absorption. Highest sorption (8.6×10^{-9} mol/g of sorbent) was obtained for Cd(II), whereas there was considerably lower sorption of Co^{2+} (Table 6.8). Although Co^{2+} had lower sorption, it had better binding with the keratin. Wool keratin was suggested to be particularly suited for sorption of transition metal ions (Naik, 2010). Extent of release of the metal ions from the sorbed wool powder was also dependent on the pH and time (Figure 6.3). Cu(II) and Cd(II) had considerably lower release when the pH was 8 compared to pH 3. Significantly lower amounts of Cu^{2+} ions were released at pH 8 compared to the other to ions, suggesting better binding with the wool keratin.

Table 6.8: Amount of metal ions absorbed by wool at equilibrium (Naik, 2010).

Wool sample	Moles ($\times 10^{-9}$) absorbed/mg of sorbent at equilibrium		
	Co(II)	Cu(II)	Cd(II)
1	3.9 ± 0.8	9.7 ± 1.8	9.3 ± 2.1
2	5.1 ± 0.8	8.7 ± 2.5	9.7 ± 6.2
3	5.4 ± 0.4	8.4 ± 1.4	9.0 ± 1.6
4	7.7 ± 1.2	9.1 ± 0.9	8.6 ± 3.2

Note: Reproduced with permission from John Wiley and Sons.

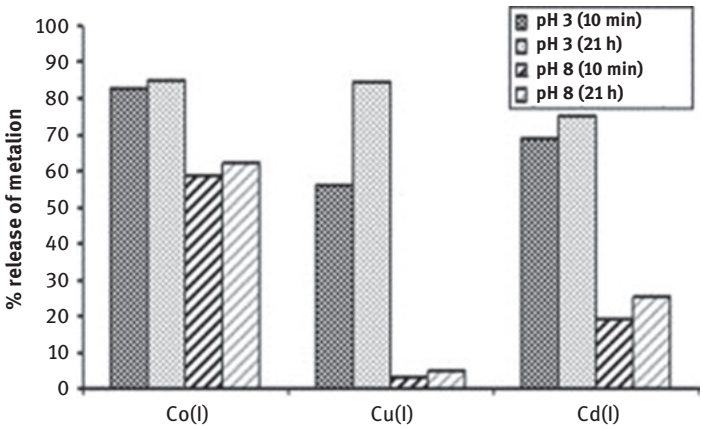

Figure 6.3: Release of the three metal ions from wool at different conditions. Reproduced with permission from John Wiley and Sons [Naik, 2010].

An investigation was done to determine the ability of keratin fibers from various sources to remove multiple metal ions from an aqueous solution. Keratin in human hair, dog hair, chicken feathers and degreased wool were used in a batch absorption experiment to sorb Cr(III), Mn(II), Ni(II), Co(II), Cu(II), Zn(II), Cd(II) and Pb(II) at a metal concentration of 0.1 mmol of each metal ion/L at pH 4.9 and 0.1 g of biosorbent in 10 mL solution. Fundamental differences were observed in the structure and properties of the different keratin fibers, which led to different levels of sorption of the metals. Extent of sorption was also dependent on the conditions such as pH and temperature. Highest sorption was observed for Pb and Cr and lowest for Mn, Ni and Co, irrespective of the keratin source. Sorption was reported to follow Langmuir isotherm model and was spontaneous (Zhang, 2019). Highest sorption of Pb was at 3.87×10^{-5} g/mol for chicken feathers followed by degreased wool. Pb(II)-loaded biofibers could also be regenerated, leading to an environmentally friendly process and products.

6.2 Keratin as sorbent for dyes

Several researchers have studied the possibility of using keratin as sorbent for dyes in wastewater. In one such study, keratin was extracted from feathers and used as a bioabsorbent for methylene blue (Aguayo-Villarreal, 2011). Influence of various sorption conditions and the kinetics of absorption were investigated. Bioabsorbent could be obtained in film form after freeze-drying and had a highly porous structure. Absorption of methylene blue was up to 150 mg/g and highly dependent on the initial dye concentration in the solution. pH above 7 showed considerably higher absorption than acidic pH. Based on isothermal studies, it was found that the maximum monolayer absorption was 157 mg/g at pH 7 (Aguayo-Villarreal, 2011). Low cost and high absorption capacity were considered to be ideal for using feathers as bioabsorbents specifically for dye removal. To further improve the absorption of methylene blue, keratin was made into nanofiber membranes and the sorption studies were conducted using batch studies (Aluigi, 2014). To prepare the nanofibers, keratin extracted from feathers was dissolved using sulfuric acid and electrospun into nanofibers with an average diameter of 223 nm. A maximum absorption of 170 mg of dye per gram of membrane was achieved, and a considerably high removal efficiency of 98% was reached. However, concentration of the membrane, pH, time and temperature determined the amount of absorption and consequently the dye removal efficiency. Large surface area and porosity of the membranes were suggested to be the reasons for the high absorption and removal (Aluigi, 2014). Also, feathers are acidic and since methylene blue solution is basic, higher sorption would be possible.

Adsorption studies were done to understand the ability of chicken feathers to remove a toxic dye “malachite green” under various sorption conditions (Mittal,

2006). In this study, feathers were cut into lengths of about 0.1 mm length and the quill was removed. The resulting barbs were treated with hydrogen peroxide to remove surface substances. When used as an absorbent, up to 85% removal of the dye was achieved at pH 7 with the absorption decreasing at lower pH. Absorption of dye followed Langmuir and Freundlich isotherms with Gibb's free energy (ΔG°) between 26 and 29 kJ/mol and enthalpy of 20 kJ/mol and entropy of 152 J/K. However, the absorption of the dye per gram of the feathers was considerably low (Mittal, 2006). Chicken feathers were directly used as a sorbent for brilliant blue FCF, a hazardous dye found in dyeing wastewater. Feathers were mechanically cut into 0.1 mm length, treated with hydrogen peroxide and later dried to remove moisture. Batch sorption studies were performed at various temperatures, pH and initial dye concentrations (Mittal, 2006). A dye removal efficiency of 70% was achieved when the pH was 2 but decreased to about 10% at pH above 4. Temperature and time during sorption also played a major role with higher temperature (50 °C) and longer time (300 min), providing a sorption of up to 90% (Mittal, 2006). Complete removal of dye was also possible when higher amounts of feathers were used but the sorption capacity of the feathers was not reported.

Powdered wool before and after chlorination were found to have different sorption capacities to acid dyes. Merino wool was milled to form particles and further subject to air milling and also to chemical processes before the absorption studies. Processing of the powdered wool changed the surface composition of the fibers and therefore the reactivity. Average particle size ranged from 61 μm to as low as 4.5 μm depending on the type of treatment. Morphological appearance also changed after the treatments. Absorption of dyes by the wool fibers was similar to that of charcoal for acid red 18 but the sorption was lower than that of the charcoal for the chopped and chemically treated fibers. Wool fibers had lower negative zeta potential, which helped the attraction of larger amounts of dye compared to charcoal (Kar, 2004).

Keratin extracted from chicken feathers was combined with cellulose nanocrystals (CNCs) (diameter of 187 nm) obtained by acid hydrolysis of cotton fabrics to develop a bioabsorbent for sorption of dyes in wastewater. The blend biosorbents were made by adding 25% by weight of nanocrystals into keratin solution and freeze-drying the solution. When necessary, the biosorbent was cross-linked using glutaraldehyde to improve the properties. A high porosity of 99% and surface area of 229 m^2/g were obtained, which facilitated high sorption of dyes. Addition of CNC substantially increased the mechanical properties of the sorbent and also the water uptake (Figure 6.4) (Song, 2017). Removal efficiency was 96% for reactive black 5 and 98% for direct red 80 at pH 2 but decreased as the pH increased. Corresponding sorption capacity was between 475 and 588 mg/g through pseudo-first and second-order mechanisms in a continuous flow reactor. The bioabsorbent also had excellent recyclability with more than 80% sorption of dyes after five desorption cycles (Figure 6.5) (Song, 2017).

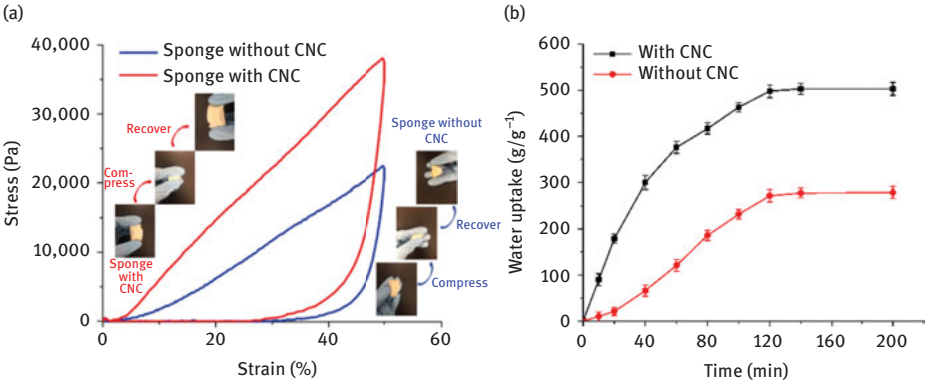

Figure 6.4: (a) and (b) Tensile strength, elongation and water uptake of keratin sponges with and without the cellulose nanocrystals (CNC) (Song, 2017). Reproduced with permission from Elsevier.

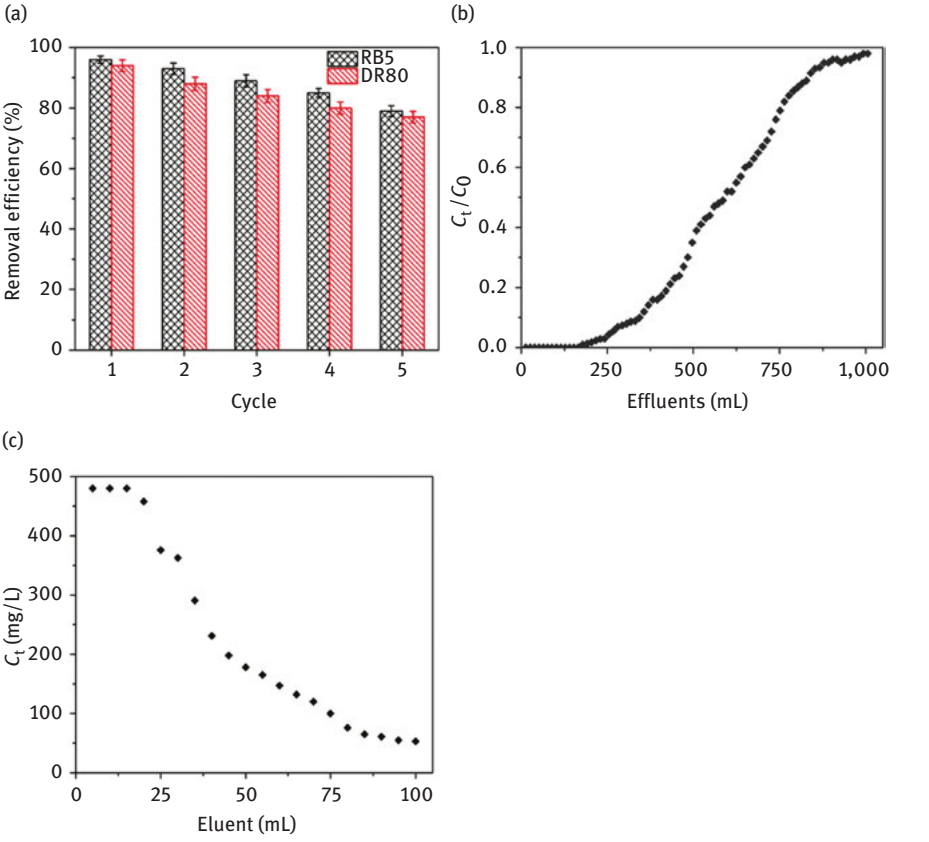

Figure 6.5: (a)–(c) Ability of the keratin–CNC sorbent to sorb and desorb two dyes for up to five cycles (Song, 2017). Reproduced with permission from Elsevier.

6.3 Sorption of oil

In addition to sorption of metals and dyes from wastewater, keratin has been considered as a potential sorbent for oil to treat oil spills. Goat hair before and after carbonization was used as sorbent for crude oil, kerosene, petrol and diesel (Nduka, 2008). Ability of the untreated goat hair and carbonized goat hair to adsorb various oils is given in Table 6.9. Amount of hydrocarbon sorbed was dependent on the molecular weight of the sorbent, contact time and particle size. Carbonization was found to favor sorption and easy recovery of the sorbed material (Nduka, 2008). In an alternative approach, keratin was extracted from pigeon feather, solubilized and lyophilized to form powder (Zhou, 2014). The keratin powder was freeze-dried and regenerated to form a sponge with surface area of 114 m^2/g and pore volume of 1.01 cm^3/g. A high sorption of up to 39 g/g of sponge and oil-holding capacity of 79% was possible.

Table 6.9: Ability of the uncarbonized and carbonized goat hair to sorb (% adsorption) various hydrocarbons at two different particle sizes and various sorption times (Nduka, 2008).

Particle size	Time (min)	Carbonized				Uncarbonized			
		C.O	Diesel	Kerosene	Petrol	C.O	Diesel	Kerosene	Petrol
325 µm	30	480	416	315	309	455	380	300	296
	60	485	437	327	320	458	384	305	312
	90	486	455	337	337	462	390	319	324
	120	510	466	367	344	471	400	330	337
625 µm	30	355	305	268	268	300	270	260	200
	60	346	314	269	269	320	276	267	206
	90	366	330	288	288	340	286	280	210
	120	381	335	300	300	360	300	284	214

Note: Reproduced with permission from Elsevier.

Chapter 7
Biocomposites

Composites are structures that contain a matrix and a reinforcing material and sometimes additives and chemicals. Composites are used in almost all industries and are primarily made using polyethylene, polypropylene (PP) and other commodity polymers. However, these composites do not degrade in the environment and hence pose considerable environmental risk after their disposal. Efforts have been made to replace the synthetic polymers with biopolymers and obtain biodegradable composites. Keratins in both their native and regenerated forms have been used as both matrix and reinforcement in composites. Since feathers are nonthermoplastic, various chemical and physical modifications have been done to utilize keratin for composite applications. In one such study, methyl methacrylate was polymerized to form poly(methyl methacrylate), and short and long keratin fibers (0–5 wt%) were mixed as reinforcement and processed into composites (Martinez-Hernandez, 2005). Addition of keratin increased the modulus continually. Although tensile strength increased, the strength starts to decrease when the amount of keratin was 5% and elongation was also observed to decrease considerably (Table 7.1). Scanning electron microscopic images of the fracture surface did not show any fiber pullouts or voids indicating good compatibility. A coating of the polymer on the surface of the fibers was observed, which also indicates compatibility between the fibers and the matrix. Although addition of keratin improved mechanical properties, the extent of improvement was limited and the amount of keratin added was also low.

Table 7.1: Mechanical properties of PMMA composites reinforced with various ratios of chicken feather fibers (Martinez-Hernandez, 2005).

Sample	Fiber volume fraction	Modulus (GPa)	Strength (MPa)	Elongation (mm/min)
0	0	5.05 ± 0.112	29.68	0.0113
1	0.0095	5.50 ± 0.336	29.33	0.0107
2	0.0190	5.66 ± 0.128	28.85	0.0120
3	0.0285	5.97 ± 0.529	34.82	0.0087
4	0.0380	6.17 ± 0.347	31.72	0.0081
5	0.04758	6.50 ± 0.202	27.89	0.0065

Note: Reproduced with permission from Elsevier.

In a simple approach, low-density polyethylene (LDPE) with a melt flow index of 0.22 g/10 min at 190 °C was combined with feather fibers and later formed into composites. The feathers had a diameter of about 5 μm and lengths ranging from 0.32 to 1.3 cm but were ground into lengths of 0.02, 0.1 and 0.2 cm before using as reinforcement (Barone, 2005a,b). Feathers and matrix were mixed in Brabender extruder at

https://doi.org/10.1515/9781501511769-007

temperatures between 171 and 180 °C. The mixture obtained was compression molded into sheets at 160 °C. Increasing the fraction of feather fibers increased the elastic modulus. It was also observed that the aspect ratio of feather fibers influenced the mechanical properties. Morphologically, the fibers showed good interaction with the matrix but considerable voids were also seen in the cross section. Direct mixing of the feathers into the matrix and developing composites was suggested to be an attractive option to develop various inexpensive feather-based consumer goods (Barone, 2005a,b). Instead of LDPE, feather fibers (20%) were compounded with high-density polyethylene (HDPE) in a twin screw extruder. Thin films extruded were combined and compression molded into dog bone-shaped samples (Barone, 2005b). Compounding conditions varied the reinforcement dimensions and hence properties of the samples. However, good compatibility was observed between the matrix and reinforcement but no mechanical property measurements were done (Barone, 2005b).

Using synthetic polymers as matrix and feathers as reinforcement results in partially biodegradable composites. To develop completely degradable composites, feather fibers were mixed with poly(lactic acid) (PLA) in 2–10% by weight and compounded in an extruder. Blends from the extruder were made into injection-molded samples for testing (Cheng, 2009). Addition of the feathers increased the modulus but considerably decreased the strength and elongation. Modulus of the composites was about 16% higher than that of neat PLA when the feather content was 5%. Dynamic mechanical analysis (DMA) also showed that the addition of feather fibers increased the stiffness due to the transfer of the stress from the PLA to the fibers. Thermal stability of the composites was also higher at a feather content of 5%. Morphological analysis did not reveal any major defects or voids in the cross section, indicating good compatibility (Cheng, 2009). Although marginal improvements were observed in the modulus of the PLA composites, only 10% feathers could be included due to difficulties in compounding and extruding. Also, the changes in the biodegradability of the samples were not studied. Controlling the aspect ratio, adding compatibilizers and increasing the amount of feathers could improve the strength and elongation.

Feather quill and PP fibers were ground into powder and mixed using a stirrer and the mixture was made into pre-pregs (Huda, 2008). When powdered quill is used as reinforcement, tensile strength and modulus were lower compared to jute fiber-reinforced composites due to their higher void content and lower mechanical properties of the feathers compared to jute. Tensile properties increased with increasing quill content from 20% to 30% but decreased at higher amounts of reinforcement (Huda, 2008). Acoustic studies showed that quill-reinforced composites had considerably higher sound absorption coefficient than the jute fibers. Instead of using neat PP as matrix, feather quills (4.4 mm long, 0.28–2.87 mm in diameter) were combined with recycled PP having a melt flow index of 6.0 per 10 min and injection molded into pellets at three different temperatures (185, 200 and 220 °C). Pellets were also compression molded at 220 °C into sheets for dynamic mechanical analysis (DMA). Good compatibility between quill and PP with few voids was noticed, and the density of the

composites increased linearly with increasing quill content. Inclusion of quill decreased the crystallinity of PP but did not affect the thermal properties (Jimenez-Cervantes Amieva, 2015).

In a different approach of using feather fibers and quills as reinforcement, separated feather fibers (no quill) were used as reinforcement and HDPE/PP fibers as matrix for lightweight composites intended for automotive applications (Huda, 2009). Feather fibers were reported to typically have tensile strength of about 1.44 g/denier, elongation of 7.7% and modulus of about 36 g/denier. These fibers were used as reinforcement, and HDPE/PP fibers in concentric sheath–core format were used as the matrix. Feathers and matrix were thoroughly mixed using water spray and pre-pregs were prepared. Feathers and quills were also powdered and mixed with the matrix fibers. Jute fibers used for comparison were in their normal form and also as powder. Pre-pregs were compression molded into composites using different temperatures, compression time, density and thickness of the pre-pregs (Huda, 2009). Increasing the amount of feathers (reinforcement) up to 35% increased the flexural strength and modulus. Addition of the feathers at a fixed thickness leads to increase in void content. Cross section of the composites revealed uniform distribution of fibers across the composites suggesting homogeneity (Huda, 2009). At similar density of the composites, quills provide considerably higher flexural strength than feather fibers, similar to that of jute fibers due to the high modulus of quill (Table 7.2). However, modulus of elasticity and impact resistance of jute fiber-reinforced composites are higher than that of both feather fibers and quill due to the inherent properties of jute fibers. Also, powdered quill provided higher strength and modulus than powdered feather fibers and jute. However, powdered specimens provide better homogeneity and reduce the number of voids and therefore do not show better sound absorption, whereas composites containing feathers and quill have higher sound absorption coefficient due to the higher number of voids (Huda, 2009).

Table 7.2: Comparison of the properties of the composites developed using various forms of feather fibers and quill (Huda, 2009).

Composite	Thickness (mm)	Density (g/cm^3)	Flexural strength (MPa)	Modulus of elasticity (MPa)	Offset yield load (N)	Impact resistance (J/m)	NRC
FF	4.2	0.36	4.2 ± 0.2	380 ± 31	41.0 ± 7.6	41.0 ± 7.6	0.17
FF	3.2	0.47	5.6 ± 0.7	548 ± 82	30.1 ± 4.1	30.1 ± 4.1	0.09
Quill	3.2	0.47	9.8 ± 1.0	805 ± 48	55.6 ± 5.0	55.6 ± 5.0	0.11
Jute	3.2	0.47	9.0 ± 0.8	1,315 ± 42	82.1 ± 5.0	82.1 ± 5.0	0.04
FF powder	2.0	0.75	9.8 ± 1.1	893 ± 85	9.5 ± 0.9	25.4 ± 5.6	0.07
Quill powder	2.0	0.75	14.4 ± 1.0	1,399 ± 114	13.2 ± 0.6	25.9 ± 5.4	0.07
Jute powder	2.0	0.75	11.2 ± 1.1	1,197 ± 124	9.0 ± 0.8	27.1 ± 7.4	0.07

Note: Reproduced with permission from Springer.

Paper-like composites were prepared by combing chicken feathers with cellulose linters, synthetic fibers and a resin. Feathers and fibers were processed in a Rapid-kothen apparatus to form sheets with mass per square meter between 50 and 140. Mechanical properties of the composite sheets show that addition of feathers influenced the strength, elongation and other properties depending on the composition of the feather, fibers and resin (Table 7.3). Substantial changes in strength and elongation are observed when the synthetic fibers and resin are added to improve binding and flexibility. Papers obtained were considered to be suitable for artistic painting (Wrzesniewska-Tosjik, 2011).

Table 7.3: Comparison of the mechanical properties of paper sheets made using feathers, cotton linters, synthetic fibers and/or resin (Wrzesneiwska-Tosik, 2011).

Parameter		Grammage (g/m^2)	Tensile strength (N m/g)	Elongation (%)	Tear index (mN)	Burst index (kPa m^2/g)	Wet strength (%)
100% cotton		140	–	–	–	–	–
100% cotton linters		100	36.2	1.3	13.6	1.55	–
20	+80% linters	140	5.67	27.0	3.9	0.29	11.9
	+3% resin + 77% linters	140	7.49	10.3	4.6	0.36	22.3
50	+50% linters	140	2.44	23.0	2.6	0.78	3.8
	+3% resin + 10% synthetic fibers + 2% linters	140	16.5	4.0	16.5	0.26	41.6
66	+3% resin + 31% linters	140	–	3.8	–	0.72	40.5
	+3% resin + 10% synthetic fibers + 2% linters	140	41.3	3.3	15.6	0.52	43.3
70	+30% synthetic fibers	95.2	2.99	10.8	21.7	0.70	98
	+3% resin, 30% synthetic fibers	91.0	5.85	16.3	18.8	1.26	97

Note: Reproduced with permission through Open Access Publishing.

Many studies combine hydrophobic synthetic polymers such as PLA with biomass to develop biodegradable composites. Unfortunately, such matrix and reinforcements have poor compatibility, leading to inferior mechanical properties. Although

chemical modifications are done to improve compatibility, these modifications are either expensive, do not provide the desired properties and/or decrease the biodegradability of the samples. In an attempt to develop completely biodegradable composites, keratin that has both hydrophilic and hydrophobic groups was combined with PLA and chitosan and made into composites (Spiridon, 2013). Feathers were made into powder with an average diameter of 50 μm and length between 0.1 and 0.2 cm, and the ratio of feathers in the composites was 2% or 4% with 30% chitosan. Addition of keratin into PLA increased strength and modulus but decreased the elongation (Table 7.4). Although chitosan decreased the strength, inclusion of keratin into chitosan and PLA composite decreased the strength and elongation but no major changes in modulus were observed. Impact strength also improved with the addition of keratin in the presence of chitosan (Spiridon, 2013). Considerable changes in mechanical properties occurred after weathering due to the exposure to humidity, temperature and UV, leading to rupture of the PLA matrix and decreased mechanical properties (Table 7.5). Impact strength decreased by more than 50%, and up to 80% decrease was seen in the tensile strength of the neat PLA matrix. Composites containing 30% chitosan had even higher strength loss of about 85% and a slightly higher

Table 7.4: Mechanical properties of PLA composites reinforced with chitosan and keratin (Spirodon, 2013).

Sample			Impact strength (kJ/m^2)	Young's modulus (GPa)	Elongation (%)	Tensile strength (MPa)
PLA	Chitosan	Keratin				
100	–	–	11.0 ± 0.3	2.6 ± 0.3	3.8 ± 0.3	58.6 ± 1.3
96	–	4	11.1 ± 0.2	3.3 ± 0.1	1.3 ± 0.2	65.1 ± 1.5
70	30	–	6.7 ± 0.5	2.9 ± 0.3	2.2 ± 0.4	49.5 ± 2.0
68	30	2	8.3 ± 0.3	2.5 ± 0.1	1.8 ± 0.1	38.1 ± 1.3
66	30	4	8.0 ± 0.2	2.3 ± 0.4	1.6 ± 0.2	35.8 ± 1.2

Note: Reproduced with permission from American Chemical Society.

Table 7.5: Mechanical properties of PLA composites reinforced with chitosan and keratin after weathering (Spirodon, 2013).

Sample			Impact strength (kJ/m^2)	Young's modulus (GPa)	Elongation (%)	Tensile strength (MPa)
PLA	Chitosan	Keratin				
100	–	–	4.1 ± 0.4	2.4 ± 0.2	1.0 ± 0.2	13.1 ± 0.2
70	30	–	4.8 ± 0.3	2.0 ± 0.1	0.6 ± 0.1	10.0 ± 0.5
68	30	2	5.7 ± 0.7	1.0 ± 0.2	0.9 ± 0.1	6.8 ± 0.3
66	30	4	8.0 ± 0.4	1.1 ± 0.2	0.9 ± 0.1	5.0 ± 0.2

Note: Reproduced with permission from American Chemical Society.

weight loss of 87% was seen for the composites containing 4% keratin, 30% chitosan and 66% PLA. Mechanical properties decreased due to addition of keratin although uniform distribution of the particles was obtained.

Composites intended for medical applications were developed using keratin extracted from chicken feather and ethyl cellulose. The ethyl cellulose was grafted onto the keratin using laccase. To improve the antimicrobial properties of the composites, various natural phenolic compounds with inherent antibacterial properties were grafted onto the keratin–cellulose composite. Phenolic compounds studied included caffeic acid (CA), gallic acid, *p*-4-hydroxybenzoic acid and thymol (T). These compounds were added (5–20 mM) onto the composites by dipping the composites in predissolved solutions of the particular phenolic compounds for 60 min at 30 °C (Iqbal, 2015). Antimicrobial activity of the treated composites was evaluated using gram-positive (*Bacillus subtilis* NCTC 3610 and *Staphylococcus aureus* NCTC 6571) and gram-negative bacteria (*Escherichia coli* NTCT 10418 and *Pseudomonas aeruginosa* NCTC 10662) (Iqbal, 2015). Biocompatibility and degradation of the composites in soil were also evaluated. Grafting parameters varied depending on the phenolic compounds used and the conditions during grafting. CA-grafted samples provided the highest graft yield and grafting efficiency. The grafting parameters and swelling ratio of the different phenolic compounds are in Figure 7.1. Antibacterial activity depended on the type of phenolic compounds used. The CA-treated samples showed excellent bactericidal and bacteriostatic activities against *E. coli* and *S. aureus*. Complete killing of the bacteria was observed for the CA-containing samples but the activity was based on the concentration of the CA used (Iqbal, 2015). Antibacterial activity of the phenolic compounds was suggested to be due to the presence of reactive acidic hydroxyl groups and delocalization of electrons in their structure. Viability of the composites was evaluated using HaCaT cells. All the samples evaluated had 100% viability after 5 days compared to the control but the composites did not promote the attachment and proliferation. In terms of morphology, the cells had similar appearance after 5 days (Figure 7.2). Degradation tests in soil showed that 100% of the keratin–ethyl cellulose (EC) composite could be degraded after 42 days. However, the phenolic compound grafted composites could degrade much faster due to their higher swelling ability and consequently higher moisture sorption (Iqbal, 2015). Although the viability of the composites was shown using qualitative means, no quantitative data was provided. More importantly, the degradation of the composites in aqueous media at different pH levels was also not reported.

7.1 Composites using wool fibers/wool keratin

Considerable amounts of wool are generated as waste during preprocessing and during processing into products. Wool waste was combined with recycled polyester fibers and made into composites (Patnaik, 2015). Two types of wool, coring wool and

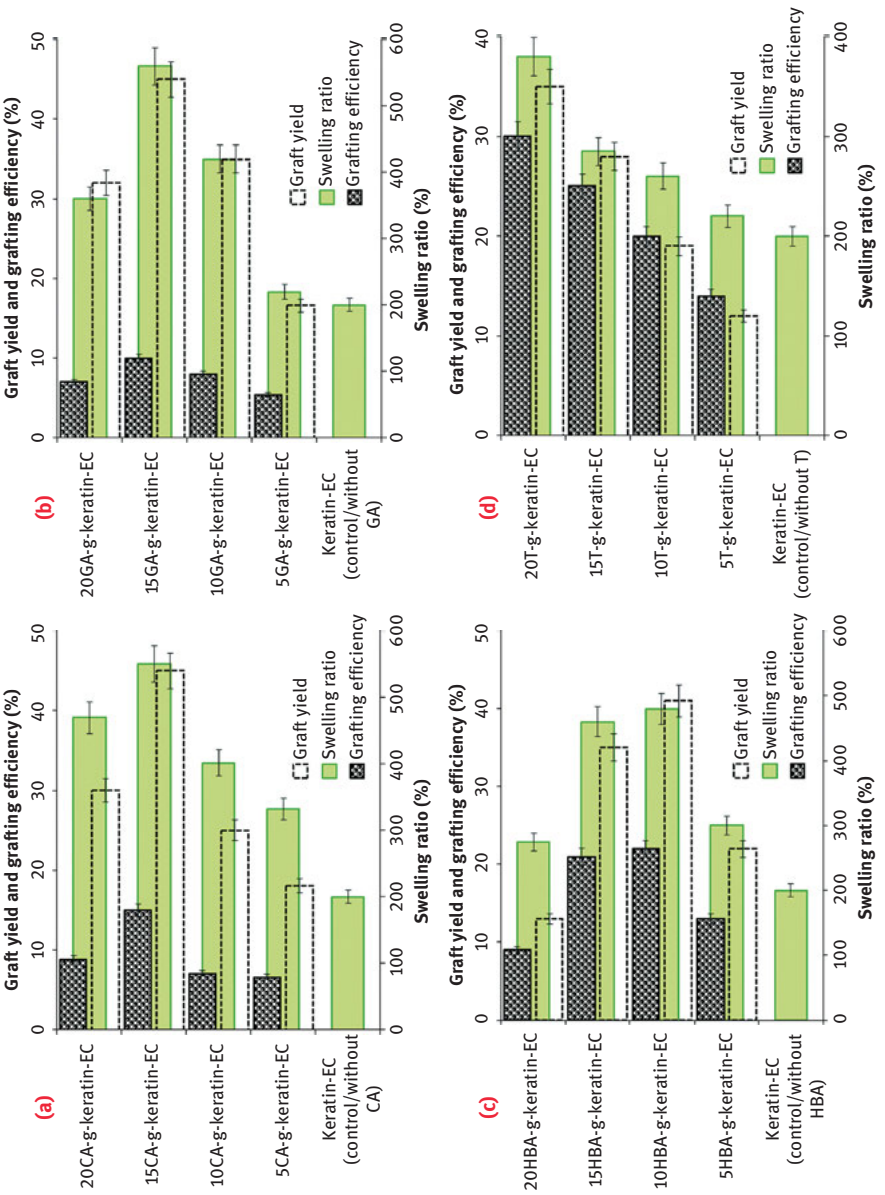

Figure 7.1: Yield, swelling ratio and grafting efficiency (Iqbal, 2015) graft yield, grafting efficiency and swelling ratio behaviours of CA, keratin EC and CA-g-keratin-EC (a), GA, keratin-EC and GA-g-keratin15 EC (b), HBA, keratin-EC and HBA-g-keratin-EC (c) and T, keratin-EC and T-g-keratin-EC (d). Reproduced with permission from Royal Society of Chemistry (Iqbal, 2015).

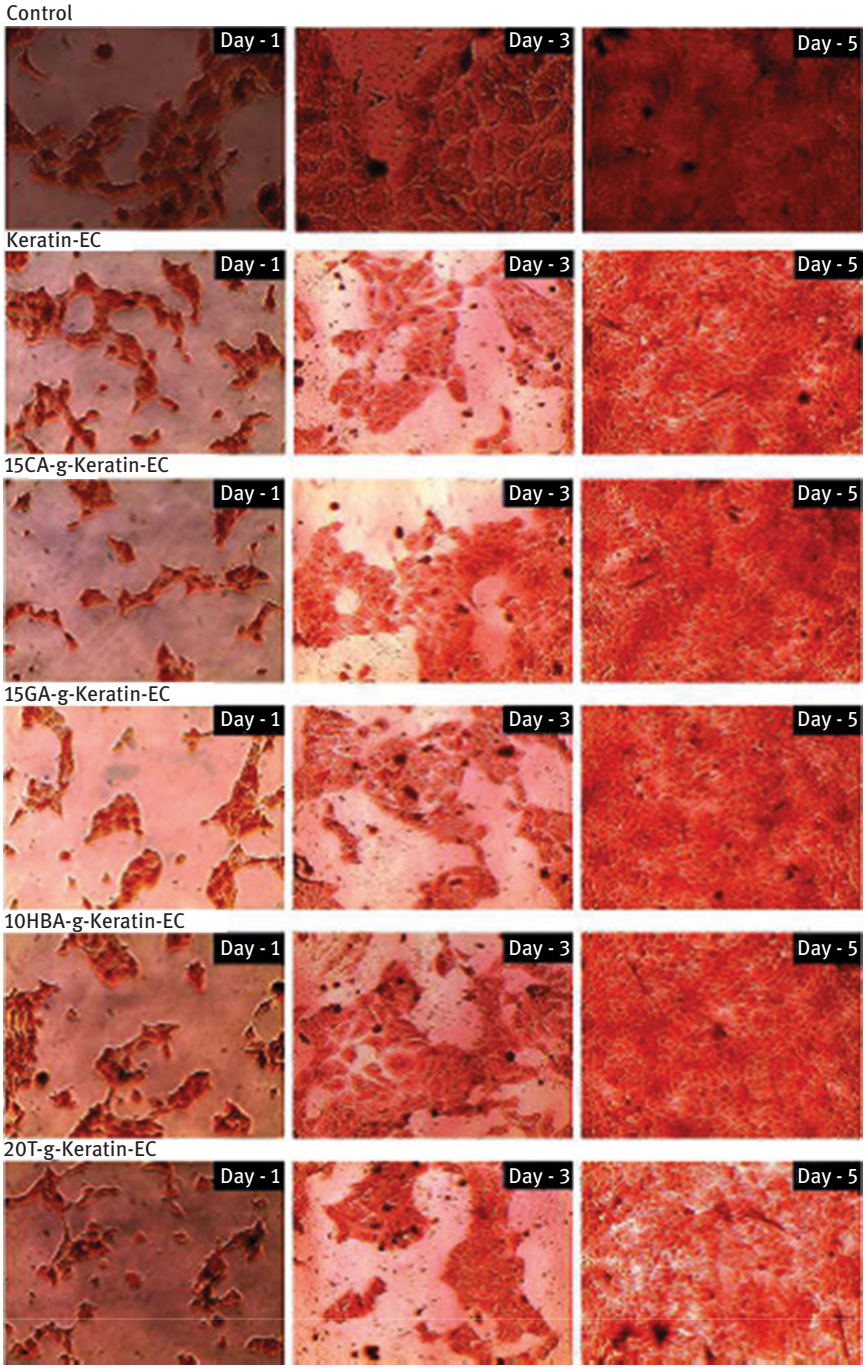

Figure 7.2: Morphology of the adherent HaCaT cells on various keratin scaffolds from 1 to 5 days of culture (Iqbal, 2015). Reproduced with permission from Royal Society of Chemistry.

dorper wool, were made into nonwoven (needle punched) mats and then combined with recycled polyester fibers. The mats developed were considered to be useful for applications in the construction industry. Thermal, acoustic and biodegradation properties of the samples developed were studied (Patnaik, 2015). Biodegradation studies were conducted using aerated compost consisting of straw/hay/mulch and chicken manure. Test samples were placed in respirometric flasks inside cylindrical glass vessels (Patnaik, 2015). Amount of carbon dioxide released from the samples was used to calculate the % biodegradability. Wool fiber mats had higher thermal insulation properties but combining with recycled polyester increased their thermal resistance. A 50/50 ratio of wool and polyester provided the highest thermal resistance. Wool fibers also have considerably higher sound absorption at all frequencies studied but the blend fiber mats absorbed more than 70% of the incident noise. As expected, the wool fibers showed easy biodegradation (up to 90% in 50 days), whereas the recycled polyester had less than 20% degradability. Blend mats developed were considered ideal for green buildings and also to reduce cost of the buildings (Patnaik, 2015).

Keratin was extracted from wool and used as filler for PP composites. To extract keratin, wool was treated in superheated water (150 °C) for 30 min in a microwave oven. After treatment, the hydrolysate obtained was filtered (0.65 μm pore size) and later freeze-dried. About 30% of the initial weight of wool was obtained as the keratin hydrolysate (Bertini, 2013). Considerable change in the amino acid content had occurred due to hydrolysis. Predominantly, the cystine content had reduced from 11.3 mol% in wool to 0.7% in the extracted keratin. There was a marginal increase in amino acids such as proline, alanine and leucine. Further, considerable changes were also observed in the molecular weight of the keratin before and after extraction. Hydrolysis results in reduction in molecular weight from about 70 kDa to less than 14 kDa. The extracted keratin was combined (5%, 10% and20%) with isotactic PP, maleic anhydride (5%) and compounded in a twin screw extruder at 190 °C for 10 min at 60 rpm. Extruded samples were compression molded into films at 180 °C. Tensile properties of the films are shown in Table 7.6. Addition of keratin increased

Table 7.6: Tensile properties of the keratin-reinforced PP composites (Bertini, 2013).

Sample	Modulus (MPa)	Stress (MPa)	Yield (%)	Elongation at break (%)
PP	2,480 ± 60	33.6 ± 0.8	2.9 ± 0.2	3.1 ± 0.2
PK	2,570 ± 59	28.9 ± 1.0	2.2 ± 0.2	2.8 ± 0.3
pgP	2,490 ± 88	36.2 ± 1.0	3.8 ± 0.3	4.0 ± 0.3
PgPK5	2,520 ± 101	36.0 ± 1.2	4.1 ± 0.3	5.1 ± 0.5
PgPK10	2,610 ± 98	34.2 ± 1.1	3.2 ± 0.3	4.0 ± 0.4
PgPK20	2,770 ± 112	32.0 ± 0.9	2.3 ± 0.3	2.5 ± 0.4

Note: Reproduced with permission from Elsevier.

the modulus by about 12% but no significant increase was seen in the strength. Samples containing 5% keratin had higher elongation than the PP films but increasing the amount of keratin decreased elongation. Although addition of keratin increased modulus and elongation, the amount of keratin used was limited and only a marginal improvement in properties was observed (Bertini, 2013). However, keratin improved the thermal properties and prevented degradation of PP. Keratin hydrolysate could also act as a nucleant and increased the crystallization rate. However, a compatibilizer was necessary to obtain good thermal and mechanical properties in the composites (Bertini, 2013). Using a similar approach of superheated steam, keratin hydrolysate obtained from wool was used as a biofiller for PP and maleated PP (Canetti, 2013). Hydrolysis was done by treating wool with superheated water at 180 °C for 30 min, which resulted in amorphous keratin powders. The extracted keratin powder (5%, 10% and 20%) was mixed with PP in a twin screw extruder and made into films. Keratin hydrolysate particles showed a spherulite structure after complete crystallization (Canetti, 2013). Morphological analysis showed that the keratin particles had uniform distribution in the matrix and the particles were in nano- to microscale. The nonchemical method of extracting keratin was considered to be a viable approach for developing biocomposites.

To improve compatibility between fibers and matrix, wool fibers (18 μm and 2 cm length) were mixed with PP along with maleic anhydride-grafted PP as compatibilizer. The mixture was compression molded into composites at 180 °C for 5 min. Morphological analysis showed that the wool fibers and PP had poor adhesion and extensive fiber pullouts were observed. Inclusion of the compatibilizer increased the compatibility and very few fiber pullouts were observed even when the fiber content was as high as 60%. Stress–strain curves showed that addition of the wool fibers decreased the stress and strain of the PP composites. However, thermal and thermo-oxidative stabilities improved due to the inclusion of wool fibers (Conzatti, 2013). Decrease in the mechanical properties was suggested to be due to the reduction in fiber length during compounding.

All keratin composites were prepared using waste wool with properties suitable for replacing petroleum-based plastics. In this approach, wool fibers were dissolved using a mixture of $CaCl_2$/water/ethanol and thioglycolate. After dissolution at different pH, temperature and time, the treated keratin was combined with raw wool fibers and compression molded at 2.2–3.3 bar pressure at 60 °C for 10–20 min to form the composite. In the composite, waste wool fibers formed the reinforcement and dissolved keratin was the matrix. Up to 60% of wool fibers could be dissolved depending on the conditions used. Composites developed had a maximum tensile strength of 15 MPa, considerably lower than the tensile strength of wool fibers (150–200 MPa) due to the porous nature of the composites. Tensile strength of all keratin composites was considered to be similar to that of soy protein-based and other regenerated keratin-based composites. The composites had higher (54–70%) moisture retention values compared to the individual fibers.

Since keratin has low flame retardancy, polyethylene/ethylene vinyl acetate (EVA) composites reinforced with chicken feathers and DNA were used to increase the flame resistance. DNA was either added onto the matrix/reinforcement and compression molded or melt blending was done, and the blend was later used for developing the composites. Addition of DNA was able to increase the Limited Oxygen Index (LOI) up to 24.5% and decreased the heat release rate by 82% (Albite-Ortega, 2019). Changes in the flame resistance properties of the composites containing DNA and magnesium hydroxide are given in Table 7.7. Inclusion of DNA was able to decrease the use of magnesium hydroxide by more than 50% and provided desired flame resistance without any major effect to the mechanical properties.

Table 7.7: Comparison of the cone calorimeter and LOI results for the keratin-reinforced and DNA-treated PE/EVA composites (Albite-Ortega, 2019). pHHR is peak heat release rate, THR is total heat release, and TTi is time to ignition.

Sample	pHHR (kW/m^2)	% reduction	THR (MJ/m^2)	TTi (Sec)	LOI (%)
PE/PVA	2,323 ± 10	–	122 ± 4	68 ± 2	17
PE/EVA/MH-55	546 ± 08	76	75 ± 3	80 ± 3	25
PE/EVA/MH-20	1,199 ± 11	48	82 ± 2	72 ± 2	22
PE/EVA/DNA	1,551 ± 09	33	100 ± 6	71 ± 1	19.5
PE/EVA/KF	1,386 ± 10	40	98 ± 5	70 ± 3	20
PE/EVA/DNA/KF	1,291 ± 12	44	96 ± 3	72 ± 2	21
PE/EVA/MH-20/DNA	630 + 06	72	89 ± 2	73 ± 2	22
PE/EVA/M-20/KF	681 ± 04	70	87 ± 4	74 ± 3	22
PE/PVA/MH-20/KF/DNA-bulk	499 ± 05	78	81 ± 3	73 ± 1	23
PE/PVA/MH-20/KF/DNA-c-surf	470 ± 03	79	79 ± 2	75 ± 1	24
PE/PVA/MH-20/KF/DNA-c-seg	395 ± 04	82	77 ± 2	77 ± 2	25

Note: Reproduced with permission from Elsevier.

7.2 Composites from horn keratin

Three-dimensional composite scaffolds were prepared by combining keratin extracted from cattle horns with either chitosan or gelatin for potential tissue engineering applications (Balaji, 2012). Keratin solution was mixed with chitosan dissolved in acetic acid, and the mixture was poured onto petri dishes and later lyophilized to form scaffolds. Similarly, keratin solution and gelatin dissolved in water were blended and made into scaffolds. Porosity, pore size, water absorption and cell proliferation of the scaffolds were studied. Addition of the gelatin and chitosan increased the load and elongation of the scaffolds (Table 7.8). Gelatin provided marginally higher strength, whereas chitosan-blended scaffolds have higher breaking elongation. Chitosan-blended scaffolds have a porosity of 27% compared to 31% for the gelatin-blended scaffolds. Respective densities were 0.0354 and 0.0273 g/cm^3. Scaffolds contained pores

Table 7.8: Mechanical properties of the pure keratin and keratin-blended samples (Balaji, 2012).

Scaffold	Maximum load (N)	Maximum extension (mm)	Elongation (%)	Tensile strength (MPa)
Keratin–chitosan	6.3 ± 0.12	5.1 ± 0.2	21.6 ± 0.1	1.6 ± 0.2
Keratin–gelatin	7.2 ± 0.18	6.1 ± 0.1	18.7 ± 0.1	1.8 ± 0.2
Keratin	0.50 ± 0.14	2.9 ± 0.2	19.7 ± 0.2	0.05 ± 0.13

Note: Reproduced with permission from Elsevier.

with size between 80 and100 μm (Balaji, 2012). Although initial attachment of cells on the pure and blend scaffolds was similar, the gelatin- and chitosan-blended scaffolds had considerably higher cell density after 48 h. Despite the scaffolds being suitable for short term for cell culture, the stability of the scaffolds under physiological conditions may not be sufficient for long-time culture.

Chapter 8
Fibers from keratin

8.1 Normal (microfibers)

Wool and silk are the only two commercially available protein fibers. These fibers have limited availability with total annual world production of about 2 million tons of the total world fiber production of about 75 million tons. Wool and silk are also expensive with selling price between $3–$8 and $8–$20 per lb of wool and silk, respectively. Hence, fibers offer one of the highest value applications for keratin. In addition to using wool in its native form, keratin has been extracted from feathers and wool and converted into regenerated fibers through various approaches. Traditional approach of extracting keratin for fiber production is to use high concentrations of urea and alkali or strong reducing agents. These approaches produce spinnable keratin solution but the properties of the fibers obtained are poor (Xu, 2014). To overcome this limitation, wool was treated with 8 M urea solution in 17:1 ratio, and cysteine (10% on weight of wool) was added as the reducing agent. The treated solution was centrifuged at 15,000 rpm for 20 min and the keratin obtained was collected. To form the fibers, the keratin obtained was dissolved in a buffer containing 10% sodium dodecyl sulfate (SDS). After aging for 24 h, the solution was heated to 90 °C for 1 h and fibers were mechanically drawn using a syringe and needle. Fibers were introduced into a coagulation bath containing 10% methanol and 10% acetic acid. Annealing of the fibers was done by heating them to 150 °C for 2 h, drawing the fibers and reannealing the fibers at 120 °C for 1 h. Amount and properties of fibers obtained were dependent on the conditions used during fiber production. Increasing the concentration of sodium hydroxide during extraction decreased the viscosity due to reduction in molecular weight, whereas increase in concentration of SDS from 5% to 8% increased the viscosity which decreased drastically with further increase in the concentration of SDS. Addition of SDS makes keratin more hydrophobic and increased its stability due to unfolding and cooperative binding (Ozdemir, 2006). However, the behavior of SDS–keratin mixture was highly dependent on pH (Ozdemir, 2006). Decrease in molecular weight and viscosity affects the tensile strength of the fibers. Tenacity of the fibers decreased to about 0.5 g/den from 0.9 g/den when alkali concentration was increased from 0% to 0.5%. Similar decrease was also seen in the crystallinity index of the fibers. Although the strength of the fibers obtained was only 0.9 g/den, considerably lower than common natural fibers, the mechanical properties of the fibers were higher than keratin products developed previously (Table 8.1) (Xu, 2014).

A few attempts have been made to produce regenerated protein fibers using keratin. However, difficulties in dissolving keratin have resulted in fibers with poor properties. To make regeneration and spinning of keratin fibers easier, PVA was added and fibers were produced by wet spinning (Liu, 2018). Keratin was extracted

https://doi.org/10.1515/9781501511769-008

Table 8.1: Comparison of the tensile properties of materials developed using keratin (Xu, 2014).

Sample	Tensile strength (MPa)	Elongation (%)
Pure keratin fibers	101 ± 15	10.9 ± 2.9
Keratin/chitosan films	34 ± 10	7 ± 2
Cross-linked keratin film	8 ± 2	8 ± 2
Cross-linked keratin film	27 ± 6	14 ± 8
Compression molded keratin film	7.9 ± 2.7	1.1 ± 0.5
Compression molded keratin film	27.8 ± 2.9	4.7 ± 0.7
Keratin–silk fibroin film	17.7 ± 4.7	1.2 ± 0.4
Keratin–silk fibroin film	27.8 ± 6.5	2.3 ± 0.6
Keratin–PVA blend fiber	87.8 ± 6.8	12.6 ± 3.2

Note: Reproduced with permission from Springer.

from wool using urea, SDS and sodium sulfide and heated at 50 °C for 8 h. PVA dissolved in water was added into the keratin solution to have a keratin concentration of 5–25%. The blend solutions had viscosities between 3.9 and 4.3 Pa s and were extruded as fibers into a coagulation bath made of saturated ammonium sulfate. Fibers obtained were further stretched to obtain a draw ratio of 2.4 and average diameter of 110 μm but with uneven surface and cross sections. Although good compatibility was observed between keratin and PVA, tensile properties decreased as the amount of keratin in the blend increased. Tensile strength decreased from 15.8 to 4.6 cN and elongation decreased from 77% to 38% when keratin content was increased from 5% to 25% (Liu, 2018). Since keratin content in the fibers was low, it is necessary to optimize processing conditions and also properties of blended keratin to obtain pure keratin or high keratin containing fibers.

Regenerated fibers were made using a blend of keratin and cellulose using ionic liquids as solvents (Kammiovirta, 2016). Cellulose for the blend was obtained from bleached pine kraft pulp and keratin from chicken feathers was dissolved using 1-ethyl-3-methylimidazolium acetate ([EMIM]AcO) separately and later combined to get a polymer concentration of 5 wt%. Ionic solvent was able to provide clear solutions of both keratin and cellulose (Figure 8.1). The blend solution was placed in a syringe and extruded through a needle into a pure ethanol coagulation bath. Filaments obtained were washed in water and dried under ambient conditions. Based on the changes in the position of peaks in Fourier transform infrared (FTIR) spectrum, it was concluded that significant unfolding of β-sheets had occurred and the proteins were disordered after dissolution. Fibers showed the presence of pores in the cross section and grooves on the surface at high keratin concentrations. It was suggested that lack of particles and no phase separation between keratin and cellulose indicated good compatibility between the two polymers. In terms of mechanical properties, increasing keratin concentration decreased the strength and elongation of the fibers but modulus increased (Table 8.2).

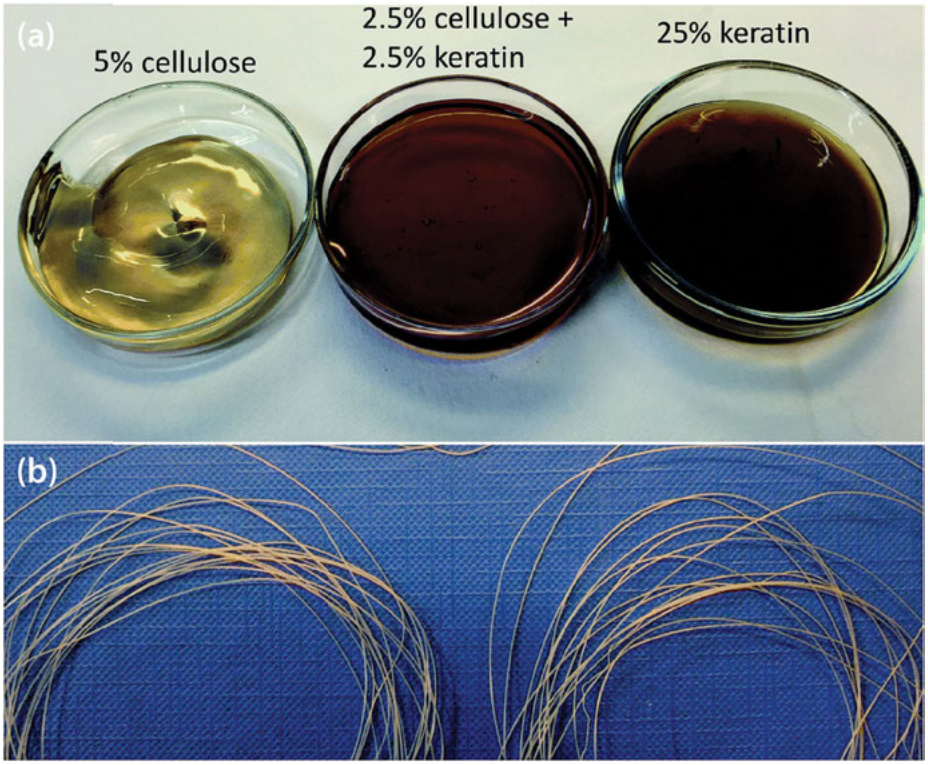

Figure 8.1: (a) Images of solutions obtained from 5% cellulose, 2.5% cellulose and 2.5% keratin blend (center) and 25% keratin using ionic solvents; (b) images of regenerated fibers obtained using 10% keratin in cellulose before (left) and after drying (right) (Kammiovirta, 2016). Reproduced with permission from Royal Society of Chemistry.

Table 8.2: Properties of regenerated cellulose fibers containing various ratios of keratin (Kammiovirta, 2016).

Cellulose (%)	Filament thickness (μm)	Fineness (tex)	Strength (MPa)	Modulus (GPa)	Stiffness (N/m)	Elongation (%)
100	232 ± 11	21.4 ± 5.6	125.4 ± 4.6	5.6 ± 0.2	5,922 ± 219	17.1 ± 4.7
90	220 ± 13	11.5 ± 1.5	142.4 ± 6.4	7.5 ± 0.7	7,166 ± 628	19.3 ± 1.1
80	222 ± 7	12.3 ± 2.7	139.9 ± 3.8	7.1 ± 0.6	6,817 ± 537	18.5 ± 2.0
50	206 ± 10	13.4 ± 2.9	134.6 ± 4.2	7.1 ± 0.5	5,917 ± 421	15.1 ± 0.8
30	221 ± 18	15.4 ± 3.8	88 ± 11.2	6.9 ± 0.5	6,347 ± 467	9.0 ± 3.7

Note: Reproduced with permission from Royal Society of Chemistry.

8.2 Keratin nanofibers

8.2.1 Keratin-PLA nanofibers

Since it is difficult to dissolve keratin in electrospinnable solvents, researchers have developed keratin-based electrospun fibers by blending keratin with other polymers. In one such attempt, keratin extracted from chicken feathers using sodium meta-bisulfite as the reducing agent was blended with various ratios of poly(lactic acid) (PLA) and electrospun into fibers (Ayutthaya, 2015). Surprisingly, considerably finer fibers were obtained when 90% keratin was used, and the diameter of the fibers increased as the PLA content increased (Table 8.3). It was observed that the electrospinning process could increase the formation of α-helix and decrease the β-sheet content in the keratin.

Table 8.3: Electrospinning conditions used and diameter of the fibers obtained with various ratios of keratin/PLA (Ayutthaya, 2015).

Keratin/ PLA (w/w)	Voltage (kV)	Distance (cm)	Feed rate (mL/min)	Diameter of needle (mm)	Diameter of fibers (nm)	Diameter of beads (nm)
90/10	20	15	0.01	0.4	91 ± 18	275 ± 86
70/30	20	15	0.01	0.4	921 ± 202	721 ± 449
50/50	20	15	0.01	0.4	341 ± 87	–
30/70	20	15	0.01	0.4	184 ± 44	–
10/90	20	15	0.01	0.8	356 ± 102	–
0/100	20	15	0.11	0.4	1,087 ± 304	–

Note: Reproduced with permission from Springer.

Blends of keratin and PLA were electrospun into fibers with the addition of nanoclay to improve morphology and filtration efficiency of the membranes (Ayutthaya, 2016). Keratin extracted from chicken feathers was blended in equal proportions with PLA. Solutions of the polymers were prepared by dissolving in chloroform/acetone and formic acid for PLA and keratin, respectively. About 1–3 pph of nanoclay was added into the keratin solution, which was later combined with the PLA solution. Electrospinning of the blend solution was done using a voltage of 19 kV and extrusion rate of 5 μL/min. Addition of clay affected the viscosity of the solution and also decreased conductivity from 423 to about 13 μs/cm. Increase in average fiber diameters was also noticed with pure keratin/PLA producing 134 nm fibers compared to 171 nm fibers when 3% clay was used. Nanoclay was predominantly located within the keratin and also between the interface of the two polymers. It was suggested that positive charge on keratin combined with the negative charge and led to uneven distribution. Addition of clay also affected the denaturation temperature and enthalpy. When used as an air filter, the electrospun fibers containing clay had a pressure drop of 21 Pa compared to 2.8 for neat PLA and 54 Pa for keratin/PLA. Considerably higher efficiency for removing

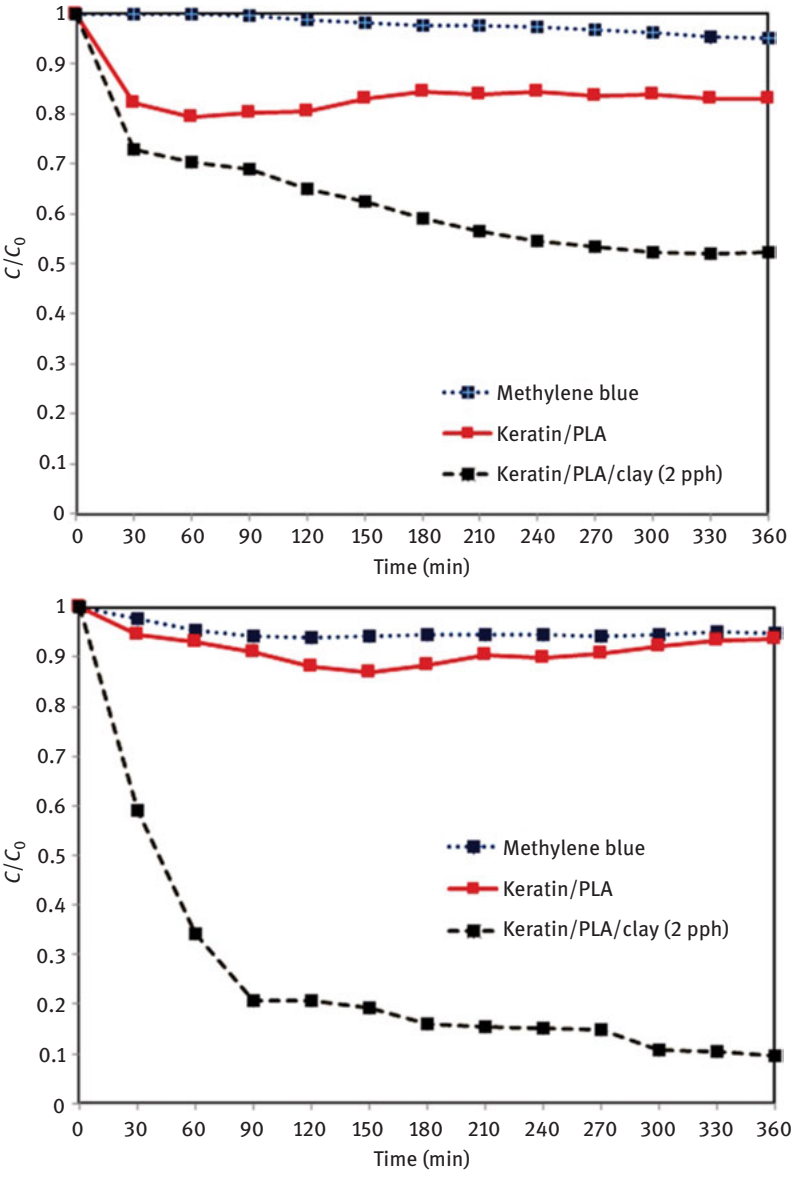

Figure 8.2: Ability of electrospun keratin/PLA electrospun membranes with and without clay to remove methylene blue in dark (top) and under illumination (bottom) (Ayutthaya, 2016). Reproduced with permission from Elsevier.

methylene blue was possible with the addition of the clay (Figure 8.2) both under dark and illumination, suggesting the suitability of the membranes for both air and water purification (Ayutthaya, 2016).

8.2.2 Keratin-PEO blends

Keratin was extracted from human hair, combined with poly(ethylene oxide) (PEO), and made into nanofibers. To extract keratin, human hair was first washed with ether and treated with 7 M urea, 2% SDS and 5% sodium metabisulfite at 95 °C for 4 h. Treated mixture was filtered and dialyzed against a cellulose membrane with 8,000–14,000 Da molecular weight cutoff and the keratin was lyophilized to obtain powder (Liu, 2015). PEO was dissolved in distilled water and the keratin powder was added into the solution. A cross-linker ethylene glycol diglycidyl ether was added to improve stability and electrospinnability. After electrospinning, the keratin/PEO mats obtained were again cross-linked using the vapors from the cross-linking agent. Initial cross-linking increased the spinnability as evinced by the reduced defects, and the second cross-linking increased water resistance as indicated by the changes in the contact angle. Although there was no major difference in thermal stability between the first and second cross-linkings, the uncross-linked samples had considerably low thermal stability. Cross-linking also led to increase in % crystallinity from 13% to 35%. Presence of PEO and the two-step cross-linking was necessary to obtain nanofibers with high keratin (90%) content.

In another study, keratin was extracted from merino wool by treating with urea and SDS at 65 °C. Solution obtained was dialyzed and concentrated. PEO was added into the keratin solution to have a total polymer concentration of 7% (Aluigi, 2008). The keratin/PEO solution was electrospun at a voltage of 20 kV, and mats obtained had a thickness between 12 and 30 μm. Solutions containing higher concentrations of keratin produced finer and uniform fibers than those containing higher levels of PEO due to the changes in viscosity (Aluigi, 2008). Based on FTIR studies, it was found that the keratin/PEO nanofibers had α-helix content of 51 and β-sheet content of 21%. In terms of tensile properties, increasing keratin content decreased the strength, elongation and modulus (Table 8.4). Blend mats produced were soluble in water and therefore had limited applicability (Aluigi, 2008). Liu et al. had extracted keratin from human hair and blended the keratin with PEO and electrospun the blend into nanofibers (Liu, 2014). Extraction of keratin was done by immersing keratin in

Table 8.4: Tensile properties of keratin/PEO blend nanofiber mats having various levels of keratin content (Aluigi, 2008).

Keratin (%)	Stress at break (MPa)	Strain at break (%)	Modulus (MPa)
10	4.7 ± 0.4	117.5 ± 11.8	12 ± 3
30	6.0 ± 1.0	46.3 ± 15.9	31 ± 3
50	1.2 ± 0.1	35.2 ± 0.7	8 ± 2
70	1.6 ± 0.3	41.2 ± 9.9	7 ± 2
90	–	–	–

Note: Reproduced with permission from Elsevier.

aqueous solution of urea, SDS and sodium bisulfite and heating the mixture at 95 °C for 4 h. Dissolved keratin was dialyzed against a molecular weight cutoff of 10,000–14, 000 Da for 36 h. A keratin solution with concentration of about 6% protein was obtained after the dialysis. Various ratios of keratin and PEO were blended together to have a total protein concentration of about 7%. The blend solution was later electrospun at a voltage between 10 and 30 kV. Keratin concentrations above 70% did not produce electrospun fibers. The diameters of the fibers obtained or the mechanical properties were not reported in this study (Liu, 2014).

A concurrent electrospinning and electrospraying method was used to develop composite scaffolds consisting of thermosensitive hydrogel particles and electrospun fibrous mats. Nonionic triblock copolymers (PEO99–PP065–PE099; Pluronic F127) were made into hydrogels and cross-linked using (1-Ethyl-3-[3-dimethylami- propyl]-carbodiimide hydrochloride) (EDC/NHS). Keratin/PEO (70:30) solution was electrospun into fibers with or without bacterial cellulose (0–5%). Concurrent electrospraying and electrospinning were done as depicted in Figure 8.3. Electrospun fibers had an average diameter of 243 nm and addition of 1% bacterial cellulose reduced the fiber diameter to 150 nm. Hydrogels developed had inner pores of about 100–300 μm and the pores were well connected. Electrospraying resulted in formation of spherical- and ellipsoid-shaped particles with sizes between 500 nm and 2 μm. These particles were simultaneously deposited onto the keratin-based nanofibers resulting in hybrid mats with improved thermal and mechanical properties. Addition of bacterial cellulose increased the hydrophilicity and also improved mechanical properties (Table 8.5). Presence of the microparticles also improved the biocompatibility and cell attachment and proliferation (Azarniya, 2019).

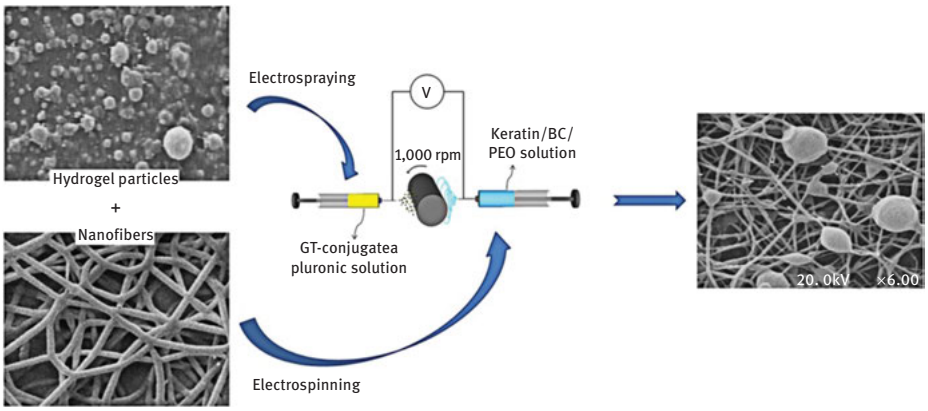

Figure 8.3: Depiction of the process of concurrent electrospraying and electrospinning to develop hybrid nanofiber-reinforced hydrogel particle scaffolds (Azarniya, 2019). Reproduced with permission from Elsevier.

Table 8.5: Comparison of the mechanical properties of hybrid scaffolds prepared from keratin using concurrent electrospinning and electrospraying in comparison to natural skin (Azarniya, 2019).

Material	Tensile strength (MPa)	Modulus (MPa)	Elongation (%)
Abdomen + thorax	2–15	18.8	–
Forehead and arm	5.7–12.6	19.5–87.1	27–59
Back	21.6 ± 8.4	83.3 ± 34.9	54 ± 17
Back	27.2 ± 9.3	98.9 ± 97	25 ± 5
BC/chitosan + 1.5% graphene oxide	35 ± 2.8	730 ± 77	9.5 ± 0.2
PEO/PVP chitosan–2% graphene oxide	14 ± 0.7	358 ± 17	10 ± 0.5
BC/PEO/chitosan–1% nanodiamond	26	458	9.9
Keratin/PEO	7.1 ± 0.8	123 ± 13	15 ± 1.7
BC/keratin/PEO	13.3 ± 1.5	250 ± 29	10.1 ± 1.2
Hybrid fiber/hydrogel	20.4 ± 2.2	361 ± 41	13.2 ± 1.5

Note: Reproduced with permission from Elsevier.

8.2.3 Nanofibers from keratin-PVA blends

Keratin has also been extracted from human hair and blended with poly(vinyl alcohol) and extruded into nanofibers. Since the blend fibers were water soluble, they were cross-linked with various amounts of glyoxal to make them insoluble. Electrospun fibers developed had diameters in the range of 100–300 nm. A keratin to PVA ratio of 2:1 and glyoxal level of 6% provided uniform fibers and with best mechanical properties (Park, 2015). Matrices developed also had good antibacterial activity and were considered to be suitable for medical applications. Keratin–PVA nanofiber membranes were also found to become highly optically transparent mats after immersion in water (Choi, 2015). Keratin extracted from human hair was blended with PVA and electrospun into mats with 10% glyoxal as the cross-linking agent. To form transparent mats, the structures were immersed in water and dried in an oven at 50 °C. Dry mats contained fibers with diameters of about 151 nm but immersion in water led to considerable increase in diameter of up to 223 nm (Choi, 2015). However, the surface roughness of the samples decreased to 73.7–105 nm after treating in water due to decrease in the interstices between the nanofibers. The blend mats had higher tensile strength and modulus but lower elongation than the transparent mats with strength of 19 MPa, modulus of 273 MPa and strain of 176% compared to 11 MPa, 72 MPa and 190%, respectively. Electrospun mats becoming highly transparent (88% transmittance) were hypothesized to be due to decrease in the surface roughness and interstice space, which reduced the scattering of the light. An in situ ultraviolet (UV) cross-linking approach was used to develop keratin-based nanofibers through electrospinning (Deniz, 2015). Human hair was hydrolyzed to obtain the keratin and the solution formed was combined with PVA and 4-vinyl benzene boronic acid–hydroxyapatite. The solution was electrospun and the fibers were cross-linked using an UV source as part of the electrospinning process. Fibers obtained had an

average diameter of about 330 nm and the scaffolds were able to support the growth of umbilical vein endothelial (ECV) 304 and sarcoma osteogenic cells suggesting that the scaffolds could be used for medical applications (Deniz, 2015).

Keratin solubilized using aqueous alkali solution was combined with PVA and made into nanofibers (Esparza, 2017) through electrospinning. Further, citric acid was used to cross-link the electrospun membranes. Amount of keratin in the solution varied from 0 to 30% and a 10% solution was used for electrospinning with conductivity ranging from 3,265 to 14,160 μS/cm. Average fiber diameter was dependent on the ratio of the two polymers and ranged from 274 to 565 nm. However, no fibers were formed when only keratin was used and 30% keratin in the solution leads to bead formation. Cross-linking improved the stability of the nanofibers in solution. Presence of keratin increased the proliferation of fibroblasts making the membranes suitable for tissue engineering and other medical applications (Esparza, 2017). In a similar study, keratin extracted from human hair was added into a solution of PVA and gelatin (1:9) and stirred overnight at room temperature. The blend solution was electrospun onto a commercial polyurethane wound dressing to form a bilayer membrane of about 160 μm in thickness (Yao, 2017). Nanofibers formed had an average diameter of 160 nm. The nanofiber membranes had high water sorption capability but a weight loss of about 10% after 4 weeks was observed in PBS solution. Fibroblast attachment and proliferation was considerably higher on the gelatin/keratin membranes compared to pure gelatin. Cells were also able to penetrate deeper into the gelatin/keratin scaffolds due to favorable porosity and interactions. When used to treat wounds on the back of rats, the gelatin/keratin membranes showed 98% wound healing after 14 days compared to 86% for commercially available gauze (Figure 8.4). It was also found that the keratin containing membranes promoted early vascularization in addition to wound healing.

8.2.4 Keratin-3-hydroxybutyric acid-co-hydroxyvaleric acid (PHBV) blends

In a similar approach, keratin was treated with SDS, mercaptoethanol, urea and sodium hydroxide. The filtrate was passed through a dialysis tube and keratin was collected. Keratin obtained was dissolved along with 3-hydroxybutyric acid-*co*-hydroxyvaleric acid (PHBV) in 1,1,1,3,3,3-hexafluoro-2-isopropanol solution (Yuan, 2009). Blend solution was electrospun at a voltage of 10 kV, and the fibers were collected on a drum. To further improve the properties of the keratin nanofibers, the mats were treated using 25% glutaraldehyde vapors for varying time periods. In vitro biodegradation of the samples in phosphate buffered saline (PBS) for 12 h at 37 °C and the ability of mats to promote attachment and proliferation of NIH3T3 cells were studied (Yuan, 2009). Depending on the conditions used for electrospinning, mats having nanofiber diameters between 487 and 815 nm were obtained. Mats obtained were soluble in water but cross-linking increased their resistance to water and decreased weight loss of the mats.

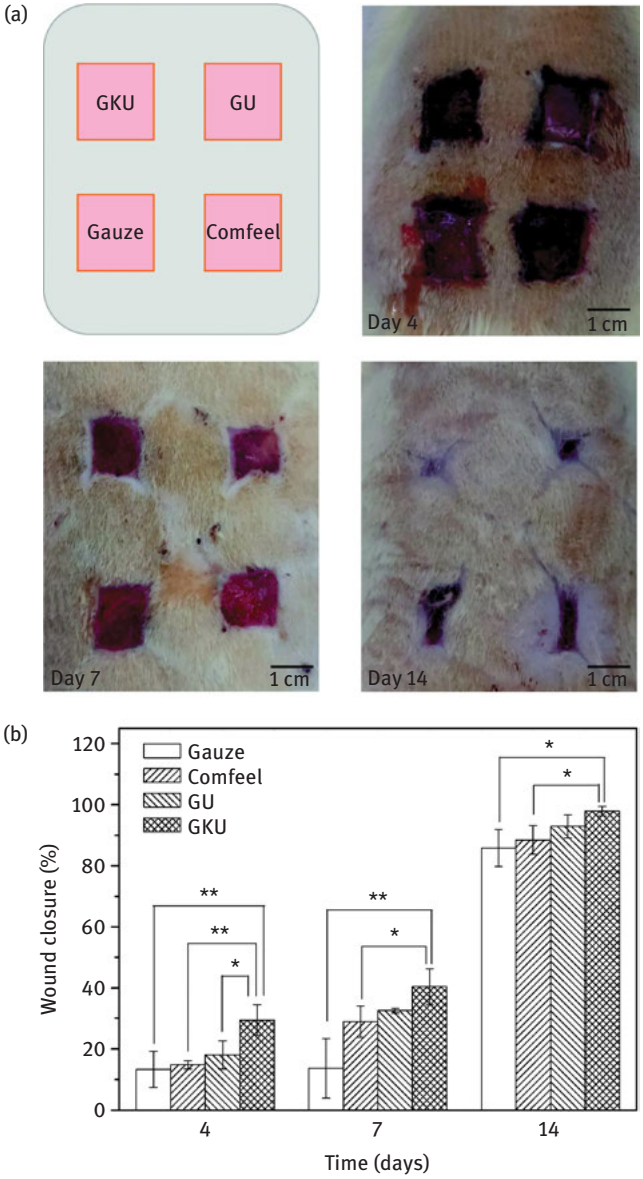

Figure 8.4: Digital images depicting the reduction in wounds on the back of mice after treating with various dressing materials including gelatin/keratin electrospun membranes (a); extent of wound closure after various days of implantation of the keratin-based and commercial wound dressings (b) (Yao, 2017). Reproduced with permission from Elsevier.

Weight loss decreased to about 2% from about 11% when the cross-linking time was increased to about 12 h. Keratin mats accelerated the adhesion and proliferation of the cells compared to the PHBV control. Nanofiber keratin mats were considered to be suitable for wound dressing and tissue engineering (Yuan, 2009).

In another study, keratin (source unknown) was modified with iodoacetic acid and later mixed with poly(hydroxybutylate-*co*-hydroxyvalerate) and electrospun into fibrous mats (Yuan, 2015). The mats were cultured with NH3T3 cells, and the ability of the mats to support attachment and proliferation was studied. Further, the pure PHBV and keratin–PHBV mats were implanted onto a wound site as dressing material in mice. Pure PHBV fibers have diameters of 815 ± 98 nm and the blended fibers had an average diameter of 720 ± 124 nm. Electrospinning of pure keratin resulted in beads, whereas combining with PEO (10%) produced fibers without any defects on the surface (Figure 8.5). 3-(4,5-dimethylthiazol-2-yl)-2,5-diphenyltetrazolium bromide (MTT) assay (Figure 8.6) showed higher cell proliferation on the keratin–PHBV mats compared to pure PHBV mats due to the presence of the cell-binding peptides on keratin. As wound dressing, PHBV–keratin matrices provided near-complete (94%) wound closure after 7 days compared to about 80% closure for the pure PHBV mats (Figure 8.7) (Yuan, 2015).

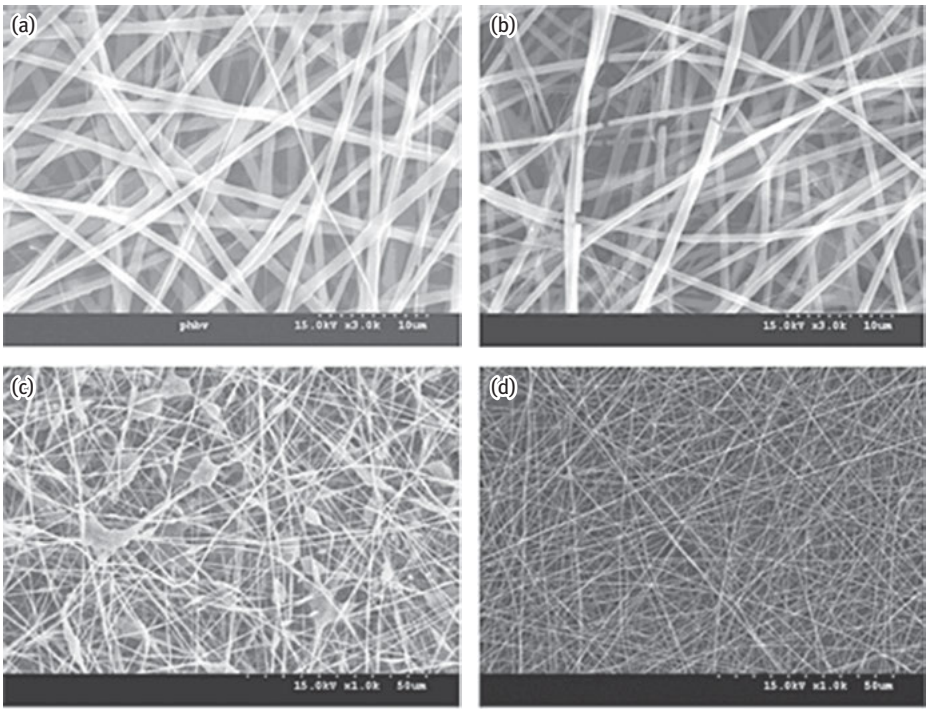

Figure 8.5: Scanning electron microscopy image of PHBV (a) and PHBV–m-keratin (7:3) (b), pure keratin (c) and PEO/keratin (1:9) mats (d) (Yuan, 2015). Reproduced with permission from John Wiley and Sons.

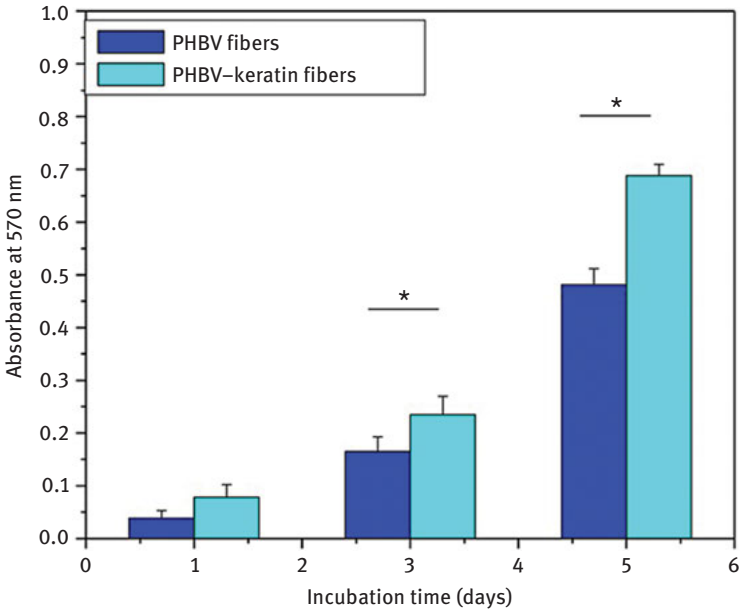

Figure 8.6: Ability of the PHBV and PHBV–keratin fibers to support the attachment and proliferation of NIH3T3 cells measured in terms of % cell viability (Yuan, 2015). Reproduced with permission from John Wiley and Sons.

8.2.5 Keratin blended with poly(caprolactone) (PCL)

Scaffolds suitable for bone tissue regeneration were prepared by electrospinning a blend of keratin and polycaprolactone (PCL). Keratin used in this study was extracted from human hair. The matrices obtained were cross-linked using glutaraldehyde and also coated with calcium phosphate to promote osteogenic differentiation (Zhao, 2015a). A new method of coating used in this study resulted in uniform distribution of calcium phosphate on the surface of the fibers. Such uniform coating of the phosphate led to substantial growth of apatite on the surface of the fibers when the fibers were immersed in simulated body fluid (Zhao, 2015a). Scanning electron microscopic images show the uniform deposition of calcium phosphate on the keratin–PCL blend fibers, which led to extensive growth of apatite on the fiber surface when the fibers were incubated in simulated body fluid (Zhao, 2015a). The blend fibers coated with calcium also had higher tensile strength (17 MPa) compared to about 7 MPa for the pure PCL. Elongation of the blend fibers was considerably lower at about 150% compared to 300% for the PCL fibers. However, pore size of the scaffolds did not show major differences and was between 2.1 and 3.1 μm. Morphological images showed that the human mesenchymal stem cells were well spread on the PCL blend nanofibers, and a high level of mineralization was observed after 14 days of culturing (Zhao, 2015a).

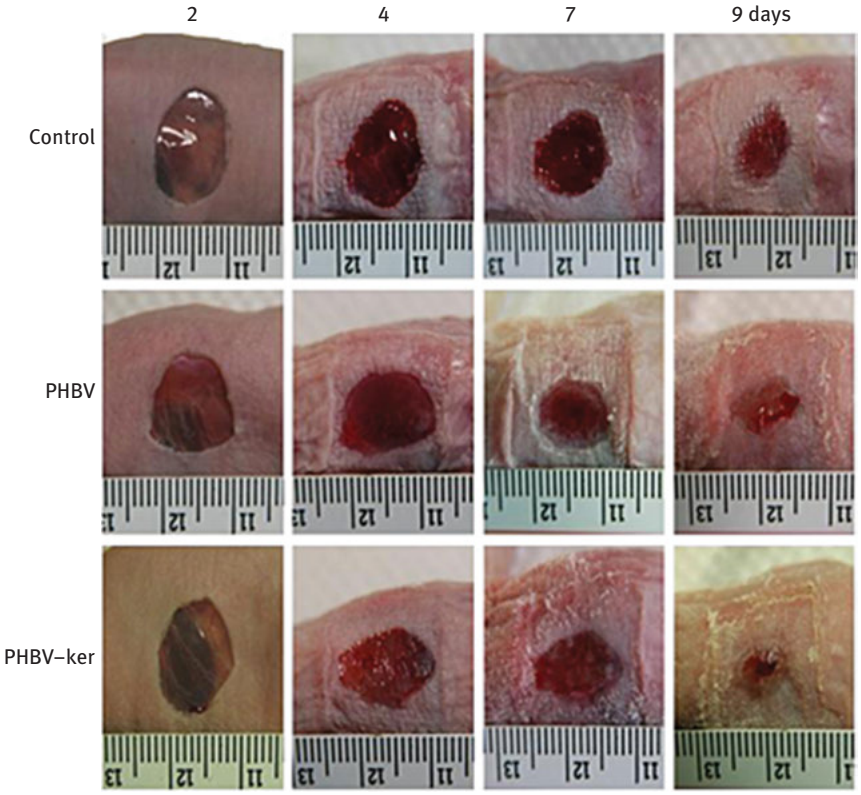

Figure 8.7: Changes in the diameter of the wound after treating with PHBV and keratin–PHBV matrices after 2–9 days of implantation (Yuan, 2015). Reproduced with permission from John Wiley and Sons.

8.2.6 Keratin blended with poly(caprolactone) (PCL)

To aid guided bone regeneration, a ternary blend of a synthetic biopolymer [poly(lactic-*co*-glycolic acid) (PLGA)], an inorganic material [carbon nanotubes (CNTs)] and a natural biopolymer (keratin) were combined together and electrospun to form membranes (Zhang, 2014). PLGA was dissolved using appropriate solvents (dimethyl formamide and trichloromethane), to which modified multiwalled CNTs and various percentages of keratin extracted from wool were added. The mixture was electrospun into fibrous membranes with diameters of the fibers ranging from 800 to 2,200 nm. Transmission electron microscopic images showed uniform distribution of the fibers and CNTs in the PLGA matrix.

Inclusion of CNTs into PLGA increased the strength marginally but the elongation increased nearly five times. Addition of 2% wool keratin increased the strength nearly three times and elongation by nearly eight times. Such substantial increase in tensile properties was considered to be due to the good interaction between the

PLGA, CNTs and wool keratin particles (Zhang, 2014). Thermal properties showed slight improvement with the addition of CNTs, and further increase was observed when the keratin particles were present (Table 8.6). When the membranes were immersed in simulated body fluid, growth of apatite particles was observed after 7 days and formation of complete membranes was observed after 14 days, suggesting that the membranes are suitable for bone tissue engineering (Zhang, 2014).

Table 8.6: Tensile and thermal properties of the pure and blend nanofiber membranes (Zhang, 2014).

Sample	Strength (MPa)	Elongation (%)	Modulus (MPa)	60% weight loss temp. (°C)
PLGA	5.60	14.35	307.12	282
PLGA/MWNTs	7.98	70.07	334.61	316
PLGA/MWNTS/0.5% keratin	7.19	79.40	234.11	316
PLGA/MWNTS/1% keratin	10.44	53.45	651.84	317
PLGA/MWNTS/2% keratin	13.93	104.02	824.30	317

Note: Reproduced with permission from Springer.

8.2.7 Keratin blends with natural polymers

Instead of blending keratin with synthetic polymers such as PHBV or PCL, keratin extracted from merino wool was dissolved using formic acid and combined with silk fibroin solution and made into films and electrospun fibers (Zocolla, 2008). Viscosity of the blend solution decreased with increasing level of keratin, whereas conductivity increased. Fibers with diameters of 207 ± 66 nm were obtained with a keratin/fibroin blend of 50/50. Thermal analysis showed the denaturation peak of the 50/50 blend at the highest temperature, suggesting that there was good interaction between the two proteins leading to increase in thermal stability. The mechanical properties, stability of the films and fibrous membranes in aqueous conditions were not known. Also, their ability to support attachment and proliferation of cells was not studied (Zocolla, 2008).

Chapter 9
Keratin micro/nanoparticles

Micro- and nanoparticles have large surface area and are able to enter into cells and organs in vitro and in vivo. Due to their large surface area, micro- and nanoparticles are also preferred as drug carriers and for loading and release of various pharma- and nutraceuticals. Hence, several studies have been done to use various sources of keratin to develop micro- and nanoparticles. Keratin in leather processing waste was retrieved and powdered to pass through a 0.1 mm mesh. The powdered keratin had particle size ranging from 146 to 185 nm. Mixing the nanoparticles with nanometric zinc oxide resulted in separation of the particles into two sizes, one between 20 and 82 nm and the other between 208 and 262 nm (Prochon, 2013). These keratin nanoparticles were incorporated into styrene as fillers, to improve flame resistance and mechanical properties. Addition of the keratin and zinc oxide-treated keratin nanoparticles resulted in significant changes in the properties of the styrene composites (Table 9.1**)**. Addition of zinc oxide decreased the water absorption and increased the compatibility with the matrix. However, mechanical properties of the elastomeric materials decreased with the addition of the nano-zinc oxide particles (Prochon, 2013). Similarly, time of burning in air increased from 283 to 345 s when 10% of keratin nanoparticles were used (Table 9.2). It was found that the thermal stability and flammability characteristics were dependent on the method of composite preparation and the quantity of added keratin. Presence of the keratin particles was also found to increase water absorption and biodegradation (Prochon, 2013).

Table 9.1: Changes in the properties of the styrene and styrene composites containing normal and nanosized keratin particles (Prochon, 2013).

Sample	LL (dNm)	ΔL (dNm)	t_{09} (min)	α_c	Z (%)	TSb (MPa)	Eb (%)	S	Z_{H2O} (%)
SBR	17	91	20	0.22	9.3	2.37	364	0.72	1.83
SBR5K	19	143	10	0.32	8.0	2.36	141	0.96	1.98
SBR10K	21	141	10	0.33	6.9	2.58	134	0.98	2.92
nSBR	16	121	10	0.27	9.1	2.11	203	1.14	1.50
nSBR5K	18	124	10	0.34	17.7	1.52	153	1.41	2.67
nSBR10K	20	127	10	0.34	19.9	1.44	145	1.41	3.11

Note: Reproduced with permission from Springer.

Keratin (20–45 kDa) was extracted from descaled wool fibers by treating with urea, mercaptoethanol and sodium dodecyl sulfate (SDS) at 70 °C for 2 h. The extracted keratin was used to prepare nanoparticles by electrospraying. Scanning electron microscopic images showed particle size distribution between 36 and 72 nm (Figure 9.1). Formation of cysteine monoxide (-SO-S-) in keratin sponge and cysteic acid and

https://doi.org/10.1515/9781501511769-009

Table 9.2: Flammability of NBR composites and nanocomposites containing keratin (Prochon, 2012).

Sample	t_S (s)	OI
N	276	0.205
N5 K	324	0.235
N5 Kr	319	0.247
N5 KZS	323	0.238
N10 K	286	0.220
N10 Kr	295	0.228
N30 Kr	336	0.238
nN	205	0.181
nN5 K	310	0.193
nN10 K	305	0.197

t_S, time of burning in air; OI, oxygen index.
Note: Reproduced with permission from Springer.

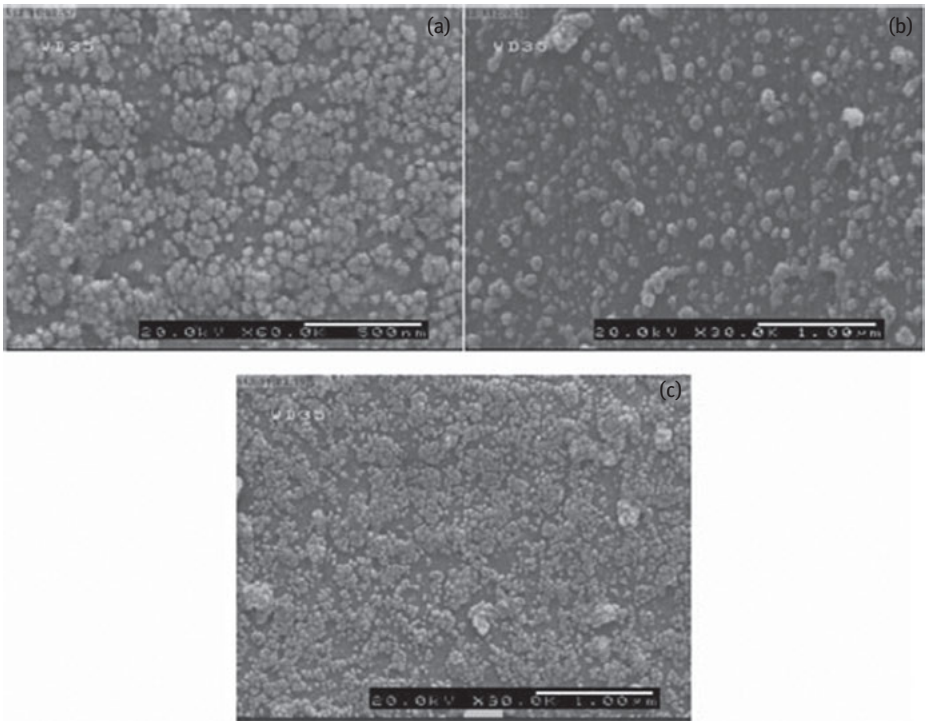

Figure 9.1: Scanning electron microscopic images (a)–(c) show the particle size distribution of the keratin nanoparticles obtained by electrospraying at different electrospinning conditions (Ebrahimgol, 2014). Reproduced with permission from John Wiley and Sons.

cysteine monoxide in the keratin nanopowder was observed (Figure 9.2). Solvents used for dissolution, concentration of the keratin solution and electrospraying conditions could be varied to control the size of the nanoparticles (Ebrahimgol, 2014). In a similar study, keratin nanopowder was produced through electrospraying with nanoparticle size as low as 53 nm (Rad, 2012). To obtain the nanoparticles, keratin was extracted from feathers using urea, mercaptoethanol, ethylenediaminetetraacetic acid (EDTA), mercaptoethanol and SDS. Extracted keratin was freeze-dried to obtain sponges (Rad, 2012). For electrospraying, the keratin sponge was dissolved in formic acid or trifluoroacetic acid (TFA). TFA provided better dissolution, and the concentration of the keratin was 0.2–1%. With a voltage of 10–20 kV, the needle to collector distance of 15–25 cm was adopted for electrospraying. X-ray diffraction studies (Figure 9.3) showed that the keratin sponge was mainly composed of β-sheets, whereas nanoparticles consisted of both the α-helix and β-sheet structures. However, there was significant reduction in % crystallinity from 63% to 51% for the particles compared to the raw keratin.

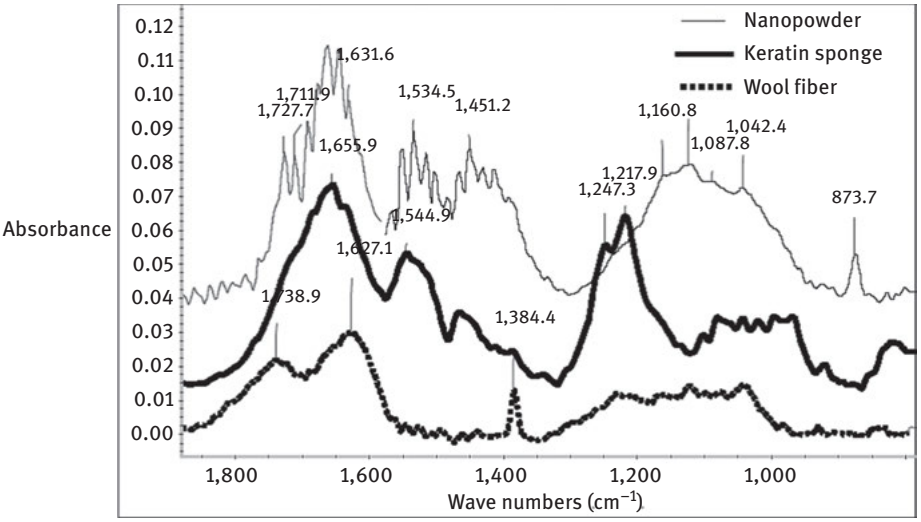

Figure 9.2: Fourier transform infrared spectrum of wool, keratin extracted from the wool and made into sponge and electrosprayed keratin nanopowder (Ebrahimgol, 2014). Reproduced with permission from John Wiley and Sons.

Keratin extracted from chicken feathers using 5% NaOH was precipitated and lyophilized to obtain protein powder. Later, the powder was suspended in 2 mL of deionized water and 8 mL of ethanol was added to form nanoparticles. Glutaraldehyde was added to cross-link and stabilize the nanoparticles. Nanoparticles with average diameters of about 150 nm were obtained and added into chitosan (1%) dissolved using acetic acid. The keratin–chitosan blend was made into scaffolds through lyophilization

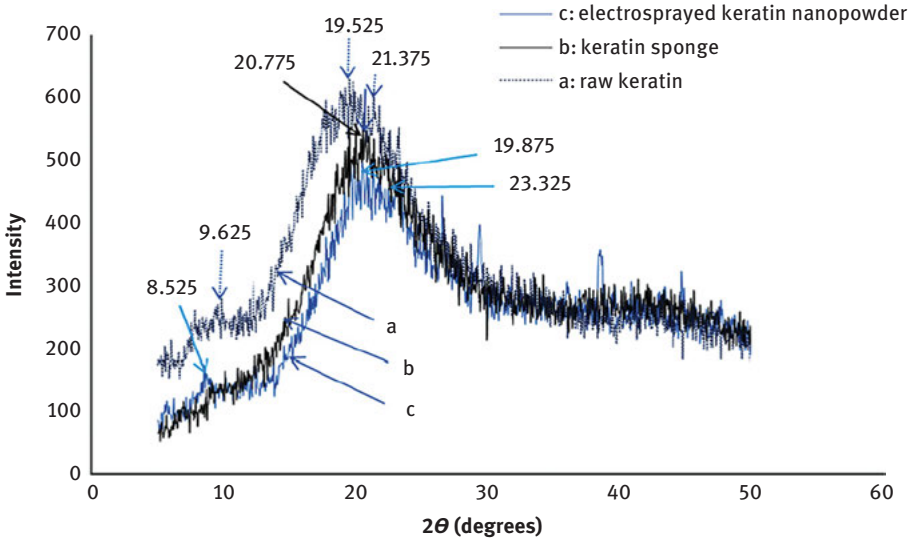

Figure 9.3: X-ray diffraction patterns of the raw keratin, keratin sponge and the electrosprayed keratin nanopowder (Rad, 2012).

(Saravanan, 2013). Morphology and porosity of the scaffolds were dependent on the conditions used for fabrication. Pure chitosan scaffolds had pore sizes between 25 and 60 μm compared to 17–30 μm for the blend scaffold. Although the swelling ratio of both the scaffolds was similar, the blend scaffold degraded by almost 30% after 48 h of incubation. When incubated with fetal bovine serum, the scaffolds containing the keratin nanoparticles showed considerably higher protein absorption due to the increased surface area and inherent properties of keratin. Scaffolds containing keratin did not show any cytotoxicity to human osteoblastic cells and were therefore considered to be suitable for medical applications (Saravanan, 2013).

One of the limitations of protein nanoparticles is their instability under aqueous conditions. Intrinsically water-stable keratin nanoparticles were prepared from feathers and used as carriers for drugs (Xu, 2014). Keratin was extracted from feathers using sodium hydroxide and sodium bisulfite. The extracted keratin was dissolved using ethylene glycol and precipitated into nanoparticles. Size of the nanoparticles varied from 50 to 130 nm (Figure 9.4) and their zeta potential was higher than 50 mV at pH below 3, whereas it was −60 mV when the pH was 10. Keratin nanoparticles promoted the growth of mouse fibroblasts when added into the culture media. The particles were also able to enter into various organs in mice but were predominantly found in the kidneys (Figure 9.5).

A unique strategy (Figure 9.6) was used to incorporate keratin nanoparticle–hydroxyapatite (HA) nanocomposite onto electrospun polylactic acid and improve

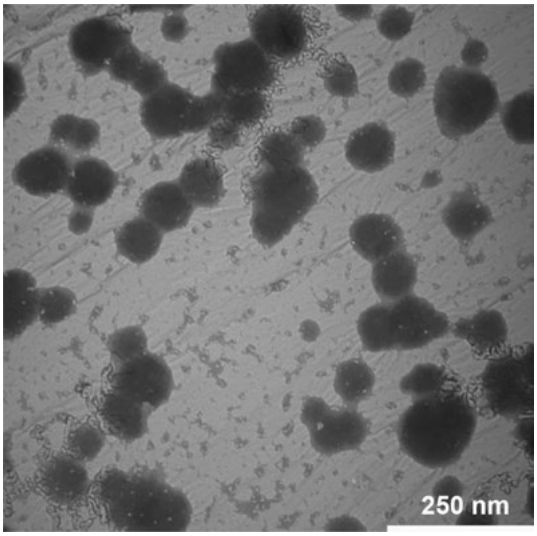

Figure 9.4: TEM images of the keratin nanoparticles show that the diameters varied from 50 to 130 nm (Xu, 2014). Reproduced with permission from American Chemical Society.

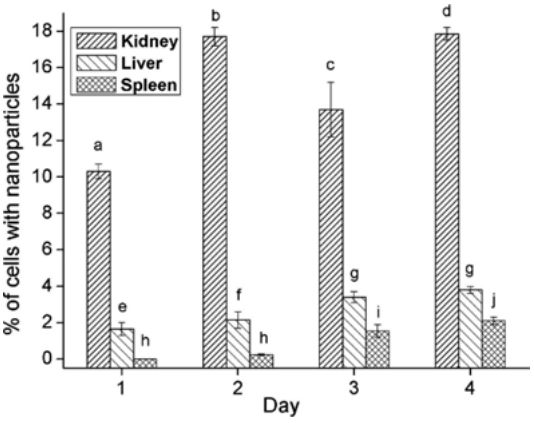

Figure 9.5: Keratin nanoparticles were able to enter various organs in mice but were predominantly found in the kidneys (Xu, 2014). Reproduced with permission from American Chemical Society.

bone formation (Li, 2013). Addition of keratin decreased the tensile strength of the electrospun matrix. However, considerably higher number of Saos-2 cells had proliferated (Figure 9.7) on the poly(L-lactic acid) (PLLA) membrane containing the nanocomposite. It was also found that the keratin–HA nanocomposite had considerably higher adhesion, spreading and formation of osteoblast cells, suggesting the suitability of keratin for tissue engineering (Li, 2013).

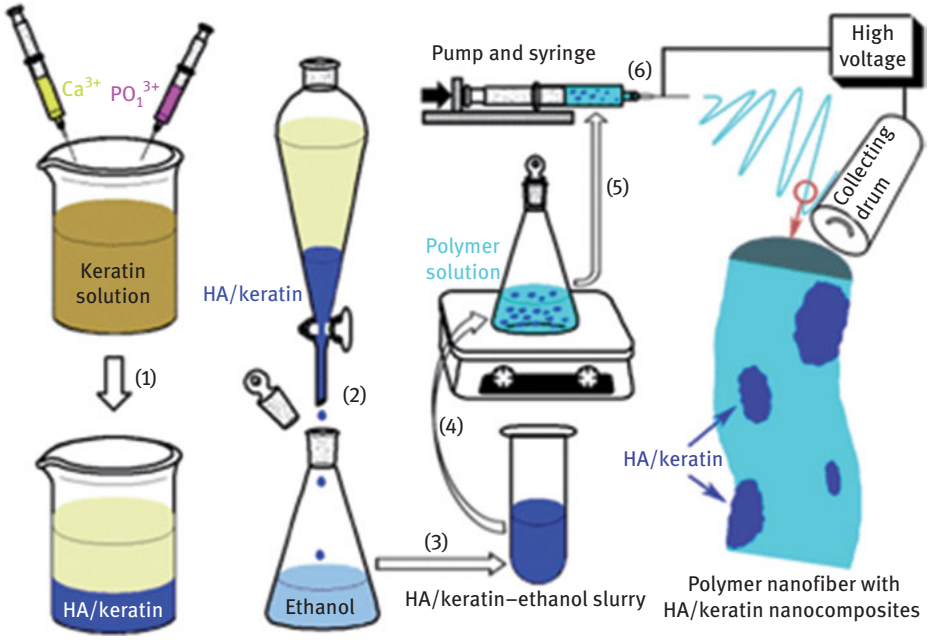

Figure 9.6: Schematic representation of the approach used to develop the keratin–HA–PLA electrospun matrices (Li, 2013). Reproduced with permission from *Journal of Materials Chemistry*.

Keratin nanoparticles were covalently conjugated with chlorin e6 (Ce6), a photosensitizer that is used in treating cancer, melanoma and other diseases (Aluigi, 2016). To prepare the nanoparticles, keratin was extracted from wool and freeze-dried into powder. This powder was conjugated with Ce6 and later made into nanoparticles by dissolving in dimethyl sulfoxide or by self-assembly. Further, the proteins were cross-linked using glutaraldehyde and during the process, self-assembly of the proteins also occurred (Aluigi, 2016). Process of formation of the conjugates and some of their properties are shown in Figure 9.8. It was found that nanoparticles had diameters of 197 and 213 nm for the self-assembling and desolvation processes, respectively. In vitro assays did not show any cytotoxicity to the keratin–Ce6 conjugates. However, irradiating the nanoparticles or the conjugates with halogen lamp caused considerable toxicity and consequently higher cell death (Figure 9.9). Ce6-loaded nanoparticles were able to cross the tumor membranes and accumulate in the cytoplasm. It was suggested that keratin–Ce6 conjugates would be effective for treating cancer and other diseases (Aluigi, 2016).

In another approach, keratin/chlorohexidine complex nanoparticles were formed via electrostatic complexation (Zhi, 2015). Complex nanoparticles obtained had an average diameter of 176 nm and zeta potential of −15 to −30 mV. A high chlorohexidine loading of 9.2% and an encapsulation efficiency of 91% was possible due to the

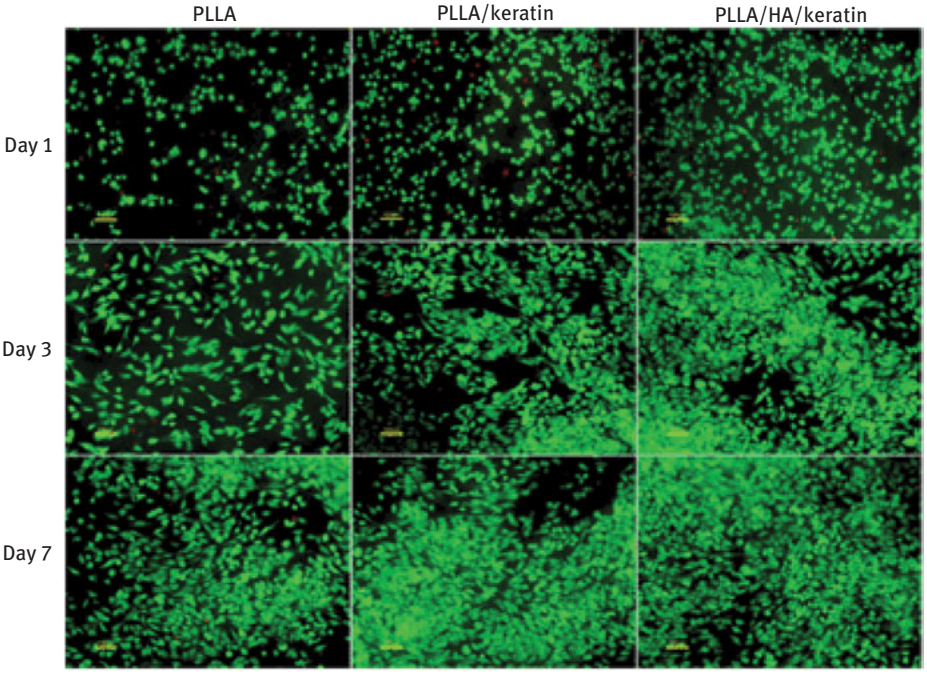

Figure 9.7: Optical images show that the proliferation of Saos-2 cells was considerably higher on the keratin–HA–PLLA electrospun matrices (Li, 2013). Reproduced with permission from *Journal of Materials Chemistry*.

electrostatic interaction between proteins and the drug molecules. Up to 50% of the drug could be released but a slight cytotoxicity was observed due to the presence of nanoparticles. However, the keratin–chlorohexidine complexes showed good antimicrobial activity against both *E. coli* and *S. aureus* (Zhi, 2015). Another study has also shown that keratin nanoparticles have better antioxidant and antibacterial activities than keratin solution (Sundaram, 2015).

Keratin nanoparticles were considered to have higher specific surface area, higher water uptake and better film-forming property, which were considered to be ideal for use as an hemostatic agent (Luo, 2016). Keratin was extracted from human hair and made into nanoparticles with size ranging from 142 to 205 nm. Both in vitro and in vivo studies showed considerably faster blood coagulation times when keratin nanoparticles were used. Such excellent coagulation was considered to be due to platelet binding and activation and polymerization of fibrinogen (Luo, 2016).

Poly(ethylene glycol) (PEG) was grafted onto keratin extracted from wool and the grafted (keratin-g-PEG) polymers were made into nanoparticles. Three levels of grafting were done to obtain nanoparticles (20–50 nm in length and 10 nm in width) with different properties (Li, 2012). The nanoparticles were cross-linked and loaded with doxorubicin (DOX). Circular dichroism (CD) spectra (Figure 9.10) showed that the

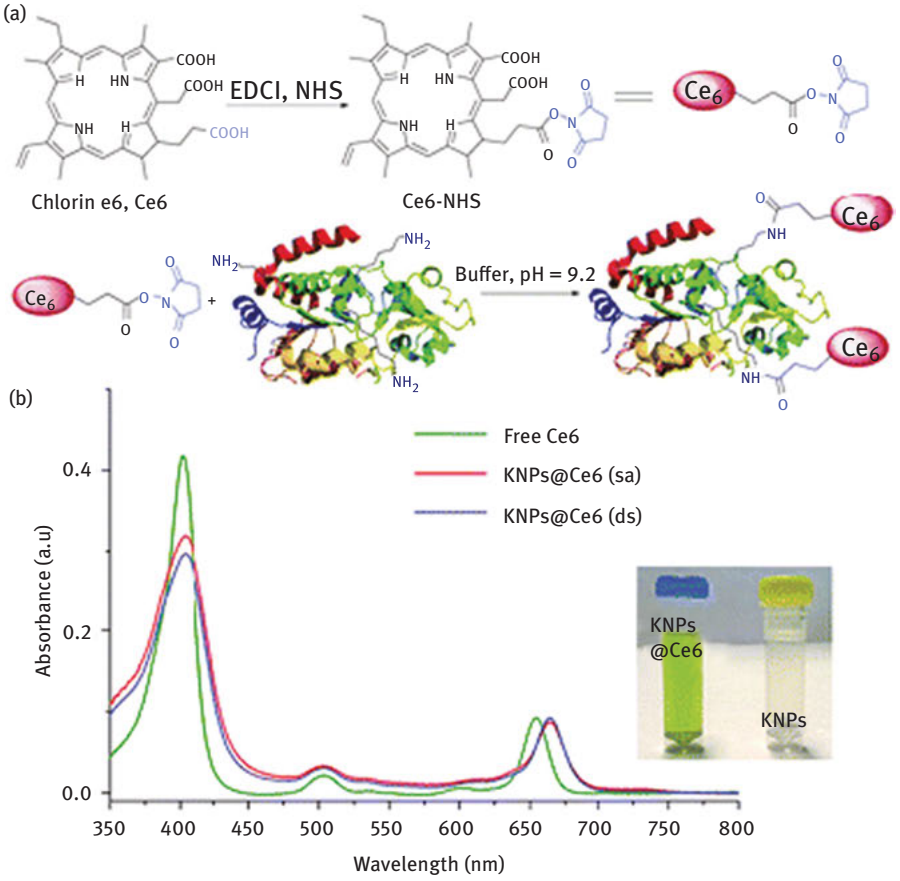

(c)

	KNPs@C6e *self-assembling*	KNPs@C6e *desolvation*
Yield (%)	24 ± 5	30 ± 5
Hydrodynamic diam. (nm)	148 ± 13	147 ± 7
Polydispersity index	0.17 ± 0.02	0.13 ± 0.5
zeta-potential (mV)	−53 ± 10	−68 ± 2
Loading ratio Ce6/ker (µg/mg)	25 ± 5	27 ± 8
Loading efficiency (%)	42 ± 8	45 ± 10

Figure 9.8: Schematic representation of the formation of the keratin–Ce6 conjugates (a), absorption spectrum of individual Ce6, keratin nanoparticles and the conjugates (b), properties of the conjugates obtained using two different approaches (c) (Aluigi, 2016). Reproduced with permission Royal Society Chemistry.

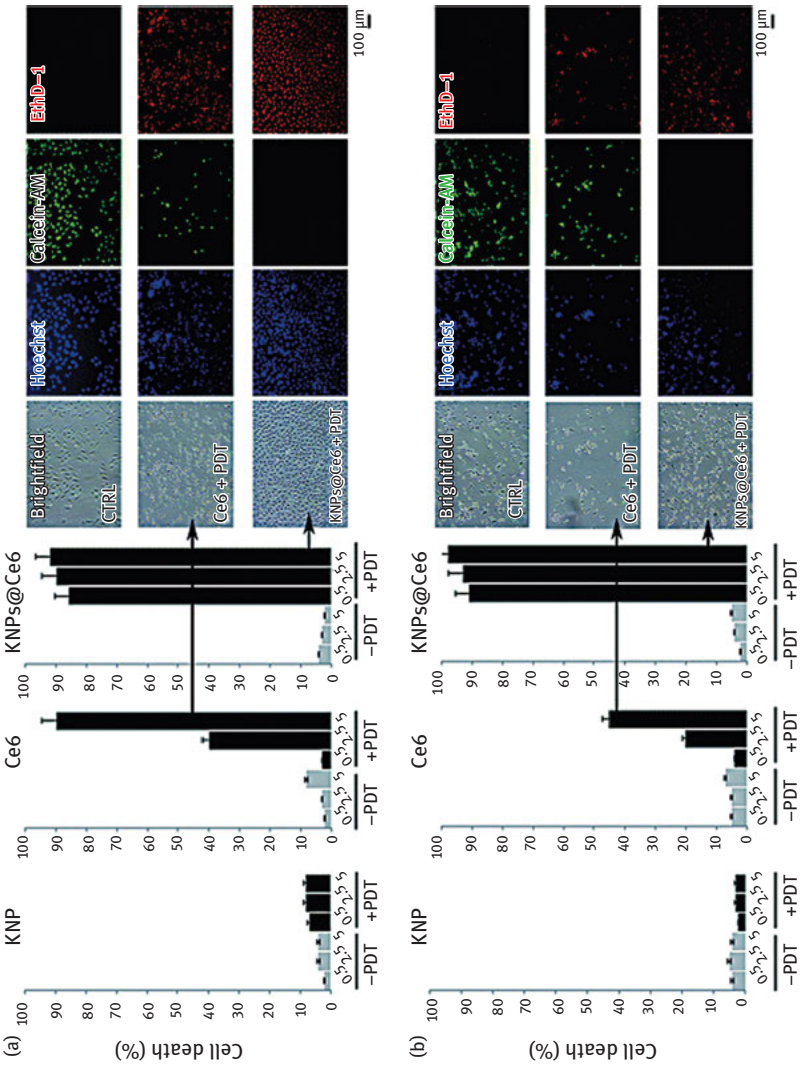

Figure 9.9: Cytotoxicity of the keratin nanoparticles (KNPs), Ce6 and conjugates KNPs@Ce6 against two cells expressed in terms of % cell death before and after irradiation. Corresponding confocal images are given on the right panel (Aluigi, 2016): (a) U2OS – osteosarcoma and (b) U87 – glioblastoma. Reproduced with permission from Royal Society Chemistry.

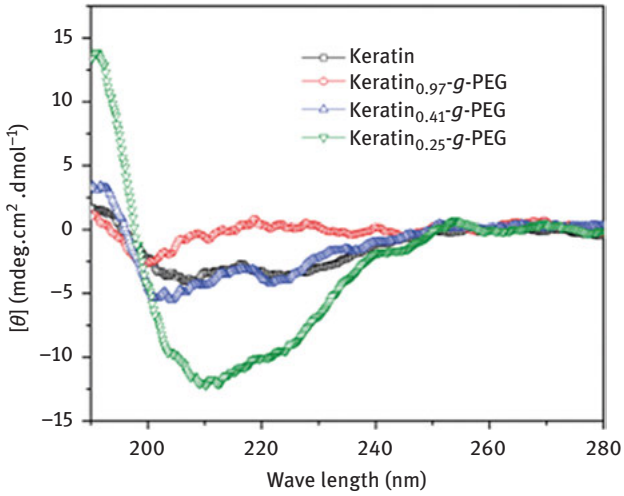

Figure 9.10: CD spectra of the unmodified and keratin grafted with PEG to three different levels of grafting (Li, 2012). Reproduced with permission from Royal Society Chemistry.

keratin nanoparticles assumed the α-helical conformation in solution. Amount of loading of the drug was dependent on the extent of grafting. Increasing grafting ratio decreased the efficiency (36–9.7%) with the corresponding decrease in drug content (18–4.9%) (Li, 2012). Release of the drug from the nanoparticles was dependent on the extent of grafting and cross-linking (Figure 9.11).

Feather keratin was made into nanoparticles for potential use as a hemostatic agent. Keratin was extracted from chicken feathers, lyophilized and made into powder. Nanoparticles were obtained by dispersing the keratin powder in acetic acid solution (pH 3.0), followed by sonication lyophilization (Wang, 2016a). Keratin obtained had molecular weight between 11 and 28 kDa and was mostly composed of β-keratin and a small proportion of α-keratin with molecular weight around 55 kDa. Amino acids desirable for extracellular matrix growth such as arginine, glycine and aspartic acid were present in the keratin. Size of the nanoparticles varied with the concentration of keratin in solution and was between 181 and 220 nm with the corresponding zeta potential between 19.6 and 18.1 mV. When hemostatic efficiency was studied in mice, feather keratin nanoparticles were able to stop bleeding much faster than keratin extracts by about 40 to 90 s. A maximum hemostasis time of 250 s and blood loss of 1.7 g were observed for keratin nanoparticles.

Keratin obtained from human hair was conjugated with DOX through hydrazine linkage and later made into nanoparticles for potential use as a pH-sensitive drug carrier (Liu, 2019). The coupling reaction was done using EDC and NHS as coupling agents. Conjugated keratin was converted into nanoparticles using the desolvation method. Here, ethanol was added into the keratin conjugate and later genipin was added and reacted for 13 h. Solution was centrifuged and later lyophilized to form

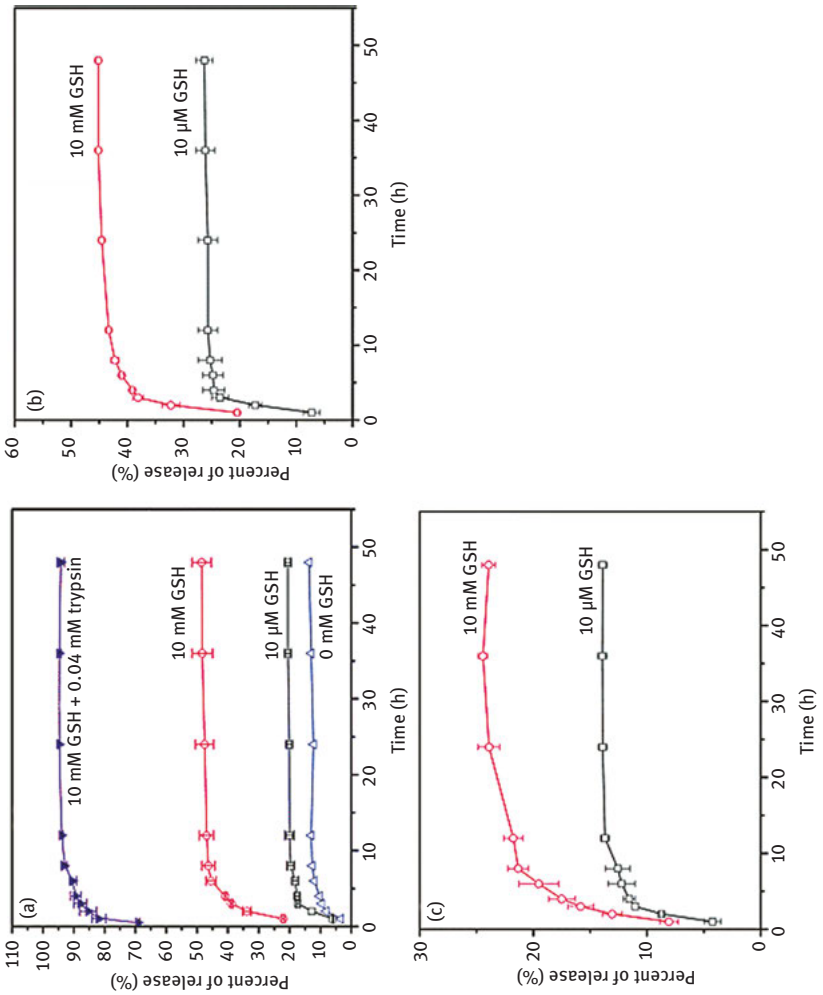

Figure 9.11: Release of drug from the keratin–PEG nanoparticles (Li, 2012): (a) keratin$_{0.25}$-*g*-PEG; (b) keratin$_{0.41}$-*g*-PEG; and (c) keratin$_{0.97}$-*g*-PEG. Reproduced with permission from Royal Society Chemistry.

the nanoparticles. Fourier transform infrared studies showed that the secondary structure of keratin was not changed but DOX was conjugated through the hydrozone bond (C=N). Average size of the nanoparticles was 230 nm and zeta potential was −30.4 ± 0.78 mV suitable for longer blood circulation. Release of DOX from the particles was heavily dependent on pH with only 5% released at pH 7.4 compared to 78% at pH 5.0. When used as an antitumor agent, up to 71% suppression was observed, suggesting that conjugated keratin particles were highly effective as antitumor agents, better than free DOX (Liu, 2019). In a similar approach, dual-responsive protein hydrogel nanoparticles were developed by combining keratin with thermoresponsive polymers for triggerable drug delivery (Ghaffari, 2018). Keratin was extracted from wool by treating with urea, sodium pyrosulfite and SDS. Solubilized keratin was lyophilized to obtain powder with molecular weight between 45 and 65 kDa. Nanoparticles having average diameter of 152 nm were prepared by conjugating keratin with pluronic block polymers. Self-assembly of the proteins and copolymers occurs, resulting in thermosensitive nanoparticles. ^{1}H-NMR studies showed successful conjugation of keratin onto pluronic through amide bond and EDC/NHS chemistry. Blend nanoparticles had a critical micelle concentration (CMC) value of 0.38 mg/mL and hence easily formed self-assembled structures. Curcumin used as a model drug was able to load up to 7.4% with encapsulation efficiency of 82%. Up to 90% curcumin retention was possible even after 30 days, and the nanoparticles had a zeta potential of −23.6 mV (Ghaffari, 2018). Both fibroblasts and HeLa cells showed high cell viability and hence biocompatibility. Since cells do not uptake free curcumin, conjugating curcumin with keratin-pluronic nanoparticles was suggested to be a viable approach for delivering curcumin with high efficiency to tumor sites for treating cancer.

Keratin extracted from feathers at two different pH was made into microparticles and studied for their antioxidant and anticancer properties (Sharma, 2017). Feathers were treated with sodium sulfide at 50 °C and converted into hydrolysate which was precipitated at pH 3.5 or 5.5 resulting in the formation of microparticles. The precipitated particles were collected after lyophilization and used for further analysis. Particles formed were spherical but were considerably agglomerated. Antioxidant studies showed significant levels of efficacies both for 2-2'-Azino-di-[3-ethylbenzthiazoline sulfonate] (ABTS) and 2,2-Diphenyl-1-picrylhydrazyl (DPPH) free radicals similar to that of ascorbic acid (Table 9.3). No major anticancer activity was recorded for any of the cell lines studied. It was suggested that the particles could be useful for developing antiaging cream, shampoo and wound healing creams (Sharma, 2017).

Nanoparticles prepared from keratin have been used as additives for polyhydroxyalkanoate-based packaging materials to improve barrier properties and other functionalities (Fabra, 2016). To extract the nanokeratin, feathers were treated with an aqueous solution of 8 M urea, 3 mM EDTA and 2-mercaptoethanol at pH 7.0 for 2 h. Liquid formed was dialyzed twice and against a 10 kDa membrane and then freeze-dried to form a fine powder. Keratin nanoparticles were combined with polyhydroxyalkanoates (PHA) and made into packaging materials using both melt compounding

Table 9.3: Antioxidant activity of keratin microparticles extracted at pH 3.5 and 5.5 in comparison to ascorbic acid (Sharma, 2017).

Particle concentration (mg/mL)	ABTS scavenging activity (%)		DPPH scavenging activity (%)	
	pH 3.5	pH 5.5	pH 3.5	pH 5.5
0.1	1.80	0.95	11.09	6.92
1	4.76	2.00	11.44	7.81
10	10.01	3.22	11.88	9.66
100	16.28	14.38	16.84	10.11
1,000	46.17	32.47	30.38	26.15
IC_{50} µg/mL	8.96 ± 0.37	5.6 ± 0.24	13.2 ± 0.33	0.02 ± 0.41
Ascorbic acid	5.04 ± 0.05	5.04 ± 0.05	12.2 ± 0.11	12.2 ± 0.11

Note: Reproduced with permission from Elsevier.

and electrospinning. Nanoparticles were added (15–50%) into 3-hydroxybutyric acid-*co*-hydroxyvaleric acid (PHBV) dissolved in 2,2,2-trifluoroethanol, and the solution was electrospun at 10–12 kV using a flow rate of 0.7 mL/h. In an alternative approach, the nanokeratin powder or electrospun fibers were combined with PHBV3 and PHBV12 by melt mixing to form pellets. The pellets were later compression molded at 165 °C using a pressure of 35 MPa and compression time of 4 min to form films. Most of the nanokeratin obtained had particle size of less than 100 nm. Addition of the nanoparticles did not affect the thermal behavior or processability of the PHBV matrices. However, substantial changes were observed in the mechanical properties and permeability behavior of the electrospun and melt compounded blends depending on the type of matrix used. Modulus of the melt blended material ranged from 1.7 to 2.3 GPa with the addition of keratin decreasing the modulus and strength, whereas elongation of the electrospun membranes increased. Oxygen and water vapor permeability decreased substantially with an increase in nanokeratin level. Reduction in water vapor permeability up to 63% was possible, indicating high barrier activity and suitability for packaging applications.

Not only pure keratin, even blends of keratin with other polymers have been made into micro- and nanoparticles. For instance, keratin from human hair, alginate and their blends were made into microparticles using the water-in-oil emulsification diffusion method. In this process, various concentrations of keratin solution were added into ethyl acetate and stirred for 30 min. Later, the acetate was evaporated to obtain the microparticles. To prepare the blends, alginate dissolved in water was added into the ethyl acetate solution in various ratios and formed into microparticles (Srisuwan, 2018). Particles with different sizes, shapes and surface features were obtained. Addition of surfactant was necessary to obtain relatively uniform particles with smaller pores (3–5 µm). Good interaction was observed between the alginate and keratin leading to higher thermal stability. Blend particles were considered to be suitable for delivering hydrophilic and hydrophobic pay loads.

Chapter 10
Miscellaneous applications of keratin

10.1 Cosmetic applications of keratin

Keratin is one of the most active ingredients in cosmetic products. The ability of keratin extracted from chicken feathers to provide antiaging properties was assessed using rabbit skin as a model. Composition of the antiaging cream containing 2 or 4 g of keratin is given in Table 10.1. Microscopical observation showed that the skin structure did not change due to the application of keratin-containing antiaging cream (Figure 10.1). However, no evidence was presented on the ability of the keratin to reduce aging (Khairunisa, 2014).

Table 10.1: Composition of the keratin-containing antiaging cream (Amir, 2014).

Ingredients	K1-L0 (g)	K2-L0 (g)	K1-L1 (g)	K2-L1(g)
Cetostearyl alcohol	3.0	3.0	3.0	3.0
Palm oil	3.0	3.0	3.0	3.0
Glycerin	4.0	4.0	4.0	4.0
Zinc oxide	2.0	2.0	2.0	2.0
Citric acid	1.0	1.0	1.0	1.0
Keratin	2.0	4.0	2.0	4.0
Distilled water	–	–	–	–
Cremophor	2.0	2.0	2.0	2.0
Lecithin	–	–	1.0	1.0

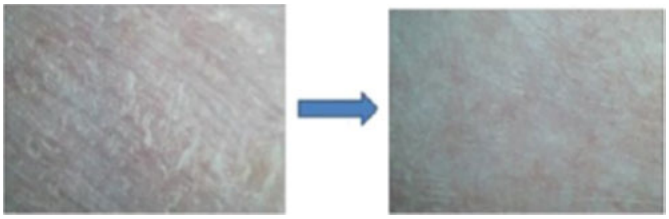

Figure 10.1: Structure of the skin after day 1 and day 90 when the keratin based antiaging cream was applied (Khairunisa, 2014). Reproduced from the University of Malaysia.

10.2 Flame retardants

Since feathers contain high amounts of nitrogen, it was hypothesized that feathers in combination with other chemicals could be useful as flame retardants. Keratin

https://doi.org/10.1515/9781501511769-010

extracted from feathers was combined with melamine and sodium pyrophosphate (5:1:8 ratio) initially and later treated with glyoxal and added into the flask and heated to 80 °C at pH 5. This reaction resulted in the formation of a yellow-colored feather-based flame retardant (Wang, 2014). Cotton fabrics were treated with borax or boric acid and the feather-based flame retardant before evaluating the flammability. Limiting oxygen index for the cotton fabrics ranged from 18 to 40 depending on the type of flame retardant much higher than that of untreated cotton.

An intumescent flame retardant that can instantaneously stop flame propagation was developed using waste wool fibers and chicken feathers as reinforcement and polypropylene as matrix (Jung, 2018). Waste wool fibers having average length of 2.4 mm or the feathers were immersed in phosphoric acid (PA) for 10 min at room temperature. Later, the keratinaceous materials were immersed in a mixture of ethylenediamine and toluene and heated to 80 °C leading to the formation of ethylene diamine phosphate (EDAP) and PA-containing fibers. Schematic of the preparation process is shown in Figure 10.2. Modified keratin fibers were combined with polypropylene in a melt blender and made into composites by compression molding at 175 °C. A two-stage mechanism was proposed, where PA provides phosphate anions to form amine phosphates, which propels the char formation. An EDAP layer forms on the surface of the fibers (Figure 10.3), providing flame retardancy with a gradient

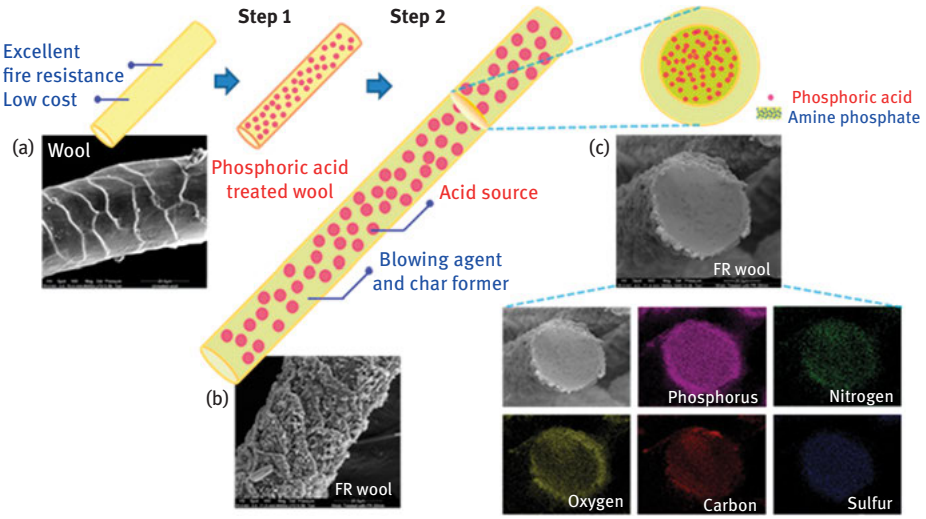

Figure 10.2: Mechanism of preparation of fire retardant keratin fibers (a), SEM image shows considerable deposits of EDAP crystals on the surface of the fibers (b) and EDX images of the cross section of the untreated and treated wool fibers (c) (Jung, 2018). Reproduced with permission from American Chemical Society.

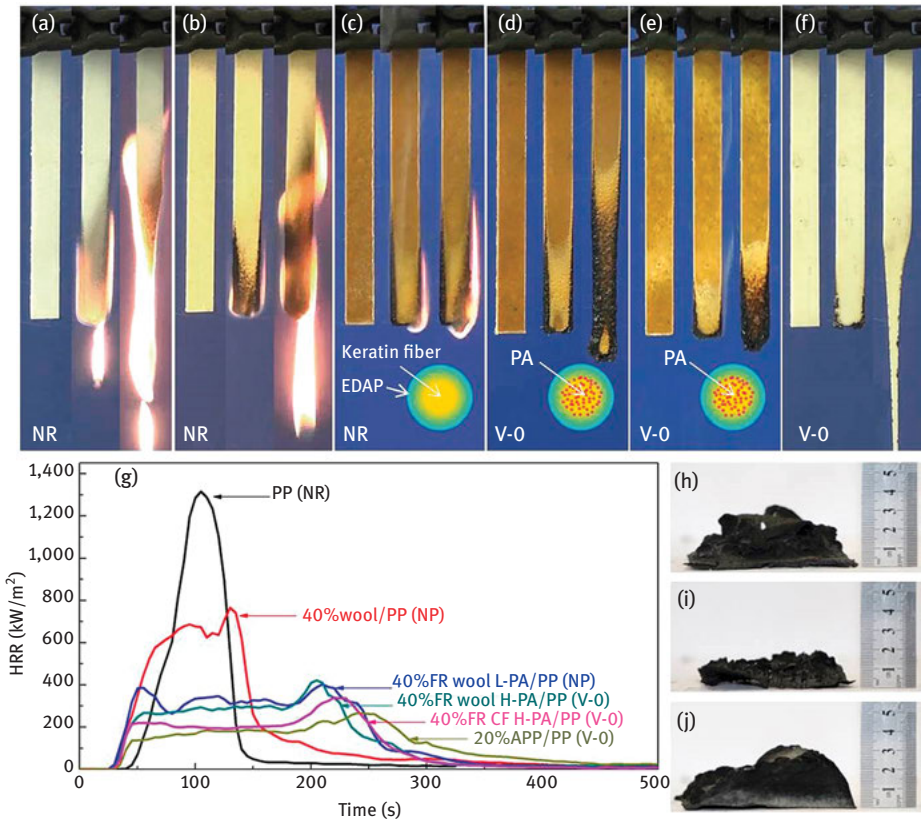

Figure 10.3: Images show the flame resistance behavior of untreated and treated wool fibers and the PP composites containing the wool fibers (a) to (f); heat release rate (HRR) curves for the various wool samples (g) and char images of composites containing 40% treated wool and L-PA/PP) (h), 40% treated wool and H-PA/PP and (j) 20% APP/PP composite after the cone calorimeter test (j) (Jung, 2018). Reproduced with permission from American Chemical Society.

in the amount of phosphorus from outside of the fibers to inside (Jung, 2018). Addition of treated keratin fibers into PP lead to substantially higher flame retardancy rating of V-0 and a 70% decrease in peak heat release rate, suggesting the suitability of composites for protection against fire (Table 10.2) (Jung, 2018).

Table 10.2: Thermal and fire retardant properties of composites containing various types of wool and feather (CF) fibers (Jung, 2018).

Sample	TTI (s)	PHRR (kW/m^2)	T_{PHRR} (s)	THR (MJ/m^2)	SPR (m^2/s)	EHC (MJ/kg)	Residue (%)
PP	24.3 ± 1.5	1,388	138	80	0.039	41.8	–
40% wool/PP	12.3 ± 1.5	859	125	77	0.032	34.1	4.2
40% FR wool L-PA/PP	14.3 ± 0.6	427	148	72	0.028	32.5	15.1
40% FR wool H-PA/PP	15.0 ± 1.7	436	182	65	0.029	31.8	20.5
40% CF wool H-PA/PP	14.7 ± 1.2	337	207	57	0.020	30.7	22.2
20% APP/PP	19.3 ± 0.5	258	251	55	0.023	30.6	26.7

THR, total heat release; EHC, effective heat of combustion; PHRR, peak heat release rate; and SPR, average smoke production rate.
Note: Reproduced with permission from American Chemical Society.

10.3 Supercapacitors

The lightweight and porous structure of feathers have been exploited to prepare supercapacitors for energy storage applications. Feathers were carbonized at different temperatures under nitrogen atmosphere for 2 h without and with pretreatment with potassium hydroxide (Zhao, 2015b). Scanning electron microscopic (SEM) images in Figure 10.4 show the porous morphological structure of the feather after carbonization. Interconnected fibrous structures that facilitate the transportation of the electrolyte ions were also seen. Substantial change in the elementary composition also occurs due to carbonization (Table 10.3). Carbon content increased from 78 to 84, whereas nitrogen decreased from 4.5% to 0.9%. Pore volume and specific surface area also changed with increasing temperature (Figure 10.5) (Zhao, 2015b). Current density was lower but energy and power density were considerably higher for the feather-based supercapacitors (Table 10.4) (Zhao, 2015b). Supercapacitance of the carbonized feathers was also found to vary with current. As given in Table 10.5, the chicken feather-based supercapacitor had the highest specific capacitance of 351 F/g compared to other common sources of activated carbon used before.

Wang et.al had prepared high-capacity carbon from feathers for supercapacitor applications (Wang, 2013). Chicken feathers were heated up to 450 °C in the presence of argon, and the obtained feather carbon was treated with potassium hydroxide in ratios from 1:1to 1:5 in the presence of ethanol. Later, the carbon was activated by heating up to 800 °C. Surface area of the feather carbon increased several thousand folds after treating with the alkali. Pore volume and average pore diameter also varied with the treatment conditions (Table 10.6) (Wang, 2013). Highest specific capacitance obtained was 302 F/g at 1 A/g comparable to results obtained by other researchers who had also carbonized feather for supercapacitor applications. However, the

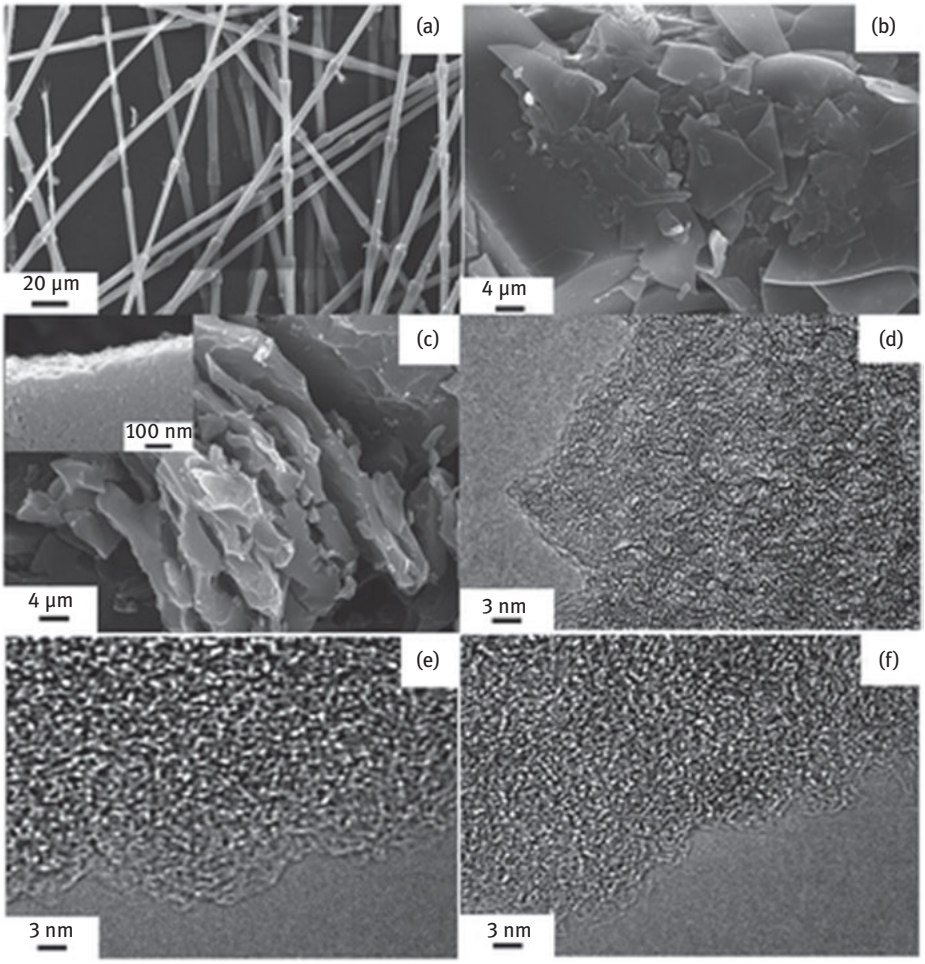

Figure 10.4: SEM images (a)–(f) of the feathers carbonized at different conditions (Zhao, 2015b). Reproduced with permission from Royal Society of Chemistry.

highest energy density reported was 7.98 Wh/kg, which is substantially higher than that reported in previous researches. Also, the specific capacitance did not show a major decrease even after 5,000 charge/recharge cycles, suggesting that charge/recharge of the carbon did not result in major structural transformations. The relatively larger pore size and wide pore distribution were suggested to provide good ion adsorption and therefore better capacitance (Wang, 2013).

Table 10.3: Changes in the elemental composition (at%) of the feathers after carbonization at various temperatures with a feather to alkali (KOH) ratio of 1:4 (Zhao, 2015b).

Samples	N	C	O	N-6	N-5	N-Q	N-X	O-1	O-II	O-III
CFC-500	4.48	78	17.2	1.87	1.13	0.48	0.99	3.20	11.21	2.78
CFAC-600	3.82	79	16.6	1.42	1.10	0.47	0.83	3.45	9.59	3.51
CFAC-650	2.46	81	16.0	0.66	0.66	0.39	0.64	0.87	10.06	5.05
CFAC-700	1.62	83	17.1	0.47	0.47	0.26	0.55	1.84	11.45	3.84
CFAC-750	1.35	83	15.0	0.49	0.49	0.22	0.41	2.46	10.52	2.05
CFAC-800	0.90	84	15.3	0.29	0.29	0.18	0.30	2.71	10.42	2.19

Note: Reproduced with permission from Royal Society of Chemistry.

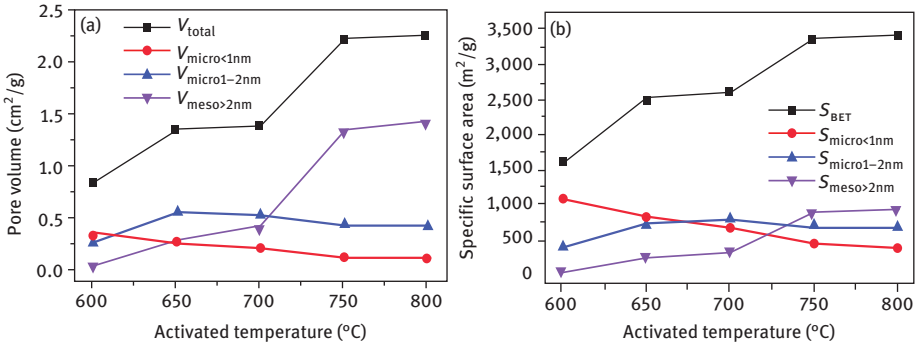

Figure 10.5: Changes in the pore volume (a) and specific surface area (b) with increase in activation temperature (Zhao, 2015b). Reproduced with permission from Royal Society of Chemistry.

Table 10.4: Variations in the specific capacitance (*C*, F/g) and energy density (*E*, W h/kg) at different currents for feathers carbonized at various temperatures and/or alkali to feather ratio (Zhao, 2015b).

Raw material	0.1 A/g		1 A/g		5 A/g		10 A/g		20 A/g		30 A/g	
	C	*E*	*C*	*E*	*C*	*E*	*C*	*E*	*C*	*E*	*C*	*E*
CFAC-600-4:1	351	31.2	244	21.7	212	18.8	183	16.3	144	12.8	142	12.6
CFAC-650-4:1	342	30.4	272	24.2	255	22.7	244	21.7	226	20.1	225	20.0
CFAC-700-4:1	256	22.8	220	19.6	208	18.5	208	18.5	204	18.1	201	17.9
CFAC-750-4:1	292	26.0	241	21.4	228	20.3	222	19.7	213	18.9	208	18.5
CFAC-800-4:1	257	22.8	227	20.2	214	19.0	207	18.4	197	17.5	190	16.9
CFAC-800-3:1	265	23.6	234	20.8	228	20.3	220	19.6	219	19.5	220	19.6
CFAC-800-5.5:1	288	25.6	264	23.5	256	22.8	258	22.9	258	22.9	260	23.1

Note: Reproduced with permission from Royal Society of Chemistry.

Table 10.5: Comparison of the performance properties of supercapacitors made using various types of biomass (Zhao, 2015b).

Raw material	Electrolyte	S_{BET} (m^2/g)	Specific capacitance (F/g)	Current density (A/g)	Energy density (W h/kg)	Powder density (kW/kg)
Human hair and glucose	KOH	849	264	0.25	7	0.045
Chicken feather	H_2SO_4	1,839	278	1	4.77	8.35
Human hair	KOH	451	192	0.3	–	–
Gizzard pepsin	KOH	2,150	198	1	–	–
Fermented rice	KOH	2,106	219	15	–	–
Fungi	$TEABF_4$	2,264	158	0.1	–	–
Watermelon	KOH	158	281	–	–	–
Chicken feather	KOH	2,515	351	0.1	23.1	11.2

Note: Reproduced with permission from Royal Society of Chemistry.

Table 10.6: Electrochemical properties and porosity of the activated carbon prepared from chicken feathers using different conditions (Wang, 2013).

Samples	BET surface area (m^2/g)	Micropore surface area (m^2/g)	Total pore volume (Cm^3/g)	Micropore volume (Cm^3/g)	Average pore diameter (nm)	ESR (Ω)
CFCA0	0.568	–	0.001	–	–	0.86
CFCA1	2,426	2,096	0.870	0.856	1.196	0.67
CFCA2	2,126	1,838	0.788	0.747	1.203	2.28
CFCA3	1,911	1,192	1.169	0.508	1.506	0.97
CFCA4	1,839	1,575	1.069	0.850	1.863	0.43
CFCA5	1,398	1,020	0.922	0.555	1.977	0.37

Note: Reproduced with permission from Elsevier.

10.4 Finishing of wool textiles

Felting (wrinkling) is one of the major draw backs of wool. Chemical and physical approaches are used to descale the surface of wool and reduce felting. Enzymes have also been used for treating wool and removing the scales (Xian-Lv, 2010). Keratinase was extracted from *Chryseobacterium* L99 sp. nov. and cultured for 30 h at 30 °C at 200 rpm using chicken feather as the substrate. The medium used for culture consisted of 40 g/L of feather keratin as the seed medium. Enzyme obtained after culture was purified, freeze-dried and stored for further use. Scoured and bleached wool fabrics were treated with 30 mM Tris–HCl buffer (pH 8.0) with a fiber to liquor ratio of 20 mL/g at 40 °C for 40 min. Amount of enzyme used was

0.5–5% on weight of the fabric for savinase 16 L and transglutaminase, and for keratinase L99 the amounts were 20, 40, 200 and 400 U/mL, respectively (Xian-Lv, 2010). Crude keratinase extracted was further purified using chromatography, the yield after purification was 29% and the molecular weight was 33 kDa (Xian-Lv, 2010). Changes in the properties of the wool fabrics including weight loss, tensile strength, dimensional stability and directional frictional effect were studied. Addition of metal ions caused considerable changes in the keratinase production. Highest activity was obtained for medium containing Mg^{2+}, and highest dry cell weight was obtained when Ca^{2+} was used. Compared to transglutaminase and savinase 16 L, keratinase significantly reduced the shrinkage and directional frictional effect but also caused weight and tensile strength loss.

Detergents contain significant amounts of keratinases. To obtain detergent and thermally stable keratinases, feather was made into powder and was used for enzyme production using marine actinobacterium *Actinoalloteichus* sp. Ma-32. Kinetics of keratinase production and the effect of various parameters including carbon and nitrogen source on keratinase activity were determined (Manivasagam, 2014). Source of carbon and nitrogen played a significant role on the production of enzymes, and the highest output was obtained with casein (nitrogen) and lowest with lactose (carbon). Production of the enzyme was highest at 120 h and the molecular weight was about 66 kDa (Manivasagam, 2014). Addition of metal ions increased but chemicals such as EDTA decreased the enzyme production. Extracted keratin was found to be stable in most detergents for up to 60 min. Enzyme-containing detergents showed considerably improved stain removal compared to the detergent without the enzyme.

Wool fabrics were treated with an acrylate monomer containing a quaternaryammonium moiety [2-(acryloyloxy)ethyl]trimethylammoniumchloride and the chemical was immobilized onto the keratin to improve antibacterial, antistatic, moisture absorption and dyeability (Yu, 2014). Treatment of the fabrics resulted in increase in surface resistivity and hence antistatic property. Considerable reduction (up to 94%) in antibacterial activity was seen on the treated fabrics. Additional advantages of the treatment include increased wettability and dye absorption (higher shade depth) of the fabrics. To avoid use of chemicals for achieving antifelting treatments, keratin was extracted from feathers using enzymes and was used to treat wool fabrics (Eslahi, 2015). Up to 20% keratin yield was obtained after treating the feathers with 1% savinase for 90 min. Keratin obtained had a molecular weight of 10 kDa. Changes in the activity and dry cell weight with change in ion concentration and pH were observed (Table 10.7) (Eslahi, 2013). Good shrink resistance that was durable to washing was obtained by treating with the keratin. Although the solubility of the fabrics in alkaline media decreased, there was no significant effect on the tensile strength of the fabrics (Eslahi, 2015). Treating with keratin was considered to be a simple, cost-effective and environmentally friendly method to impart shrink resistance to wool fabrics.

Table 10.7: Level of activity of enzymes depending on pH and ions (Eslahi, 2013).

Type of ion	Keratinase activity (%)	pH	Dry cell weight (g/L)
K^+	107.0	5.88	9.4
Na^+	106.5	6.13	8.7
Ca^{2+}	114.8	5.93	9.5
Mg^{2+}	120.5	5.80	7.8
Zn^{2+}	115.6	5.74	8.0
Mn^{2+}	102.2	5.66	8.7
Cu^{2+}	114.0	5.92	8.7
Co^{2+}	66.7	5.85	6.7
Fe^{3+}	40.2	5.74	7.3

Note: Reproduced with permission from Sage Publications.

10.5 Microbial fuel cell

Microbial fuel cells are considered to be one of the most promising technologies for green energy. Chicken feathers were hydrolyzed using *Pseudomonas aeruginosa* strain SDS3, and the effect of various sources on their degradation was studied and the degraded feathers were used as a source for production of electricity using a microbial fuel cell (Figure 10.6). Extent of degradation of the feathers was dependent on the culture conditions and the bacterial strain used. The strain SDS3 was capable of completely degrading 0.1% and 0.5% of feathers in 3 and 5 days, respectively, but at 1% concentration, only 80% of the feathers degraded even after 7 days. Further, the presence of sources such as carbon and nitrogen significantly affected the activity and

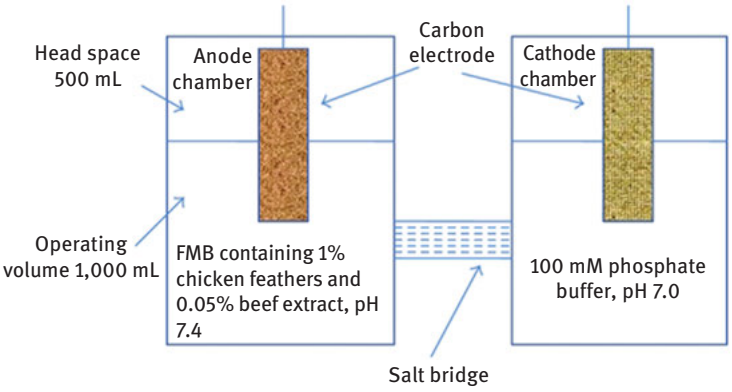

Figure 10.6: Depiction of a microbial fuel cell connected with a salt bridge (Chaturvedi, 2014). Reproduced from Hindawi Publishing Corporation.

production of the enzyme (Chaturvedi, 2014) (Tables 10.8 and 10.9). Unfortunately, addition of either glucose or nitrogen reduced the activity of keratinase. Power density and voltage varied with time and the percentage of feathers used (Figure 10.7). A maximum voltage of 141 mV was obtained after 14 days of incubation and the maximum power density was 1,206.8 mW/m^2 and maximum current density was 8.6 mA/m^2. It was suggested that chicken feathers could be a good substrate for microbial fuel cells to produce electricity (Chaturvedi, 2014).

Table 10.8: Effect of carbon sources on growth, soluble protein and keratinase activity (Chaturvedi, 2014).

Carbon source (0.1% w/v)	Growth (OD 600 nm)	Protein (g/mL)	Keratinase activity (U/mL)
Control	0.282 ± 0.015	139.7 ± 9.7	7.1 ± 0.3
Glycerol	0.249 ± 0.011	102.9 ± 4.9	6.4 ± 0.32
Fructose	0.214 ± 0.007	124.2 ± 4.6	6.8 ± 0.26
Galactose	0.243 ± 0.012	60.2 ± 4.6	5.2 ± 0.25
Sucrose	0.506 ± 0.014	79.4 ± 3.4	6.5 ± 0.3
Glucose	0.164 ± 0.022	68.4 ± 2.6	4.5 ± 0.24
Maltose	0.211 ± 0.013	130.8 ± 7.2	7.5 ± 0.35
Mannitol	0.32 ± 0.019	109.5 ± 7.9	5.5 ± 0.21
Malt extract	0.237 ± 0.018	175.3 ± 9.4*	8.6 ± 0.31*
Lactose	0.319 ± 0.006	128.7 ± 9.1	6.3 ± 0.32
Starch	0.28 ± 0.011	169.7 ± 8.5*	8.0 ± 0.14*

Table 10.9: Effect of nitrogen sources on growth, soluble protein and keratinase activity (Chaturvedi, 2014).

Nitrogen source (0.05% w/v)	Growth (OD 600 nm)	Protein (g/mL)	Keratinase activity (U/mL)
Control	0.304 ± 0.011	142.7 ± 2.3	7.4 ± 0.4
Casein	0.352 ± 0.014	112.3 ± 3.1	7.5 ± 0.3
Yeast extract	0.326 ± 0.012	160.6 ± 4.4	12.5 ± 0.34*
Urea	0.394 ± 0.018	158.9 ± 4.1	12.8 ± 0.4*
Ammonium sulfate	0.202 ± 0.014	87.6 ± 4.0	5.3 ± 0.31
Potassium nitrate	0.271 ± 0.014	65.8 ± 2.6	7.5 ± 0.33

Table 10.9 (continued)

Nitrogen source (0.05% w/v)	Growth (OD 600 nm)	Protein (g/mL)	Keratinase activity (U/mL)
Ammonium chloride	0.294 ± 0.016	63.01 ± 2.9	7.1 ± 0.26
$NH_4H_2PO_4$	0.295 ± 0.0009	112.3 ± 5.8	6.5 ± 0.15
Ammonium nitrate	0.275 ± 0.010	139.9 ± 5.2	6.9 ± 0.31
Sodium nitrite	0.255 ± 0.011	79.4 ± 2.1	5.8 ± 0.21
Sodium nitrate	0.277 ± 0.012	87.6 ± 2.8	6.4 ± 0.24
Skim milk	0.319 ± 0.012	168.2 ± 3.7*	9.6 ± 0.34*
Tryptone	0.459 ± 0.018	187.3 ± 4.2*	13.2 ± 0.36*
Beef extract	0.319 ± 0.007	219.2 ± 7.5*	13.4 ± 0.27*

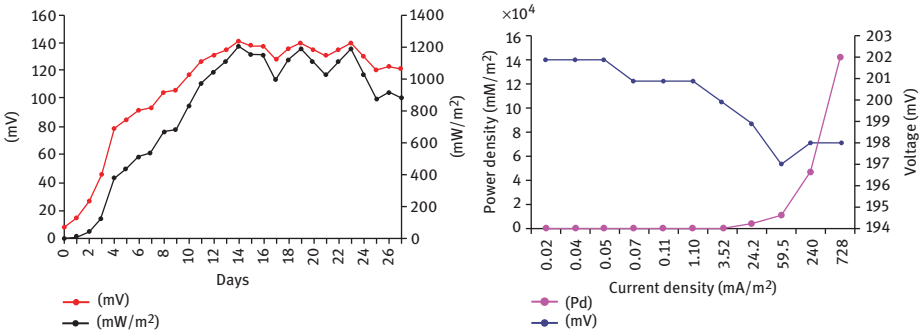

Figure 10.7: Ability of the keratin-based microbial fuel cells to generate current and voltage when the density and time were varied (Chaturvedi, 2014). Reproduced from Hindawi Publishing Corporation.

10.6 Substitutes for nail plates

Treating nail-related diseases is a challenge due to the difficulties in obtaining adequate number of nails for drug penetration and other related studies. Although bovine hoofs have been used as a substitute for human nail plates, there are substantial differences between human and animal nails and the results obtained may not be directly applicable. In a novel study, the potential of developing substitute human nail plates using keratin extracted from human hair was studied (Lusiana, 2011). Blonde hair was used to extract keratin by the Shindai method. In this method, powdered hair was treated with urea, thiourea and mercaptoethanol at 50 °C for 72 h. After treatment, the dissolved solution was filtered and dialyzed

against a MWCO of 6,000–8,000 Da. Solution obtained was poured into teflon rings to form films (110, 120 and 130 μm thickness and about 2 cm inner diameter). Films were further cured at 110 °C for 3 h, which resulted in water-insoluble films. For comparison, bovine hoofs from the sole part were collected and sliced to a thickness of about 100 μm and diameter of 15 mm.

Permeation studies were done in diffusion cells having donor and receiver compartments. The hoof membranes and the keratin films were placed between the donor and receiver compartments, which were filled with marker [sodium fluorescein (SF) with a MW of 376, rhodamine B (RB) with a MW of 443 and fluorescein isothiocyanate–dextran (FD) with a MW of 4,400] solution containing nail penetration enhancers (urea, thioglycolic acid and papain). Diffusion was carried out at 32 °C for various time periods. After the permeation, samples were rinsed in water and the markers extracted using 1 mL aqueous NaOH solution for 3 days. Intensity of the marker in the extracted solution was measured using calibration curves. The permeability coefficient of SF, RB and FD 4 was (5, 18 and 0.6) × 10^{-7} cm/s for the hoof and 5.9, 32 and 0.4 for the keratin film. Permeation coefficients of the hoofs and the films were identical to each other and the permeated amounts were also similar. As can be expected, the thicker keratin films provide lower permeation. However, films having a thickness of 120 μm had accumulated nearly 60% higher RB than the hoof. Treating with permeation enhancers increased accumulation of the markers significantly (Lusiana, 2011). Based on the results obtained, it was suggested that the keratin films were ideal substitutes to study the penetration in nail plates but caution should be expressed when using permeation enhancers to prevent over estimation (Lusiana, 2011).

In an unique approach, dielectric measurements of the nail plate have been used to detect diabetes (Jablecka, 2009). Nails from the middle fingers of diabetic and nondiabetic patients were collected in two 4-week intervals. These nails were washed with dilute sodium chloride solution to remove fat and covered with silver paste to act as electrodes. Dielectric properties (relative permittivity and dielectric loss) were measured using an LCR bridge at frequencies between 100 Hz and 100 kHz (Jablecka, 2009) and temperatures between 22 and 200 °C. It was observed that the relative permittivity at the same temperature and frequency was lower in the nails from the diabetic patients compared to healthy patients. This difference was suggested to be due to the damage to the hydrogen bonds and polar side chains of keratin in the diabetic nails. Dielectric measurements were considered to be a useful noninvasive procedure and good indicators for diabetics (Jablecka, 2009).

10.7 Keratin as fertilizer

Wool keratin containing about 90% protein was hydrolyzed using 0.15 M KOH and 0.05 M NaOH at 120 °C for 20 min for potential use as fertilizer. The hydrolysate was added (0.17–1 g of hydrolysate per 100 g of soil) into soil for cultivation of rye grass.

The grass was grown for up to 9 months under controlled conditions. Growth curves showed that rye grass growth was highest for soil with the higher level of hydrolysate. Three times increase in carbon content and nearly double the level of nitrogen were detected in the soil containing 1% hydrolysate compared to the control. It was concluded that addition of the hydrolysate enhances the development of microflora in the soil (Gousterova, 2003).

Chicken feather hydrolysate and feather keratin compost were used to treat leaves and also used as fertilizer to improve plant growth (Kucinska, 2014). The hydrolysate was sprayed onto leaves and the compost was used with the soil. Influence of the hydrolysate and the compost on chlorophyll content and metabolic activity was studied using tomato, cucumber, cabbage and maize plants. Considerable increase in fresh weight was observed for those plants treated with the compost but the hydrolysate did not increase the plant biomass. Among the different plants studied, only cucumber showed increase in leaf chlorophyll after treating with the feather compost. It was concluded that use of the hydrolysate or the compost resulted in increased enzymatic activity in the plants and that feather was suitable to be used as fertilizer (Kucinska, 2014).

10.8 Scaffolds for tissue engineering

Keratin extracted from chicken feathers were combined with alginate and made into porous scaffolds for potential tissue engineering scaffolds (Gupta, 2016). Scaffolds had a porosity of 96% with pore size between 10 and 200 μm and tensile strength of 0.33 MPa and elongation of 23%. When *E. coli* and *B. subtilis* were incubated on the scaffolds, zone of inhibitions of 2 and 2.2 cm, respectively, were observed. When incubated in PBS at 37 °C, the scaffolds lost 66% of their weight but the porous morphology was maintained. Although no cell culture and cytocompatibility studies were conducted, it was concluded that the blend scaffolds were suitable for tissue engineering (Gupta, 2016).

10.9 Devices and electronic applications

Novel transient resistive switches for use in memory devices were developed using human hair keratin (Lin, 2019). Hair fibers were washed with a surfactant (0.5% w/w %) and later treated with 0.5 M thioglycolic acid at pH 11 for 15 h to reduce the feathers. Later, dialysis was done using low molecular filtration membrane of 5,000 Da. Powder keratin formed was lyophilized and dried. Solubilized keratin was spun coated onto a fluorine-doped tin oxide (FTO)/glass substrate at 2,000 rpm for 30 s and later heated on a baking plate at 60 °C for 30 min. Silver electrodes were deposited on the keratin films and vacuum evaporated to form the Ag/keratin/FTO memory

devices (Lin, 2019) as shown schematically in Figure 10.8. Thickness of the keratin film in the device was about 180 nm compared to 100 nm for the Ag electrode. Assembled device was highly transparent with transmittance values between 85% and 90%. Films also had a smooth surface with roughness of 1.96 nm and root mean square roughness of 2.47 nm (Lin, 2019). The device fabricated was called a resistive switching random access memory device, which is supposed to have transient characteristics and resistance to water. Such devices are also supposed to be able to have writeable and erasable memory at specific voltages. Cyclic resistance voltage and clockwise hysteretic switching from low resistance to high resistance was also possible (Figure 10.9).

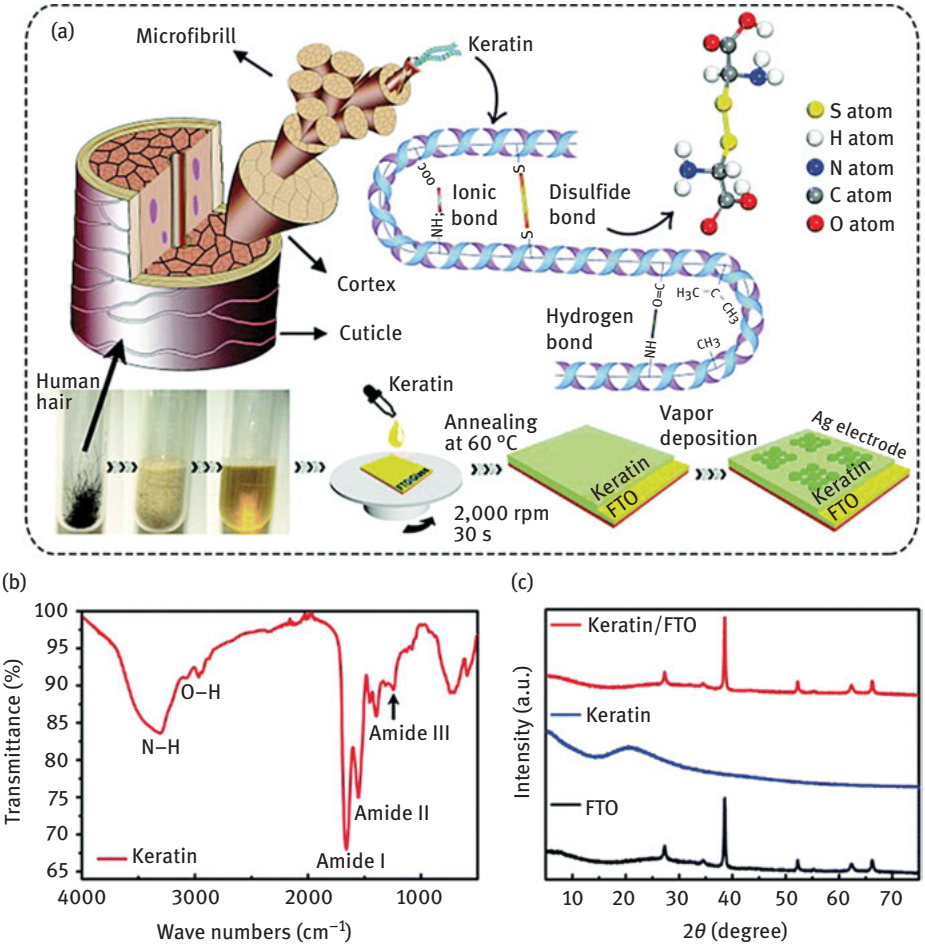

Figure 10.8: Schematic representation of the process used to prepare the transient switches (a) and FTIR spectra (b) and XRD diffraction patterns (c) of keratin, FTO and their blends (Lin, 2019). Reproduced with permission from Royal Society of Chemistry.

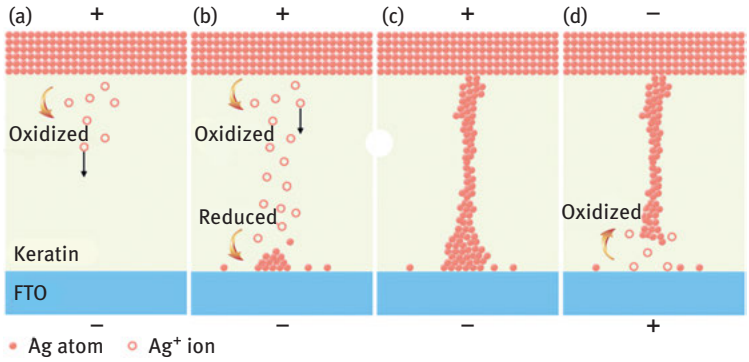

Figure 10.9: Proposed mechanism of switching through oxidation and reduction by the keratin/FTO blend films (Lin, 2019). Reproduced with permission from Royal Society of Chemistry.

A resistance ratio larger than 10^3 OFF/ON function and retention time of 10^4 s was obtained for nonvolatile memory applications. The device was also found to have good durability after testing for 80 continuous voltage exposures (Lin, 2019). The devices could be dissolved in water within 30 min making them biodegradable and environmentally friendly. Similar resistive switching devices were developed using human hair keratin with Ag/keratin/indium tin oxide (ITO) structure. ITO-coated Si/SiO_2 substrate was spin coated with aqueous keratin. Coated substrate was then used to thermally deposit Ag electrodes with an area of about 1 mm^2 (Guo, 2019). Fabricated device had excellent switching and ON/OFF function resistance for as many as 150 consecutive cycles, and the retention time was up to 3,000 s (Figure 10.10). The switching performance of the device could be tailored to the desired level by doping with Ag/graphite nanoparticles. Based on the characteristics, the device was suggested to be useful for biomaterial-based nonvolatile memory devices.

Keratin films could act as humidity sensors when made into electrodes having interdigitated and rectangular spiral shape. Keratin in wool was extracted by alkaline hydrolysis and the solution obtained was drop casted onto films. Two types of electrodes were developed: one having six fingers and surface area of 100 mm^2 and the other a rectangular spiral (Figure 10.11) having surface area of 180 mm^2. Keratin solution was poured onto the pattern and dried to form the sensors (Hamouche, 2018). Although the main amide structures of keratin were maintained, a decrease in crystallinity had occurred. Films deposited had a contact angle of 53°, suggesting that the surface was hydrophilic. Capacitance of the sensor increased with increasing humidity. Sensitivity of the spiral sensor was higher than that of the interdigitated sensor (Figure 10.12). Compared to other capacitive humidity sensors, a considerably low hysteresis of 3.5% was obtained even at 72% relative humidity (RH) when measured at 100 Hz. The electrodes also had considerably quick response time between 30 and 36 s, and recovery time was between 51 and 55 s suggesting the suitability for humidity sensing. A

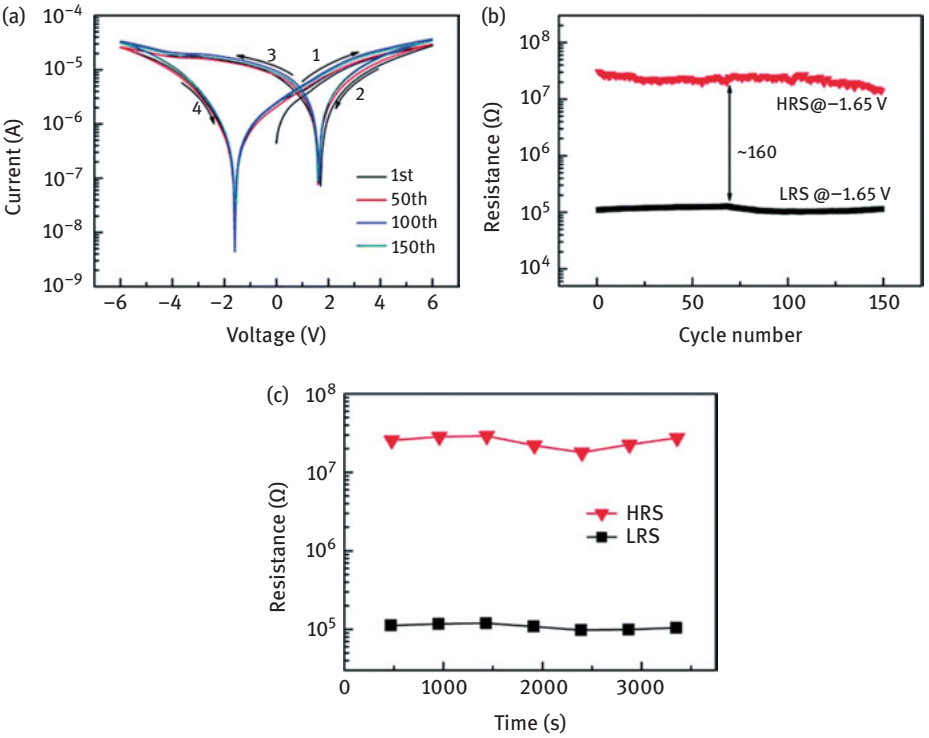

Figure 10.10: Performance of the keratin-based resistance switching device at high and low resistance switching (Guo, 2019) (a) Typical I–V curves with different laps under single logarithmic coordinates. (b) Distribution of the HRS and LRS over 150 consecutive cycles. (c) Retention characteristics of both resistance states. Reproduced with permission through Open License Publishing.

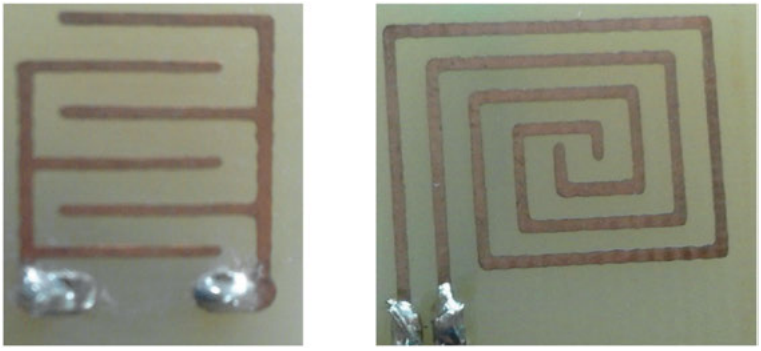

Figure 10.11: The interdigitized and spiral electrodes used to prepare the keratin-based humidity sensors (Hamouche, 2018). Reproduced with permission from Elsevier.

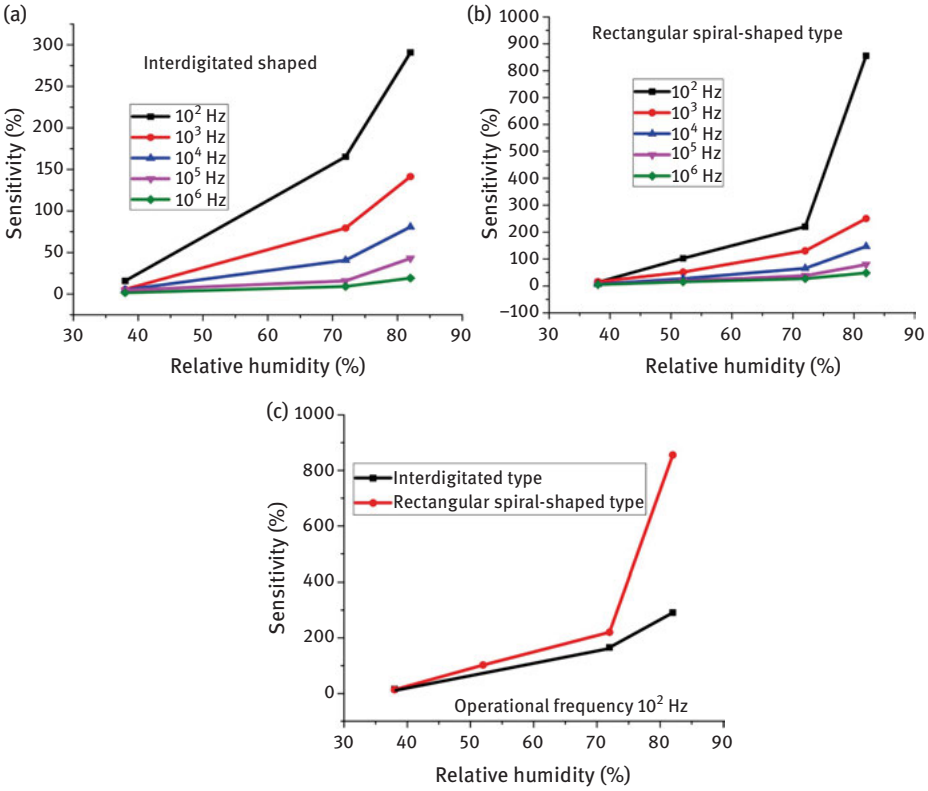

Figure 10.12: Sensitivity of the keratin-based humidity sensors operated at two different frequencies (Hamouche, 2018). (a) Interdigitated type; (b) Rectangular spiral-shaped type at 100 Hz; (c) The comparison of the sensitivity between Interdigitated type. Reproduced with permission from Elsevier.

bendable and free-standing electrode system was developed using keratin for detection of humidity (Figure 10.13) (Natali, 2019). Wool keratin solutions were spin coated onto glass/ITO substrates and later dried at room temperature. Coated films were placed between ITO and gold electrodes and treated with glutaraldehyde to make keratin insoluble. In addition, free standing keratin sensors were prepared by spin coating keratin/glutaraldehyde and glycerol solution onto glass/ITO substrates through gold electrode sublimation process at a pressure of 10^{-6} mbar and growth rate of 0.1 nm/s. In addition, the keratin sensors were treated with melanin extracted from yak fibers to improve ion conductivity or interlaced with Pd-based protodes to enhance proton extraction/injection and transport characteristics. All types of keratin-based sensors developed showed excellent sensitivity to low hysteresis (Figure 10.14). Ability of the keratin sensors to bend and be insoluble in water makes them suitable for external and even as implantable biosensors for humidity or other sensing (Natali, 2019).

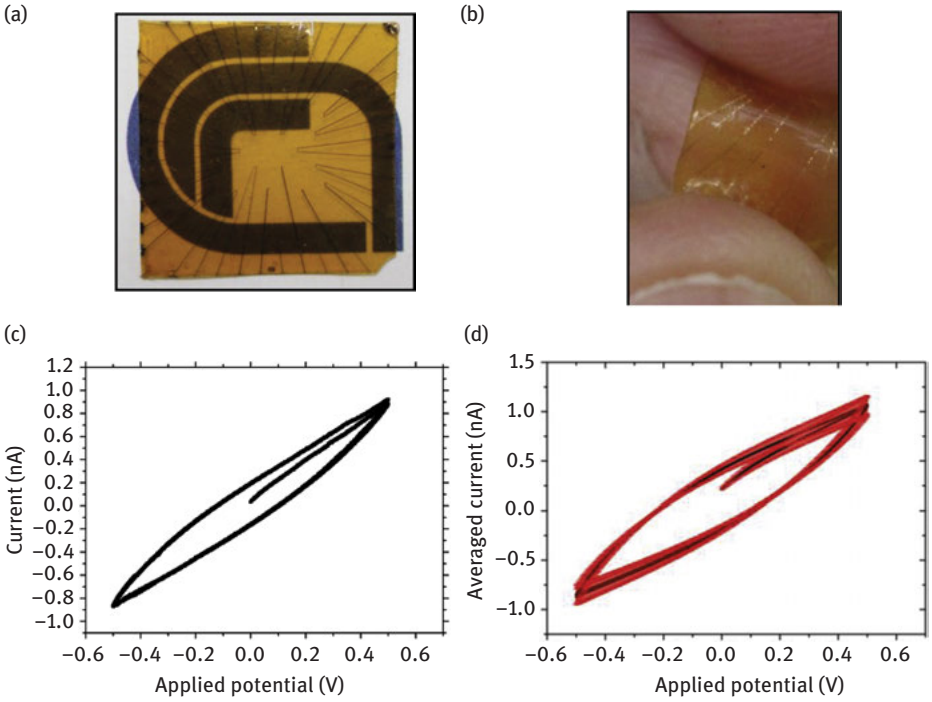

Figure 10.13: Digital image of a free-standing insoluble keratin-based microelectrode (a); ability of the biosensor to bend (b); multiple cycle cyclic voltammetry at 60% RH from keratin electrode (c) and from the developed three different keratin-based sensor systems (d) (Natali, 2019). Reproduced with permission from Elsevier.

10.10 Electronic skin

Electronic skin or e-skin was developed using keratin and thermoplastic polyurethane (TPU) with coefficient of friction (0.26) equivalent to that of leg skin and surface roughness (RA of 0.047) equivalent to that of cheek skin and positive triboelectric properties (Li, 2018). To obtain such a unique material, keratin was extracted from human hair and later melt blended with TPU and made into films of 0.5 mm thickness. A single-electrode triboelectric nanogenerator (STENG) was fabricated using films containing 10% keratin and TPU. Considerable extent of hydrogen bonding was observed between keratin and TPU leading to increased thermal stability and flexibility (Figure 10.15). The keratin–TPU-based STENG was able to differentiate (Figure 10.16) between various tactile sensations required for biological sensing applications (Li, 2018).

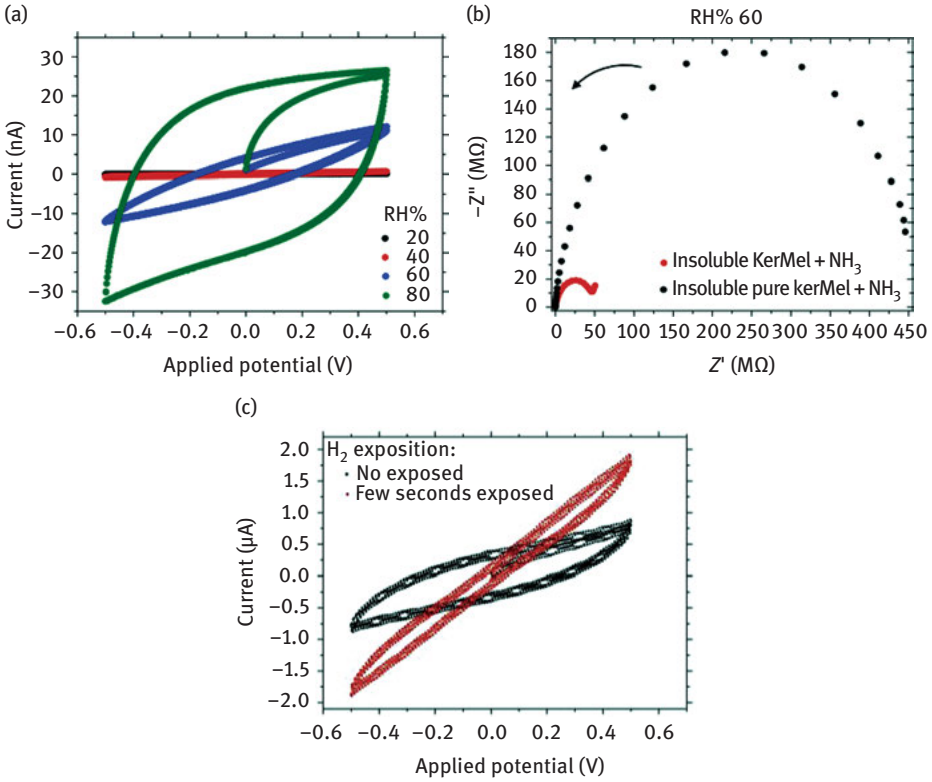

Figure 10.14: Performance of keratin humidity sensor at different pH (a), Nyquist plot of pure keratin compared to melanin-treated keratin biosensor (b) and cyclic voltammetry of soluble keratin at constant RH, Pd electrodes compared to PdHx protodes (c) (Natali, 2019). Reproduced with permission from Elsevier.

10.11 Detection of chemicals, metals and bioentities

A composite (film) made of keratin extracted from wool was combined with PVA, potassium iodide and silver nanoparticles for detection of chlorine (Taleb, 2020) based on the difference in absorbance. Extent of absorbance was dependent on the concentration of chlorine and iodine in the solution. Films containing silver nanoparticles showed substantial inhibition against *E. coli* and *S. aureus*. It was suggested that quantitative detection of chlorine in water could be done using treated films having of specific color (Figure 10.17) (Taleb, 2020).

Keratin was used as a substrate to prepare silver nanocrystals to develop a pluorometric probe for detection of mercury (Zhou 2019). To prepare the nanocrystals, $AgNO_3$ was injected into keratin solution for 5 min and later NaOH solution was added followed by $NaBH_4$ solution. Nanoclusters were formed within 30 min and were filtered

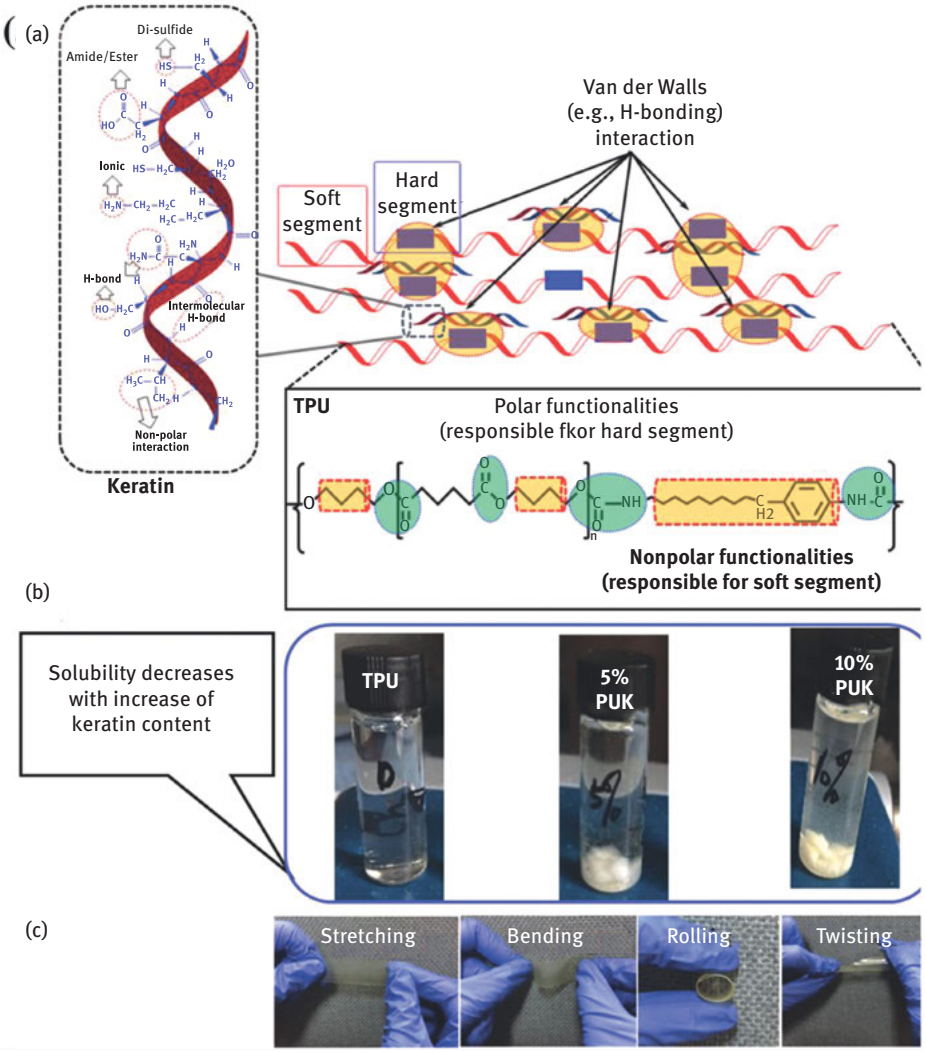

Figure 10.15: Schematic representation of bonding between keratin and TPU (a); images of TPU–keratin solutions with increasing keratin content (b) and ability of the blend films to be deformed (c) (Li, 2018). Reproduced with permission from Elsevier.

and collected. Presence of cysteine-rich keratin and easier purification were considered essential for development of the detector. The AgNCs showed fluorescent behavior dependent on the amount of keratin and amount of NaOH and $NaBH_4$ added. Average size of AgNCs was 2.5 nm and yield was about 1.7% obtained within a synthesis time of less than 1 h. The particles had an emission peak at 705 nm at an excitation wavelength of 400 nm. Close interaction was detected between Hg^{2+} and AgNCs, which enabled a wide detection range of 13.7 nM to 10 μm even at a low detection limit of

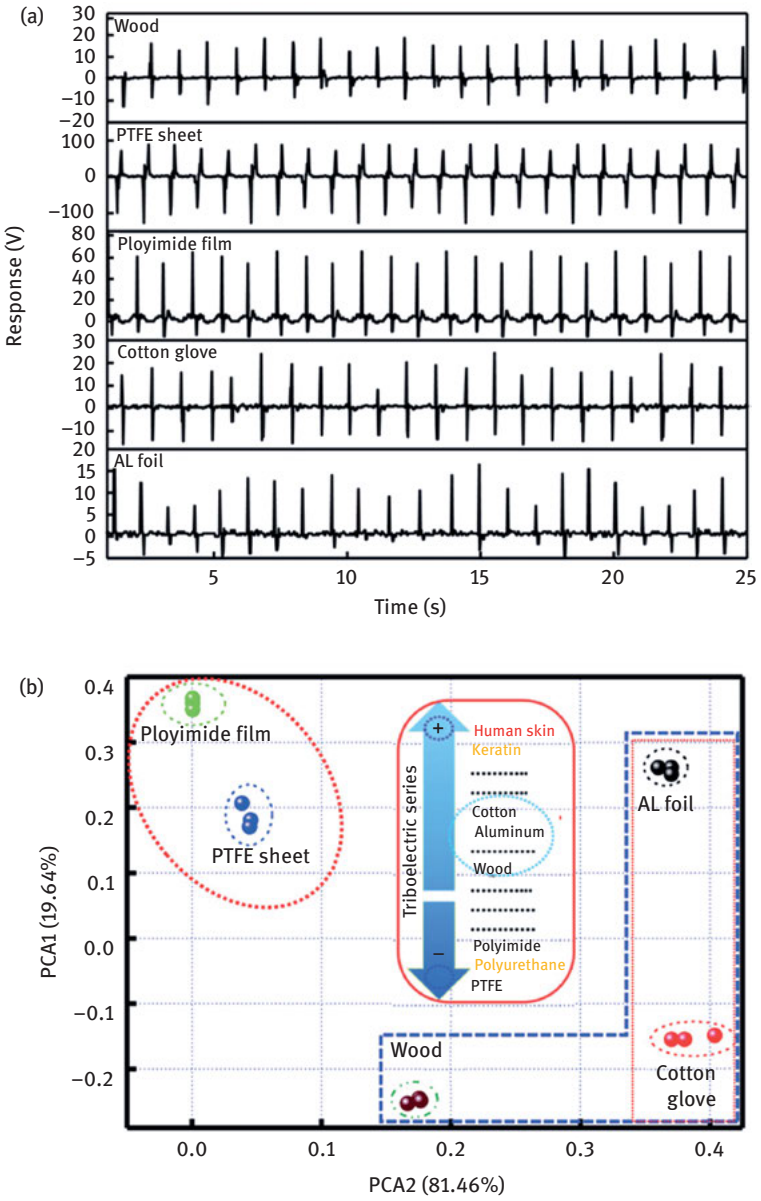

Figure 10.16: Comparison of the ability of TPU–keratin e-skin to respond to various stimuli (Li, 2018). (a) Triboelectric responses of STENG toward different objects; (b) Principal component analysis (PCA) plot. Reproduced with permission from Elsevier.

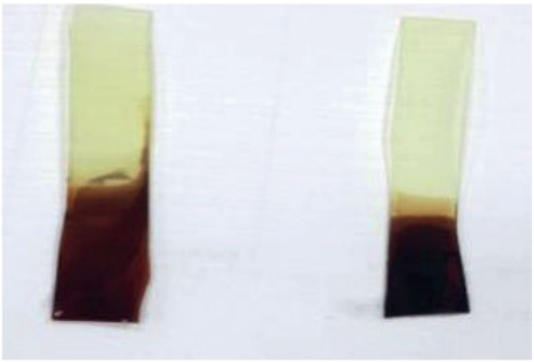

Figure 10.17: Images of keratin-based films treated with PVA, KI and silver nanoparticles exhibit different colors when immersed in varying concentrations of chlorine in water (Taleb, 2020). Reproduced with permission from Elsevier.

6.5 nM. The particles retained their fluorescence for up to 3 months (Figure 10.18). To further increase the properties of gold templated keratin particles for detection of mercury, addition of silver was considered (Wang, 2018). Various concentrations of $HAuCl_4$ were added into the keratin solution and stirred vigorously for 2 min at 37 °C. NaOH was added into the solution and the mixture was stirred at 37 °C for 12 h to form the AuNCs containing keratin (about 2.2–2.6 nm in diameter). Similarly, the AuNCs–Ag–keratin clusters were prepared by adding the gold–keratin solution into $AgNO_3$ solution and incubating the mixture at room temperature for 6 h. Keratin-based gold nanoclusters had fluorescent emission at 705 nm and quantum yields of 6.5%. Addition of Ag^+ ions substantially increased the emissions, as high as five times that of the gold keratin nanoclusters (Figure 10.19). The silver-containing nanoclusters had stable fluorescent emission even after 3 months but fluorescence was highest at pH 4. It was proposed that the silver ions could interact with gold and also with the disulfide bonds in keratin. Interaction between gold and silver would decrease surface defects and improve brightness, whereas silver–keratin interactions improved stability and dispersibility (Wang, 2018). Au–Ag–keratin particles had a wide range of detection (2.44–2,500 nM) and low detection limit (2.3 nM) and highly selective detection of Hg^{2+} in both lab and practical tests. Further, combining Cu^{2+} to the gold-capped keratin nanocrystals (AgNCs) enables selective detection of glucose (Ma, 2019). Inclusion of Cu^{2+} ions increased the catalytic activity and stability of the gold nanoclusters and also imparted a yellow color to the solution. The ability of the AuNC–Cu–keratin particles to change color was used to develop a colorimetric system for detection of glucose. A detection range of 1.56–800 μM with a limit of detection of 0.61 μM for glucose detection was observed. Up to 94.6–96.7% detection of glucose in serum was possible using the keratin-based system (Ma, 2019).

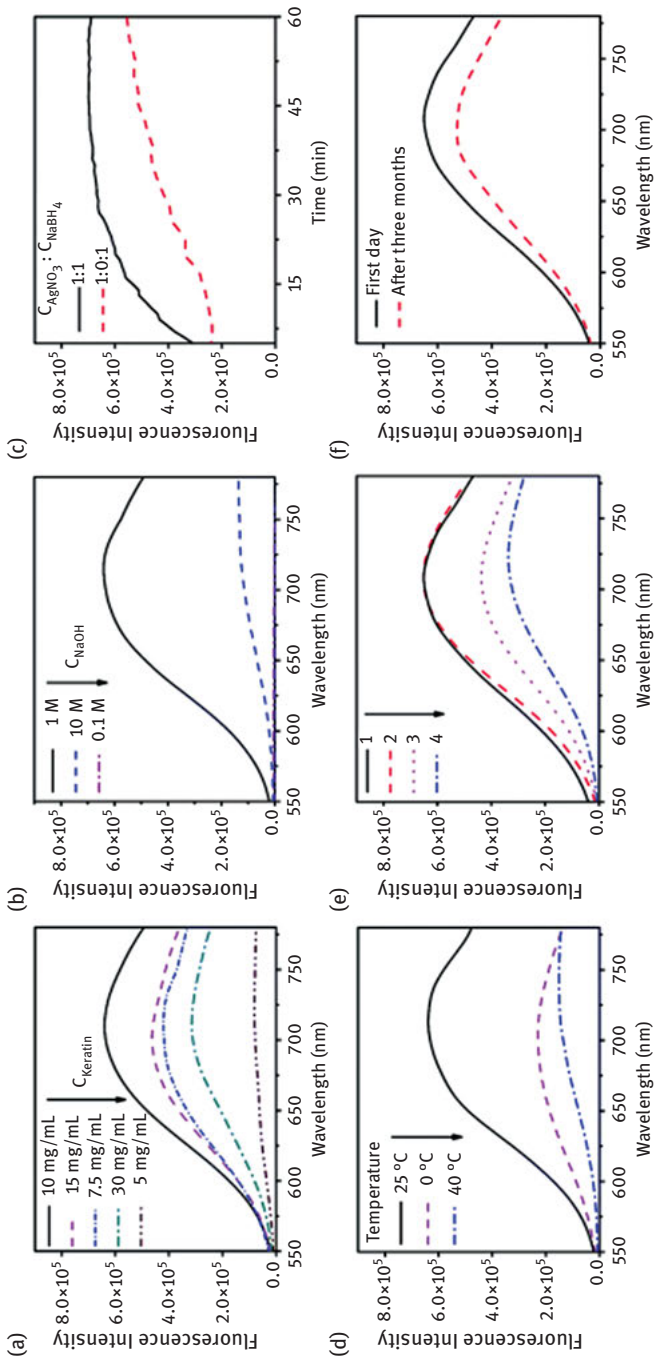

Figure 10.18: Effect of various preparation conditions on the fluorescence intensity of silver nanocrystals prepared using keratin as template (Zhou, 2019). AgNCs prepared with different concentrations of (a) keratin, (b) NaOH, and (c) NaBH4 and (d) prepared at different temperatures. (e) Fluorescence emission spectra of AgNCs prepared using different termination reaction methods. Line 1: freshly prepared AgNCs, line 2: AgNCs purified by SEC, line 3: AgNCs neutralized with BR buffer (pH = 6), and line 4: AgNCs without any termination operation after 3 h. (f) The time stability of AgNCs (1 mg mL−1, 4 °C). Reproduced with permission from Royal Society of Chemistry.

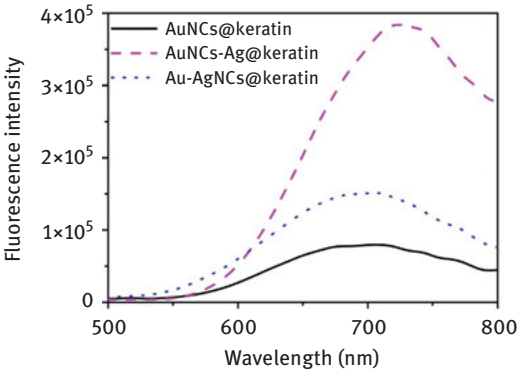

Figure 10.19: Fluorescence intensity of keratin-based silver and gold nanoparticles (Wang, 2018). Reproduced with permission from Elsevier.

With the intent to develop films for bioimaging, biosensors and catalysis, feather keratin was combined with egg white containing luminescent Au particles (Xing, 2016). Keratin extracted using urea, sodium sulfite and SDS was dialyzed against 8–10 kDa membrane and the protein was concentrated to 200 mg/mL. Au nanoparticles (clusters) containing egg white was added to the keratin solution, and the mixture was cast into films. Addition of Au particles imparted luminescent properties and the films appeared red under visible light (Figure 10.20). The Au particles not only affected the appearance but also caused considerable changes in the α-helix and β-sheet content. Increase in β-sheet and decrease in α-helices were observed as the amount of Au particles was increased. Similarly, the extent of luminescence could also be controlled by limiting the amount of egg white-Au particles added (Xing, 2016).

Luminescent gold particles were also prepared using goose feathers. In a simple process, goose feathers were soaked in aqueous solution of $HAuCl_4$ under vigorous stirring at 80 °C for 10 min. NaOH solution was added into the solution and heated at 45 min at 80 °C. The treated feathers were subject to Tris(2-carboxyethyl)-phosphone (TCEP) and cysteamine-induced chemical etching. Gold-coated feathers were also immersed in TCEP solution for 1 h and incubated with various concentrations of Cd^{2+} to impart desired properties (Shu, 2018). Bright luminescence of different colors was exhibited by the feathers after treatment. Feathers from different sources showed luminescence to specific colors (Figure 10.21). Maximum luminescence was observed at 513 nm, and the intensity of luminescence was found to increase with increase in Cd^{2+} concentration. These luminescent feathers were suggested to be suitable for use in bioimaging, optoelectronics, light-emitting diodes and others.

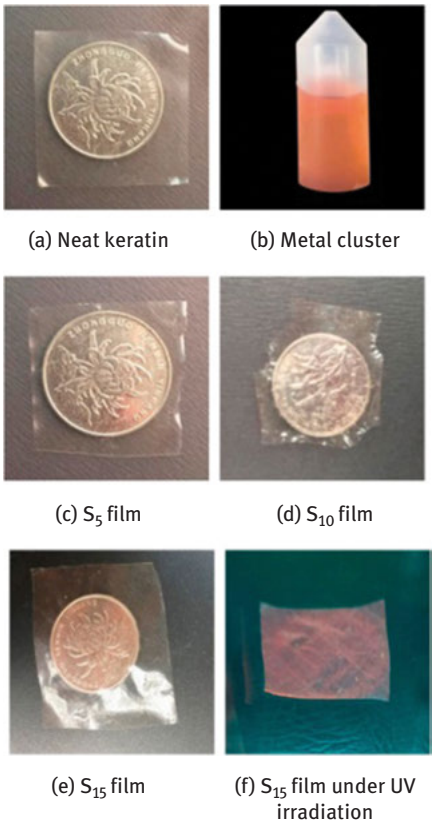

(a) Neat keratin (b) Metal cluster

(c) S_5 film (d) S_{10} film

(e) S_{15} film (f) S_{15} film under UV irradiation

Figure 10.20: Images of films made from pure keratin (a), dispersion of Au particles in alginate solution (b) and with blends of gold particles containing alginate 5% (c), 10% (d) and 15% (e) films and 15% films under UV irradiation (f) (Xing, 2016).

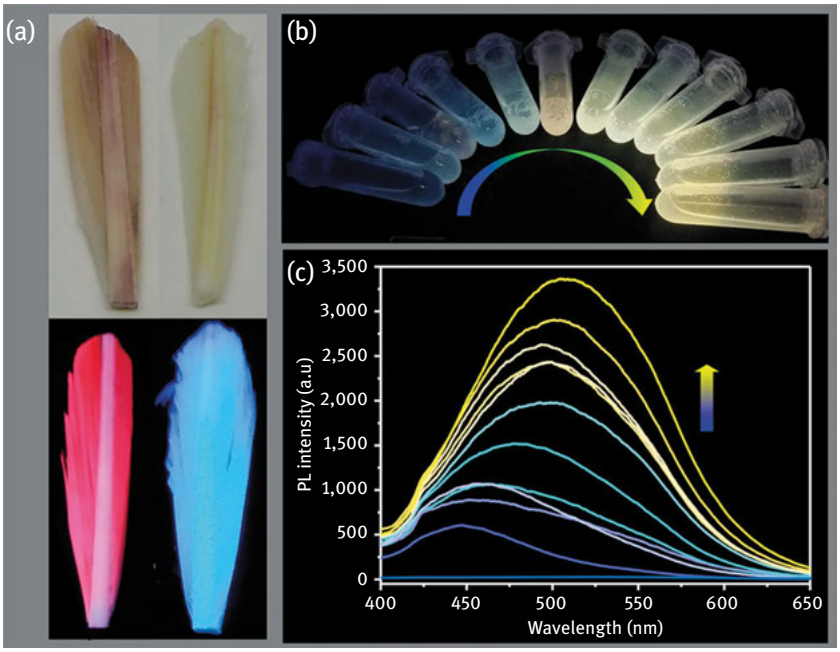

Figure 10.21: Digital picture of gold-treated feathers before (left) and after (right) etching with TCEP under visible (top) and UV light (bottom) (a); images (b) and luminescent spectra (c) of TCEP-etched solutions containing different amounts of Cd^{2+} (Shu, 2018). Reproduced with permission from American Chemical Society.

References

Aboushwareb, T., Eberli, D., Ward, C., Broda, C., Holcomb, J., Atala, A. and Dyke, M.V. 2009. A keratin biomaterial gel hemostat derived from human hair: Evaluation in a rabbit model of lethal liver injury, Journal of Biomedical Materials Research Part B Applied Biomaterials, 90B: 45–54.

Adler, S. A., Rasa, S., Kaisu, H. and Anne-Kristin, L. 2018. In vitro pepsin digestibility and amino acid composition in soluble and residual fractions of hydrolyzed chicken feathers, Poultry Science, 97(9): 3343–3357.

Agarwal, V., Arpana, G. P., Sushma, I. and Kaushik, C. 2019. Comparative study of keratin extraction from human hair, International Journal of Biological macromolecules, 133: 382–390.

Aguayo-Villarreal, I.A., Bonilla-Petriciolet, A., Hernandez-Montoya, V., Montes-Moran, M.A. and Reynel-Avila, H.E. 2011. Batch and column studies of Zn2+ removal from aqueous solution using chicken feathers as sorbents, Chemical Engineering Journal, 167: 67–76.

Akhlaghi, S., Sharif, A., Kalaee, M., Nouri, A. and Manafi, M. 2012. Morphology, nanomechanical and thermodynamic surface characteristics of nylon6/feather keratin blend films: An atomic force microscopy investigation, Polymer International, 61: 646–656.

Al-Asheh, S. and Fawzi, B. 2003. Beneficial reuse of chicken feathers in removal of heavy metals from wastewater, Journal of Cleaner Production, 11(3): 321–326.

Albite-Ortega, J., Sánchez-Valdes, S., Ramirez-Vargas, E., Nuñez-Figueredo, Y., Ramos deValle, L.F., Martínez-Colunga, J. G. and Graciano-Verdugo, A. Z. 2019. Influence of keratin and DNA coating on fire retardant magnesium hydroxide dispersion and flammability characteristics of PE/EVA blends, Polymer Degradation and Stability, 165: 1–11.

Aluigi, A., Rombaldoni, F., Tonetti, C. and Jannoke., L. 2014. Study of Methylene Blue adsorption on keratin nanofibrous membranes, Journal of Hazardous Materials, 268: 156–165.

Aluigi, A., Sotgiu, G., Torreggiani, A., Zamboni, R., Guerrini, A., Varchi, G. and Orlandi., V. T. 2016. Raman spectroscopic characterisation of photo-active keratin doped with Methylene Blue for wound dressings and tissue engineering, Biomedical Spectroscopy and Imaging, 5(2): 207–215.

Aluigi, A., Tonetti, C., Rombaldoni, F., Puglia, D., Fortunati, E., Armentano, L., Santulli, C., Torre, L. and Kenny, J.M. 2014. Keratins extracted from Merino wool and Brown Alpaca fibers as potential fillers for PLLA-based composites, Journal of Materials Science, 49: 6257–6269.

Aluigi, A., Tonetti, C., Vineis, C., Tonin, C. and Mazzuchetti., G. 2011. Adsorption of copper (II) ions by keratin/PA6 blend nanofibres, European Polymer Journal, 47(9): 1756–1764.

Aluigi, A., Vineis, C., Varesano, A., Mazzuchetti, G., Ferrero, F. and Tonin, C. 2008. Structure and properties of keratin/PEO blend nanofibers, European Polymer Journal, 44: 2465–2475.

Aluigi, A., Zoccola, M., Vineis, C., Tonin, C., Ferrero, F. and Canetti, M. 2007. Study on the structure and properties of wool keratin regenerated from formic acid, International Journal of Biological Macromolecules, 41: 266–273.

Ayutthaya, S.I., Tanpichal, S. and Wootthikannokkhan, J. 2015. Keratin extracted from chicken feather waste: Extraction, preparation and structural characterization of the keratin and keratin/biopolymer films and electrospuns, Journal of Polymers and the Environment, 23: 506–516.

Ayutthaya, S. I. N., Supachok, T., Weradesh, S. and Jatuphorn, W. 2016. Effect of clay content on morphology and processability of electrospun keratin/poly (lactic acid) nanofiber, International Journal of Biological Macromolecules, 85: 585–595.

Azarniya, A., Elnaz, T., Niloofar, E. and Abdolreza, S. 2019. Modification of bacterial cellulose/keratin nanofibrous mats by a tragacanth gum-conjugated hydrogel for wound healing, International Journal of Biological Macromolecules, 134: 280–289.

https://doi.org/10.1515/9781501511769-011

Bach, E., Lopes, F.C. and Brandelli, A. 2015. Biodegradation of α and β keratins by gram negative bacteria, International Biodeterioration and Biodegradation, 104: 136–141.

Balaji, S., Kumar, R., Sripriya, R., Kakkar, P., Ramesh, D.V., Reddy, P.N.K. and Sehgal, P.K. 2012. Preparation and comparative characterization of keratin-chitosan and keratin-gelatin composite scaffolds for tissue engineering applications, Materials Science and Engineering C, 32: 975–982.

Barone, J.R. and Schmidt, W.F. 2005c. Polyethylene reinforced with keratin fibers obtained from chicken feathers, Composites Science and Technology, 65: 173–181.

Barone, J.R., Schmidt, W.F. and Liebner, C.F.E. 2005a. Compounding and molding of polyethylene composites reinforced with keratin feather fiber, Composite Science and Technology, 65: 683–692.

Barone, J.R., Schmidt, W.F. and Liebner, C.F.E. 2005b. Thermally processed keratin films, Journal of Applied Polymer Science, 97: 1644–1651.

Berstch, A. and Coello, N. 2005. A biotechnological process for treatment and recycling poultry feathers as feed ingredient, Bioresource Technology, 96: 1703–1708.

Bertini, F., Canetti, M., Patrucco, A. and Zoccola, M. 2013. Wool keratin polypropylene composites: Properties and thermal degradation, Polymer Degradation and Stability, 98: 980–987.

Bhari, R., Manpreet, K. and Ram, S. S. 2019. Thermostable and halotolerant keratinase from *Bacillus aerius* NSMk2 with remarkable dehairing and laundry applications, Journal of Basic Microbiology, 59(6): 555–568.

Bhavsar, P., Marina, Z., Alessia, P., Alessio, M., Giorgio, R. and Claudio, T. 2017. Comparative study on the effects of superheated water and high temperature alkaline hydrolysis on wool keratin, Textile Research Journal, 87(14): 1696–1705.

Bose, A., Pathan, S., Pathak, K. and Keharia, H. 2014. Keratinolytic protease production by *Bacillus amyloliquefaciens* 6B using feather meal as substrate and application of feather hydrolysate as organic nitrogen input for agricultural soil, Waste Biomass Valorization, 5: 595–605.

Bragulla, H.H. and Homberger, D.G. 2009. Structure and functions of keratin proteins in simple, stratified, keratinized and cornified epithelia, Journal of Anatomy, 214: 516–559.

Bryson, W. G., Duane, P. H., Jonathan, P. C., James, A. V., Richard, J. W., Joy, L. W., Shinobu, N., Takashi, I. and Kenzo, K. 2009. Cortical cell types and intermediate filament arrangements correlate with fiber curvature in Japanese human hair, Journal of Structural Biology, 166(1): 46–58.

Cai, C., Lou, B. and Zheng, X. 2008. Keratinase production and keratin degradation by a mutant strain of Bacillus subtilis, Journal of Zheijang University Science B, 9(1): 60–67.

Caldwell, J. P., David, N. M., Joy, L. W. and Warren, G. B. 2005. The three-dimensional arrangement of intermediate filaments in Romney wool cortical cells, Journal of Structural Biology, 151(3): 298–305.

Călin, M., Diana, C., Elvira, A., Iuliana, R., Mihaela, B. D., Melania-Liliana, A., Florin, O., Luiza, J. and Veronica, L. 2017. Degradation of keratin substrates by keratinolytic fungi, Electronic Journal of Biotechnology, 28: 101–112.

Canetti, M., Adriana, C. and Fabio, B. 2013. Structural characterization and thermal behaviour of wool keratin hydrolizates-polypropylene composites, Journal of Polymer Research, 20(7): 181–193.

Canetti, M., Cacciamani, A. and Bertini, F. 2013. Structural characterization and thermal behaviour of wool keratin hydrolizates-polypropylene composites, Journal of Polymer Research, 20: 181–192.

Cao, Y., Yiqian, Y., Ying, L., Xuexia, Y., Zhangjun, C. and Guang, Y. 2019. Tunable keratin hydrogel based on disulfide shuffling strategy for drug delivery and tissue engineering, Journal of Colloid and Interface Science, 544: 121–129.

Cao, Z.J., Lu, D., Luo, L.S., Deng, Y.X., Bian, Y.G., Zhang, X.Q. and Zhou, M.H. 2011. Composition analysis and application of degradation products of whole feathers through a large scale of fermentation, Environmental Science and Pollution Research International, 19(7): 2690–2696.

Cardamone, J.M. 2010. Investigating the microstructure of keratin extracted from wool:peptide sequence (MALDI-TOF/TOF) and protein conformation (FTIR), Journal of Molecular Structure, 969: 97–105.

Cavello, I.A., Cavalitto, S.F. and Hours, R.A. 2012. Biodegradation of a keratin waste and the concomitant production of detergent stable serine proteases from Paecilomyceslilacinus, Applied Biochemistry and Biotechnology, 167: 945–958.

Cavello, I.A., Chesini, M., Hours, R.A. and Cavalitto, S.F. 2013. Study of the production of alkaline keratinases in submerged cultures as an alternative for solid waste treatment generated in leather technology, Journal of Microbial Biotechnology, 23(7): 1004–1014.

Chaturvedi, V. and Verma, P. 2014. Metabolism of chicken feathers and concomitant electricity generation by Pseudomonos aeruginosa by employing microbial fuel cells (MFC), Journal of Waste Management. http://dx.doi.org/10.1155/2014/928618.

Chen, B., Yao, X., Weidong, Y. and Hongling, L. 2018a. Wool keratin and silk sericin composite films reinforced by molecular network reconstruction, Journal of Materials Science, 53(7): 5418–5428.

Chen, J., Ding, S., Ji, Y., Ding, J., Yang, X., Zou, M. and Li, Z. 2015. Microwave enhanced hydrolysis of poultry feather to produce amino acid, Chemical Engineering and Processing, 87: 104–109.

Chen, X., Shufang, W., Minghao, Y., Jianfang, G., Guoqiang, Y. and Xinming, L. 2018b. Preparation and physicochemical properties of blend films of feather keratin and poly(vinyl alcohol) compatibilized by tris(hydroxymethyl)aminomethane, Polymers, 10(10): 1054–1062.

Cheng, S., Lau, K., Liu, T., Zhao, Y., Lam, P. and Yin, Y. 2009. Mechanical and thermal properties of chicken feather fiber/PLA green composites, Composites Part B, 40: 650–654.

Choi, J., Panthi, G., Liu, Y., Kim, J., Chae, S, Lee, C., Park, M. and Kim, H. 2015. Keratin/poly(vinyl alcohol) blended nanofibers with high optical transmittance, Polymer, 58: 146–152.

Cocean, I., Alexandru, C., Cristina, P., Valentin, P., Nicanor, C., Georgiana, B., Felicia, I. and Silviu, G. 2019. Alpha keratin amino acids BEHVIOR under high FLUENCE laser interaction, Medical applications. Applied Surface Science, 488: 418–426.

Conzatti, L., Giunco, F., Stagnaro, P., Patrucco, A., Marano, C., Rink, M. and Marsano, E. 2013. Composites based on polypropylene and short wool fibers, Composites Part A, 47: 165–171.

Coulombe, P.A. and Omary, M.B. 2002. Hard and soft principles defining the structure, function and regulation of keratin intermediate filaments, Current Opinion in Cell Biology, 14: 110–122.

Coward-Kelly, G., Agbogbo, F.K. and Holtzapple, M.T. 2006b. Lime treatment of keratinous materials for the generation of highly digestible animal feed: 2. Animal hair, Bioresource, Technology, 97: 1344–1352.

Coward-Kelly, G., Chang, V.S., Agbogbo, F.K. and Holtzapple, M.T. 2006a. Lime treatment of keratinous materials for the generation of highly digestible animal feed: 1. Chicken feathers, Bioresource Technology, 97: 1337–1343.

Cui, L., Gong, J., Fan, X., Wang, P., Wang, Q. and Qiu, Y. 2013. Transglutaminase-modified wool keratin films and its potential application in tissue engineering, Engineering in Life Sciences, 13(2): 149–155.

Deb-Choudhury, S., Jeffrey, E. P., Kelsey, R., Erin, L., Chikako, K., Stefan, C., Jolon, M. D. and Duane, P. H 2015. Mapping the accessibility of the disulfide crosslink network in the wool fiber cortex, Proteins: Structure, Function, and Bioinformatics, 83(2): 224–234.

Deivasigamani, B. and Alagappan, K.M. 2008. Industrial application of keratinase and soluble proteins from feather keratins, Journal of Environmental Biology, 29(6): 933–936.

Deniz, D.Y., Kahraman, M.V. and Kuruca, S.E. 2015. UV-reactive electrospinning of keratin/4-vinyl benzene boronic acid hydroxyapatite/poly(vinyl alcohol) composite nanofibers, Polymer Composites, 38(7): 1371–1377.

Dias, G.J., Mahoney, P., Swain, M., Kelly, R.J., Smith, R.A. and Ali, M.A. 2010. Keratin-hydroxyapatite composites: Biocompatibility, osseointegration, and physical properties in an ovine model, Journal of Biomedical Materials Research Part A, 95A: 1084–1095.

Dou, Y., Huang, X., Zhang, B., He, M., Yin, G. and Cui, Y. 2015. Preparation and characterization of a dialdehyde starch crosslinked feather keratin film for food packaging application, RSC Advances, 5: 27168–27177.

Duer, M.J., McDongal., N. and Murray, R.C. 2003. A solid state NMR study of the structure and molecular mobility of α-keratin, Physical Chemistry and Chemical Physics, 5: 2894–2899.

Ebrahimgol, F., Tavanai, H., Alihosseini, F. and Khayamian, T. 2014. Electrosprayed recovered wool keratin nanoparticles, Polymers Advanced Technologies, 25: 1001–1007.

Eslahi, N., Moshggoo, S., Azar, S.K., Dadashian, F. and Nejad, N.H. 2015. Application of extracted feather protein to improve the shrink resistance of wool fabrics, Journal of Industrial Textiles, 44(6): 835–548.

Esparza, Y., Aman, U., Yaman, B. and Jianping, W. 2017. Preparation and characterization of thermally crosslinked poly (vinyl alcohol)/feather keratin nanofiber scaffolds, Materials & Design, 133: 1–9.

Fabra, M. J., Pablo, P., Marta, M., Amparo, L. and Lagarón, J. M. 2016. Combining polyhydroxyalkanoates with nanokeratin to develop novel biopackaging structures, Journal of Applied Polymer Science, 133(2): 42695–42704.

Falco, F. C., Roall, E., Birte, S., Krist, V. G. and Anna, E. L 2019. An integrated strategy for the effective production of bristle protein hydrolysate by the keratinolytic filamentous bacterium Amycolatopsis keratiniphila D2, Waste Management, 89: 94–102.

Fan, J., Tong-Da, L., Jia, L., Pei-Yu, Z., Yong-Heng, W., Fu-Yuan, C. and Yong, L. 2016. High protein content keratin/poly (ethylene oxide) nanofibers crosslinked in oxygen atmosphere and its cell culture, Materials & Design, 104: 60–67.

Fan, J. and Yi, W. 2012. High yield preparation of keratin powder from wool fiber, Fibers and Polymers, 13(8): 1044–1049.

Fernández-d'Arlas, B. 2019. Tough and functional cross-linked Bioplastics from Sheep Wool Keratin.", Scientific Reports, 9(1): 1–12.

Feughelman, M. 2002. Natural protein fibers, Journal of Applied Polymer Science, 83(3): 489–507.

Fitz-Binder, C., Tung, P. and Thomas, B. 2019. A second life for low-grade wool through formation of all β-keratin composites in cystine reducing calcium chloride–water–ethanol solution, Journal of Chemical Technology & Biotechnology, 94(10): 3384–3392.

Forgacs, G., Lundin, M., Taherzadeh, M.J. and Horvath, I.S. 2013. Pretreatment of chicken feather waste for improved biogas production, Applied Biochemistry and Biotechnology, 169: 2016–2028.

Fortunati, E., Aluigi, A., Armentano, L., Morena, F., Emiliani, C., Martino, S., Santulli, C., Torre, L., Kenny, J.M. and Puglia, D. 2015. Keratins extracted from Merino wool and Brown Alpaca Fibers: Thermal, mechanical and biological properties of PLLA based biocomposites, Materials Science and Engineering C, 47: 394–406.

Fortunato, G. M., Francesco, D. R., Samuele, B., Aurora, De., A., Francesco, B., Anna, L. and Chiara, M. 2019. Electrospun structures made of a hydrolyzed keratin-based biomaterial for development of in vitro tissue models, Frontiers in Bioengineering and Biotechnology, 7: 174–180.

Galaburri, G., María, L. P., Juan, M. L., Roberto, F. L., María, I. A., María, E. V. and Guillermo, J. C. 2019. pH and ion-selective swelling behaviour of keratin and keratose 3D hydrogels, European Polymer Journal, 118: 1–9.

Gao, J., Lei, Z., Yusheng, W., Tianyan, C., Xianyan, J., Kai, Y., Jiahong, Y., Bin, T., Xiaochun, S. and Jiabo, H. 2019. Human hair keratins promote the regeneration of peripheral nerves in a rat sciatic nerve crush model, Journal of Materials Science: Materials in Medicine, 30(7): 82–88.

Gao, P., Kanzhu, L., Zhenhong, L., Baojiang, L., Chunyan, M., Gang, X. and Meihua, Z 2014. Feather Keratin deposits as biosorbent for the removal of Methylene Blue from aqueous solution: Equilibrium, kinetics, and thermodynamics studies, Water, Air, & Soil Pollution, 225(5): 1946–1959.

Gao, P., Li, K., Liu, Z., Liu, B., Ma, C., Xue, G. and Zhou, M. 2014a. Feather keratin deposits as biosorbent for the removal of methylene blue from aqueous solution: Equilibrium, kinetics and thermodynamics studies, Water Air Soil Pollution, 225: 1946–1955.

Gao, P., Liu, Z., Wu, X., Cao, Z., Zhuang, Y., Sun, W., Xue, G. and Zhou, M. 2014b. Biosorption of chromium (VI) ions by deposits produced from chicken feathers after soluble keratin extraction, CLEAN soil, Air and Water, 42(11): 1558–1566.

Ghaffari, R., Niloofar, E., Elnaz, T. and Abdolreza, S. 2018. Dual-sensitive hydrogel nanoparticles based on conjugated thermoresponsive copolymers and protein filaments for triggerable drug delivery, ACS Applied Materials & Interfaces, 10(23): 19336–19346.

Ghosh, A., Clerens, S., Deb-choudhury, S. and Dyer, J.M. 2014. Thermal effects of ionic liquid dissolution, on the structures and properties of regenerated wool keratin, Polymer Degradation and Stability, 108: 108–115.

Ghosh, M., Prajapati, B.P., Kango, N. and Dey, K.K. 2019. A comprehensive and comparative study of the internal structure and dynamics of natural β– keratin and regeneratedβ– keratin by solid state NMR spectroscopy, Solid State Nuclear Magnetic Resonance, 101: 1–11.

Gong, H., Huitong, Z., Jiqing, W., Shaobin, L., Yuzhu, L. and Jonathan, G.H.H. 2019. Characterisation of an Ovine Keratin Associated Protein (KAP) Gene, Which Would Produce a Protein Rich in Glycine and Tyrosine, but Lacking in Cysteine, Genes, 10(11): 848–856.

Gousterova, A., Nustorova, M., Goshev, I., Christov, P., Braikova, D., Tishinov, K., Haertle, T. and Nedkov, P. 2003. Alkaline hydrolysate of waste sheep wool aimed as fertilizer, Biotechnology and Biotechnological Equipment, 17(2): 140–145.

Grazziotin, A., Pimentel, F.A, de Jong, E.V. and Brandelli, A 2006. Nutritional improvement of feather protein by treatment with microbial keratinase, Animal Feed Science and Technology, 126: 135–144.

Grazziotin, A., Pimentel, F.A., Sangali, S., Jong, E.V. and Brandelli, A. 2007. Production of feather protein hydrolysate by keratinolytic bacterium Vibrio sp. Kr 2, Bioresource Technology, 98: 3172–3175.

Grkovic, M., Stojanovic, D.B., Kojovic, A., Strnad, S., Kreze, T., Aleksic, R. and Uskokovic, P.S. 2015. Keratin polyethylene oxide bio-nanocomposites reinforced with ultrasonically functionalized graphene, RSC Advances, 5: 91280–91289.

Guo, B., Bai, S., Wentao, H., Yuanzheng, C., Shouhui, Z., Suangsuo, M., Liang, Z., Ming, L., Bing, L. and Guoqiang, F. 2019. A sustainable resistive switching memory device based on organic keratin extracted from hair, RSC Advances, 9(22): 12436–12440.

Guo, J., Pan, S., Yin, X., He, Y., Li, T. and Wang, R. 2015. pH sensitive keratin based polymer hydrogel and its controllable drug release behavior, Journal of Applied Polymer Science, 132: 41572–41579.

Gupta, P. and Nayak, K.K. 2016. Optimization of keratin/alginate scaffold using RSM and its characterization for tissue engineering, International Journal of Biological Macromolecules, 85: 141–149.

Gupta., R. and Ramnani, P. 2006. Microbial keratinases and their prospective applications: an overview, Applied Microbial Biotechnology, 70: 21–33.

Guzman, R.C., Merrill, M.R., Richter, J.R., Hamzi, R.I., Greengauz-Roberts, O.K. and Dyke, M.E.V. 2011. Mechanical and biological properties of keratose biomaterials, Biomaterials, 32: 8205–8207.

Hamasaki, S., Tachibana, A., Tada, D, Yamauchi, K. and Tanabe, T. 2008. Fabrication of highly porous keratin sponges by freeze drying in the presence of calcium alginate beads, Materials Science and Engineering C, 28: 1250–1254.

Hamouche, H. S., Makhlouf, A. C. and Laghrouche., M. 2018. Humidity sensor based on keratin bio polymer film, Sensors and Actuators A: Physical, 282: 132–141.

Harland, D.P., Jonathan, P., Caldwell, J. L.W., Richard, J. W. and Warren, G. B. 2011. Arrangement of trichokeratin intermediate filaments and matrix in the cortex of Merino wool, Journal of Structural Biology, 173(1): 29–37.

Harland, D.P., Veronika, N., Marina, R., Sailakshmi, V., Mihnea, B. and John, M. A. 2019. Helical twist direction in the macrofibrils of keratin fibres is left handed, Journal of Structural Biology, 206(3): 345–348.

He, M., Buning, Z., Yao, D., Guoqiang, Y. and Yingde, C. 2017. Blend modification of feather keratin-based films using sodium alginate, Journal of Applied Polymer Science, 134(15): 44680–44689.

He, Y., Qing, Q., Tiantian, L., Yuhua, G., Zongkun, H., Jia, D., Yingqian, X., Bochu, W. and Shilei, H. 2019. Human hair keratin hydrogels alleviate rebleeding after intracerebral hemorrhage in a rat model, ACS Biomaterials Science & Engineering, 5(2): 1113–1122.

Hémonnot, C.Y.J., Reinhardt, J., Saldanha, O., Patommel, J., Rita, G., Britta, W., Manfred, B., Christian, G. S. and Sarah, K. 2016. X-rays reveal the internal structure of keratin bundles in whole cells, ACS Nano, 10(3): 3553–3561.

Hill, P.S., Apel, P.J., Barnwell, J., Smith, T., Koman, L.A., Atala, A. and Dyke, M.V. 2011. Repair of peripheral nerve defects in rabbits using keratin hydrogel scaffolds, Tissue Engineering, 11(12): 1499–1507.

Hirata, Y., Yuasa, R., Takahashi, R., Takigami, M. and Takigami, S. 2013. Preparation and characterization of soluble wool keratin for human hair care, Transaction of Materials Research Society Japan, 38(2): 195–198.

Hmidet, N., Ali, N.E.H., Zouari-Fakhfakh, N., Haddar, A., Nasri, M. and Sellemi-Kamoun, A. 2010. Chicken feathers: A complex substrate for the production of α-amylase and proteases by B. licheniformis NH1, Journal of Industrial and Microbial Biotechnology, 37: 983–990.

Huang, W., Alireza, Z., Wen, Y., David, K., Robert, O. R., Horacio, E. and Joanna, M. 2019. How Water Can Affect Keratin: Hydration-Driven Recovery of Bighorn Sheep (Ovis Canadensis) Horns, Advanced Functional Materials, 29(27): 1901077–1901086.

Huda, S. and Yang, Y. 2008. Composites from ground chicken quill and polypropylene, Composites Science and Technology, 68: 790–798.

Huda, S. and Yang, Y. 2009. Feather fiber reinforced light weight composites with good acoustic properties, Journal of Polymer Environment, 17: 131–142.

Inácio, F., Alessandro, F. M., Alex, G. C., Tatiane, B., Rosane, M.P., Cristina, G. and Souza, M. 2018a. Biodegradation of human keratin by protease from the basidiomycete Pleurotus pulmonarius, International Biodeterioration & Biodegradation, 127: 124–129.

Inácio, F., Alessandro, F. M., Alex, G. C., Tatiane, B., Rosane, M. P. and Cristina, G. M. 2018b. Biodegradation of human keratin by protease from the basidiomycete, Pleurotus pulmonarius. International Biodeterioration & Biodegradation, 127: 124–129.

Iqbal, H.M.N., Kyazze, G., Locke, I.C., Tron, T. and Keshavarz, T. 2015. In situ development of self-defensive antibacterial biomaterials:phenol-g-keratin-EC based biocomposites with characteristics for biomedical applications, Green Chemistry, 17: 3858–3869.

Jablecka, A., Olszewski, J. and Marzec, E. 2009. Dielectric properties of keratin water system in diabetic and heatly human fingernails, Journal of Non-crystalline Solids, 233: 2436–2480.
James, V. 2011. The molecular architecture for the intermediate filaments of hard α-keratin based on the superlattice data obtained from a study of mammals using synchrotron fibre diffraction, Biochemistry Research International. doi: 10.1155/2011/198325.
Ji, Y., Chen, J., Lv, J., Li, Z., Xing, L. and Ding, S. 2014. Extraction of keratin with ionic liquids from poultry feathers, Separation Science and Technology, 132: 577–583.
Jimenez-Cervantes, E., Velasco-Santos, C., Martinez-Hernandez, A.L., Rivera-Armenta, J.L., Mendoza-Martinez, A.M. and Castano, V.M. 2015. Composites from chicken feathers quill and recycled polypropylene, Journal of Composite Materials, 49(3): 275–283.
Jung, D. and Debes, B. 2018. Keratinous fiber based intumescent flame retardant with controllable functional compound loading, ACS Sustainable Chemistry & Engineering, 6(10): 13177–13184.
Kadir, M., Xinwei, W., Bowen, Z., Jing, L., Duane, H. and Crisan, P. 2017. The structure of the "amorphous" matrix of keratins, Journal of Structural Biology, 198(2): 116–123.
Kakkar, P. and Madhan, B. 2016. Fabrication of keratin-silica hydrogel for biomedical applications, Materials Science and Engineering: C, 66: 178–184.
Kakkar, P., Madhan, B. and Shanmugam, G. 2014. Extraction and characterization of keratin from bovine hoof: A potential material for biomedical applications, Springer Plus, 3: 596–607.
Kammiovirta, K., Anna-Stiina, J., Lauri, K., Ulla, H., Arja, P., Anna, S. and Hannes, O. 2016. Keratin-reinforced cellulose filaments from ionic liquid solutions, RSC Advances, 6(91): 88797–88806.
Kannahi, M. and Ancy, R.J. 2012. Keratin degradation and enzyme producing ability of Aspergillus Flavus and Fusarium Solani from soil, Journal of Chemical and Pharmaceutical Research, 4(6): 3245–3248.
Kar, P. and Misra, M. 2004. Use of keratin fiber for separation of heavy metals from water, Journal of Chemical Technology & Biotechnology: International Research in Process, Environmental & Clean Technology, 79(11): 1313–1319.
Karthikeyan, R., Balaji, S. and Sehgal, P.K. 2007. Industrial applications of keratins-A review, Journal of Scientific and Industrial Research, 66: 710–715.
Katoh, K., Shibayama, M., Tanabe, T. and Yamauchi, K. 2004a. Preparation and physiochemical properties of compression molded keratin films, Biomaterials, 25: 2265–2272.
Katoh, K., Tanabe, T. and Yamauchi, K. 2004b. Novel approach to fabricate keratin sponge scaffolds with controlled pore size and porosity, Biomaterials, 25: 4255–4262.
Kavitha, A., Boopalan, K., Radhakrishnan, G., Sankaran, S., Das, B.N. and Sastry, T.P. 2005. Preparation of feather keratin hydrolysate-gelatin composites and their graft copolymers, Journal of Macromolecular Science Part A Pure and Applied Chemistry, 42(12): 1703–1713.
Khairunisa, S. N., Amir, M., Gupta, A., Saufi, S. M., Chik, T. and Kausar, A. 2014. Development of Anti-Ageing Cream from Chicken Feathers. Research Journal of Pharmaceutical, Biological and Chemical Sciences, 5(6): 389–393.
Khosa, M.A. and Aman, U. 2014. In-situ modification, regeneration, and application of keratin biopolymer for arsenic removal, Journal of Hazardous Materials, 278: 360–371.
Kucinska, J.K., Magnucka, E.G., Oksinska, M.P. and Pietr, S.J. 2014. Bioefficacy of hen feather keratin hydrolysate and compost on vegetable plant growth, Compost Science and Utilization, 22: 179–187.
Kurimoto, A., Tanabe, T., Tachibana, A. and Yamauchi, K. 2003. Keratin sponge: Immobilization of lysozyme, Journal of Bioscience and Bioengineering, 96(3): 307.
Latshaw, J.D., Musharaf, N. and Retrum, R. 1994. Processing of feather meal to maximize its nutritional value for poultry, Animal Feed Science and Technology, 47: 179–188.

Lee, H., Hwang, Y., Lee, H., Choi, S., Kim, Y., Moon, J., Kim, J., Kim, K.C., Han, D., Park, H. and Bae, H. 2015. Human hair keratin based biofilm for potent application to periodontal tissue regeneration, Macromolecular Research, 23(3): 300–308.

Li, B., Jinbo, Y., Jiarong, N., Jianyong, L., Le, W., Mao, F. and Yanli, S. 2018a. Effects of Graphene Oxide on the Structure and Properties of Regenerated Wool Keratin Films, Polymers, 10(12): 1318–1326.

Li, H., Tridib, K., Sinha, J. L., Jeong, S.O., Youngjoon, A. and Jin, K. K. 2018b. Melt-Compounded Keratin-TPU Self-Assembled Composite Film as Bioinspired e-Skin, Advanced Materials Interfaces, 5(19): 1800635–1800644.

Li, J., Liu, X., Zhang, J., Zhang, Y., Han, Y., Hu, J. and Li, Y. 2012. Synthesis and characterization of wool keratin/hydroxyapatite nanocomposite, Journal of Biomedical Materials Research Part B: Applied Biomaterials, 100B: 896–902.

Li, J., Yi, L., Xuan, L., Jing, Z. and Yu, Z. 2013. Strategy to introduce an hydroxyapatite–keratin nanocomposite into a fibrous membrane for bone tissue engineering, Journal of Materials Chemistry B, 1(4): 432–437.

Li, Q., Lijun, Z., Ruigang, L., Da, H., Xin, J., Ning, C., Zhuang, L, Xiaozhong, Q., Hongliang, K. and Yong, H. 2012. Biological stimuli responsive drug carriers based on keratin for triggerable drug delivery, Journal of Materials Chemistry, 22(37): 19964–19973.

Li, R. and Wang, D. 2013. Preparation of regenerated wool keratin films from wool keratin-ionic liquid solutions, Journal of Applied Polymer Science, 127: 2648–2653.

Liebeck, B., Natalia, H., Georg, Roth., Crisan, P. and Alexander, B. 2017. Synthesis and characterization of methyl cellulose/keratin hydrolysate composite membranes, Polymers, 9(3): 91.

Lin, C., Yi-Kai, C., Min, L., Kuo-Long, L. and Jiashing, Y. 2018. Photo-Crosslinked Keratin/Chitosan Membranes as Potential Wound Dressing Materials, Polymers, 10(9): 987–994.

Lin, Q., Shilei, H., Wei, H., Ming, W., Zhigang, Z., Linna, Z., Juan, D. and Xiaosheng, T. 2019. Human hair keratin for physically transient resistive switching memory devices, Journal of Materials Chemistry C, 7(11): 3315–3321.

Liu, P., Qiong, W., Yanmei, L., Pengfei, L., Jiang, Y., Xianwei, M. and Yinghong, X. 2019. DOX-Conjugated Keratin Nanoparticles for pH-Sensitive Drug Delivery, Colloids and Surfaces B: Biointerfaces, 181(1): 1012–1018.

Liu, R., Liang, L., Shuping, L., Shujing, L., Xueying, Z., Mengmeng, Y. and Xilin, L. 2018. Structure and properties of wool keratin/poly (vinyl alcohol) blended fiber, Advances in Polymer Technology, 37(8): 2756–2762.

Liu, S., Kaibing, H., Han, Y. and Fenxia, W. 2018. Bioplastic based on 1, 8-octanediol-plasticized feather keratin: A material for food packaging and biomedical applications, Journal of Applied Polymer Science, 135(30): 46516–46528.

Liu, X., Yi, N., Xianglei, M., Zhenlei, Z., Xiangping, Z. and Suojiang, Z. 2017. DBN-based ionic liquids with high capability for the dissolution of wool keratin, RSC Advances, 7(4): 1981–1988.

Liu, Y., Li, J., Fan, J. and Wang, M. 2014. Preparation and characterization of electrospun human hair keratin/poly(ethylene oxide) composite nanofibers, Revista Materia, 19(4): 382–388.

Liu, Y., Yin, R. and Yu, W. 2010. Preparation and characterization of keratin-$k_2Ti_6O_{13}$ whisker composite film, African Journal of Biotechnology, 9(20): 2884–2890.

Liu, Y., Yu, X., Li, J., Fan, J., Wang, M., Lei, T., Liu, J. and Huang, D. 2015. Fabrication and properties of high content keratin/poly(ethylene oxide blend nanofibers using two step crosslinking process), Journal of Nanomaterials. http://dx.doi.org/10.1155/2015/803937.

Lopez, F.C., Silva, L.A.D., Tichota, D.M., Daroit, D.J., Velho, R.V., Pereira, J.Q., Correa, A.P.F. and Brandelli, A. 2011. Production of proteolytic enzymes by a keratin degrading, Aspergillus niger, Enzyme Research. doi:10.4061/2011/487093.

Luo, T., Shilei, H., Xiaoliang, C., Ju, W., Qian, Y., Yazhou, W., Yulan, W., Huimin, W., Jin, Z. and Bochu, W. 2016. Development and assessment of kerateine nanoparticles for use as a hemostatic agent, Materials Science and Engineering: C, 63: 352–358.

Lusiana, S.R. and Christel, C.M. 2011. Keratin film made of human hair as a nail plate model for studying drug permeation, European Journal of Pharmaceutics and Biopharmaceutics, 78: 432–440.

Ma, B., Qisong, S., Jing, Y., Jakpa, W., Xiuliang, H. and Yiqi, Y. 2017. Degradation and regeneration of feather keratin in NMMO solution, Environmental Science and Pollution Research, 24(21): 17711–17718.

Ma, B., Xue, Q., Xiuliang, H. and Yiqi, Y. 2016. Pure keratin membrane and fibers from chicken feather, International Journal of Biological Macromolecules, 89: 614–621.

Ma, S., Jinjie, W., Guang, Y., Jingxia, Y., Derun, D. and Min, Z. 2019. Copper (II) ions enhance the peroxidase-like activity and stability of keratin-capped gold nanoclusters for the colorimetric detection of glucose, Microchimica Acta, 186(5): 271–282.

Manivasagan, P., Sivakumar, K., Gnanam, S., Venkatesan, J. and Kim, S. 2014. Production, biochemical characterization and detergents application of keratinase from the marine actinobacterium Actinoalloteichus Sp. MA-32, Journal of Surfactants and Detergents, 17: 669–682.

Martelli, S.M. and Laurindo, J.B. 2012. Chicken feather keratin films plasticized with polyethylene glycol, International Journal of Polymeric Materials, 61: 17–29.

Martelli, S.M., Moore, G.R.P. and Laurindo, J.B. 2006. Mechanical properties, water vapor permeability and water affinity of feather keratin films plasticized with sorbitol, Journal of Polymers and the Environment, 14: 215–222.

Martinez-Hernandez, A.L., Velasco-Santos, C., Icaza, M. and Castano, V.M. 2005. Mechanical properties evaluation of new composites with protein biofibers reinforcing poly(methyl methacrylate), Polymer, 46: 8233–8238.

McKittrick, J., Chen, P.Y., Bodde, S.G., Yang, W., Novitskaya, E.E. and Meyers, M.A. 2012. The structure, functions and mechanical properties of keratin, Journal of Materials, 64(4): 449–469.

Mi, X., Helan, X. and Yiqi, Y. 2019. Submicron amino acid particles reinforced 100% keratin biomedical films with enhanced wet properties via interfacial strengthening, Colloids and Surfaces B: Biointerfaces, 177: 33–40.

Mittal, A. 2006. Adsorption kinetics of removal of a toxic dye, Malachite Green, from wastewater by using hen feathers, Journal of Hazardous Materials, 133(1-3): 196–202.

Mokrejs, P., Svoboda, P., Hrncirik, J., Janacova, D. and Vasek, V. 2010. Processing poultry feathers into keratin hydrolysate through alkaline-enzymatic hydrolysis, Waste Management and Research, 29(3): 260–267.

Moll, R., Divo, M. and Langbein, L. 2008. The human keratins: biology and pathology, Histochemical Cell Biology, 129: 705–733.

Moore, G.R.P., Martelli, S.M., Gandolfo, C., Sobral, P.J.D.A. and Laurindo, J.B. 2006. Influence of the glycerol concentration on some physical properties of feather keratin films, Food Hydrocolloids, 20: 975–982.

Mori, H. and Masayuki, H. 2018. Transparent biocompatible wool keratin film prepared by mechanical compression of porous keratin hydrogel, Materials Science and Engineering: C, 91: 19–25.

Naik, R., Wen, G., Ms, D., Hureau, S., Uedono, A., Wang, X., Liu, X., Cookson, P.G. and Smith, S.V. 2010. Metal ion binding properties of novel wool powders, Journal of Applied Polymer Science, 115(3): 1642–1650.

Nakata, R., Osumi, Y., Miyagawa, S., Tachibana, A. and Tanabe, T. 2015. Preparation of keratin and chemically modified keratin hydrogels and their evaluation as cell substrate with drug releasing ability, Journal of Bioscience and Bioengineering, 120(1): 111–116.

Natali, M, Campana, A., Posati, T., Benvenuti, E., Prescimone, F., Sanchez Ramirez, D. O. and Varesano, A. 2019. Engineering of keratin functionality for the realization of bendable all-biopolymeric micro-electrode array as humidity sensor, Biosensors and Bioelectronics, 141(15): 111480–111492.

Navarro, J., Jay, S., Max, L., Marco, S. and John, P. F. 2019. Development of keratin-based membranes for potential use in skin repair, Acta Biomaterialia, 83: 177–188.

Nduka, J. K., Linus, O. E. and Emmanuel, T. E. 2008. Comparison of the mopping ability of chemically modified and unmodified biological wastes on crude oil and its lower fractions.", Bioresource Technology, 99(16): 7902–7905.

Nuutinen, E., Pia, W., Tommi, V., Alice, M., Lauri, K., Raija, L. and Anna-Stiina, J. 2019. Green process to regenerate keratin from feathers with an aqueous deep eutectic solvent, RSC Advances, 9(34): 19720–19728.

Ozaki, Y., Takagi, Y., Mori, H. and Hara, M. 2014. Porous hydrogel of wool keratin prepared by a novel method: An extraction with guanidine/2-mercaptoethanol solution followed by a dialysis, Materials Science and Engineering C, 42: 146–154.

Ozdemir, G. and Sezgin, O.E. 2006. Keratin rhamnolipids and keratin sodium deodecyl sulfate interactions at the air/water interface, Colloids and Surfaces B: Biointerfaces, 52: 1–7.

Papadopoulos, M. C., El Boushy, A. R. and Ketelaars, E. H. 1985. Effect of different processing conditions on amino acid digestibility of feather meal determined by chicken assay, Poultry Science, 64(9): 1729–1741.

Park, M., Kim, B., Shin, H., Park, S. and Kim, H. 2013. Preparation and characterization of keratin based biocomposites hydrogels prepared by electron beam irradiation, Materials Science and Engineering C, 33(8): 5051–5052.

Park, M., Shin, H.Y., Panthi, G., Rabbani, M.M., Alam, A., Choi, J., Chung, H, Hong, S. and Kim, H. 2015. Novel preparation and characterization of human hair based nanofibers using electrospinning process, International Journal of Biological Macromolecules, 76: 45–48.

Patnaik, A., Mvubu, M., Muniyaswamy, S., Botha, A. and Anandjiwala, R.D. 2015. Thermal and sound insulation materials from waste wool and recycled polyester fibers and their biodegradation studies, Energy and Building, 92: 161–169.

Patrucco, A., Cristofaro, F., Simionati, M., Zoccola, M., Bruni, G., Fassina, L., Visai, G., Magenes, R., Mossotti, A., Montarsolo, A. and Tonin, C. 2015. Wool fibril sponges with perspective biomedical applications, Materials Science and Engineering C. doi: 10.1016/j.msec.2015.11.073.

Patrucco, A., Zoccola, M., Consonni, R. and Tonin, C. 2013. Wool cortical cell based porous films, Textile Research Journal, 83(15): 1563–1573.

Peng, Z., Juan, Z., Guocheng, D. and Jian, C. 2019. Keratin Waste Recycling Based on Microbial Degradation: Mechanisms and Prospects, ACS Sustainable Chemistry & Engineering, 7(11): 9727–9736.

Plowman, E., Clerens, S., Lee, E. and Harland, D.P. 2014. Ionic liquid-assisted extraction of wool keratin proteins as an aid to MS identification, Analytical Methods, 6: 7305–7312.

Poole, A.J. and Church, J.S. 2015. The effects of physical and chemical treatments of Na_2S produced feather keratin films, International Journal of Biological Macromolecules, 73: 99–108.

Poole, A.J., Lyons, R.E. and Church, J.S. 2011. Dissolving feather keratin using sodium sulfide for biopolymer applications, Journal of Polymer and Environment, 19: 995–1004.

Popescu, C. and Hartwig, H. 2007. Hair—the most sophisticated biological composite material, Chemical Society Reviews, 36(8): 1282–1291.

Potter, N.A. and Mark, V. D. 2018. Effects of Differing Purification Methods on Properties of Keratose Biomaterials, ACS Biomaterials Science & Engineering, 4(4): 1316–1323.

Pourjavaheri, F., Saeideh, O. P., Oliver, A.H. J., Peter, M. S., Robert, B., Frank, S., Ewan, W.B., Arun, G. and Robert, A.S. 2019. Extraction of keratin from waste chicken feathers using sodium sulfide and l-cysteine, Process Biochemistry, 82: 205–214.

Prochon, M., Janowska, G., Przepiorkowska, A. and Kucharska-Jastrzabek, A.K. 2012. Thermal properties and combustibility of elastomer-protein composites, Part I Composites SBR-keratin, Journal of Thermal Analysis and Calorimetry, 109: 1563–1570.

Prochon, M., Janowska, G., Przepiorkowska, A. and Kucharska-Jastrzabek, A.K. 2013. Thermal properties and combustibility of elastomer-protein composites, Part II Composites NBR-keratin, Journal of Thermal Analysis and Calorimetry, 113: 933–938.

Rad, Z.P., Tavanai, H. and Moradi, A.R. 2012. Production of feather keratin nanopowder through electrospraying, Journal of Aerosol Science, 51: 49–56.

Rafik, M., Jean, D. and Fatma, B. 2004. The intermediate filament architecture as determined by X-ray diffraction modeling of hard α-keratin, Biophysical Journal, 86(6): 3893–3904.

Ramakrishnan, N., Swati, S., Arun, G. and Basma, Y. A. 2018. Keratin based bioplastic film from chicken feathers and its characterization, International Journal of Biological Macromolecules, 111: 352–358.

Ramos, M. L. P., Gonzalo, G. J. A. G., Claudio, J. P., María, E.V. and Guillermo, J. 2018. Influence of GO reinforcement on keratin based smart hydrogel and its application for emerging pollutants removal, Journal of Environmental Chemical Engineering, 6(6): 7021–7028.

Reakasame, S., Daniela, T., Rainer, D. and Aldo, R. B. 2018. Cell laden alginate-keratin based composite microcapsules containing bioactive glass for tissue engineering applications, Journal of Materials Science: Materials in Medicine, 29(12): 185–195.

Reddy, N., Chen, L. and Yang, Y. 2013. Biothermoplastics from hydrolyzed and citric acid crosslinked chicken feathers, Materials Science and Engineering C, 33: 1203–1208.

Reddy, N., Hu, C., Yan, K. and Yang, Y. 2011. Thermoplastic films from cyanoethylated chicken feathers, Materials Science and Engineering C, 31: 1706–1710.

Reichl, S. 2009. Films based on human hair keratin as substrates for cell culture and tissue engineering, Biomaterials, 30: 6854–6886.

Rouse, J.G. and Dyke, M.E.V. 2010. A review of keratin based biomaterials for biomedical applications, Materials, 3: 999–1014.

Sadeghi, S., Dadashian, F. and Eslahi., N. 2019. Recycling chicken feathers to produce adsorbent porous keratin-based sponge, International Journal of Environmental Science and Technology, 16(2): 1119–1128.

Sando, L., Kim, M., Colgrave, M.L., Ramshaw, J.A.M., Werkmesiter, J.A. and Elvin, C.M. 2010. Photochemical crosslinking of soluble wool keratins produced a mechanically stable biomaterial that supports cell adhesion and proliferation, Journal of Biomedical Materials Research Part A, 95A: 901–911.

Saravanan, S., Sameera, D.K., Moorthi, A. and Selvamurugan, N. 2013. Chitosan scaffolds containing chicken feather keratin nanoparticles for bone tissue engineering, International Journal of Biological Macromolecules, 6: 481–486.

Saucedo-Rivalcoba, V., Martínez-Hernández, A. L., Martínez-Barrera, G., Velasco-Santos, C., Rivera-Armenta, J. L. and Castaño, V. M. 2011. Removal of hexavalent chromium from water by polyurethane–keratin hybrid membranes. Water, Air, & Soil, Pollution, 218(1-4): 557–571.

Sayed, S. A., Saleh, S. M. and Hasan., E. E. 2005. Removal of some polluting metals from industrial water using chicken feathers, Desalination, 181(1-3): 243–255.

Schweizer, J., Bowden, P.E., Coulombe, P.A., Langbein, L., Lane, E.B., Magin, T.M., Maltais, L., Omary, M.B., Parry, D.A.D., Rogers, M.A. and Wright, M.W. 2006. New consensus nomenclature for mammalian keratins, The Journal of Cell Biology, 174(2): 169–174.

Sekimoto, Y., Okiharu, T., Nakajima, H., Fujii, T., Shirai, K. and Moriwaki, H. 2013. Removal of Pb(II) from water using keratin colloidal solution obtained from wool, Environmental Science and Pollution Research, 20: 6531–6538.

Senoz, E. and Wool, R.P. 2010. Microporous carbon-nitrogen fibers from keratin fibers by pyrolysis, Journal of Applied Polymer Science, 118: 1752–1765.

Shanmugasundaram, O. L., Syed, Z. A. K., Sujatha, K., Ponnmurugan, P., Srivastava, A., Ramesh, R., Sukumar, R. and Elanithi, K. 2018. Fabrication and characterization of chicken feather keratin/polysaccharides blended polymer coated nonwoven dressing materials for wound healing applications, Materials Science and Engineering: C, 92: 26–33.

Sharma, S., Arun, G., Ashok, K., Chua, G. K., Hesam, K. and Syed, M. S. 2018. An efficient conversion of waste feather keratin into ecofriendly bioplastic film, Clean Technologies and Environmental Policy, 20(10): 2157–2167.

Sharma, S., Arun, G., Syed, M.S., Chik, T., Chua, G. K., Bhupendra, M. M., Doo, H. K. and Gaurav, S. 2017. Characterization of keratin microparticles from feather biomass with potent antioxidant and anticancer activities, International Journal of Biological Macromolecules, 104: 189–196.

Shavandi, A., Alaa, E. A. B., Alan, C. and Adnan, B. 2017. Evaluation of keratin extraction from wool by chemical methods for bio-polymer application, Journal of Bioactive and Compatible Polymers, 32(2): 163–177.

Shavandi, A., Tiago, H. S., Adnan, A. B. and Alaa, E. A. B. 2017. Keratin: Dissolution, extraction and biomedical application. Biomaterials, Science, 5(9): 1699–1735.

Shu, T., Xiaojun, C., Jianxing, W., Xiangfang, L., Ziping, Z., Lei, S. and Xueji, Z. 2018. Synthesis of luminescent gold nanoclusters embedded goose feathers for facile preparation of Au (I) complexes with aggregation-induced emission, ACS Sustainable Chemistry & Engineering, 7(1): 592–598.

Sierpinski, P., Garrett, J., Ma, J., Apel, J., Klorig, D., Smith, T., Koman, L.A., Atala, A. and Dyke, M.V. 2008. The use of keratin biomaterials derived from human hair for the promotion of rapid regeneration of peripheral nerves, Biomaterials, 29: 118–128.

Silva, R., Singh, R., Sarker, B., Papageorgiou, D.G., Juhasz, J.A., Roether, J.A., Cicha, I., Kaschta, J., Schubert, D.W., Chrissafis, K., Detsch, R. and Boccaccini, A.R. 2014. Hybrid hydrogels based on keratin and alginate for tissue engineering, Journal of Materials Chemistry B, 2: 5442–5452.

Singaravelu, S., Ramanathan, G., Raja, M.D., Barge, S. and Sivagnanam, U.T. 2015. Preparation and characterization of keratin based biosheet from bovine horn waste as wound dressing material, Materials Letters, 152: 90–93.

Singh, I. and Kushwaha, R.K.S. 2015. Keratinases and microbial degradation of keratin, Advances in Applied Science Research, 6(2): 74–82.

Song, K., Helan, X., Lan, X. and Yiqi Yang, Kongliang, X. 2017. Cellulose nanocrystal-reinforced keratin bioadsorbent for effective removal of dyes from aqueous solution, Bioresource Technology, 232: 254–262.

Spiridon, I., Paduraru, O.M., Zaltariov, M.F. and Darie, R.N. 2013. Influence of keratin on polylactic acid/chitosan composite properties. Behavior upon accelerated weathering, Industrial and Engineering Chemistry Research, 52: 9822–9833.

Srisuwan, Y. and Prasong, S. 2018. Preparation and characterization of keratin/alginate blend microparticles, Advances in Materials Science and Engineering. https://doi.org/10.1155/2018/8129218, accessed January 2020.

Srivastava, A., Sharma, A. and Suneetha, V. 2011. Feather waste biodegradation as a source of Amino acids, European Journal of Experimental Biology, 1(2): 56–63.

Stanić, V., Jefferson, B., Fabiano, E. M., Aaron, S. and Kenneth, E. 2015. Local structure of human hair spatially resolved by sub-micron X-ray beam, Scientific Reports, 5: 17347–17353.

Su, C., Jin-Song, G., Yu-Xin, S., Jiufu, Q., Shen, Z., Heng, L., Hui, L., Zhen-Ming, L., Zheng-Hong, X. and Jin-Song, Shi 2019. Combining Pro-peptide Engineering and Multisite Saturation Mutagenesis To Improve the Catalytic Potential of Keratinase, ACS Synthetic Biology, 8(2): 425–433.

Sun, K., Juhua, G., Yufeng, H., Pengfei, S., Yubing, X. and Rong-Min, W. 2016. Fabrication of dual-sensitive keratin-based polymer hydrogels and their controllable release behaviors, Journal of Biomaterials Science, Polymer Edition, 27(18): 1926–1940.

Sun, M., Hua, S., Steven, H. and David, A. S. 2018. Effects of feather-fiber reinforcement on poly (vinyl alcohol)/clay aerogels: Structure, property and applications, Polymer, 137: 201–208.

Sun, P., Zhao-Tie, L. and Zhong-Wen, L. 2009. Chemically modified chicken feather as sorbent for removing toxic chromium (VI) ions, Industrial & Engineering Chemistry Research, 48(14): 6882–6889.

Sun, Z., Zeng, Y., Huaiying, Z., Xiaomin, M., Wen, S., Xiaoyu, S. and Xudong, L. 2017. Bio-responsive alginate-keratin composite nanogels with enhanced drug loading efficiency for cancer therapy, Carbohydrate Polymers, 175: 159–169.

Sundaram, M., Legadevi, R., Afrin, N.B., Gayathri, V. and Palanisammy., A. 2015. A study on anti bacterial activity of keratin nanoparticles from chicken feather waste against Staphylococcus aureus (Bovine Mastitis Bacteria) and its anti oxidant activity, European Journal of Biotechnology and Biosciences, 3: 1–5.

Szewciw, L. J., Kerckhove, D. G. D., Grime, G. W. and Douglas, S. F. 2010. Calcification provides mechanical reinforcement to whale baleen α-keratin, Proceedings of the Royal Society B: Biological Sciences, 277(1694): 2597–2605.

Tachibana, A., Furuta, Y., Takeshima, H., Tanabe, T. and Yamauchi, K. 2002. Fabrication of wool keratin sponge scaffolds for long term cell cultivation, Journal of Biotechnology, 93: 165–170.

Tachibana, A., Kaneko, S., Tanabe, T. and Yamauchi, K. 2005. Rapid fabrication of keratin-hydroxyapatite hybrid sponges toward osteoblast cultivation and differentiation, Biomaterials, 26: 297–302.

Tachibana, A., Nishikawa, Y., Nishino, M., Kaneko, S., Tanabe, T. and Yamuchi, K. 2006. Modified keratin sponge: Binding of bone morphogenic protein-2 and osteoblast differentiation, Journal of Bioscience and Bioengineering, 102(5): 425–429.

Taleb, M.A., Salwa, M. and Hosam, E. 2020. Utilization of keratin or sericin-based composite in detection of free chlorine in water, Journal of Molecular Structure, 1202: 127379–127386.

Tanabe, T., Okitsu, N., Tachibana, A. and Yamuchi, K. 2002. Preparation and characterization of keratin chitosan composite film, Biomaterials, 23: 817–825.

Tanabe, T., Okitsu, N. and Yamauchi, K. 2004. Fabrication and characterization of chemically crosslinked keratin films, Materials Science and Engineering C, 24: 441–446.

Thibaut, S., Collin, C., Langbein, L., Schweizer, J., Gautier, B. and Bernard, B.A. 2003. Hair keratin pattern in human hair follicles grown in vitro, Experimental Dermatalogy, 12: 160–164.

Thomas, A., Harland, D.P., Clerens, S., Deb-Choudhury, S., Vernon, J.A., Krsinic, G.L., Walls, R.J., Cornellison, C.D., Plowman, J.E. and Dyer, J.M. 2012. Interspecies comparison of morphology, ultrastructure and proteome of mammalian keratin fibers of similar diameter, Journal of Agricultural and Food Chemistry, 60: 2434–2446.

Toni, M., Luisa, D. V. and Lorenzo, A. 2007. Hard (Beta-) keratins in the epidermis of reptiles: Composition, sequence, and molecular organization, Journal of Proteome Research, 6(9): 3377–3392.

Tran, C. D. and Tamutsiwa, M. M. 2016. Cellulose, chitosan and keratin composite materials: Facile and recyclable synthesis, conformation and properties, ACS Sustainable Chemistry & Engineering, 4(3): 1850–1861.

Tsuda, Y. and Nomura, Y. 2014. Properties of alkaline hydrolysed waterfowl feather keratin, Animal Science Journal, 85: 180–185.

Tu, H., Weidong, Y. and Ling, D. 2016. Structural studies and macro-performances of hydroxyapatite-reinforced keratin thin films for biological applications, Journal of Materials Science, 51(21): 9573–9588.

Uttani, V. and Aruna, K. 2018. Optimization of production and partial characterization of keratinase produced by Bacillus thuringiensis strain Bt407 isolated from poultry soil, International Journal of Current Microbiology and Applied Sciences, 7(4): 596–626.

Valle, D.L., Nardi, A., Bonazza, G., Zuccal, C., Emera, D. and Alibardi, L. 2010. Forty keratin-associated β-proteins (β-keratins) form the hard layers of scales, claws, and adhesive pads in the green anole lizard, Anolis carolinensis, Journal of Experimental Zoology Part B: Molecular and Developmental Evolution, 314(1): 11–32.

Verma, V., Verma, P., Ray, P. and Ray, A.R. 2008. Preparation of scaffolds from human hair proteins for tissue engineering applications, Biomedical Materials, 3: 025007–14.

Villa, A. L.V., Aragao, M.R.S., Santos, E.P., Mazotto, A.M., Zingali, R.B., Souza, E.P. and Vermelho, A.B. 2013. Feather keratin hydrolysates obtained from microbial keratinases: Effect on hair fiber, BMC Biotechnology, 13: 15–26.

Wang, B., Wen, Y., Vincent, R. S. and Marc, A. M. 2016b. Pangolin armor: Overlapping, structure, and mechanical properties of the keratinous scales, Acta Biomaterialia, 41: 60–74.

Wang, B., Yang, W., McKittrick, J. and Meyers, M.A. 2016a. Keratin: Structure, mechanical properties occurrence in biological organisms and efforts at bioinspiration, Progress in Materials Science, 76: 226–318.

Wang, D. and Ren-Cheng, T. 2018a. Dissolution of wool in the choline chloride/oxalic acid deep eutectic solvent, Materials Letters, 231: 217–220.

Wang, D., Wenfeng, L., Yumei, W., Haimeng, Y., Yi, D., Jingou, J., Bochu, W. and Shilei, H. 2019. Fabrication of an expandable keratin sponge for improved hemostasis in a penetrating trauma, Colloids and Surfaces B: Biointerfaces, 182: 110367–110375.

Wang, J., Shilei, H., Tiantian, L., Zhongjun, C., Wenfeng, L., Feiyan, G., Tingwang, G., Yuhua, G. and Bochu, W. 2017. Feather keratin hydrogel for wound repair: Preparation, healing effect and biocompatibility evaluation, Colloids and Surfaces B: Biointerfaces, 149: 341–350.

Wang, J., Shuyi, M., Jicun, R., Jinxia, Y., Yi, Q., Derun, D., Min, Z. and Guang, Y. 2018. Fluorescence enhancement of cysteine-rich protein-templated gold nanoclusters using silver (I) ions and its sensing application for mercury (II), Sensors and Actuators B: Chemical, 267: 342–350.

Wang, K., Li, R., Ma, J.H., Jian, Y.K. and Che, J.N. 2016c. Extracting keratin from wool by using L-cysteine, Green Chemistry, 18(2): 476–481.

Wang, L., Cheng, G., Ren, Y., Dai, Z., Zhao, Z., Liu, F., Li, S., Wei, Y., Xiong, J., Tang, X. and Tang, B. 2015. Degradation of intact chicken feathers by Thermoactinomyces sp. CDF and characterization of its kertinolytic protease, Applied Microbiology and Biotechnology, 99: 3949–3959.

Wang, Q., Cao, Q., Wang, X., Jing, B., Kuang, H. and Zhou, L. 2013. A high capacity carbon prepared from renewable chicken feather biopolymer for supercapacitors, Journal of Power Sources, 225: 101–107.

Wang, X., Lu, C. and Chen, C. 2014. Effect of chicken feather protein based flame retardant on flame retarding performance of cotton fabric, Journal of Applied Polymer Science, 131: 40584–40596.

Wang, Y. and Cao, X. 2012. Extracting keratin from chicken feathers by using a hydrophobic ionic liquid, Process Biochemistry, 47: 896–899.

Wattie, B., Marie-Josée, D. and Mark, L. 2018. Synthesis and properties of feather keratin-based superabsorbent hydrogels, Waste and biomass valorization, 9(3): 391–400.

Wrzesniewska-Tosjik, K., Marcinkowska, M., Niekraszewicz, A., Potocka, D.A., Mik, T. and Palczynska, M. 2011. Fibrous composites based on keratin from chicken feathers, Fibers & Textiles in Eastern Europe, 19(6): 118–123.

Xian Lv, L., Sim, M., Li, Y., Min, J., Feng, W., Guan, W. and Li, Y 2010. Production, characterization and application of a keratinase from Chryseobacterium L99 sp. nov, Process Biochemistry, 45: 1236–1244.

Xie, H., Li, S. and Zhang, S. 2005. Ionic liquids as novel solvents for the dissolution and blending of wool keratin fibers, Green Chemistry, 7: 606–608.

Xing, Y., Hongling, L. and Weidong, Y. 2016. Preparation and characterization of keratin and chicken egg white-templated luminescent Au cluster composite film, Journal of Molecular Structure, 1106: 53–58.

Xu, H., Ma, Z. and Yang, Y. 2014. Dissolution and regeneration of wool via controlled degradation and disentanglement of highly crosslinked keratin, Journal of Materials Science, 49: 7513–7521.

Xu, H., Zhen, S., Reddy, N. and Yang, Y. 2014. Intrinsically water-stable keratin nanoparticles and their in vivo biodistribution for targeted delivery, Journal of Agricultural and Food Chemistry, 62(37): 9145–9150.

Yang, X., Zhang, H., Yuan, X. and Cui, S. 2009. Wool keratin: A novel building block for layer-by-layer self-assembly, Journal of Colloid and Interface Science, 336: 756–760.

Yang, Y.J., Ganbat, D., Aramwit, P., Bucciarelli, A., Chen, J., Migliaresi, C. and Motta, A. 2019. Processing keratin from camel hair and cashmere with ionic liquids, eXPRESS Polymer Letters, 13(2): 97–109.

Yao, C., Chia-Yu, L., Chiung-Hua, H., Yueh-Sheng, C. and Kuo-Yu, C. 2017. Novel bilayer wound dressing based on electrospun gelatin/keratin nanofibrous mats for skin wound repair, Materials Science and Engineering: C, 79: 533–540.

Yu, D., Cai, J.Y., Liu, X., Church, S. and Wang, L. 2014. Novel immobilization of a quaternary ammonium moiety on keratin fibers for medical applications, International Journal of Biological Macromolecules, 70: 236–240.

Yu, Y., Wen, Y., Bin, W. and Marc, A. 2017c. Structure and mechanical behavior of human hair, Materials Science and Engineering: C, 73: 152–163.

Yu, Y., Wen, Y. and Marc, A. 2017b. Viscoelastic properties of α-keratin fibers in hair, Acta Biomaterialia, 64: 15–28.

Yuan, J., Geng, J., Xing, Z, Shim, K., Han, I., Kim, J., Kang, I. and Shen, J. 2015. Novel wound dressing based on nanofibrous PHBV-keratin mats, Journal of Tissue Engineering and Regenerative Medicine, 9: 1027–1035.

Yuan, J., Xing, Z., Park, S., Geng, J. and Kang, I. 2009. Fabrication of PHBV/keratin composite nanofibrous mats for biomedical applications, Macromolecular Research, 17(11): 850–855.

Zhang, H., Fernando, C., Montserrat, L. and Cristina, P. 2019. Valorization of keratin biofibers for removing heavy metals from aqueous solutions, Textile Research Journal, 89(7): 1153–1165.

Zhang, H., Wang, J., Yu, N. and Liu, J. 2014. Electrospun PLGA/multiwalled carbon nanotubes/wool keratin composite membranes: Morphological, mechanical, and thermal properties and their bioactivities in vitro, Journal of Polymer Research, 21: 329–337.

Zhang, Q., Shan, G., Cao, P., He, J., Lin, Z., Huang, Y. and Ao, N. 2015b. Mechanical and biological properties of oxidized horn keratin, Materials Science and Engineering C, 47: 125–134.

Zhang, Y., Zhao, W. and Yang, R. 2015a. Steam flash explosion assisted dissolution of keratin from feathers, ACS Sustainable Chemistry and Engineering, 3: 2036–2042.

Zhang, Z., Xiaochun, Z., Yi, N., Hui, W., Shuangshuang, Z. and Suojiang, Z. Effects of water content on the dissolution behavior of wool keratin using 1-ethyl-3-methylimidazolium dimethylphosphate, Science China Chemistry, 60(7): 934–941.

Zhang, Z., Yi, N., Qiansen, Z., Xue, L., Wenhui., T., Xiangping, Z. and Suojiang, Z. 2017. Quantitative change in disulfide bonds and microstructure variation of regenerated wool keratin from various ionic liquids, ACS Sustainable Chemistry & Engineering, 5(3): 2614–2622.

Zhao, X., Lui, Y.S., Choo, C.K.C., Sow, W.T., Huang, C.L., Ng, K.W., Tan, L.P. and Loo, J.S.C. 2015. Calcium phosphate coated keratin-PCL scaffolds for potential bone tissue regeneration, Materials Science and Engineering C, 49: 746–753.

Zhao, Z., Wang, Y., Li, M. and Yang, R. 2015. High performance N-doped porous activated carbon based on chicken feather for supercapacitors and CO_2 capture, RSC Advances, 5: 34803–34811.

Zheng, D., Sheng, H., Lu, X., Chu-Xin, L., Ke, L., Si-Xue, C. and Xian-Zheng, Z. 2018. Hierarchical Micro-/Nanostructures from Human Hair for Biomedical Applications, Advanced Materials, 30(27): 1800836–1800844.

Zheng, S., Nie, Y., Zhang, S., Zhang, X. and Wang., L. 2015. Highly efficient dissolution of wool keratin by dimethylphosphate ionic liquids, ACS Sustainable Chemistry and Engineering, 3: 2925–2932.

Zhi, X., Yanfang, W., Pengfei, L., Jiang, Y. and Jian, S. 2015. Preparation of keratin/chlorhexidine complex nanoparticles for long-term and dual stimuli-responsive release, RSC Advances, 5(100): 82334–82341.

Zhou, L., Guang, Y., Xue-Xia, Y., Zhang-Jun, C. and Mei-Hua, Z. 2014. Preparation of regenerated keratin sponge from waste feathers by a simple method and its potential use for oil adsorption, Environmental Science and Pollution Research, 21(8): 5730–5736.

Zhou, Y., Jinjie, W., Guang, Y., Shuyi, M., Min, Z. and Jingxia, Y. 2019. Cysteine-rich protein-templated silver nanoclusters as a fluorometric probe for mercury (ii) detection, Analytical Methods, 11(6): 733–738.

Zoccola, M., Aluigi, A. and Tonin, C. 2009. Characterization of keratin biomass from butchery and wool industry wastes, Journal of Molecular Structure, 938: 35–40.

Zoccola, M., Aluigi, A., Vineis, C., Tonin, C., Ferrero, F. and Piacentino, M.G. 2008. Study on cast membranes and electrospun nanofibers made from keratin/fibroin blends, Biomacromolecules, 9: 2918–2825.

Index

https://doi.org/10.1515/9781501511769-012